UNIVERSITY OF CALIFORNIA,
IRVINE

The Synthesis of Rare Earth Complexes for the Optimization of Single-Molecule Magnets

DISSERTATION

submitted in partial satisfaction of the requirements
for the degree of

DOCTOR OF PHILOSOPHY

in Chemistry

by

Jordan Faye Corbey

Dissertation Committee:
Professor William J. Evans, Chair
Professor A.S. Borovik
Professor Alan F. Heyduk

2015

DEDICATION

To

My Father and Mother

Tom & Ronelle

You bring me to Life … over and over.

"Man suffers only because he takes seriously what the gods made for fun."

- Alan W. Watts

TABLE OF CONTENTS

LIST OF FIGURES

LIST OF TABLES

ACKNOWLEDGMENTS

To my adviser Professor William J. Evans, thank you for being the example of what it means to work diligently, efficiently and to be utterly successful while still treating your students like real people. Despite your staggeringly busy schedule, you find time to meet with your group members whenever they need, and you see them as individuals with unique paths and attributes. In addition to learning valuable laboratory techniques and rare earth chemistry in your laboratory over the past five years, I've also deepened my understanding of what it means to respect others and their ideas by approaching problems with an open mind. Even today, I'm discovering new wisdom and insight in words you said to me years ago. Therefore, I have no doubt the lessons you've taught me will stick with me through the rest of my professional career. Thank you Bill, for reminding me every day through your actions and advice, that the greatest decision I've made thus far in my career was joining your research group.

To Professor A. S. Borovik, thank you for opening your door to me. During my graduate career, if ever I felt worried about exams or anxious about classes, you were willing to talk me through my concerns and remind me that everything will work out okay so that I always felt more at ease after leaving your office. I am honored Andy to have you as part of my defense committee, and I'll miss stopping by your lab or office just to say hello.

To Professor Alan F. Heyduk, thank you for serving on my second year report committee, my advancement committee and now my defense committee; you really have been with me every step of the way. Thank you for your support as my Inorganic Chemistry graduate adviser and for truly caring about the needs and lives of the graduate students in the UCI Chemistry Program.

To Dr. Joseph W. Ziller, thank you for your patience in teaching me everything I know about X-ray crystallography. Thank you for taking the time Joe, to be a friend as well as an adviser.

To Dr. Ming Fang, thank you for your kindness and diligence in teaching me laboratory techniques and for continuing to be a mentor to me even after your time in the Evans lab. Thank you for reading drafts, sending edits and still asking me how I'm doing once in a while.

To past Evans group members, especially Dr. Tom Mueller, Dr. Ian Casely, Dr. Nate Siladke and Dr. Matt MacDonald, thank you for your words of wisdom, continued friendship and complimentary beer tasters from each new batch of homebrew.

To Megan Fieser, thank you for caring. You did a lot of that for both of us. Thank you for working beside me these past five years and helping me pull all-nighters to finish assignments or prepare samples for our collaborators or practice our presentations. Thanks for always being there, even when I didn't make it easy.

To current Evans group members, especially Chris Kotyk, Ryan Langeslay, Cory Windorff, David Woen, Chad Palumbo and Casey Johnson, thank you for helping to make these last few years in graduate school memorable to say the least. Each of you brings unique character to our group that is irreplaceable.

To our collaborators, Professor Jeffrey R. Long, Katie Meihaus, and Dr. Selvan Demir, thank you for providing all of the magnetic data described in this dissertation. Thank you also for hosting me in your lab over the summer. Your expertise has been invaluable to me.

To my parents, Tom and Ronelle Corbey, thank you for your *Agape*. Your love, faith, strength of heart and clarity of mind has contributed so much to the person I am today. I feel blessed simply to know you, let alone, have you for my parents. I am astounded daily by the fact

that I have been gifted with you to help guide me through my life. You are the reason I am anything today.

To my cousin SSgt Daniel S. Arcand, thank you for putting my difficulties into perspective. Your perspective is one I think everyone needs to see.

Finally, to the incredible individuals, the deep thinkers, who I met during my time in Southern California, thank you for helping me to develop and discover my true self and for teaching me about the ways of this world. You know who you are. I thank you.

CURRICULUM VITAE

Jordan F. Corbey

2010	Bachelor of Science in Chemistry and Biochemistry, Eastern Washington University
2010-2015	Graduate Student Researcher/Teaching Assistant, University of California, Irvine
2012-2015	X-ray Crystallography Laboratory Assistant, University of California, Irvine
2015	Ph.D. in Chemistry, University of California, Irvine

PUBLICATIONS

"Field-induced *XY* and Ising Ground States in a Quasi-Two-Dimensional *S*=1/2 Heisenberg Antiferromagnet" Yoshimitsu Kohama, Marcelo Jaime, Oscar E. Ayala-Valenzuela, Ross D. McDonald, Eun Deok Mun, Jordan F. Corbey, and Jamie L. Manson *Physical Review B*, **2011**, *84*, 184402.

"Dimensionality Selection in a Molecule-Based Magnet" Paul A. Goddard, Jamie L. Manson, John Singleton, Isabel Franke, Tom Lancaster, Andrew J. Steele, Stephen J. Blundell, Christopher Baines, Francis L. Pratt, Ross D. McDonald, Oscar E. Ayala-Valenzuela, Jordan F. Corbey, Heather I. Southerland, Pinaki Sengupta, and John A. Schlueter *Physical Review Letters*, **2012**, *108*, 077208.

"Varying the Lewis Base Coordination of the Y_2N_2 Core in the Reduced Dinitrogen Complexes $\{[(Me_3Si)_2N]_2(L)Y\}_2(\mu\text{-}\eta^2\text{:}\eta^2\text{-}N_2)$ (L = Benzonitrile, Pyridines, Triphenylphosphine Oxide, and Trimethylamine *N*-Oxide)" Jordan F. Corbey, Joy H. Farnaby, Jefferson E. Bates, Joseph W. Ziller, Filipp Furche and William J. Evans *Inorganic Chemistry*, **2012**, *51*,7867.

"Magnetic Exchange in $(N_2)^{3-}$ Bridged Bimetallic Rare Earth Single-Molecule Magnets Isolated Using an External NdFeB Magnet" Katie R. Meihaus, Jordan F. Corbey, Ming Fang, Joseph W. Ziller, Jeffrey R. Long, and William J. Evans *Inorganic Chemistry*, **2014**, *53*, 3099.

"Co-crystallization of $(\mu\text{-}S_2)^{2-}$ and $(\mu\text{-}S)^{2-}$ and Formation of an $[\eta^2\text{-}S_3N(SiMe_3)_2]$ Ligand From Chalcogen Reduction by $(N_2)^{2-}$ in a Bimetallic Yttrium Amide Complex" Jordan F. Corbey, Ming Fang, Joseph W. Ziller, and William J. Evans *Inorganic Chemistry*, **2014**, *54*, 801-807.

"Accessing Record Single-Ion Magnetic Moments through a Mixed Electronic Configuration in the Divalent Lanthanide Complexes $[(C_5H_4SiMe_3)_3Ln]^-$" Katie R. Meihaus, Megan E. Fieser, Jordan F. Corbey, William J. Evans, and Jeffrey R. Long *Submitted*.

"Isolation and Structure of the Bis(allyl) and Bis(ammonia) Cyclopentadienyl Dysprosium Complexes, $(C_5Me_5)Dy(C_3H_5)_2(THF)$ and $[(C_5Me_5)_2Dy(NH_3)_2][BPh_4]$, from the Synthesis of $[(C_5Me_5)_2Dy][(\mu\text{-}Ph)_2BPh_2]$" Jordan F. Corbey, Selvan Demir, Miguel Gonzalez, Joseph W. Ziller, Jeffrey R. Long, William J. Evans *Manuscript in preparation*.

"Ligand Effects in the Synthesis of Ln^{2+} Complexes by Reduction of Tris(cyclopentadienyl) Precursors Including C–H Bond Activation of an Indenyl Anion" Jordan F. Corbey, David H. Woen, Chad T. Palumbo, Megan E. Fieser, Joseph W. Ziller, Fillip Furche and William J. Evans *Manuscript in preparation.*

"Synthesis and Structure of Nitrile-Solvated Rare Earth Metallocene Cations $[Cp_2Ln(NCR)_3][BPh_4]$ (Cp = C_5Me_5, $C_5H_4SiMe_3$; R = Me, ^{t}Bu, Ph)" Jordan F. Corbey, Joseph W. Ziller, and William J. Evans *Manuscript in preparation*.

"Raman, X-ray Crystallographic and Theoretical Studies of N=N Bond Reduction in Rare Earth Dinitrogen Complexes" Megan E. Fieser, David H. Woen, Jordan F. Corbey, Thomas J. Mueller, Joseph W. Ziller, Filipp Furche, William J. Evans *Manuscript in preparation.*

PUBLICATIONS CONTAINING ACKNOWLEDGMENTS FOR X-RAY CRYSTALLOGRAPHY

"Insertion of CO_2 and COS into Bi−C Bonds: Reactivity of a Bismuth NCN Pincer Complex of an Oxyaryl Dianionic Ligand, $[2,6\text{-}(Me_2NCH_2)_2C_6H_3]Bi(C_6H_2{}^tBu_2O)$" Douglas R. Kindra, Ian J. Casely, Megan E. Fieser, Joseph W. Ziller, Filipp Furche, and William J. Evans *J. Am. Chem. Soc.*, **2013**, *135*, 7777.

"Reactivity of U^{3+} Metallocene Allyl Complexes Leads to a Nanometer-Sized Uranium Carbonate, $[(C_5Me_5)_2U]_6(\mu\text{-}\kappa^1\text{:}\kappa^2\text{-}CO_3)_6$" Christopher L. Webster, Joseph W. Ziller, and William J. Evans *Organometallics*, **2013**, *32*, 4820.

"Synthetic Aspects of $(C_5H_4SiMe_3)_3Ln$ Rare-Earth Chemistry: Formation of $(C_5H_4SiMe_3)_3Lu$ via $[((C_5H_4SiMe_3)_2Ln]^+$ Metallocene Precursors" Jeffrey K. Peterson, Matthew R. MacDonald, Joseph W. Ziller, and William J. Evans *Organometallics*, **2013**, *32*, 2625.

"Nitric Oxide Insertion Reactivity with the Bismuth–Carbon Bond: Formation of the Oximate Anion, $[ON=(C_6H_2{}^tBu_2O)]^-$, from the Oxyaryl Dianion, $(C_6H_2{}^tBu_2O)^{2-}$" Douglas R. Kindra, Ian J. Casely, Joseph W. Ziller, and William J. Evans *Chem. Eur. J.* **2014**, *20*, 15242.

"Structural Complexity in the Rare Earth Metallocene Hydride Complexes, $[(C_5Me_5)_2LnH]_2$" Shan-Shan Liu, Song Gao, Joseph W. Ziller and William J. Evans *Dalton Trans.*, **2014**, *43*, 15526.

"A Half-Sandwich Organometallic Single-Ion Magnet with Hexamethylbenzene Coordinated to the Dy(III) Ion" Shan-Shan Liu, Joseph W. Ziller, Yi-Quan Zhang, Bing-Wu Wang, William J. Evans and Song Gao *Chem. Commun.*, **2014**, *50*, 11418.

"Reactivity of Organothorium Complexes with TEMPO" Ryan R. Langeslay, Justin R. Walensky, Joseph W. Ziller, and William J. Evans *Inorg. Chem.*, **2014**, *53*, 8455.

"Synthesis and Structure of Bis- and Tris-Benzyl Bismuth Complexes" Douglas R. Kindra, Jeffrey K. Peterson, Joseph W. Ziller, and William J. Evans *Organometallics*, **2015**, *34*, 395.

"Synthesis, Structure, and Reactivity of Crystalline Molecular Complexes of the $\{[C_5H_3(SiMe_3)_2]_3Th\}^{1-}$ Anion Containing Thorium in the Formal +2 Oxidation State" Ryan R. Langeslay, Megan E. Fieser, Joseph W. Ziller, Filipp Furche and William J. Evans *Chem. Sci.*, **2015**, 6, 517.

PRESENTATIONS

"Diversifying Coordination Environments in Bimetallic Rare Earth Reduced Dinitrogen Complexes that are Precursors to Single Molecule Magnets" Jordan F. Corbey, Joseph W. Ziller, and William J. Evans, Poster presented at the Western Regional Meeting of the American Chemical Society, Pasadena, CA, November 11, 2011.

"Synthesis of New Bimetallic Rare Earth Reduced Dinitrogen Complexes for the Optimization of Single-Molecule Magnets" Jordan F. Corbey, Joseph W. Ziller, and William J. Evans, Oral Presentation at the 243rd National Meeting of the American Chemical Society, San Diego, CA, March 27, 2012.

"Crystallization and Chalcogen Reactivity Studies of Bimetallic Rare Earth Reduced Dinitrogen Complexes Supported by Bis(trimethylsilyl)amide Ancillary Ligands" Jordan F. Corbey, Joseph W. Ziller and William J. Evans, Oral Presentation at the 248th National Meeting of the American Chemical Society, San Francisco, CA, August 10, 2014.

"Ligand Effects in the Synthesis of Ln^{2+} Complexes by Reduction of Tris(cyclopentadienyl) Precursors Including C–H Bond Activation of an Indenyl Ligand" Jordan F. Corbey, Chad Palumbo, David Woen, Joseph W. Ziller and William J. Evans, Oral Presentation at the 249th National Meeting of the American Chemical Society, Denver, CO, March 22, 2015.

AWARDS

2015	Associate Graduate Student (AGS) Travel Grant
2014	Travel Award from the Division of Inorganic Chemistry (DIC) of the American Chemical Society
2013	Committee on Research Award for "Fostering Development of Single-Molecule Magnets" – University of California, Irvine
2010	Funded as a summer researcher at the University of California, Irvine through ChaMP (Chemical and Materials Research Program)
2010	Graduated *Summa Cum Laude* – Eastern Washington University
2010	Outstanding Chemistry Graduate Award (one of six) – Eastern Washington University
2006	Orland B. Killin Honors Scholarship (one of two), highest academic four-year scholarship – Eastern Washington University, 2006-2010
2006	Dean's list twelve consecutive quarters – Eastern Washington University, 2006 2010

VOLUNTEER

2012-2013	LEAPS (Laboratory Experiments and Activities in the Physical Sciences) for grade school children, University of California, Irvine
2009-2010	WaTep tutor for Washington state funded universities tutoring college students, Easter Washington University
2009-2010	Science Olympiad volunteer, Eastern Washington University
2005-2006	Teen Aid Project Tutor

ABSTRACT OF THE DISSERTATION

The Synthesis of Rare Earth Complexes for the Optimization of Single-Molecule Magnets

By

Jordan Faye Corbey

Doctor of Philosophy in Chemistry

University of California, Irvine, 2015

Professor William J. Evans, Chair

This dissertation describes the synthesis and physical characterization of a variety of rare earth-containing molecules that have been targeted for the purpose of better understanding the roles that rare earth elements play in molecular magnetism. The complexes described here also contribute to fundamental understanding of rare earth coordination chemistry. Many of these results and conclusions have been developed in collaboration with the group of Professor Jeffrey R. Long at the University of California, Berkeley.

Chapters 1 through 4 of this dissertation focus on modifying different aspects of the known $(N_2)^{3-}$-bridged bimetallic single-molecule magnet (SMM) system $\{[(Me_3Si)_2N]_2(THF)Ln\}_2(\mu\text{-}\eta^2\text{:}\eta^2\text{-}N_2)[K(18\text{-crown-}6)(THF)_2]$, whose Tb analog had the highest blocking temperature ever observed for a SMM when it was published in 2011. Variations in the ancillary ligands, the metals, and the bridging unit were investigated to determine their effects on magnetic properties. In Chapter 1, the variation in the Lewis base L in the precursor to the $(N_2)^{3-}$ complexes, the $(N{=}N)^{2-}$ complexes, $\{[(Me_3Si)_2N]_2(L)Ln\}_2(\mu\text{-}\eta^2\text{:}\eta^2\text{-}N_2)$, was explored. Previously, only L = THF was known. It was found with the diamagnetic Ln = Y analog that L = pyridines, nitriles, and triphenylphosphine oxide can also support this reduced dinitrogen

$(N=N)^{2-}$ system. However, further reduction to obtain a radical $(N_2)^{3-}$ complex was not achieved. Density functional theory (DFT) calculations suggest this is due to the presence of lower lying orbitals based on the new neutral donors.

Chapter 2 analyzes how structural modifications in the previously reported SMMs $\{[(Me_3Si)_2N]_2(THF)Ln\}_2(\mu\text{-}\eta^2\text{:}\eta^2\text{-}N_2)[K(18\text{-crown-}6)(THF)_2]$ (Ln = Tb, Dy) can affect the molecular magnetism when the K^+ counter cation is incorporated into the inner sphere of the magnetic core. The new series of SMMs that resulted, $\{[(Me_3Si)_2N]_2(THF)Ln\}_2(\mu_3\text{-}\eta^2\text{:}\eta^2\text{:}\eta^2\text{-}N_2)K$ (Ln = Tb, Dy), displays blocking temperatures lower than the outer sphere K^+ analogs. This result is thought to be due in part to the crystallographically-observed bending of the previously planar Ln_2N_2 core. In Chapter 3, a more drastic modification in the bridging unit of these bimetallic rare earth complexes was achieved: the $(N_2)^{2-}$ anion in $\{[(Me_3Si)_2N]_2(THF)Y\}_2(\mu\text{-}\eta^2\text{:}\eta^2\text{-}N_2)$ can reduce elemental sulfur and selenium to generate bridging E^{2-} and $(E_2)^{2-}$ chalcogenide complexes, where E = S, Se. Finally, Chapter 4 investigates the Tb analog of the first reported molecular example of an $(NO)^{2-}$-containing complex, the radical bridged $\{[(Me_3Si)_2N]_2(THF)Y\}_2(\mu\text{-}\eta^2\text{:}\eta^2\text{-}NO)$, and demonstrates the importance of obtaining additional spectral characterization data to support X-ray crystallographic findings.

Chapter 5 describes synthetic aspects of complexes containing the $[(C_5Me_5)_2Ln]^{1+}$ moiety, which is an important component in rare earth starting materials, and Chapter 6 shows how this is used to design phenazine radical $(phz)^{1-}$-containing SMMs. Although the targeted complexes, $\{[(C_5Me_5)_2Ln]_2(phz)\}\{BPh_4\}$ (Ln = Tb, Dy; phz = phenazine), could be synthesized and crystallographically characterized, magnetic data suggest the presence of multiple magnetic products in the crystalline sample. In Chapter 7, $(C_5Me_5)^{1-}$ metallocenes are investigated from

another perspective. Attempts were made to obtain linear monometallic trivalent rare earth metallocene cations, as previously demonstrated for U^{4+}, to determine their potential as single-ion magnets (SIMs).

The origin of the research presented in Chapter 8 was the recent discovery that the +2 oxidation state is accessible for all the lanthanides in molecular species with formula [K(2.2.2-cryptand)][Cp'_3Ln] ($Cp' = C_5H_4SiMe_3$) and that the Ho^{2+} analog of these complexes possesses the highest magnetic moment ever measured for a single metal ion, 11.4 μ_B. The synthesis and isolation of more molecular examples of these highly reactive divalent ions were pursued with the indenide ligand, $(C_9H_7)^{1-}$. However, reduction of $Cp^{In}{}_3Ln$ ($Cp^{In} = C_9H_7$) resulted in C–H bond activation of an indenyl ligand and the first example of the indenyl dianion, $(C_9H_6)^{2-}$.

Appendix A is a collection of results on miscellaneous projects not covered in the previous eight chapters. The results in this appendix are presented in chronological order and span a collection of ventures from dinitrogen reduction using lithium to inelastic neutron scattering (INS) experiments and finally a collaborative project with the group of Professor Alan F. Heyduk at the University of California, Irvine, presenting the mixed metal lanthanide/transition metal species $(C_5Me_5)_2Dy[M(SNS)_2]$ (M = Mo, W). These latter complexes were synthesized to probe whether magnetic coupling of the mixed metal centers could occur. They truly exemplify the purpose of the research presented in this dissertation which is to explore the frontiers of molecular magnet design.

INTRODUCTION

The purpose of the research presented in this dissertation is to explore the properties of rare earth-containing molecules that may be valuable in the realm of molecular magnetism. This research not only aims to expand this area, but it also broadens on what is known about fundamental rare earth coordination chemistry. This introduction includes background information in three areas critical to the utilization of rare earth metals in magnetic molecules: the intrinsic properties of the rare earths, single-molecule magnets (SMMs), and finally the chemistry that changed the field of molecular magnetism and inspired many of the projects described in the following chapters.

The Rare Earths. The rare earth elements include scandium, yttrium, and the lanthanides, and are shown in orange in Figure 0.1. The lanthanides are some of the heaviest metals in the periodic table. They contain f electrons and are most commonly found in the +3 oxidation state. Due to the limited radial extension of the f orbitals, as shown in Figure 0.2, the lanthanides are known to form primarily ionic complexes and generally demonstrate less metal-ligand overlap than the d orbitals of transition metals.[1] Although scandium and yttrium are technically transition metals, they are closed-shell ions in the +3 oxidation state and often display chemistry analogous to that of the lanthanides. Yttrium has a nuclear spin of I = ½, is diamagnetic in its +3 oxidation state and is similar in size (0.900 Å)[2] to Ho^{3+} (0.901 Å) and Er^{3+} (0.890 Å).[2] As such, yttrium is a spectroscopically useful surrogate for the smaller paramagnetic lanthanides (i.e. Gd, Tb, Dy, Ho, Er, Tm, Yb).

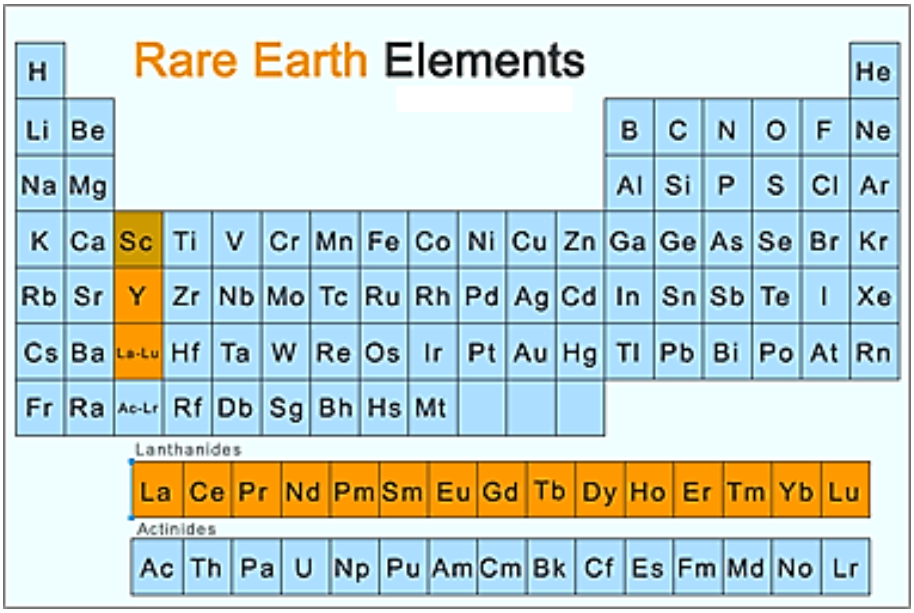

Figure 0.1. Periodic table of the elements displaying the rare earth elements in orange.

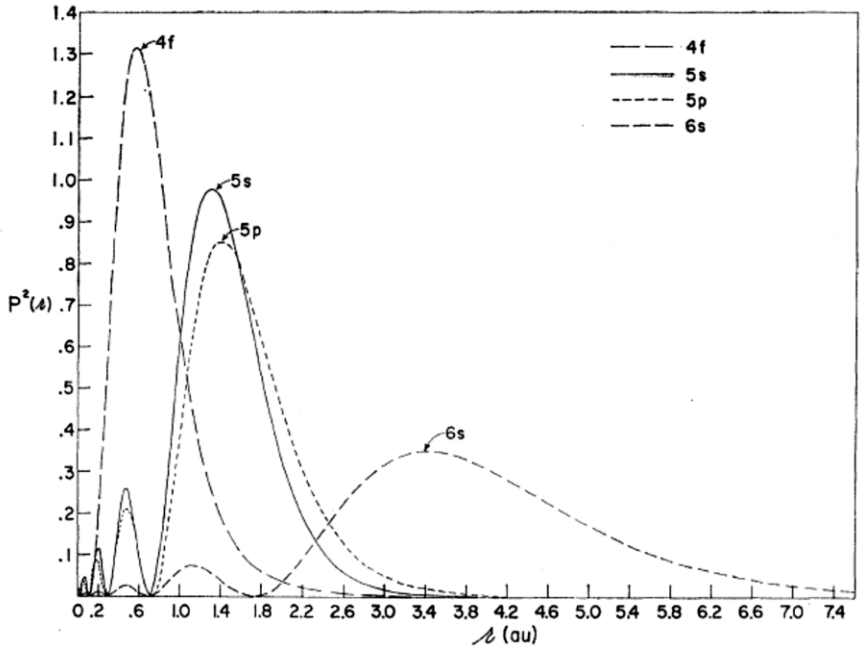

Figure 0.2. Probability distribution of the 4f, 5s, 5p, and 6s electrons for the Gd^{3+} ion (electron configuration $[Xe]4f^7$) as a function of radial distance.[1]

With seven f orbitals available to the lanthanides, they have the potential to retain more unpaired electrons than most other elements in the periodic table. Therefore, they tend to possess higher total spin (S_T) values. Additionally, with the contracted nature of the f orbitals and limited metal-ligand orbital overlap, orbital angular momentum is not quenched as it is with transition metals, and spin-orbit coupling effects play a much more significant role in determining the electronic structure and magnetism of the f elements than in transition metals. These spin-orbit coupling (J) effects contribute to the large single-ion anisotropies often exhibited by the f elements. Maximum S_T and maximum J are ideal in molecular magnets. Problematic magnetic relaxation pathways are also less likely due to the isolated spin manifold of the f elements. The metal ions in the second half of the lanthanide series such as Tb^{3+}, Dy^{3+}, Ho^{3+}, and Er^{3+}, where S and L add to make large J values, are good candidates for single-molecule magnets.[3-5]

Single-Molecule Magnets (SMMs). It was first realized in 1993 that a single molecule could possess a barrier to magnetic relaxation of its molecular spin that was large enough to observe magnetic hysteresis.[3,6,7] Since that time, the utility of lanthanides in the field of single-molecule magnetism has been demonstrated in a variety of systems,[5,8-15] due in part to the large single-ion anisotropies the f elements can possess.[3] Although the special properties of the lanthanides have been employed in bulk magnetic materials since the 1960s to generate some of the strongest magnets currently known, such as $Nd_2Fe_{14}B$ and $SmCo_5$,[16-18] their role in molecular magnetism was not widely accepted until the early 2000s.[3,15]

Perhaps the most prominent obstacle in the way of utilizing SMMs for practical purposes is the low temperature regime at which they function, with most traversing their thermal barriers to magnetic relaxation below 4 K.[3,5] Much of the exploratory synthetic chemistry in this field

has been done to determine which molecular properties are required to boost the working temperatures of SMMs. Although valuable theoretical[3,19] and experimental results have shed light on some of these characteristics, there is still much to be determined regarding the molecular architectures necessary in the design of useful molecular magnets.[20]

A breakthrough in the field of SMMs occurred in 2011 with the discovery that some radical bridging ligands containing diffuse spin orbitals can enhance magnetic communication in bimetallic lanthanide complexes.[4,11,12,21,22] Weak magnetic exchange coupling is typically observed for lanthanides due to the contracted nature of the f electrons[1,3] however, in the radical-bridge systems described in the next section, strong coupling was observed and this led to the best SMMs known to date.

Rare Earth Reduced Dinitrogen Complexes. The rare earth reduced dinitrogen chemistry pioneered by Evans and coworkers via the LnA_3/M (Ln = Y, lanthanide; A = anionic ligand; M = Na, K, KC_8) reduction system[23-28] has influenced many areas of chemistry including, but not limited to, small molecule activation,[29-31] molecular magnetism,[11,12,32] and fundamental redox properties of heavily-studied metal ions.[33-37] Exploration of the reactivity of the $(N{=}N)^{2-}$ complexes $[A_2(THF)Ln]_2(\mu\text{-}\eta^2{:}\eta^2\text{-}N_2)$ (Ln = Dy or Y; A = $[OC_6H_3(^tBu)_2\text{-}2,6]^-$ or $[N(SiMe_3)_2]^-$, respectively) led to isolation of the first molecular examples of the $(N_2)^{3-}$ radical ion in species such as $[A_2(THF)Ln]_2(\mu\text{-}\eta^2{:}\eta^2\text{-}N_2)[K(THF)_6]$, eq 0.1.[26,27]

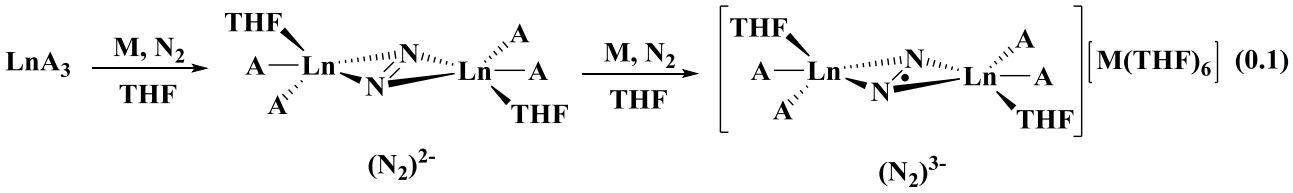

(0.1)

It has been found that these highly reactive reduced dinitrogen complexes can act as reducing agents themselves and activate other substrates such as dioxygen,[38] nitric oxide,[29] carbon monoxide,[39] phenazine,[39] cyclooctatetraene,[39] as well as other organic molecules.[39] Eqs 0.2 and 0.3 display reactions of two of the above mentioned examples, and Chapter 3 of this dissertation discusses analogous findings with chalcogen reduction.

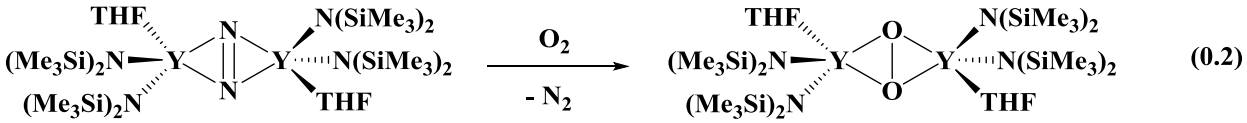

(0.2)

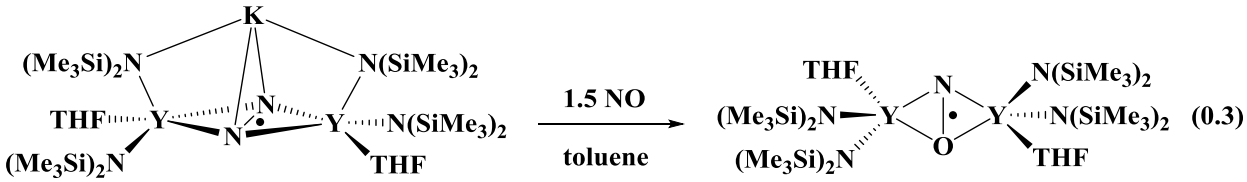

(0.3)

Rare earth reduced dinitrogen complexes entered the field of molecular magnetism in 2011 when it was discovered, in collaboration with the laboratory of Professor Jeffrey R. Long at the University of California, Berkeley, that the radical bridge of the $(N_2)^{3-}$-containing species [K(18-crown-6)(THF)$_2$]{[(Me$_3$Si)$_2$N]$_2$(THF)Ln}$_2$(μ-η^2:η^2-N$_2$) (Ln = Gd, Dy, Tb), Figure 0.3, can strongly couple the unpaired electrons of the trivalent lanthanide ions leading to record breaking magnetic blocking temperatures.[11,12] The low temperature magnetic hysteresis data for [K(18-crown-6)(THF)$_2$]{[(Me$_3$Si)$_2$N]$_2$(THF)Ln}$_2$(μ-η^2:η^2-N$_2$) (Ln = Dy, Tb) are shown in Figure 0.4[11,12] and provide evidence for the large anisotropy barrier to spin reversal present in these systems. In the $(N_2)^{3-}$ radical complexes discussed above, it is believed that the radical unit in the planar Ln$_2$N$_2$ core enables a unique exchange pathway between the lanthanide centers that exploits their high anisotropy and isolated spins.[19]

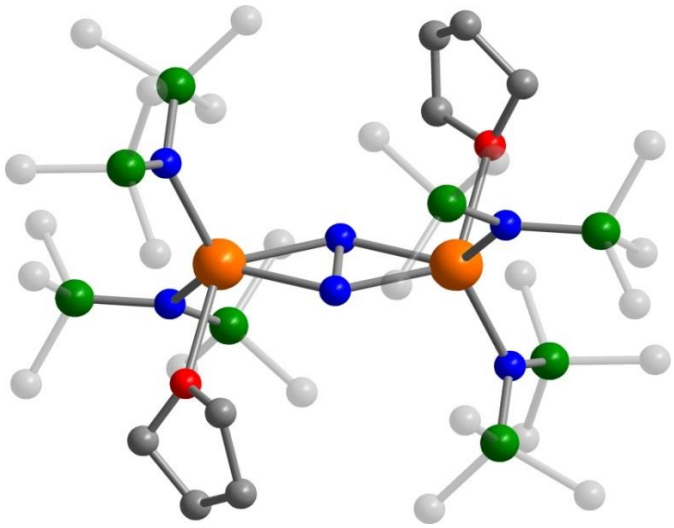

$Ln^{3+}\ (N_2)^{3-\bullet}\ Ln^{3+}$

Figure 0.3. Crystal structure of the anion in $[K(18\text{-crown-}6)(THF)_2]\{[(Me_3Si)_2N]_2(THF)Ln\}_2(\mu\text{-}\eta^2\text{:}\eta^2\text{-}N_2)$.[11,12]

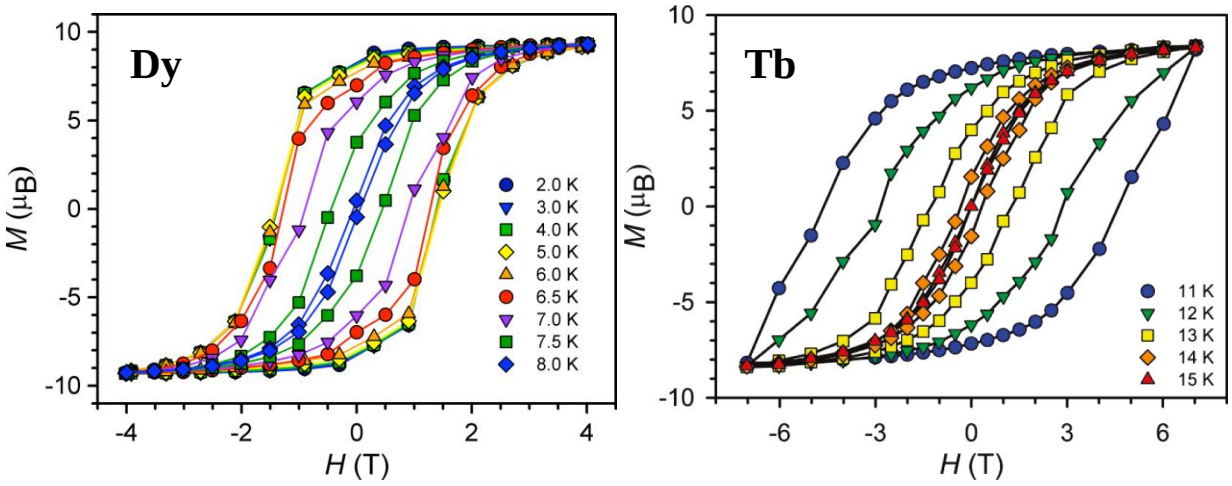

Figure 0.4. Variable-field magnetization data for (left) $[K(18\text{-crown-}6)(THF)_2]\{[(Me_3Si)_2N]_2(THF)Dy\}_2(\mu\text{-}\eta^2\text{:}\eta^2\text{-}N_2)$ and (right) $[K(18\text{-crown-}6)(THF)_2]\{[(Me_3Si)_2N]_2(THF)Tb\}_2(\mu\text{-}\eta^2\text{:}\eta^2\text{-}N_2)$.[11,12]

The projects discussed in this dissertation aim to identify advantageous features of SMMs by building on the success of the $(N_2)^{3-}$ radical complexes while taking lessons from novel species in the literature. The notion of being able to control the magnetization of a molecule-sized magnet has also caused research toward this end to flourish in the areas of spintronics,[40-42] nanodevices,[43] and quantum computing[44] which exist at the triple point between synthetic chemistry, physics, and materials science.

References

(1) Freeman, A. J.; Watson, R. E. *Physical Review* **1962**, *127*, 2058.

(2) Shannon, R. *Acta Crystallographica Section A* **1976**, *32*, 751.

(3) Rinehart, J. D.; Long, J. R. *Chemical Science* **2011**, *2*, 2078.

(4) Demir, S.; Jeon, I.-R.; Long, J. R.; Harris, T. D. *Coordination Chemistry Reviews* **2015**, *289–290*, 149.

(5) Woodruff, D. N.; Winpenny, R. E. P.; Layfield, R. A. *Chemical Reviews* **2013**, *113*, 5110.

(6) Sessoli, R.; Tsai, H. L.; Schake, A. R.; Wang, S.; Vincent, J. B.; Folting, K.; Gatteschi, D.; Christou, G.; Hendrickson, D. N. *Journal of the American Chemical Society* **1993**, *115*, 1804.

(7) Sessoli, R.; Gatteschi, D.; Caneschi, A.; Novak, M. A. *Nature* **1993**, *365*, 141.

(8) Ishikawa, N.; Mizuno, Y.; Takamatsu, S.; Ishikawa, T.; Koshihara, S.-y. *Inorganic Chemistry* **2008**, *47*, 10217.

(9) Lin, P.-H.; Burchell, T. J.; Ungur, L.; Chibotaru, L. F.; Wernsdorfer, W.; Murugesu, M. *Angewandte Chemie International Edition* **2009**, *48*, 9489.

(10) Guo, Y.-N.; Xu, G.-F.; Gamez, P.; Zhao, L.; Lin, S.-Y.; Deng, R.; Tang, J.; Zhang, H.-J. *Journal of the American Chemical Society* **2010**, *132*, 8538.

(11) Rinehart, J. D.; Fang, M.; Evans, W. J.; Long, J. R. *Nature Chemistry* **2011**, *3*, 538.

(12) Rinehart, J. D.; Fang, M.; Evans, W. J.; Long, J. R. *Journal of the American Chemical Society* **2011**, *133*, 14236.

(13) Hewitt, I. J.; Tang, J.; Madhu, N. T.; Anson, C. E.; Lan, Y.; Luzon, J.; Etienne, M.; Sessoli, R.; Powell, A. K. *Angewandte Chemie International Edition* **2010**, *49*, 6352.

(14) Jiang, S.-D.; Wang, B.-W.; Sun, H.-L.; Wang, Z.-M.; Gao, S. *Journal of the American Chemical Society* **2011**, *133*, 4730.

(15) Ishikawa, N.; Sugita, M.; Ishikawa, T.; Koshihara, S.-y.; Kaizu, Y. *Journal of the American Chemical Society* **2003**, *125*, 8694.

(16) Halbach, K. *Nuclear Instruments and Methods* **1980**, *169*, 1.

(17) Narasimhan, K. S. V. L. *Journal of Applied Physics* **1985**, *57*, 4081.

(18) Sugimoto, S. *Journal of Physics D: Applied Physics* **2011**, *44*, 064001.

(19) Rajeshkumar, T.; Rajaraman, G. *Chemical Communications* **2012**, *48*, 7856.

(20) Neese, F.; Pantazis, D. A. *Faraday Discussions* **2011**, *148*, 229.

(21) Demir, S.; Nippe, M.; Gonzalez, M. I.; Long, J. R. *Chemical Science* **2014**, *5*, 4701.

(22) Demir, S.; Zadrozny, J. M.; Nippe, M.; Long, J. R. *Journal of the American Chemical Society* **2012**, *134*, 18546.

(23) Evans, W. J.; Lee, D. S.; Ziller, J. W. *Journal of the American Chemical Society* **2003**, *126*, 454.

(24) Evans, W. J.; Lee, D. S.; Rego, D. B.; Perotti, J. M.; Kozimor, S. A.; Moore, E. K.; Ziller, J. W. *Journal of the American Chemical Society* **2004**, *126*, 14574.

(25) Evans, W. J.; Lee, D. S.; Lie, C.; Ziller, J. W. *Angewandte Chemie International Edition* **2004**, *43*, 5517.

(26) Evans, W. J.; Fang, M.; Zucchi, G. l.; Furche, F.; Ziller, J. W.; Hoekstra, R. M.; Zink, J. I. *Journal of the American Chemical Society* **2009**, *131*, 11195.

(27) Fang, M.; Bates, J. E.; Lorenz, S. E.; Lee, D. S.; Rego, D. B.; Ziller, J. W.; Furche, F.; Evans, W. J. *Inorganic Chemistry* **2011**, *50*, 1459.

(28) Fang, M.; Lee, D. S.; Ziller, J. W.; Doedens, R. J.; Bates, J. E.; Furche, F.; Evans, W. J. *Journal of the American Chemical Society* **2011**, *133*, 3784.

(29) Evans, W. J.; Fang, M.; Bates, J. E.; Furche, F.; Ziller, J. W.; Kiesz, M. D.; Zink, J. I. *Nature Chemistry* **2010**, *2*, 644.

(30) Fang, M.; Farnaby, J. H.; Ziller, J. W.; Bates, J. E.; Furche, F.; Evans, W. J. *Journal of the American Chemical Society* **2012**, *134*, 6064.

(31) Corbey, J. F.; Fang, M.; Ziller, J. W.; Evans, W. J. *Inorganic Chemistry* **2014**.

(32) Meihaus, K. R.; Corbey, J. F.; Fang, M.; Ziller, J. W.; Long, J. R.; Evans, W. J. *Inorganic Chemistry* **2014**, *53*, 3099.

(33) MacDonald, M. R.; Ziller, J. W.; Evans, W. J. *Journal of the American Chemical Society* **2011**, *133*, 15914.

(34) MacDonald, M. R.; Bates, J. E.; Fieser, M. E.; Ziller, J. W.; Furche, F.; Evans, W. J. *Journal of the American Chemical Society* **2012**, *134*, 8420.

(35) MacDonald, M. R.; Bates, J. E.; Ziller, J. W.; Furche, F.; Evans, W. J. *Journal of the American Chemical Society* **2013**, *135*, 9857.

(36) MacDonald, M. R.; Fieser, M. E.; Bates, J. E.; Ziller, J. W.; Furche, F.; Evans, W. J. *Journal of the American Chemical Society* **2013**, *135*, 13310.

(37) Langeslay, R. R.; Fieser, M. E.; Ziller, J. W.; Furche, F.; Evans, W. J. *Chemical Science* **2015**, *6*, 517.

(38) Farnaby, J. H.; Fang, M.; Ziller, J. W.; Evans, W. J. *Inorganic Chemistry* **2012**, *51*, 11168.

(39) Evans, W. J.; Lee, D. S.; Ziller, J. W.; Kaltsoyannis, N. *Journal of the American Chemical Society* **2006**, *128*, 14176.

(40) Rocha, A. R.; Garcia-suarez, V. M.; Bailey, S. W.; Lambert, C. J.; Ferrer, J.; Sanvito, S. *Nature Materials* **2005**, *4*, 335.

(41) Bogani, L.; Wernsdorfer, W. *Nature Materials* **2008**, *7*, 179.

(42) Candini, A.; Klyatskaya, S.; Ruben, M.; Wernsdorfer, W.; Affronte, M. *Nano Letters* **2011**, *11*, 2634.

(43) Affronte, M. *Journal of Materials Chemistry* **2009**, *19*, 1731.

(44) Leuenberger, M. N.; Loss, D. *Nature* **2001**, *410*, 789.

CHAPTER 1

Varying the Lewis Base Coordination of the Y_2N_2 Core in the Reduced Dinitrogen Complexes $\{[(Me_3Si)_2N]_2(L)Y\}_2(\mu\text{-}\eta^2\text{:}\eta^2\text{-}N_2)$ (L = Tetrahydrofuran, Benzonitrile, Pyridines, Triphenylphosphine Oxide, and Trimethylamine *N*-Oxide)

Introduction[†]

One of the common methods of making reduced dinitrogen complexes of the rare earth metals involves the combination of a trivalent complex, LnA_3 (Ln = Sc, Y, lanthanide; A = monoanion), with an alkali metal, M.[1-10] This LnA_3/M reduction method generally works best in THF, and hence the resulting $(N=N)^{2-}$ complexes are commonly isolated as THF solvates, $[A_2(THF)_xLn]_2(\mu\text{-}\eta^2\text{:}\eta^2\text{-}N_2)$, where x = 1 or 2. When the anion A is $[N(SiMe_3)_2]^{1-}$, x = 1 for both large (Ln = Nd) and small (Ln = Lu) rare earth complexes.[11-14]

Due to the prevalence of THF solvates, the effect of the neutral donor ligand, L, on the structure and reactivity of $[A_2(L)_xLn]_2(\mu\text{-}\eta^2\text{:}\eta^2\text{-}N_2)$ complexes had not been examined. Variation in the coordinating ligand L was of interest not only for the $(N=N)^{2-}$ complexes but also for the $(N_2)^{3-}$ complexes $K\{[A_2(L)_xLn]_2(\mu\text{-}\eta^2\text{:}\eta^2\text{-}N_2)\}$ formed from these $(N=N)^{2-}$ complexes.[15] Since the $(N_2)^{3-}$ complexes of paramagnetic rare earths can function as single-molecule magnets,[16,17] it was of interest to vary the coordination environment around the Ln_2N_2 core to determine the effects on the magnetism. Since only THF adducts were previously known, analysis of the effects of variation in L had not previously been carried out.

Formation of $[A_2(L)_xLn]_2(\mu\text{-}\eta^2\text{:}\eta^2\text{-}N_2)$ complexes with L ≠ THF was examined with the yttrium complex, $\{[(Me_3Si)_2N]_2Y(THF)\}_2(\mu\text{-}\eta^2\text{:}\eta^2\text{-}N_2)$, **1**, since it is a well-studied, diamagnetic

[†]Portions of this chapter have been published: Corbey, J. F.; Farnaby, J. H.; Bates, J. E.; Ziller, J. W.; Furche, F.; Evans, W. J. *Inorg. Chem.* **2012**, *51*, 7867.

example of an $(N=N)^{2-}$ complex.[15] Initial attempts at substitution gave only crystals of the starting material, **1**, but conditions were subsequently found that allowed isolation and structural characterization of five new $\{[(Me_3Si)_2N]_2(L)Y\}_2(\mu\text{-}\eta^2\text{:}\eta^2\text{-}N_2)$ complexes: L = PhCN, **2**; py, **3**; DMAP, **4**; Ph_3PO, **5**; Me_3NO, **6**.

Results

Synthesis. Addition of benzonitrile, pyridine, 4-dimethylaminopyridine, and triphenylphosphine oxide to toluene solutions of $\{[(Me_3Si)_2N]_2(THF)Y\}_2(\mu\text{-}\eta^2\text{:}\eta^2\text{-}N_2)$, **1**, causes color changes that could occur due to coordination of the added L. Removal of solvent gave solids that were examined in benzene-d_6 by ^{1}H NMR spectroscopy. Complex **1** was not present and resonances were observed that are consistent with formation of a single substitution product $\{[(Me_3Si)_2N]_2(L)Y\}_2(\mu\text{-}\eta^2\text{:}\eta^2\text{-}N_2)$ in quantitative yield. However, initial attempts to obtain crystals from the benzonitrile reaction in a glovebox containing THF gave only the THF solvate, **1**. To ensure the absence of THF, after the solvent was removed from the $\{[(Me_3Si)_2N]_2(THF)Y\}_2(\mu\text{-}\eta^2\text{:}\eta^2\text{-}N_2)$ / L reactions, the solids were transferred to a glovebox free of THF for crystallization. This produced crystals of $\{[(Me_3Si)_2N]_2(L)Y\}_2(\mu\text{-}\eta^2\text{:}\eta^2\text{-}N_2)$ for L = benzonitrile (**2**), pyridine (**3**), 4-dimethylaminopyridine (**4**), and triphenylphosphine oxide (**5**) in yields of over 65% in each case, eq 1.1. The trimethylamine *N*-oxide complex, $\{[(Me_3Si)_2N]_2(Me_3NO)Y\}_2(\mu\text{-}\eta^2\text{:}\eta^2\text{-}N_2)$, **6**, could be prepared from **1** in 88% yield in THF, and single crystals could be grown from THF/Et_2O solutions.

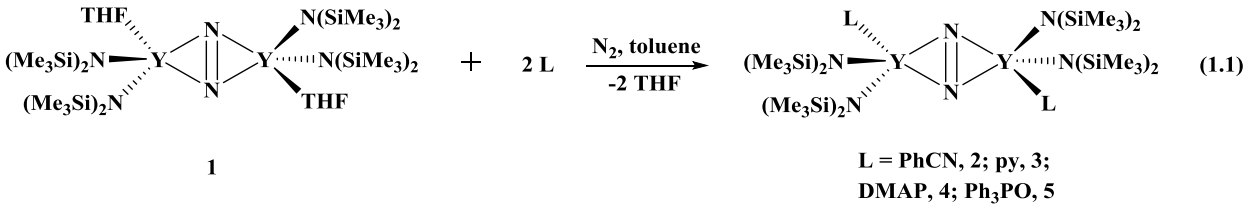

(1.1)

Exchange Reactions. The ^{1}H NMR resonances of the $[(Me_3Si)_2N]^{1-}$ ligands for **1**-**6** are 0.35, 0.50, 0.33, 0.48, 0.37, and 0.45 ppm in benzene-d_6, respectively. Addition of up to 40 equiv of THF to solutions of **3**-**6** in benzene-d_6 causes only minor shifts in the amide resonances, but addition of just four equiv of THF to **2** generates the shift of **1** and free benzonitrile in the ^{1}H NMR spectrum. This is consistent with the fact that attempts to grow crystals of **2** in the presence of THF give **1**. The $[(Me_3Si)_2N]^{1-}$ ^{1}H NMR resonances for **1**-**6** in THF-d_8 are 0.09, 0.09, 0.15, 0.04, 0.00, and 0.07 ppm, respectively.

Crystallographic Analysis. The structures of complexes **2**-**6** are shown in Figures 1.1-1.5. With all of the L ligands investigated, the new complexes formed have just one L per metal as with THF in **1** and have an overall structure similar to that of **1** with the L ligands oriented in a trans fashion around the Y_2N_2 core. Complexes **2**, **3, 5** and **6** crystallize in the $P\bar{1}$ space group like **1**, whereas **4** crystallizes in *P2$_1$/c*. As shown in Table 1.1, the Y–L bond distances vary considerably, i.e. 2.361(1) Å for L = THF, 2.480(1) Å for L = PhCN, 2.519(2) Å for L = py, 2.459(1) Å for L = DMAP, 2.254(1) Å for L = Ph_3PO, and 2.197(1) Å for L = Me_3NO, but they are not unusual in comparison to other Y–L adducts.[18-25]

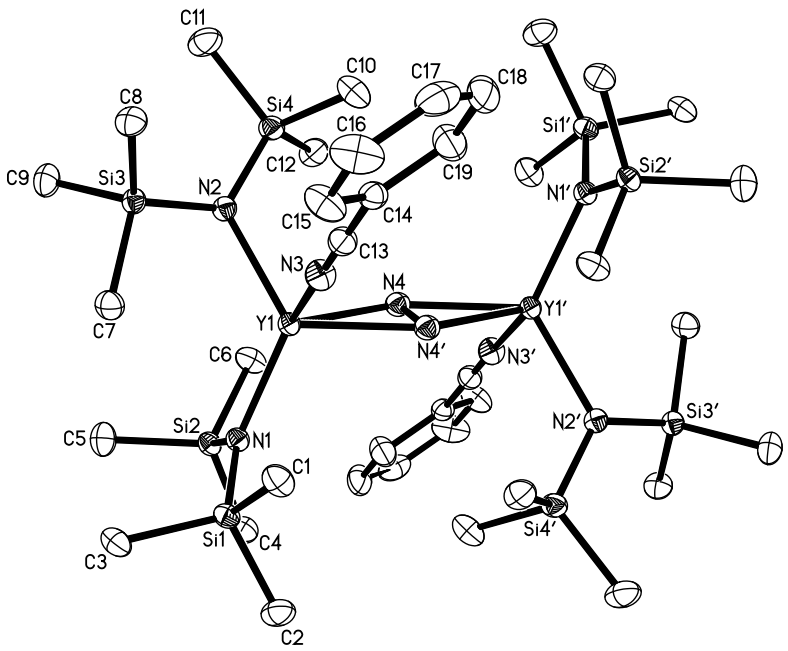

Figure 1.1. Thermal ellipsoid plot of $\{[(Me_3Si)_2N]_2(PhCN)Y\}_2(\mu\text{-}\eta^2\text{:}\eta^2\text{-}N_2)$, **2**, drawn at the 50% probability level. Hydrogen atoms are omitted for clarity.

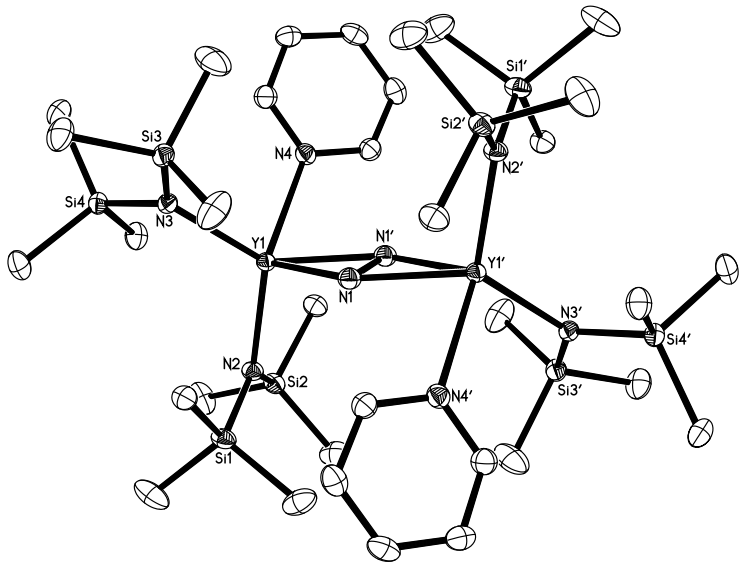

Figure 1.2. Thermal ellipsoid plot of $\{[(Me_3Si)_2N]_2(py)Y\}_2(\mu\text{-}\eta^2\text{:}\eta^2\text{-}N_2)$, **3**, drawn at the 50% probability level. Hydrogen atoms are omitted for clarity.

Despite the varying Y–L distances in **1**-**5**, the structural features of the Y_2N_2 core are not significantly different from complex to complex with the N–N bond distances in the narrow range of 1.255(3) Å (**4**) to 1.274(3) Å (**1**). Similarly, the angles within the Y_2N_2 core are essentially equivalent in structures **1**-**5**, and the Y–N[$N(SiMe_3)_2$] distances are similar. In contrast, analysis of the crystal data on **6** yields a significantly shorter N–N bond distance of 1.198(3) Å. The Y–O distance of 2.197(1) in **6** is also the shortest Y–L donor atom length of the series. Although trimethylamine *N*-oxide is most commonly used as a decarbonylation/decomplexation agent in organometallic chemistry or as an oxidant in organic synthesis,[26] when it acts only as a ligand, it is a strong donor. It has been shown to be a better donor than pyridine *N*-oxide[27,28] and displaces triphenylphosphine oxide in some cases.[29] The shorter Y–O bond length in **6** could be explained by a greater anionic contribution at oxygen due to the zwitterionic character of the Me_3NO ligand. However, the Y–O distance is still longer than a typical anionic Y–O bond,[30] and the N–O distance of 1.382(2) Å in **6** is unchanged from that observed experimentally for free trimethylamine *N*-oxide, 1.388(5) Å.[31,32] The IR spectrum of **6** has two absorptions in the region expected for an *N*-oxide[33] at 982 and 940 cm^{-1}. The absorption at 982 cm^{-1} is the stronger of the two and is assigned as the ν_{NO} on the basis of the DFT analysis described below.

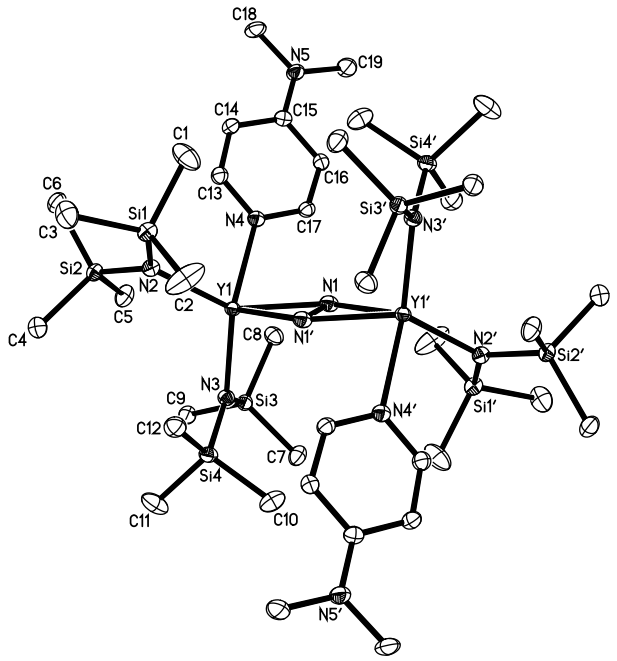

Figure 1.3. Thermal ellipsoid plot of $\{[(Me_3Si)_2N]_2(DMAP)Y\}_2(\mu\text{-}\eta^2\text{:}\eta^2\text{-}N_2)$, **4**, drawn at the 50% probability level. Hydrogen atoms are omitted for clarity.

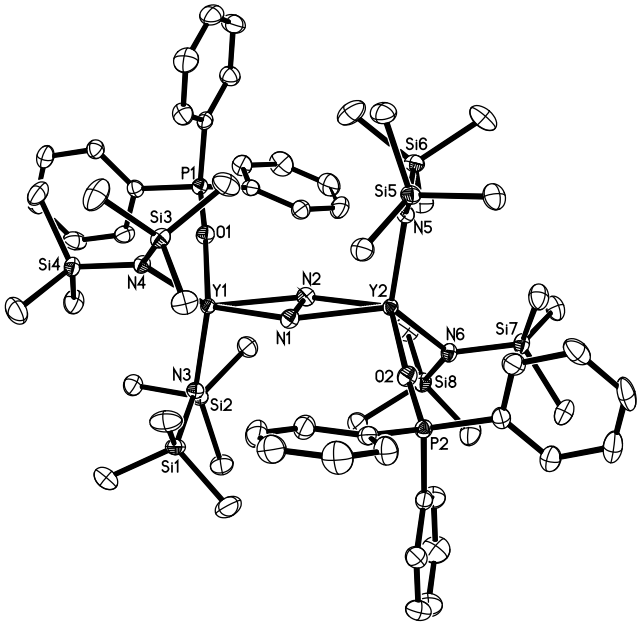

Figure 1.4. Thermal ellipsoid plot of $\{[(Me_3Si)_2N]_2(Ph_3PO)Y\}_2(\mu\text{-}\eta^2\text{:}\eta^2\text{-}N_2)$, **5**, drawn at the 50% probability level. Hydrogen atoms and co-crystallized toluene molecules are omitted for clarity.

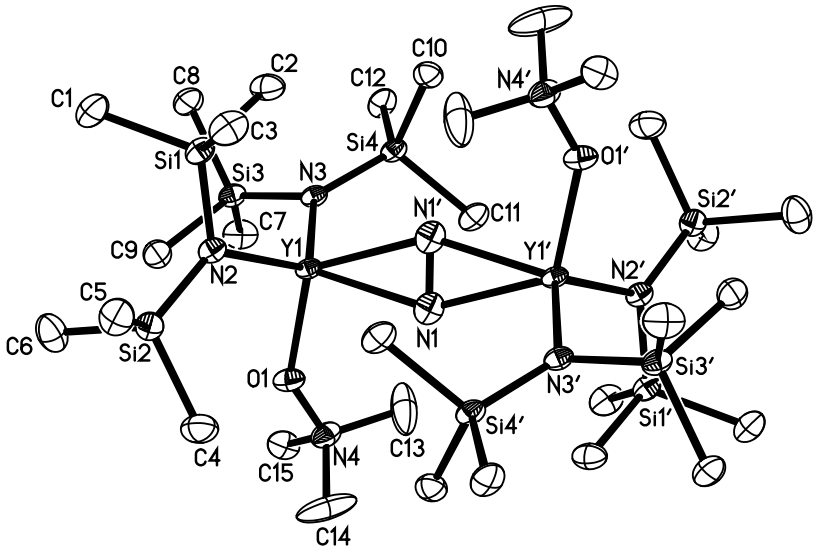

Figure 1.5. Thermal ellipsoid plot of $\{[(Me_3Si)_2N]_2(Me_3NO)Y\}_2(\mu\text{-}\eta^2\text{:}\eta^2\text{-}N_2)$, **6**, drawn at the 50% probability level. Hydrogen atoms and co-crystallized diethyl ether molecules are omitted for clarity.

Table 1.1. Selected bond lengths (Å) and angles (deg) in complexes **1-6** where N_B refers to bridging nitrogen and Y–N* refers to the yttrium-nitrogen distance for the $[N(SiMe_3)_2]^-$ ligands.

Compounds	N–N	Y–N_B	Y–L	Y–N*	N–Y–N′	Y–N–Y′
$\{[Me_3Si)_2N]_2(THF)Y\}_2(\mu\text{-}\eta^2\text{:}\eta^2\text{-}N_2)$, **1**	1.274(3)	2.297(2) 2.308(2)	2.361(1)	2.248(1) 2.263(1)	32.11(7)	147.89(7)
$\{[(Me_3Si)_2N]_2(PhCN)Y\}_2(\mu\text{-}\eta^2\text{:}\eta^2\text{-}N_2)$, **2**	1.258(2)	2.285(1) 2.309(1)	2.480(1)	2.240(1) 2.250(1)	31.78(6)	148.22(6)
$\{[(Me_3Si)_2N]_2(py)Y\}_2(\mu\text{-}\eta^2\text{:}\eta^2\text{-}N_2)$, **3**	1.255(3)	2.292(2) 2.311(2)	2.519(2)	2.242(1) 2.271(1)	31.65(7)	148.35(7)
$\{[(Me_3Si)_2N]_2(DMAP)Y\}_2(\mu\text{-}\eta^2\text{:}\eta^2\text{-}N_2)$, **4**	1.259(2)	2.298(1) 2.313(1)	2.459(1)	2.256(1) 2.288(1)	31.69(5)	148.31(5)
$\{[(Me_3Si)_2N]_2(Ph_3PO)Y\}_2(\mu\text{-}\eta^2\text{:}\eta^2\text{-}N_2)$, **5**	1.262(2)	2.300(1) 2.302(1)	2.254(1)	2.262(1) 2.296(1)	31.82(5)	147.73(7)
$\{[(Me_3Si)_2N]_2(Me_3NO)Y\}_2(\mu\text{-}\eta^2\text{:}\eta^2\text{-}N_2)$, **6**	1.198(3)	2.292(2) 2.294(2)	2.197(1)	2.282(1) 2.290(1)	30.27(8)	149.73(8)

UV-Vis Spectroscopy. The UV-Vis spectra of **1-6** are shown in Figures 1.6 and 1.7. Each complex has a high energy absorption at a wavelength ≤ 210 nm that is also observed in the spectra of $Y[N(SiMe_3)_2]_3$ and $K[N(SiMe_3)_2]$. Complexes **2-6** also each have an absorption in the 220-300 nm range that matches an absorption in the free ligand L. The most interesting feature of these spectra is that they display a low energy, low intensity absorption around 700 nm. This absorption is unique to the complexes and does not appear in the lanthanide precursors or L. Density functional theory, in collaboration with the group of Professor Filipp Furche at UC Irvine, was employed to understand this transition.

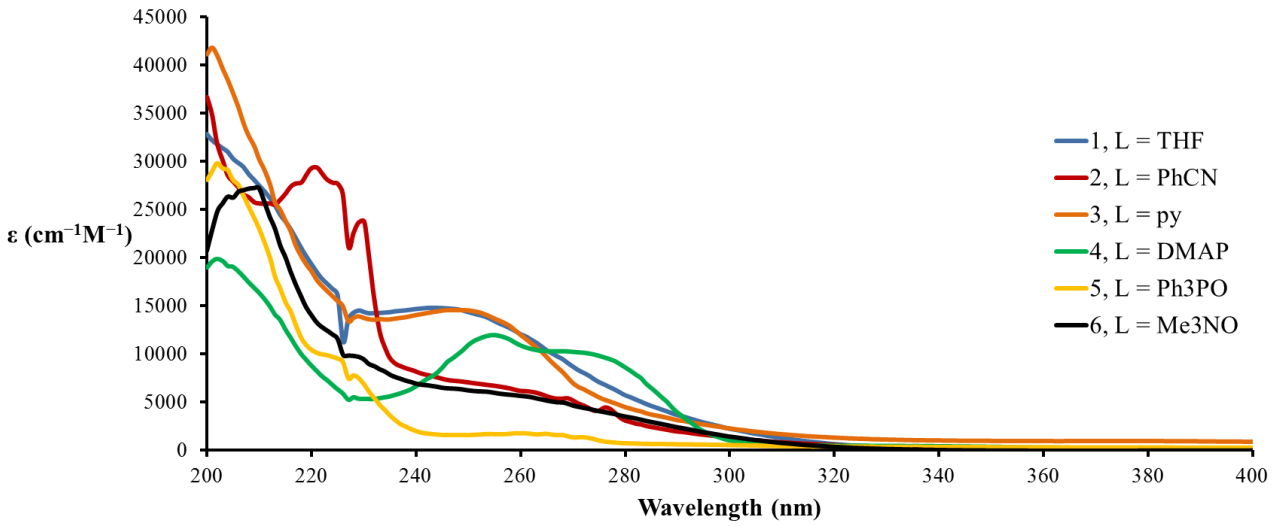

Figure 1.6. UV spectra of $\{[(Me_3Si)_2N]_2(THF)Y\}_2(\mu\text{-}\eta^2\text{:}\eta^2\text{-}N_2)$, **1**, $\{[(Me_3Si)_2N]_2(PhCN)Y\}_2(\mu\text{-}\eta^2\text{:}\eta^2\text{-}N_2)$, **2**, $\{[(Me_3Si)_2N]_2(py)Y\}_2(\mu\text{-}\eta^2\text{:}\eta^2\text{-}N_2)$, **3**, and $\{[(Me_3Si)_2N]_2(DMAP)Y\}_2(\mu\text{-}\eta^2\text{:}\eta^2\text{-}N_2)$, **4**. $\{[(Me_3Si)_2N]_2(Ph_3PO)Y\}_2(\mu\text{-}\eta^2\text{:}\eta^2\text{-}N_2)$, **5**, and $\{[(Me_3Si)_2N]_2(Me_3NO)Y\}_2(\mu\text{-}\eta^2\text{:}\eta^2\text{-}N_2)$, **6** in Et_2O.

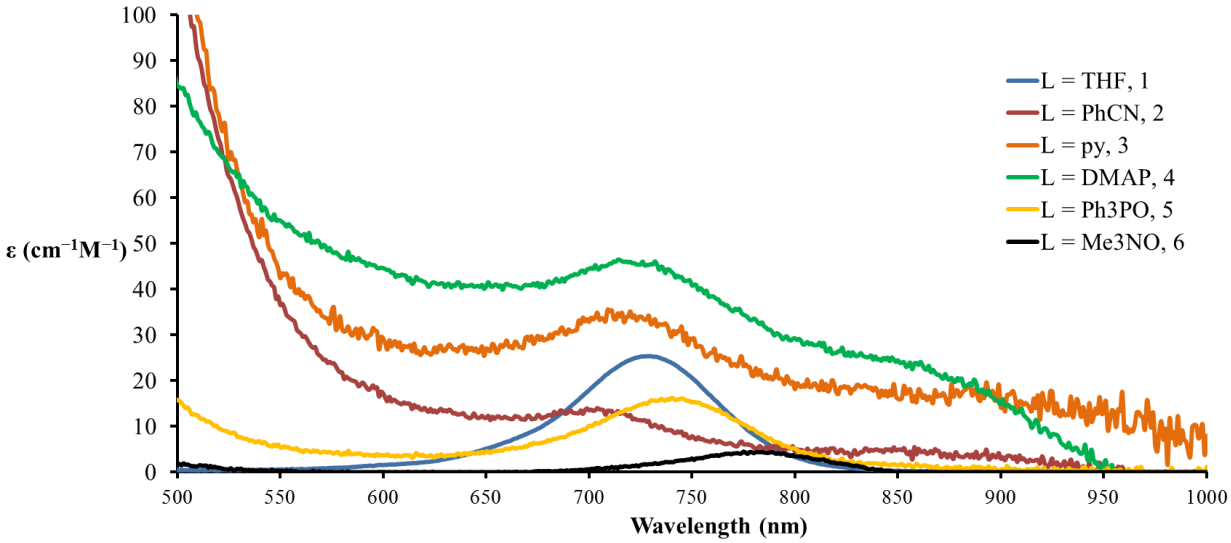

Figure 1.7. Vis-IR spectra of $\{[(Me_3Si)_2N]_2(THF)Y\}_2(\mu\text{-}\eta^2\text{:}\eta^2\text{-}N_2)$, **1**, $\{[(Me_3Si)_2N]_2(PhCN)Y\}_2(\mu\text{-}\eta^2\text{:}\eta^2\text{-}N_2)$, **2**, $\{[(Me_3Si)_2N]_2(py)Y\}_2(\mu\text{-}\eta^2\text{:}\eta^2\text{-}N_2)$, **3**, and $\{[(Me_3Si)_2N]_2(DMAP)Y\}_2(\mu\text{-}\eta^2\text{:}\eta^2\text{-}N_2)$, **4**. $\{[(Me_3Si)_2N]_2(Ph_3PO)Y\}_2(\mu\text{-}\eta^2\text{:}\eta^2\text{-}N_2)$, **5**, and $\{[(Me_3Si)_2N]_2(Me_3ON)Y\}_2(\mu\text{-}\eta^2\text{:}\eta^2\text{-}N_2)$, **6** in toluene.

DFT Analysis. DFT analysis of **1**-**4** and **6** starting with the crystal data gives optimized theoretical structures that matched the experimental data in geometry and in Y–L distances typically within ~0.05 Å at the SV(P) level. The computed results indicate that **2**, **3**, **4**, and **6** have very similar Y_2N_2 binding to that of **1**[34] in which the dinitrogen–Y bonding results from a strong interaction between an yttrium 4*d* orbital and the antibonding π^* orbital of N_2 in the Y_2N_2 plane. The qualitative molecular orbital (MO) diagram that describes the interaction between the metal fragments and the dinitrogen bridge is given in Figure 1.8.

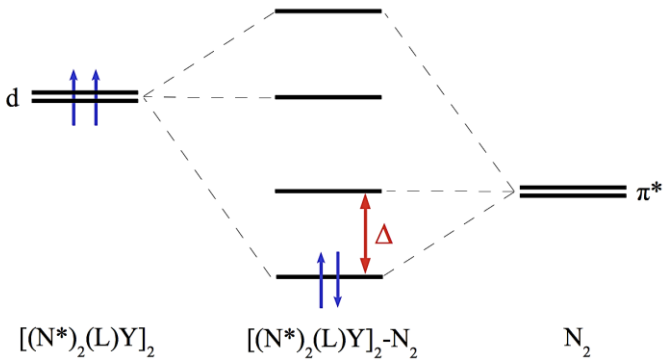

Figure 1.8. Qualitative molecular orbital diagram which depicts the interaction between degenerate π^* orbitals for free N_2 and the yttrium 4*d* orbitals to form $(N_2)^{2-}$ in the complex, where L is a neutral donor and N* = $[(Me_3Si)_2N]^-$. The splitting, Δ, is directly impacted by the electronic structure of the metal cores and gives rise to a very weak electronic transition between calculated wavelengths of 730 and 840 nm. Transitions to the higher unoccupied non-bonding orbitals are predicted to be between 230 and 280 nm, but have small oscillator strengths in comparison to the intra-ligand excitations in that frequency range.

While the doubly occupied N_2 π^* orbital is the HOMO for **1**-**4**, and **6**, the LUMO for these compounds shows some variation with neutral ligand coordination. For **1**,**4**, and **6,** the unperturbed N_2 π^* orbital is the LUMO for the complex. Compounds **2** and **3** do not follow this trend, however, and the lowest unoccupied orbitals are actually those of the neutral donors (Fig 1.9), while the LUMO+2 is the usual unperturbed π^* orbital. Representative plots for compounds **3** and **6** can be found in Figure 1.10. To test the sensitivity of this result to solvation effects, single-point energy calculations at the TPSSh/def2-SV(P) level were performed on the converged structures for **1**-**4**, and **6** using the COSMO[35] solvation model with a dielectric constant of 7.52, corresponding to that of THF. THF was chosen since it has a larger dielectric

constant than the solvent used during synthesis (toluene). These additional calculations did not lead to any changes in the energetic ordering of the unoccupied orbitals. For compounds **2** and **3**, solvent effects may play a more important role for computing excitation energies. The variation in unoccupied orbitals in the complex also reveals the competition between unoccupied orbitals on the neutral donor and those on the N_2 bridge. Such variations may play a role in the reactivity of the complexes as reduction could potentially occur on the neutral donors rather than the bridge.

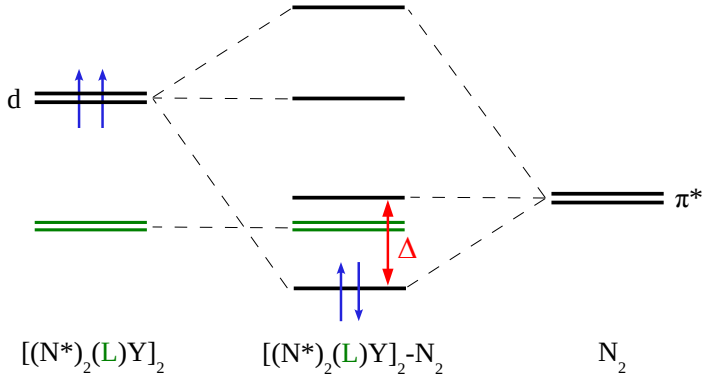

Figure 1.9. Complete frontier molecular orbital diagram for **2** and **3**. Charge transfer excitations from the doubly occupied orbital to the unoccupied neutral ligand orbitals are predicted by TDDFT, but their energies vary strongly with the chosen functional and cannot be used as a probe of $Y–N_2$ interactions.

Charge transfer excitations from the doubly occupied orbital to the unoccupied neutral ligand orbitals are also predicted by TDDFT, but the excitation energy for these transitions varies strongly with functional. For instance, PBE0 and BHLYP predict excitation energies that differ by nearly 200 nm using SV(P) basis sets. Much like the transitions to higher unoccupied 4*d*

orbitals, the oscillator strengths are predicted to be smaller than the intra-ligand transitions and for similar reasons cannot be used as an indication of metal-dinitrogen interactions.

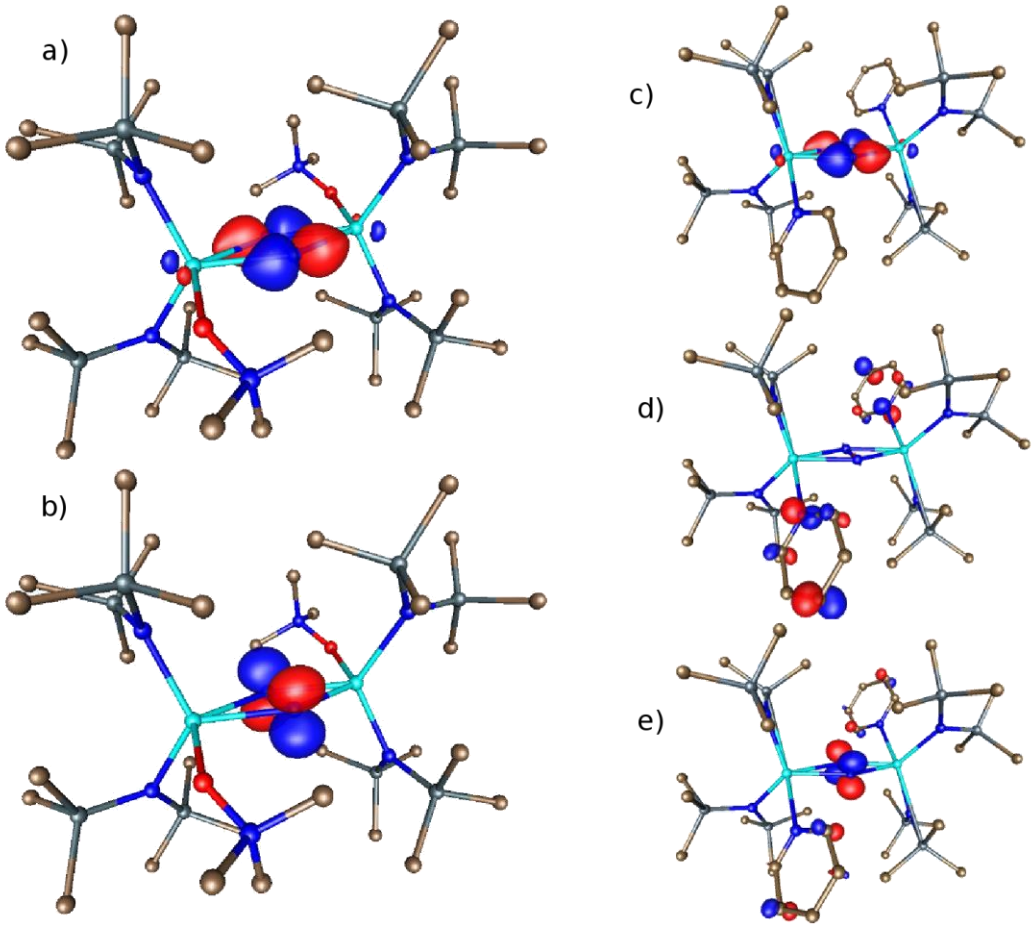

Figure 1.10. PBE0 molecular orbitals of a_g symmetry for **3** and **6** computed using def2-SV(P) basis sets. Plots a) and b) are the HOMO and LUMO for **6** as shown in Fig 1.8. Plots c), d), and e) are the HOMO and two unoccupied orbitals, respectively, for **3**. The contour value for all plots is 0.08.

Table 1.2. Selected computed bond lengths (Å) in complexes **1**-**4** and **6** where N_B refers to bridging nitrogen. SV(P) basis sets for light atoms and TZVP basis sets for Y were used for each complex in conjunction with the TPSSh density functional. The numbers reported here are from the second optimization with tighter convergence criterion.

Compounds	N–N	Y–N_B	Y–L
1	1.249	2.329	2.399
		2.344	
2	1.239	2.328	2.431
		2.361	
3	1.247	2.321	2.523
		2.339	
4	1.249	2.320	2.491
		2.338	
6	1.253	2.349	2.237
		2.363	

Table 1.3. Selected excitations computed with TDDFT using PBE0, SV(P) basis sets for light atoms, and TZVP basis sets for Y. The lowest a_g transition is reported for each compound and corresponds to an N_2 π^* to π^* transition. The predicted oscillator strength is identically 0 since the transition is symmetry forbidden.

Compounds	Excitation Energy (nm)
1	771
2	754
3	745
4	739
6	835

Inspection of the frontier molecular orbitals computed from DFT indicate that the weak electronic transition in the visible region shown in Figure 1.7 corresponds to an excitation between degenerate π^* orbitals arising from free N_2 that are split in the $(N{=}N)^{2-}$ complexes, because one becomes bonding and is occupied while the other remains non-bonding and unoccupied (Fig. 1.8). Since both of these orbitals are of a_g symmetry, the transition is formally electric-dipole forbidden and therefore low in intensity.

This weak, long wavelength absorption can provide a fingerprint of the electronic structure in the Y_2N_2 core, since the splitting of the degenerate N_2 π^* orbitals is a direct result of the interaction with the metal cores, which are themselves slightly influenced by the different donors. All of the computational methods tested here predict an absorption with exactly zero spectral intensity (because it is formally symmetry forbidden) between 730 and 840 nm for **1**-**4** and **6** (Table 1.3), regardless of the choice of density functional (complex **5** was not examined). This is a clear indication that this transition is not a false charge-transfer intruder state but does indeed correspond to the transition observed experimentally.

The relative energetic ordering of the N_2 π^* to π^* transition for compounds **1**-**4** is incorrectly predicted by the present approach, however both theory and experiment agree that **6** has the lowest energy transition. Since the π^* to π^* absorptions in **1**-**4** occur over a narrow frequency range (~50 nm), incorporation of solvent effects may be required to correctly predict the trend in this excitation for these compounds. Excitations from the doubly occupied orbital in Figure 1.8 to higher unoccupied 4*d* orbitals are found between 230 and 280 nm for **1**-**4** and **6**, but the oscillator strengths are much smaller than those of the intra-ligand transitions that dominate in this frequency range. As a result, these higher energy transitions cannot be easily detected experimentally and used as a probe of the metal-ligand interaction strength.

DFT calculations at the SV(P) level on **6** did not match the experimental data as well as for **1**-**4**. The optimized N–N bond length in the bridge for **6** is predicted to be 1.252 Å, not the 1.198(3) Å observed, although the 2.237 Å calculated Y–O distance is within 0.04 Å of that experimentally found. Further structural optimization with TZVP basis sets for all atoms was also done for **6**, but the larger basis sets only improve the agreement for the N–N bond length by 0.01 Å. If this difference between experiment and theory is computational, it may be due to the increased local ionic character in the real system, which semi-local DFT does not completely capture due to known problems such as self-interaction error. On the other hand, if the difference arises from an inconsistency in the crystallography, it is not evident from the crystal data. This discrepancy has stimulated discussion as to which method is the most accurate for measuring the N–N bond lengths in these systems.[36] Preliminary Raman data obtained with the assistance of Megan Fieser for **6** displays a peak at 1419 cm^{-1} assigned to the N–N bond which is consistent with resonances observed for **1** (1425 cm^{-1}),[34] **2** (1426 cm^{-1}), **3** (1428 cm^{-1}), **4** (1426 cm^{-1}), and **5** (1410 cm^{-1}). In this case, the Raman measurements support the theoretical predictions that **6** may not have an unusual N–N bond which contradicts the crystallographic model that fits best with a short N–N bond distance. The computed structure for **6** yields an N–O distance of 1.376 Å which is close to the free trimethylamine *N*-oxide value and that measured experimentally in the complex.

The computed N–O vibrational frequency for **6** is a strong vibration at 994 cm^{-1}. Experimentally the IR spectrum of **6** has two absorptions in the region expected for an *N*-oxide[33] at 982 and 940 cm^{-1}. The absorption at 982 cm^{-1} is the stronger of the two and is assigned as the ν_{NO} on the basis of the DFT analysis. This is a significant shift from the 937 cm^{-1} [37] absorption of free Me_3NO and is indicative of metal coordination. However, it has been shown that the

variation in ν_{NO} when coordinated to a transition metal is not an accurate measure of the "activation" of the ligand.[23]

Discussion

The reactions of $\{[(Me_3Si)_2N]_2Y(THF)\}_2(\mu\text{-}\eta^2\text{:}\eta^2\text{-}N_2)$, **1**, with PhCN, py, DMAP, Ph_3PO, and Me_3NO demonstrate that the THF ligands are not essential to the isolation of the $(N{=}N)^{2-}$ ligand in bis(trimethylsilyl)amide rare earth complexes. The substitution reactions and the crystal structures of **2**-**6** suggest that a wide range of adducts should be accessible. It is worth noting that the $(N{=}N)^{2-}$ ligand can be a potent reductant and has been found to reductively homologate CO[38] and dimerize CO_2[39] in cyclopentadienyl complexes. However, in this bis(trimethylsilyl)amide system, **1** does not reduce any of the added ligands, even in the case of trimethylamine *N*-oxide which can be used as an oxygen delivery reagent.[23,26]

Although there is variety in the nature of L in $\{[(Me_3Si)_2N]_2(L)Y\}_2(\mu\text{-}\eta^2\text{:}\eta^2\text{-}N_2)$, the structures of the Y_2N_2 cores in **2**-**5** were surprisingly similar. In view of the similarity of **2**-**5**, the variation in the N–N distance in the trimethylamine *N*-oxide complex, **6**, was unexpected, particularly since this was not predicted by the DFT calculations. If the crystallographic data are reliable, the fact that Me_3NO has the shortest Y–L distance of **1**-**6** may be a factor in changing the N–N distance.

In many classes of transition metal complexes, addition of a stronger L donor puts more electron density into the system[40] which in turn reduces further the other ligands in the complex. In these reduced dinitrogen molecules, addition of strong donors could reduce the N–N linkage further and make the bond longer. However, from inspection of the experimental Vis-IR spectra (Fig 1.7) and comparison of the computed excitations (Table 1.3), it is clear that the π^* to π^*

transition in **6** has shifted to the longest wavelength of the compounds reported here. The red shift compared to **1** indicates that the splitting between the $(N_2)^{2-}$ π^* orbitals has been decreased. This decrease implies that the $(N{=}N)^{2-}$ bridge interaction with the metal centers has been reduced, which in principle leads to a shorter N–N bond length as observed in the crystallographic analysis. Even in light of this argument, the shift in excitation energy is small, ~0.12 eV, and cannot be taken as definitive proof alone.

Numerous attempts to reduce **2**-**5** using KC_8 were performed to see if the $(N_2)^{2-}$ bridging ligand could be reduced to the $(N_2)^{3-}$ radical. However, these experiments had to be carried out in noncoordinating solvents, and no reactions were observed during the lifetime of the $(N_2)^{2-}$ complexes which are thermally unstable. Even addition of KC_8 to **6** in THF did not lead to EPR active species or new isolable products. Addition of free L to the $(N_2)^{3-}$ complex $K\{[(Me_3Si)_2N]_2(THF)Y\}_2(\mu_3\text{-}\eta^2{:}\eta^2{:}\eta^2\text{-}N_2)$ yielded the corresponding Lewis base adducts (**2** for L = PhCN, **3** for L = py, **4** for L = DMAP, **5** for L = Ph_3PO) observable by NMR spectroscopy as well as unidentified pale insoluble products. The DFT studies above indicate for **2** and **3** that lower lying LUMOs localized on the neutral donor ligands could lead to reduction of the Lewis base rather than the dinitrogen bridge, which may contribute to the formation of unisolable mixed products in these reactions. However, this still does not explain why reduction of **6** does not lead to the desired $(N_2)^{3-}$ radical species, since the LUMO of **6** is predicted to be a π^* orbital localized on the N_2 bridge. It is possible an $(N_2H_2)^{2-}$ -containing product could form, such as $\{[(Me_3Si)_2N]_2Y(ONMe_3)\}_2(\mu\text{-}N_2H_2)$, via reduction of the $(N_2)^{2-}$ precursor **6**, analogous to the THF adduct,[41] however, there is no evidence for an $(\mu\text{-}N_2H_2)$ moiety in the NMR.

Crystallographic and DFT results suggest that in **2**-**6**, there is a competition between the L donor and the $(N{=}N)^{2-}$ bridge for interaction with the metal. The stronger the donor, the less the

interaction that occurs with dinitrogen. This implies that weakly coordinating ligands may be optimum for activating dinitrogen with complexes of this type, a possibility that will require additional examples before it can be considered reliable.

One further point of discussion involves the isolation of crystalline samples of the THF solvate **1** from reaction solutions of $\{[(Me_3Si)_2N]_2Y(PhCN)\}_2(\mu\text{-}\eta^2\text{:}\eta^2\text{-}N_2)$, **2**. This reinforces the fact that evidence from single crystals in a reaction can be misleading.

Conclusion

The THF in $\{[(Me_3Si)_2N]_2(THF)Y\}_2(\mu\text{-}\eta^2\text{:}\eta^2\text{-}N_2)$, **1**, can be displaced with the neutral donors benzonitrile, pyridine, 4-dimethylamino pyridine, and triphenylphosphine oxide to form new $\{[(Me_3Si)_2N]_2(L)Y\}_2(\mu\text{-}\eta^2\text{:}\eta^2\text{-}N_2)$ complexes, but these substitutions do not significantly affect the structural or electronic properties of the Y_2N_2 core. In contrast, when THF is replaced by Me_3NO, the $\{[(Me_3Si)_2N]_2(L)Y\}_2(\mu\text{-}\eta^2\text{:}\eta^2\text{-}N_2)$ product contains an $(N{=}N)^{2-}$ ligand with an N–N distance that is shorter on the basis of the crystallographic model. This raises the possibility that ligands with zwitterionic character and donor atoms with increased anionic character may be useful in manipulating metrical parameters in bimetallic rare earth reduced dinitrogen complexes.

Experimental

All syntheses and manipulations described below were conducted under nitrogen with rigorous exclusion of air and water using glovebox, Schlenk, and vacuum line techniques. Solvents used were dried over columns containing Q-5 and molecular sieves. Benzene-d_6 and THF-d_8 were dried over sodium-potassium alloy, degassed using three freeze-pump-thaw cycles,

and vacuum transferred before use. Potassium and sodium were washed with hexanes and scraped to provide fresh surfaces before use. Ph_3PO, Me_3NO and 4-$Me_2NC_5H_4N$ (DMAP) were sublimed prior to use. C_5H_5N (py) and PhCN were dried over molecular sieves and degassed using three freeze-pump-thaw cycles prior to use. $\{[(Me_3Si)_2N]_2(THF)Y\}_2(\mu\text{-}\eta^2\text{:}\eta^2\text{-}N_2)$, **1**, was synthesized according to literature methods.[15] ^1H and ^{13}C NMR spectra were obtained on a Bruker CRYO500 MHz spectrometer at 25 ºC. ^{31}P NMR spectra were obtained on a Bruker DRX400 MHz spectrometer at 25 ºC, and resonances were referenced with H_3PO_4 (δ = 0 ppm) as an external standard. The ^{13}C and ^{31}P NMR spectra are reported as proton decoupled unless otherwise specified. IR samples were prepared as KBr pellets on a Varian 1000 FT-IR system. Elemental analyses were performed on a PerkinElmer Series II 2400 CHNS analyzer. Raman experiments were performed on crystalline samples in a quartz cell sealed with a Teflon stopcock with a Renishaw inVia confocal Raman microscope using 532 nm laser excitation (laser power 10%, laser focus 50% at 200 s exposure) and a 5 X objective lens. Electronic absorption spectra were collected in Et_2O at 25 ºC using a Varian Cary 50 Scan UV-Vis spectrophotometer and in toluene at 25 ºC using an Ocean Optics USB Red Tide UV-Vis spectrophotometer.

$\{[(Me_3Si)_2N]_2(PhCN)Y\}_2(\mu\text{-}\eta^2\text{:}\eta^2\text{-}N_2)$, 2. In a nitrogen-filled glovebox containing THF, PhCN (10 μL, 0.10 mmol) was added to a stirred pale blue solution of **1** (50 mg, 0.05 mmol) in toluene (4 mL) causing an immediate color change to amber. After 10 min, solvent was removed under vacuum to produce an orange powder that was transferred to a nitrogen-filled glovebox free of THF. Recrystallization of the powder in hexane at −30 ºC overnight produced orange/brown crystals of **2** (36 mg, 68%) suitable for X-ray diffraction. ^1H NMR (500 MHz, benzene-d_6): δ 0.48 (s, 36H, N(Si*Me*$_3$)$_2$), 6.64 (m, 2H, *m*-NC*Ph*), 6.81 (m, 1H, *p*-NC*Ph*), 7.32 (m, 2H, *o*-NC*Ph*). ^{13}C NMR (126 MHz, benzene-d_6): δ 5.59 (s, N(Si*Me*$_3$)$_2$), 108.97 (s, *i*-*Ph*CN),

110.66 (s, N*C*Ph), 129.77 (s, *m*-NC*Ph*), 133.05 (s, *o*-NC*Ph*), 134.99 (s, *p*-NC*Ph*). IR: 2946m, 2893m, 2254s, 1597w, 1449s, 1245s, 992s, 940w, 869s, 833s, 772m, 756s, 673m, 609m, 554w, 527s cm^{-1}. Anal. Calcd for $C_{38}H_{82}N_8Si_8Y_2$, **2**: C, 43.32; H, 7.84; N, 10.64. Found: C, 43.25; H, 8.26; N, 10.31. UV-Vis λ_{max} (nm), ε ($M^{-1}cm^{-1}$): (Et_2O) 220, 29000; (C_7H_8) 700, 50.

{[(Me$_3$Si)$_2$N]$_2$(py)Y}$_2$(μ-η^2:η^2-N$_2$), 3. Following the procedure for **2**, addition of pyridine (8 μL, 0.10 mmol) to **1** (50 mg, 0.05 mmol) in toluene (4 mL) gave an immediate color change to orange. After 5 min, solvent was removed under vacuum to produce an orange powder that was recrystallized from toluene in a THF-free glovebox to form orange crystals of **3** (43 mg, 85%) suitable for X-ray diffraction. ^{1}H NMR (500 MHz, benzene-d_6): δ 0.33 (s, 36H, N(Si*Me*$_3$)$_2$), 6.76 (m, 2H, *m*-NC$_5$*H*$_5$), 6.90 (m, 1H, *p*-NC$_5$*H*$_5$), 9.63 (bs, 2H, *o*-NC$_5$*H*$_5$). ^{13}C NMR (126 MHz, benzene-d_6): δ 5.76 (s, N(Si*Me*$_3$)$_2$), 125.27 (s, *m*-N*C*$_5$H$_5$), 139.88 (s, *p*-N*C*$_5$H$_5$), 151.74 (s, *o*-N*C*$_5$H$_5$). IR: 2947m, 2894w, 1602m, 1489w, 1444sh, 1243s, 1185w, 1153w, 1068w, 1040m, 987s, 866s, 828s, 773s, 752s, 700m, 668s, 607m, 518w cm^{-1}. Anal. Calcd for $C_{34}H_{82}N_8Si_8Y_2$, **3**: C, 40.61; H, 8.22; N, 11.14. Found: C, 41.00; H, 8.61; N, 11.02. UV-Vis λ_{max} (nm), ε ($M^{-1}cm^{-1}$): (Et_2O) 250, 22000; (C_7H_8) 710, 40.

{[(Me$_3$Si)$_2$N]$_2$(DMAP)Y}$_2$(μ-η^2:η^2-N$_2$), 4. In a nitrogen-filled glovebox containing THF, addition of 4-dimethylaminopyridine (DMAP) (12 mg, 0.10 mmol) to a stirred pale blue solution of **1** (50 mg, 0.05 mmol) in toluene (4 mL) caused an immediate color change to green. After 5 min, solvent was removed under vacuum to yield a pale green powder that was recrystallized in a THF-free glovebox from hot toluene. The green solution was allowed to cool to room temperature without agitation. After 24 h, green crystals of **4** suitable for X-ray diffraction were obtained (55 mg, 100%). ^{1}H NMR (500 MHz, benzene-d_6): δ 0.48 (s, 36H, N(Si*Me*$_3$)$_2$), 2.01 (bs, 6H, NC$_5$H$_4$N*Me*$_2$), 6.16 (d, 2H, $^3J_{HH}$ = 5.9 Hz, *m*-NC$_5$*H*$_4$NMe$_2$), 9.43 (bs, 2H, *p*-NC$_5$*H*$_4$NMe$_2$).

^{13}C NMR (126 MHz, benzene-d_6): δ 6.09 (s, N(SiMe_3)$_2$), 38.46 (s, $NC_5H_4NMe_2$), 106.79 (s, *m*-$NC_5H_4NMe_2$), 110.68 (s, *p*-$NC_5H_4NMe_2$), 151.34 (s, *o*-$NC_5H_4NMe_2$). IR: 2944s, 2893m, 2832w, 2571w, 2360w, 1769w, 1618s, 1537s, 1445m, 1392m, 1351w, 1244s, 1116w, 1065m, 1005s, 868s, 829s, 769m, 661m, 603m, 616s cm^{-1}. Anal. Calcd for $C_{38}H_{92}N_{10}Si_8Y_2$, **4**: C, 41.81; H, 8.49; N, 12.83. Found: C, 41.53; H, 9.02; N, 12.50. UV-Vis λ_{max} (nm), ε ($M^{-1}cm^{-1}$): (Et_2O) 260, 12000; (C_7H_8) 710, 50.

{[(Me$_3$Si)$_2$N]$_2$(Ph$_3$PO)Y}$_2$(μ-η^2:η^2-N$_2$), 5. Following the procedure for **4**, addition of Ph_3PO (28 mg, 0.10 mmol) to **1** (50 mg, 0.05 mmol) in toluene (4 mL) gave an immediate color change to yellow. After 5 min, a pale yellow precipitate formed. Solvent was removed under vacuum to yield a yellow powder that was recrystallized in a THF-free glovebox from hot toluene (3 mL). The yellow solution was allowed to cool to room temperature without agitation. After 24 h, yellow crystals of **5** (62 mg, 77%), suitable for X-ray diffraction, were obtained. ^{1}H NMR (500 MHz, benzene-d_6): δ 0.36 (s, 36H, N(SiMe_3)$_2$), 7.24 (m, 6H, *m*-Ph_3PO), 7.76 (m, 3H, *p*-Ph_3PO), 7.90 (m, 6H, *o*-Ph_3PO). ^{13}C NMR (126 MHz, benzene-d_6): δ 6.60 (s, N(SiMe_3)$_2$), 128.87 (d, $^3J_{CP}$ = 11.5 Hz, *m*-Ph_3PO), 131.85 (d, $^1J_{CP}$ = 2.8 Hz, Ph_3PO), 132.78 (d, $^4J_{CP}$ = 9.5 Hz, *p*-Ph_3PO), 133.84 (d, $^2J_{CP}$ = 11 Hz, Ph_3PO). ^{31}P NMR (162 MHz, benzene-d_6): δ 39.73 (d, $^2J_{PY}$ = 11.5 Hz, Ph_3PO). IR: 4053w, 3058m, 3025m, 2944s, 2894m, 1972w, 1904s, 1851w, 1826w, 1686s, 1592m, 1495m, 1439s, 1391w, 1313w, 1246s, 1154s, 1124s, 1094s, 988s, 880s, 827s, 771sh, 747m, 727s, 693s, 665m, 606m, 539s, 513m, 463s, 412w cm^{-1}. Anal. Calcd for $C_{60}H_{102}N_6O_2P_2Si_8Y_2 \bullet (C_7H_8)_2$, **5**: C, 55.96; H, 7.49; N, 5.29. Found: C, 55.97; H, 7.66; N, 5.12. UV-Vis λ_{max} (nm), ε ($M^{-1}cm^{-1}$): (Et_2O) 260, 1800; (C_7H_8) 740, 20.

{[(Me$_3$Si)$_2$N]$_2$(ONMe$_3$)Y}$_2$(μ-η^2:η^2-N$_2$), 6. In a nitrogen-filled glovebox, a pale blue solution of **1** (100 mg, 0.10 mmol) in THF (3 mL) was added to a suspension of Me_3NO (16 mg,

0.20 mmol) in THF (2 mL) and the mixture was stirred at room temperature for 90 min. The solution was centrifuged and filtered and the solvent was removed under vacuum to yield **6** as a very pale blue powder (91 mg, 88%). Crystals suitable for X-ray diffraction were grown from a THF/Et_2O solution at −35 ºC. ^{1}H NMR (500 MHz, benzene-d_6): δ 0.45 (s, 36H, N(SiMe_3)$_2$), 2.72 (s, 9H, ONMe_3). ^{13}C NMR (126 MHz, benzene-d_6): δ 6.7 (s, N(SiMe_3)$_2$), 60.7 (s, ONMe_3). IR: 3009w, 2950s, 2398w, 2364w, 2334w, 1469m, 1385w, 1250s, 1133w, 1105w, 982s, 940m, 872m, 832s, 774w, 669w, 607w, 498m cm^{-1}. Anal. Calcd for $C_{30}H_{90}N_8O_2Si_8Y_2$, **6** minus $(Et_2O)_2$: C, 36.12; H, 9.09; N, 11.23. Found: C, 35.95; H, 9.51; N, 10.82. UV-Vis λ_{max} (nm), ε ($M^{-1}cm^{-1}$): (Et_2O) 260, 5600; (C_7H_8) 780, 10.

X-ray Data Collection, Structure Solution and Refinement for {[(Me$_3$Si)$_2$N]$_2$(PhCN)Y}$_2$(μ-η^2:η^2-N$_2$), 2. A yellow crystal of approximate dimensions 0.12 x 0.14 x 0.25 mm was mounted on a glass fiber and transferred to a Bruker SMART APEX II diffractometer. The APEX[42] program package was used to determine the unit-cell parameters and for data collection (60 sec/frame scan time for a sphere of diffraction data). The raw frame data was processed using SAINT[43] and SADABS[44] to yield the reflection data file. Subsequent calculations were carried out using the SHELXTL[45] program. There were no systematic absences nor any diffraction symmetry other than the Friedel condition. The centrosymmetric triclinic space group $P\bar{1}$ was assigned and later determined to be correct. The structure was solved by direct methods and refined on F^2 by full-matrix least-squares techniques. The analytical scattering factors[46] for neutral atoms were used throughout the analysis. Hydrogen atoms were located from a difference-Fourier map and refined (x,y,z and U_{iso}). The molecule was located about an inversion center. At convergence, wR2 = 0.0565 and Goof = 1.032 for 417

variables refined against 6949 data (0.74Å), R1 = 0.0240 for those 6246 data with I > 2.0σ(I). Details are given in Table 1.4.

X-ray Data Collection, Structure Solution and Refinement for {[(Me$_3$Si)$_2$N]$_2$(py)Y}$_2$(μ-η^2:η^2-N$_2$), 3. A pale yellow crystal of approximate dimensions 0.14 x 0.18 x 0.27 mm was mounted in a loop and transferred to a Bruker SMART APEX II diffractometer. The APEX2[42] program package was used to determine the unit-cell parameters and for data collection (25 sec/frame scan time for a sphere of diffraction data). The raw frame data was processed using SAINT[43] and SADABS[44] to yield the reflection data file. Subsequent calculations were carried out using the SHELXTL[45] program. There were no systematic absences nor any diffraction symmetry other than the Friedel condition. The centrosymmetric triclinic space group $P\bar{1}$ was assigned and later determined to be correct. The structure was solved by direct methods and refined on F^2 by full-matrix least-squares techniques. The analytical scattering factors[46] for neutral atoms were used throughout the analysis. Hydrogen atoms were located from a difference-Fourier map and refined (x,y,z and U_{iso}). The molecule was located about an inversion center. At convergence, wR2 = 0.0621 and Goof = 1.017 for 399 variables refined against 6350 data (0.75Å), R1 = 0.0280 for those 5386 data with I > 2.0σ(I). Details are given in Table 1.4.

X-ray Data Collection, Structure Solution and Refinement for {[(Me$_3$Si)$_2$N]$_2$(DMAP)Y}$_2$(μ-η^2:η^2-N$_2$), 4. A green crystal of approximate dimensions 0.18 x 0.26 x 0.30 mm was mounted on a glass fiber and transferred to a Bruker SMART APEX II diffractometer. The APEX2[42] program package was used to determine the unit-cell parameters and for data collection (20 sec/frame scan time for a sphere of diffraction data). The raw frame data was processed using SAINT[43] and SADABS[44] to yield the reflection data file. Subsequent

calculations were carried out using the SHELXTL[45] program. The diffraction symmetry was 2/*m* and the systematic absences were consistent with the monoclinic space group $P2_1/c$ that was later determined to be correct. The structure was solved by direct methods and refined on F^2 by full-matrix least-squares techniques. The analytical scattering factors[46] for neutral atoms were used throughout the analysis. Hydrogen atoms were placed in calculated positions then allowed to refine freely (x,y,z and U_{iso}). The molecule was located about an inversion center. At convergence, wR2 = 0.0546 and Goof = 1.037 for 446 variables refined against 7351 data (0.74Å), R1 = 0.0225 for those 6489 data with $I > 2.0\sigma(I)$. Details are given in Table 1.4.

X-ray Data Collection, Structure Solution and Refinement for {[(Me$_3$Si)$_2$N]$_2$(Ph$_3$PO)Y}$_2$(μ-η^2:η^2-N$_2$), 5. A yellow crystal of approximate dimensions 0.20 x 0.21 x 0.33 mm was mounted on a glass fiber and transferred to a Bruker SMART APEX II diffractometer. The APEX2[42] program package was used to determine the unit-cell parameters and for data collection (20 sec/frame scan time for a sphere of diffraction data). The raw frame data was processed using SAINT[43] and SADABS[44] to yield the reflection data file. Subsequent calculations were carried out using the SHELXTL[45] program. There were no systematic absences nor any diffraction symmetry other than the Friedel condition. The centrosymmetric triclinic space group $P\bar{1}$ was assigned and later determined to be correct. The structure was solved by direct methods and refined on F^2 by full-matrix least-squares techniques. The analytical scattering factors[46] for neutral atoms were used throughout the analysis. Hydrogen atoms were initially included in calculated positions then allowed to refine (x,y,z and U_{iso}). The methyl hydrogen atoms associated with the toluene solvent molecules were included using a riding model. At convergence, wR2 = 0.0720 and Goof = 1.015 for 1297 variables refined

against 19767 data (0.74Å), R1 = 0.0291 for those 16366 data with I > 2.0σ(I). Details are given in Table 1.4.

X-ray Data Collection, Structure Solution and Refinement for $\{[(Me_3Si)_2N]_2(ONMe_3)Y\}_2(\mu\text{-}\eta^2\text{:}\eta^2\text{-}N_2)$, 6. A colorless crystal of approximate dimensions 0.09 x 0.31 x 0.42 mm was mounted on a glass fiber and transferred to a Bruker SMART APEX II diffractometer. The APEX2[42] program package was used to determine the unit-cell parameters and for data collection (30 sec/frame scan time for a sphere of diffraction data). The raw frame data was processed using SAINT[43] and SADABS[44] to yield the reflection data file. Subsequent calculations were carried out using the SHELXTL[45] program. There were no systematic absences nor any diffraction symmetry other than the Friedel condition. The centrosymmetric triclinic space group $P\bar{1}$ was assigned and later determined to be correct. The structure was solved by direct methods and refined on F^2 by full-matrix least-squares techniques. The analytical scattering factors[46] for neutral atoms were used throughout the analysis. Hydrogen atoms were included using a riding model. The molecule was located about an inversion center. There were two molecules of diethyl ether solvent present. At convergence, wR2 = 0.0868 and Goof = 1.051 for 288 variables refined against 7564 data (0.75Å), R1 = 0.0328 for those 6630 data with I > 2.0σ(I). Details are given in Table 1.4.

Table 1.4. X-ray data collection parameters for $\{[(Me_3Si)_2N]_2(PhCN)Y\}_2(\mu\text{-}\eta^2\text{:}\eta^2\text{-}N_2)$, **2**, $\{[(Me_3Si)_2N]_2(py)Y\}_2(\mu\text{-}\eta^2\text{:}\eta^2\text{-}N_2)$, **3**, $\{[(Me_3Si)_2N]_2(DMAP)Y\}_2(\mu\text{-}\eta^2\text{:}\eta^2\text{-}N_2)$, **4,** $\{[(Me_3Si)_2N]_2(Ph_3PO)Y\}_2(\mu\text{-}\eta^2\text{:}\eta^2\text{-}N_2)$, **5**, and $\{[(Me_3Si)_2N]_2(Me_3NO)Y\}_2(\mu\text{-}\eta^2\text{:}\eta^2\text{-}N_2)$, **6**.

	$C_{38}H_{82}N_8Si_8Y_2$	$C_{34}H_{82}N_8Si_8Y_2$	$C_{38}H_{92}N_{10}Si_8Y_2$	$C_{60}H_{102}N_6O_2P_2Si_8Y_2 \bullet (C_7H_8)_2$	$C_{30}H_{90}N_8O_2Si_8Y_2 \bullet (C_4H_{10}O)_2$
	2	**3**	**4**	**5 • $(C_7H_8)_2$**	**6 • $(C_4H_{10}O)_2$**
formula weight	1053.66	1005.62	1091.76	1588.22	1145.88
T(K)	88(2) K	88(2)	88(2)	143(2)	88(2) K
crystal system	Triclinic	triclinic	Monoclinic	Triclinic	Triclinic
space group	$P\bar{1}$	$P\bar{1}$	$P2_1/c$	$P\bar{1}$	$P\bar{1}$
a (Å)	11.6982(5)	11.4313(19)	11.7078(4)	13.2550(8)	11.3035(12)
b (Å)	12.1360(5)	11.5217(19)	21.3898(8)	17.3303(11)	11.3174(12)
c (Å)	12.7580(9)	11.842(4)	11.8653(4)	20.6793(13)	13.1070(14)
α (deg)	105.9500(10)	97.537(3)	90	106.5289(7)	97.7530(12)
β (deg)	114.4570(10)	96.112(3)	95.1065(5)	91.0252(7)	101.8936(12)
γ (deg)	104.4850(10)	116.989(2)	90	108.2521(7)	94.6340(12)
volume Å^3	1441.74(13)	1353.2(5)	2959.60(18)	4294.9(5)	1615.5(3)
Z	1	1	2	2	1
ρ_{calced} (Mg/m^3)	1.214	1.234	1.225	1.228	1.178
μ (mm^{-1})	2.200	2.341	2.147	1.537	1.973
R1[a] [I > 2.0σ(I)]	0.0240	0.0280	0.0225	0.0291	0.0328
wR2[b] (all data)	0.0565	0.0621	0.0546	0.0720	0.0868

[a] $R1 = \Sigma||F_o|-|F_c|| / \Sigma|F_o|$. [b] $wR2 = [\Sigma[w(F_o^2-F_c^2)^2] / \Sigma[w(F_o^2)^2]\ ]^{1/2}$

References

(1) MacDonald, M. R.; Ziller, J. W.; Evans, W. J. *Journal of the American Chemical Society* **2011**, *133*, 15914.

(2) Evans, W. J.; Le, D. S.; Lie, C.; Ziller, J. W. *Angewandte Chemie International Edition* **2004**, *43*, 5517.

(3) Evans, W. J.; Rego, D. B.; Ziller, J. W. *Inorganic Chemistry* **2006**, 45, 10790.

(4) Demir, S.; Lorenz, S. E.; Fang, M.; Furche, F.; Meyer, G.; Ziller, J. W.; Evans, W. J. *Journal of the American Chemical Society* **2010**, *132*, 11151.

(5) Jaroschik, F.; Momin, A.; Nief, F.; Le Goff, X. F.; Deacon, G. B.; Junk, P. C. *Angewandte Chemie International Edition* **2009**, *48*, 1117.

(6) Evans, W. J.; Lee, D. S.; Ziller, J. W. *Journal of the American Chemical Society* **2004**, *126*, 454.

(7) Evans, W. J.; Lee, D. S.; Rego, S. B.; Perotti, J. M.; Kozimor, S. A.; Moore, E. K.; Ziller, J. W. *Journal of the American Chemical Society* **2004**, *126*, 14574.

(8) Evans, W. J.; Lee, D. S.; Johnston, M. A.; Ziller, J. W. *Organometallics* **2005**, *24*, 6393.

(9) Evans, W. J.; Lee, D. S. *Canadian Journal of Chemistry* **2005**, *83*, 375.

(10) Evans, W. J. *Inorganic Chemistry* **2007**, *46*, 3435.

(11) Evans, W. J.; Zucchi, G.; Ziller, J. W. *Journal of the American Chemical Society* **2003**, *125*, 10.

(12) Evans, W. J.; Lee, D. S.; Ziller, J. W. *Journal of the American Chemical Society* **2004**, *126*, 454.

(13) Evans, W. J.; Lee, D. S.; Rego, S. B.; Perotti, J. M.; Kozimor, S. A.; Moore, E. K.; Ziller, J. W. *Journal of the American Chemical Society* **2004**, *126*, 14574.

(14) Cheng, J.; Takats, J.; Ferguson, M. J.; McDonald, R. *Journal of the American Chemical Society* **2008**, *130*, 1544.

(15) Fang, M.; Bates, J. E.; Lorenz, S. E.; Lee, D. S.; Rego, D. B.; Ziller, J. W.; Furche, F.; Evans, W. J. *Inorganic Chemistry* **2011**, *50*, 1459.

(16) Rinehart, J. D.; Fang, M.; Evans, W. J.; Long, J. R. *Journal of the American Chemical Society* **2011**, *133*, 14236.

(17) Rinehart, J. D.; Fang, M.; Evans, W. J.; Long, J. R. *Nature Chemistry* **2011**, *3*, 538.

(18) Holler, C. J.; Muller-Buschbaum, K. *Inorganic Chemistry* **2008**, *47*, 10141.

(19) Kirillov, E.; Lehmann, C. W.; Razavi, A.; Carpentier, J. *European Journal of Inorganic Chemistry* **2004**, *2004*, 943.

(20) Pfeiffer, D.; Ximba, B. J.; Liable-Sands, L. M.; Rheingold, A. L.; Heeg, M. J.; Coleman, D. M.; Schlegel, H. B.; Kuech, T. D.; Winter, C. H. *Inorganic Chemistry* **1999**, *38*, 4539.

(21) Clegg, W.; Sage, I.; Oswald, I.; Brough, P.; Bourhill, G. *Acta Crystallographica* **2000**, *C56*, 1323.

(22) Deakin, L.; Levason, W.; Popham, M. C.; Reid, G.; Webster, M. *Journal of the Chemical Society, Dalton Transactions* **2000**, 2439.

(23) Hong, S.; Gupta, A. K.; Tolman, W. B. *Inorganic Chemistry* **2009**, *48*, 6323 and references therein.

(24) Jin, S.; Nieuwenhuyzen, M.; Wilkins, C. J. *Journal of the Chemical Society, Dalton Transactions* **1992**, 2071 and references therein.

(25) Nubel, O. P.; Wilson, S. R.; Brown, T. L. *Organometallics*, **1983**, *2*, 515 and references therein.

(26) Pearson, A. J.; Yamamoto, Y. Trimethylamine N-oxide. *e-EROS: encyclopedia of reagents for organic synthesis*. Wiley Interscience, 2001.

(27) Jin, S.; Nieuwenhuyzen, M.; Robinson, W. T.; Wilkins, C. J. *Acta Crystallographica* **1992**, *C48*, 274.

(28) Drago, R. S.; Donoghue, J. T.; Herlocker, D. W. *Inorganic Chemistry* **1965**, *4*, 836.

(29) Schindler, F.; Schmidbaur, H. *Chemische Berichte* **1967**, *100*, 3655.

(30) Klooster, W. T.; Brammer, L.; Schaverien, C. J.; Budzelaar. P. H. M. *Journal of the American Chemical Society* **1999**, *121*, 1381.

(31) Caron, A.; Palenik, G. J.; Goldish, E.; Donohue, J. *Acta Crystallographica* **1964**, *17*, 102.

(32) Haaland, A.; Thomassen, H.; Svenstrøm, S. *Journal of Molecular Structure* **1991**, *263*, 299.

(33) *N*-oxide IR range: Pretsch, E.; Buehlmann, P.; Badertscher, M. *Structure Determination of Organic compounds: Tables of Spectral Data*; Springer: Berlin, 2009, Vol. 4, pp 296, 297.

(34) Evans, W. J.; Fang, M.; Zucchi, G.; Furche, F.; Ziller, J. W.; Hoekstra, R. M.; Zink. J. I. *Journal of the American Chemical Society* **2009**, *131*, 11195.

(35) Klamt, A.; Schüürmann, G. *Journal of the Chemical Society, Perkin Transactions 2,* **193**, *5,* 799.

(36) Mansell, S. M.; Farnaby, J, H.; Germeroth, A. I.; Arnold, P. L. *Organometallics*, **2013**, *32*, 4214.

(37) Voltz, H.; Gartner, H. *European Journal of Organic Chemistry* **2007**, 2791.

(38) Evans, W. J.; Lee, D. S.; Ziller, J. W.; Kaltsoyannis. N. *Journal of the American Chemical Society* **2006**, *128*, 14176.

(39) Evans, W. J.; Lorenz, S. E.; Ziller. J. W. *Inorganic Chemistry* **2009**, *48*, 2001.

(40) Hartwig, J. *Organotransition Metal Chemistry: From Bonding to Catalysis*; Murdazek, J.; University Science Books, 2010; pp 33-36, 481-50.

(41) Fang, M.; Lee, D. S.; Ziller, J. W.; Doedens, R. J.; Bates, J. E.; Furche, F.; Evans, W. J. *Journal of the American Chemical Society* **2011**, *133*, 3784.

(42) APEX2 Version 2011.4-1, Bruker AXS, Inc.; Madison, WI 2011.

(43) SAINT Version 7.68a, Bruker AXS, Inc.; Madison, WI 2009.

(44) Sheldrick, G. M. SADABS, Version 2008/1, Bruker AXS, Inc.; Madison, WI 2008.

(45) Sheldrick, G. M. SHELXTL, Version 2008/4, Bruker AXS, Inc.; Madison, WI 2008.

(46) International Tables for Crystallography 1992, Vol. C., Dordrecht: Kluwer Academic Publishers.

CHAPTER 2

Influence of an Inner-Sphere K^+ Ion on the Magnetic Behavior of $(N_2)^{3-}$ Radical-Bridged Dilanthanide Complexes Isolated Using an External Magnetic Field

Introduction[†]

Determining the relationship between structure and magnetic properties is a fundamental goal in the study of lanthanide molecular magnetism. In mononuclear lanthanide species, the combination of inherently large magnetic anisotropy with the appropriate ligand field symmetry has been used to rationalize slow magnetic relaxation in many different coordination environments.[1] Even for multinuclear complexes, single-ion anisotropy and symmetry often trump exchange interactions as the most relevant criteria for promoting slow relaxation,[2] and this is due to the fact that the contracted 4f orbitals usually promote only very weak magnetic exchange.[3] The advent of a small contingent of dinuclear radical-bridged lanthanide complexes demonstrated that strong magnetic exchange can be facilitated by diffuse $(N_2)^{3-}$ or 2,2′-bipyrimidine$^-$ radical units.[4,5] For example, the series of complexes [K(18-crown-6)(THF)$_2$]{[$(R_2N)_2$(THF)Ln]$_2$(μ-η^2:η^2-N_2)} (**2-Ln**; Ln = Gd, Tb, Dy, Ho, Er; R = $SiMe_3$), where a bridging $(N_2)^{3-}$ radical ligand leads to an exchange constant of $J = -27$ cm^{-1}, represents the strongest magnetic exchange coupling observed to date for a Gd^{III} compound.[4a] Importantly, this strong coupling also leads to a blocking temperature of 14 K for the Tb^{III} analog, the highest for any single-molecule magnet (SMM)[4b] at the time of publication. DFT calculations for the Gd complex suggest that the coupling interaction is a result of overlap of the lanthanide 4f orbitals

[†]Portions of this chapter have been published: Meihaus, K. R.; Corbey, J. F.; Fang, M.; Ziller, J. W.; Long, J. R.; Evans, W. J. *Inorg. Chem.* **2014**, *53*, 3099.

with the N_2^{3-} ligand orbitals and thus, as the dihedral angle between the lanthanide and radical ligand deviates from planarity, the strength of the coupling is predicted to decrease.[6]

To probe this computational result, the synthesis and structural characterization of $\{K[(R_2N)_2(THF)Ln]_2(\mu_3\text{-}\eta^2\text{:}\eta^2\text{:}\eta^2\text{-}N_2)\}$ (**1-Ln**; Ln = Gd, Tb, Dy), was carried out to determine the effects of the unsolvated K^+ counterion on the magnetism. **1-Ln** was previously reported only for diamagnetic Y^{3+}: **1-Y** could be crystallized from toluene in the absence of 18-crown-6 and coordinating solvent.[7] X-ray structural characterization revealed that interaction of the K^+ ion with the $(N_2)^{3-}$ radical leads to a folding of the planar Ln_2N_2 unit present in the $[K(18\text{-crown-}6)(THF)_2]^+$ salt.[8] This chapter describes the extension of this synthetic methodology to analogous complexes featuring the paramagnetic lanthanide centers Ln = Gd, Tb, and Dy. Notably, the isolation of these compounds in pure form is facilitated through utilization of an external $Nd_2Fe_{13}B$ magnet during crystal growth. Full magnetic characterization of the series performed in collaboration with the group of Professor Jeffrey Long at UC Berkeley reveals non-negligible antiferromagnetic coupling between the Ln^{3+} centers in addition to antiferromagnetic Ln-$(N_2)^{3-}$ coupling, which leads to significantly lower magnetic relaxation barriers and blocking temperatures for **1-Tb** and **1-Dy**.

Results and Discussion

Synthesis. The $(N_2)^{3-}$ radical-bridged complexes **1-Ln** were synthesized by routes analogous to the one previously established for Y, as presented in Figure 2.1.[7] Here, potassium graphite reduction of the corresponding neutral $(N_2)^{2-}$-bridged complexes $[(R_2N)_2(THF)Ln]_2(\mu\text{-}\eta^2\text{:}\eta^2\text{-}N_2)$, **3-Ln**,[9,10] followed by filtration and removal of THF, yielded the desired products as yellow or orange powders. If left at room temperature, these powders will decompose to form

pale products within 24 h, though they are stable when stored at −30 °C. Crystallization of the isolated powders from toluene at −30 °C leads to a mixture of crystals of **1-Ln** and the neutral (N_2^{2-})-bridged complex, **3-Ln**, as determined by X-ray crystallography. ^{1}H NMR spectroscopy on isolated samples of **1-Y** show decomposition to **3-Y** occurs within hours in solution.

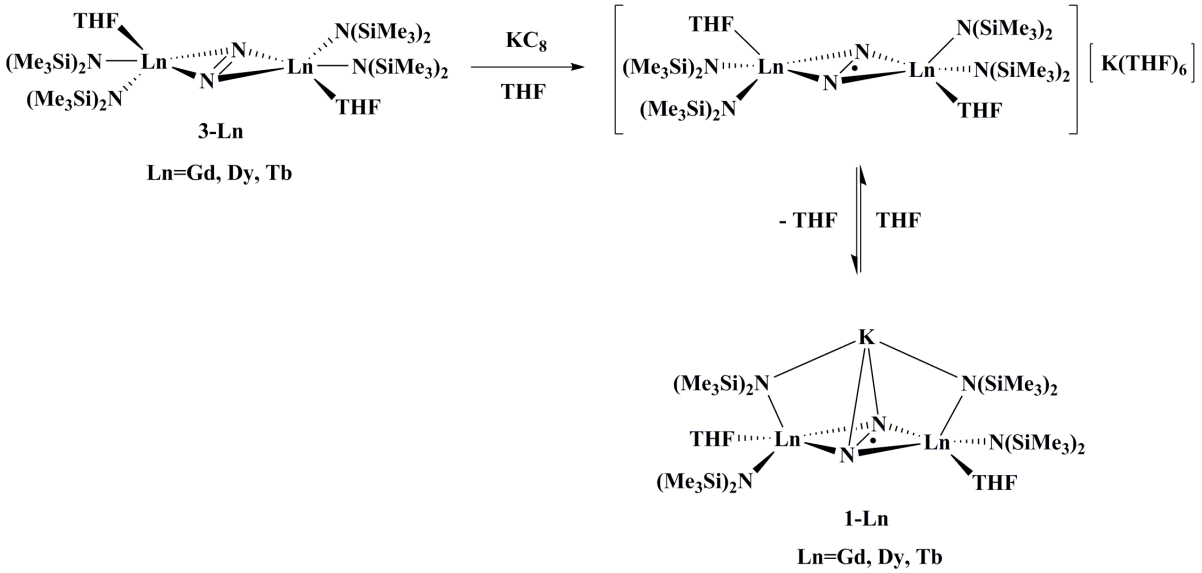

Figure 2.1. Synthesis of the $(N_2)^{3-}$ radical-bridged complexes **1-Ln**, featuring an inner-sphere K^+ counterion.

It was subsequently found that using excess KC_8 in the reduction of $[(R_2N)_2(THF)Ln]_2(\mu$-η^2:η^2-$N_2)$ gave samples of **1-Ln** with higher purity. While excess KC_8 was previously avoided owing to its potential for degrading the reduced product,[7] it can evidently be tolerated in the short reaction times used here. This is consistent with the sensitive nature of this multi-component reduction system, where the reaction times, order of KC_8 addition, and reaction concentration are all important variables.[7] A combination of short reaction times with excess

KC_8 and crystallizations in the presence of a $Nd_2Fe_{13}B$ magnet (*vide infra*) produced pure crystals of **1-Ln** suitable for magnetic studies.

Crystallization Using a $Nd_2Fe_{13}B$ Magnet. Due to the difficulty in isolating pure **1-Ln** using standard recrystallization techniques, alternative routes to purification were investigated. Notably, the use of magnetic fields to effect the separation of various materials has been well-established since the 1960s and 1970s,[11] largely tailored toward mineralogical applications. Magnetic fields produced by rare earth magnets have more recently been employed in many other applications, such as iron ore refinement[12] and water purification,[13] and on a laboratory scale in the fractionation and manipulation of magnetic nanoparticles.[14] An extensive body of work also exists on the use of magnetic levitation (MagLev) for the separation of various diamagnetic materials. In this technique, diamagnetic substances are placed in an aqueous paramagnetic solution that is then positioned between two $Nd_2Fe_{13}B$ magnets, with like poles facing.[15] Materials are separated within the solution based on a balance between their magnetic susceptibilities and their differing densities. MagLev has very recently been extended to address the often difficult task of separating diamagnetic crystal polymorphs.[16]

In light of these results, the use of a strong external $Nd_2Fe_{13}B$ magnet to purify the highly anisotropic paramagnetic **1-Ln** was examined. Rare earth magnets had not previously been reported to effect the crystallization of paramagnetic molecules in solution. Such a technique would rest on the fact that paramagnetic molecules will be much more strongly attracted to a magnet than say, diamagnetic impurities, or less paramagnetic substances (e.g. complexes with smaller spin). A magnet-driven concentration gradient in solution should thus lead to more rapid and preferential crystallization of the most paramagnetic substance. Indeed, it was found that crystals of **1-Ln** could be cleanly and swiftly crystallized without accompanying formation of **3-**

Ln by positioning a $Nd_2Fe_{13}B$ magnet adjacent to the crystallization vessel (Figures 2.2 and 2.3). While crystals also grow elsewhere in the vial, the majority are observed to form on the wall to which the magnet is attached. What is fascinating to note is that in some cases, the individual crystallites seem to form in a pattern defined by magnetic field lines (Figures 2.2 and 2.7).

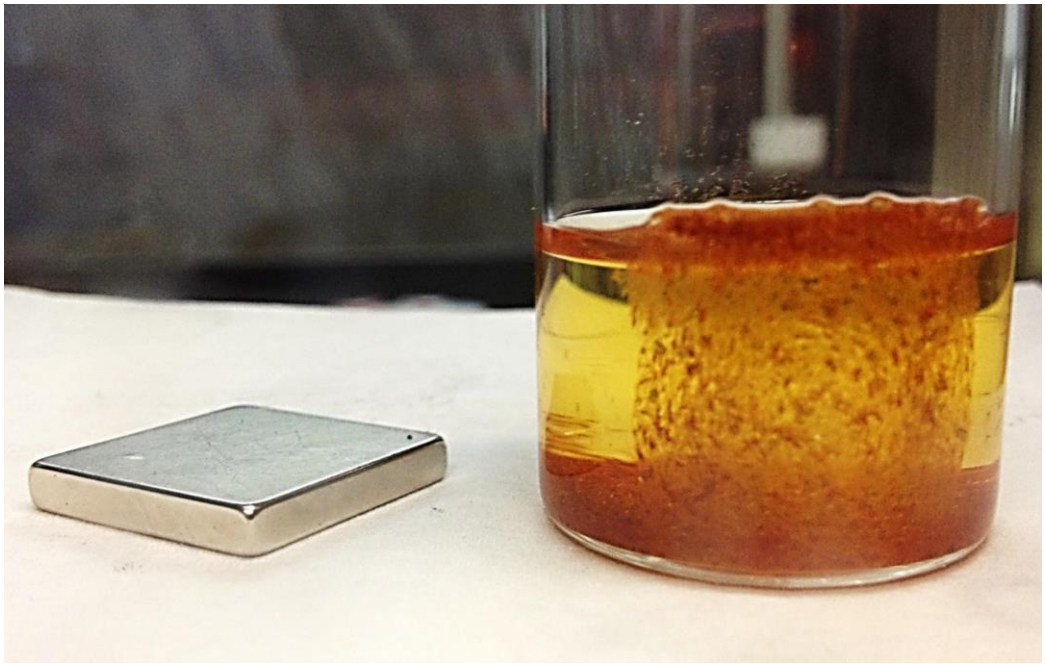

Figure 2.2. Crystals of $\{K[(R_2N)_2(THF)Dy]_2(\mu_3\text{-}\eta^2\text{:}\eta^2\text{:}\eta^2\text{-}N_2)\}$, **1-Dy**, grown with the aid of a $Nd_2Fe_{13}B$ magnet. A cluster of crystals can be seen along the side of the vial in a square formation where the magnet was attached to the outer wall.

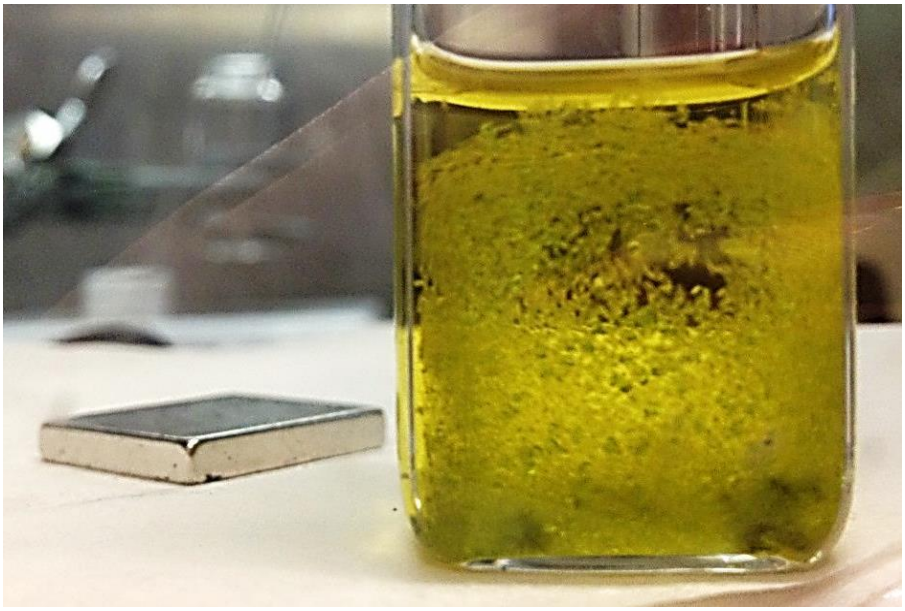

Figure 2.3. Crystals of {K[$(R_2N)_2$(THF)Tb]$_2$(μ_3-η^2:η^2:η^2-N_2)}, **1-Tb**, grown along the side of the square vial where the square $Nd_2Fe_{13}B$ magnet shown to the left had been attached.

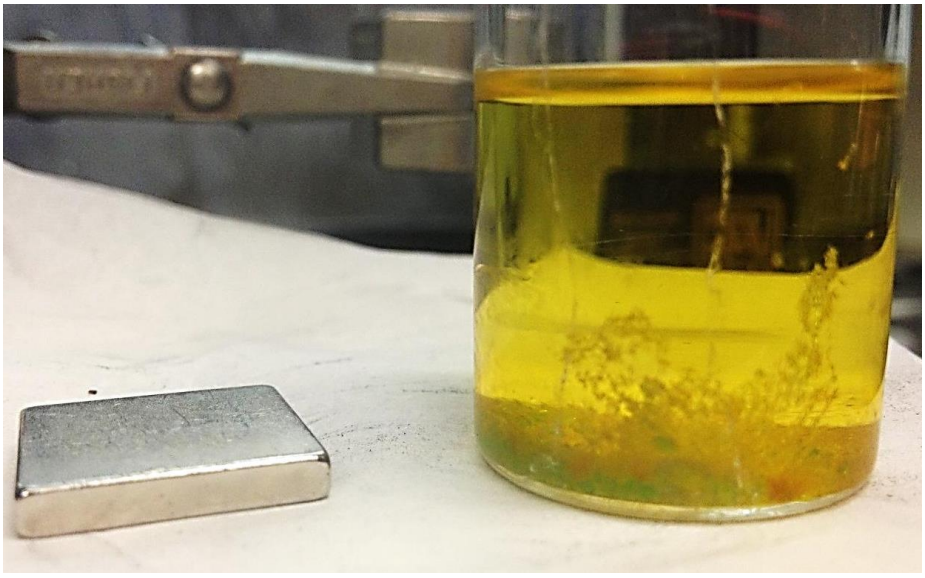

Figure 2.4. Crystals of {K[$(R_2N)_2$(THF)Gd]$_2$(μ_3-η^2:η^2:η^2-N_2)}, **1-Gd**, grown along the side of the vial where the square $Nd_2Fe_{13}B$ magnet shown to the left had been attached. Blue crystals of **3-Gd** are also observed to grow near the base of the vial.

Among **1-Ln**, this effect is most pronounced for Dy (Figure 2.2) and Tb (Figure 2.3), with less efficient crystal growth observed for the magnetically isotropic complex Gd (Figure 2.4). The effect is not noticeable for **1-Y**, which has only one unpaired electron per molecular unit. Given the greater effect on crystallization noted for **1-Tb** and **1-Dy** over **1-Gd**, this effect seems to be strongly correlated with large anisotropy, concentration and a high number of unpaired electrons. It is likely, however, that this technique is most useful in enhancing the rate of crystallization for the present complexes, as opposed to selectively crystallizing **1-Ln** from **3-Ln**. Such a conclusion is rationalized by the fact that magnet-induced crystal growth was also found to occur readily for **3-Tb** and **3-Dy** (Figures 2.5 and 2.6).

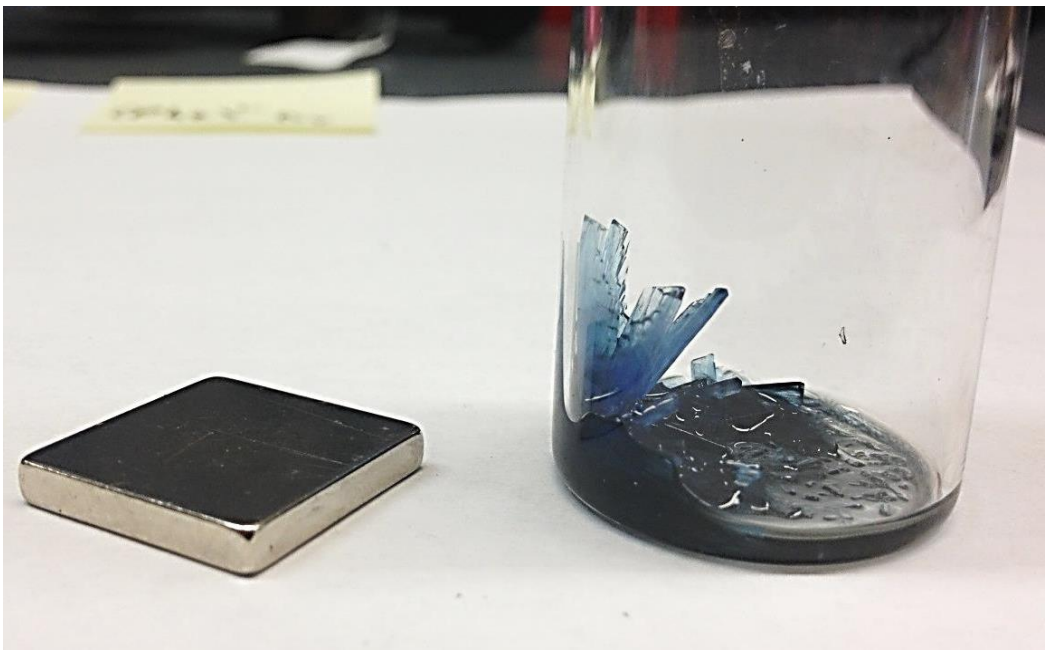

Figure 2.5. Crystals of $[(R_2N)_2Tb(THF)]_2(\mu\text{-}\eta^2\text{:}\eta^2\text{-}N_2)$, **3-Tb**, grown along the side of the vial where the square $Nd_2Fe_{13}B$ magnet shown to the left had been attached.

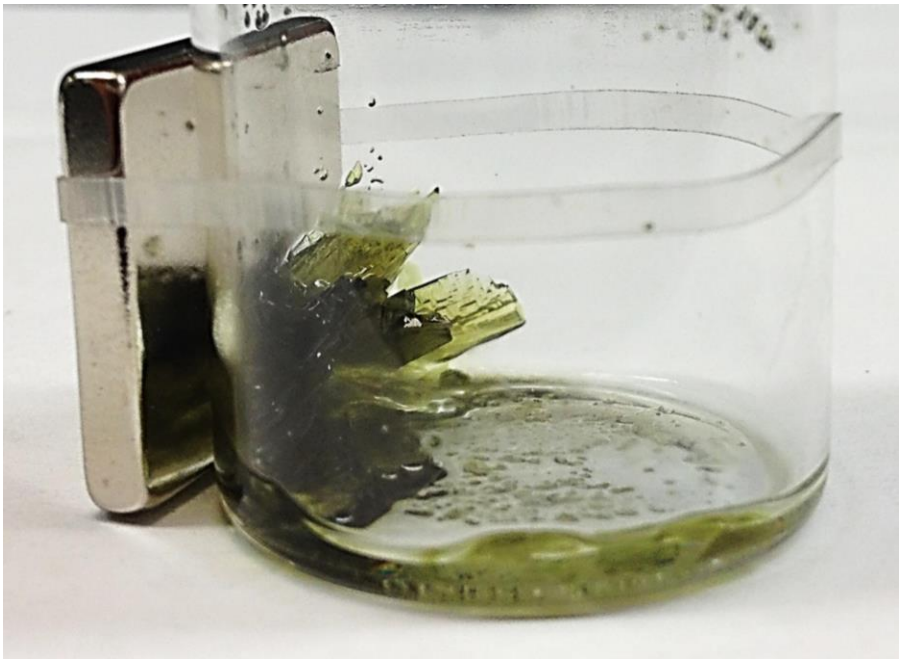

Figure 2.6. Crystals of $[(R_2N)_2Dy(THF)]_2(\mu\text{-}\eta^2\text{:}\eta^2\text{-}N_2)$, **3-Dy**, grown along the side of the vial where the square $Nd_2Fe_{13}B$ magnet is attached.

However, this technique should generally be useful in the efficient crystallization and separation of other highly paramagnetic complexes (see Figures 2.7-2.9) from diamagnetic or less paramagnetic molecular species in solution. Shown below are images of crystals of the monometallic $(C_5Me_5)_2Ln(C_3H_5)$ (Ln = Tb, Fig 2.7; Dy, Fig.2.8) complexes grown in the presence of an external magnetic field as a proof-of-concept. The previously reported **2-Tb** was also crystallized using this technique and is included in Figure 2.9.

Figure 2.7. Crystals of $(C_5Me_5)_2Tb(C_3H_5)$ grown using a square $Nd_2Fe_{13}B$ magnet attached to the side, demonstrating this phenomenon can be generalized to many different paramagnetic species.

Figure 2.8. Crystals of $(C_5Me_5)_2Dy(C_3H_5)$ grown using a square $Nd_2Fe_{13}B$ magnet attached to the top side of the vial from which the mother liquor has been removed to demonstrate the external magnet elicits crystal growth on the wall with which it is in direct contact.

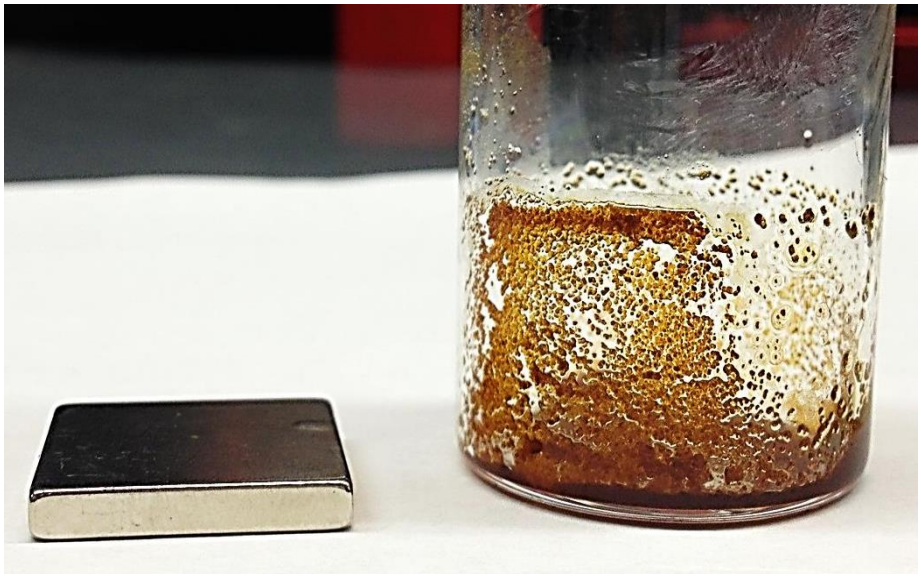

Figure 2.9. Crystals of the SMM {K(18-crown-6)(THF)$_2$}{[(R$_2$N)$_2$(THF)Tb]$_2$(μ-η^2:η^2-N$_2$)}, **2-Tb**, grown along the side of the vial where the square Nd$_2$Fe$_{13}$B magnet shown to the left had been attached.

X-ray Crystallographic Studies. Complexes **1-Ln** crystallize in the monoclinic space group $P2_1/n$ and are isomorphous with the previously reported Y analogue[7] (Figure 2.10). In the absence of coordinating solvent or other encapsulating agents, the K^+ cation is found above the $(N_2)^{3-}$ bridge and the N atoms of two NR_2 ligands orient inward to form a dative interaction with the metal cation. The K–N distances involving the $(N_2)^{3-}$ bridge are 2.844(3) to 2.888(2) Å, close to those of **1-Y** and at the long end of the 2.714(6)-2.800(6) Å range observed for other K–(η^2-N$_2$) distances in the literature.[17-19] The distances of 2.959(2) to 2.988(3) Å for K–N(NR$_2$) are much longer than the 2.760(1) Å K–N distance in (18-crown-6)K(NR$_2$),[20] as expected, and are similar to the 2.908 Å bridging K–N[μ-NR$_2$] distance in [(R$_2$N)Sm(μ-NR$_2$)$_2$K]$_n$.[21]

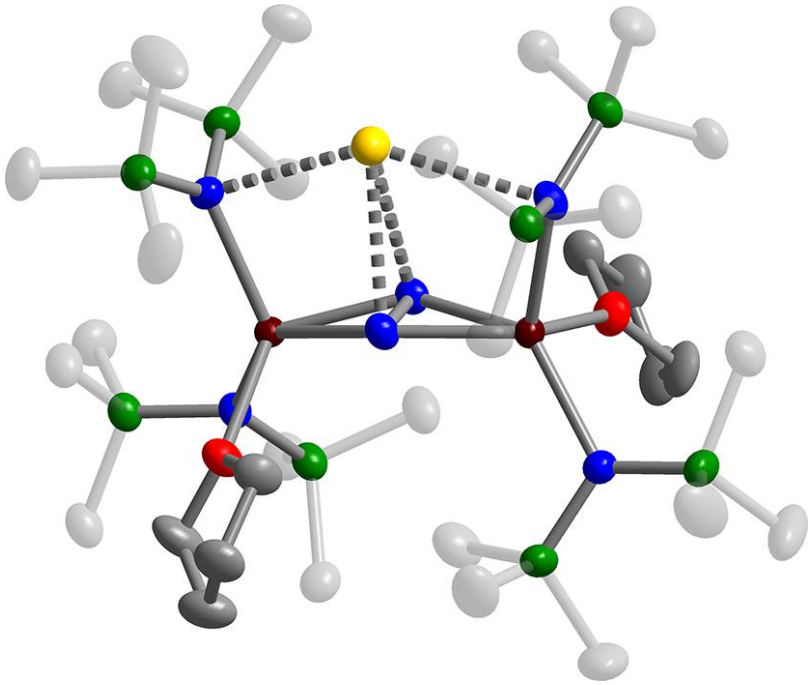

Figure 2.10. Structure of the $(N_2)^{3-}$ radical-bridged complex **1-Tb** with thermal ellipsoids drawn at the 70% probability level. Dark red, blue, green, red, grey, and yellow ellipsoids represent Tb, N, Si, O, C, and K atoms, respectively. Hydrogen atoms have been omitted for clarity.

A comparison of the metrical parameters for **1-Ln** and **2-Ln** (Table 2.1) reveals the N–N distances within the $(N_2)^{3-}$ radical bridges to be the same within error, and the Ln–N(NR_2) distances to decrease slightly as a function of ionic radii (in the order Gd > Tb > Dy). The Ln–O(THF) distances of **1-Ln** are slightly shorter than those of **2-Ln**, which could be due to a decrease in steric interactions of the ligands as the amides orient toward the inner sphere K^+ ion in **1-Ln**. The most notable structural change in **1-Ln** is a folding of the previously planar Ln_2N_2 core unit found in **2-Ln** to generate dihedral angles between the two LnN_2 planes of 13.64° in **1-Gd**, 16.12° in **1-Tb**, and 15.27° in **1-Dy**.

Table 2.1. Selected interatomic distances (Å) and angles (º) for {K[$(R_2N)_2$(THF)Ln]$_2$(μ_3-η^2:η^2:η^2-N_2)} (**1-Ln**) and [K(18-crown-6)(THF)$_2$]{[$(R_2N)_2$(THF)Ln]$_2$(μ-η^2:η^2-N_2)} (**2-Ln**).[4]

	N–N (Å)	K–N(N_2^{3-}) (Å)	K–(NR_2) (Å)	Ln–(NR_2) (Å)	Ln–O (Å)	Ln–N–N–Ln dihedral angle (°)
1-Gd	1.395(3)	2.875(2) 2.888(2)	2.959(2) 2.971(2)	2.354(2) 2.378(2)	2.425(2)	13.64
2-Gd[4a]	1.401(4)	- -	- -	2.357(2) 2.382(2)	2.480(2)	0
1-Tb	1.401(3)	2.844(3) 2.868(3)	2.977(3) 2.988(3)	2.337(2) 2.358(2)	2.413(2)	16.12
2-Tb[4b]	1.394(3)	- -	- -	2.331(2) 2.360(2)	2.479(1)	0
1-Dy	1.404(5)	2.852(4) 2.870(4)	2.968(4) 2.980(4)	2.324(4) 2.347(4)	2.392(3)	15.27
2-Dy[4a]	1.399(2)	- -	- -	2.314(1) 2.343(1)	2.455(1)	0

Static Magnetic Susceptibility Measurements. Temperature-dependent dc magnetic susceptibility measurements were carried out in the lab of Professor Jeffrey Long at the University of California, Berkeley for complexes **1-Ln** between 1.8 and 300 K at fields of 0.1 or 1 T. Comparison of the values of $\chi_M T$ versus T for **1-Ln** with data previously reported for the **2-Ln**[4] complexes without inner sphere K^+ ions reveals stark differences in the magnetism of the two series (Figure 2.11). For **1-Gd** (Figure 2.11a, green circles), $\chi_M T$ is 16.28 emu·K/mol at 300 K, larger than that observed for **2-Gd** (15.25 emu·K/mol).[4b] The susceptibility reaches a maximum of 18.25 emu·K/mol at 18 K for **1-Gd**, which is much lower than the maximum of 23.83 emu·K/mol occurring for **2-Gd** at 9 K.[4b] For **1-Gd**, a good fit to the data is achieved by considering intramolecular Gd-(N_2^{3-}) and Gd-Gd coupling, owing to the non-zero dihedral angle between the two GdN_2 planes not present in **2-Gd**.

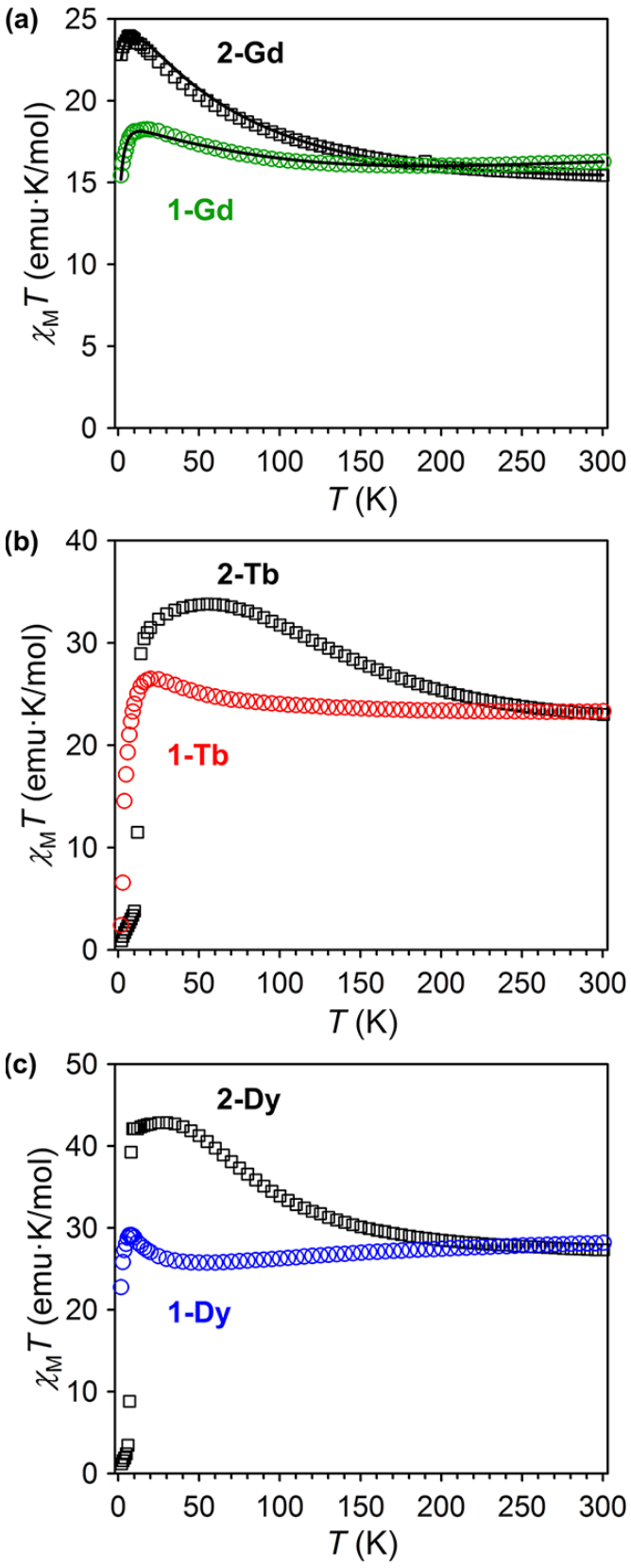

Figure 2.11. Plot of the product of the molar magnetic susceptibility and temperature ($\chi_M T$) with respect to temperature (T) for **1-Ln** (colored circles) and **2-Ln** (black squares). Data for the Gd and Dy complexes were collected under H_{dc} = 0.1 T, while data for the Tb^{III} complexes were collected under H_{dc} = 1 T to compare with the previously reported literature data for **2-Tb**. Fits are represented by black lines.

The improvement in the fit (largely below 40 K) with the inclusion of this intramolecular term (J' = −2.28(1) cm^{-1}) indicates that the coupling between Gd centers is significant only below this temperature,[22] and therefore, such an interaction is also likely to influence the magnetic relaxation behavior of **1-Tb** and **1-Dy**. Notably, the Gd-(N_2^{3-}) coupling constant obtained for **1-Gd** matches the value of J = –27 cm^{-1} previously reported for **2-Gd**.[4a] Thus, the small bend in the Gd-(N_2^3)$^-$-Gd unit appears to have little impact on the strength of the Gd-(N_2^{3-}) coupling. Given the large separation of 4.267 Å between Gd centers in **1-Gd**, it is likely that the mechanism for Gd-Gd coupling is via superexchange through the N_2^{3-} ligand. For comparison, an exchange of J = −0.49 cm^{-1} was observed for the planar $(N_2)^{2-}$-bridged species **3-Ln**[4a] indicating that the strength of the exchange increases considerably upon reduction of the bridging intermediary to $(N_2)^{3-}$ and folding of the Gd_2N_2 core unit.

The competing Gd-Gd exchange interaction that arises in **1-Gd** has a dramatic effect on its magnetic susceptibility data, as manifested in a suppression of the magnetic moment at low temperatures when compared to **2-Gd** (see Figure 2.11a). Our collaborators were able to use fits to the susceptibility data to generate diagrams of the spin state energy level structures for each of these complexes, as shown in Figure 2.12. Here, the simple level ordering of **2-Gd** expected for strong antiferromagnetic exchange between an $S = {}^1/_2$ radical and two $S = {}^7/_2$ Gd^{3+} centers is disrupted by the antiferromagnetic Gd-Gd exchange. Namely, whereas the $S = {}^{13}/_2$ ground state of **2-Gd** is well-isolated from an $S = {}^{11}/_2$ excited state, for **1-Gd**, the ground state is a lower $S = {}^9/_2$ spin state that is separated by only 0.29 cm^{-1} from an $S = {}^{11}/_2$ excited state, which facilitates faster magnetic relaxation in this system.

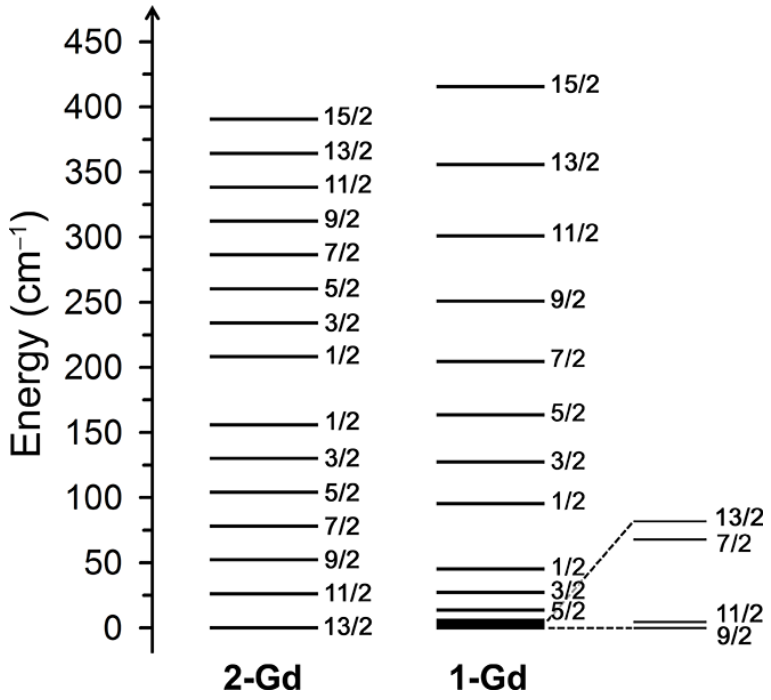

Figure 2.12. Spin state energy level diagrams for [K(18-crown-6)(THF)$_2$]{[(R$_2$N)$_2$(THF)Gd]$_2$(μ-η^2:η^2-N$_2$)}, **2-Gd**, and {K[(R$_2$N)$_2$(THF)Gd]$_2$(μ_3-η^2:η^2:η^2-N$_2$)}, **1-Gd**, as obtained from fitting to the susceptibility data.

Dc magnetic susceptibility measurements performed on **1-Tb** and **1-Dy** reveal similar trends to those observed for **1-Gd** (Figure 2.11b and c, colored circles) from which the general results may be extended to gain a qualitative understanding of the magnetism. In particular, we would anticipate for these compounds that the moment of the ground state is reduced as a result of antiferromagnetic Tb-Tb and Dy-Dy exchange interactions. Maxima in $\chi_M T$ are observed for **1-Tb** and **1-Dy** at 10 and 8 K, respectively, with corresponding $\chi_M T$ values of 28.44 and 29.12 emu·K/mol. Again, these maxima are much less than those for **2-Tb** and **2-Dy** at 33.76 emu·K/mol and 42.54 emu·K/mol, consistent with competing antiferromagnetic interactions between Ln centers, as observed in **1-Gd**. While a sharp decline in the susceptibility behavior of

1-Tb is indicative of magnetic blocking, the same phenomenon is lacking for **1-Dy**, indicating the latter has a much lower blocking temperature.

Dynamic Magnetic Susceptibility Measurements. To probe for slow relaxation of the magnetization, ac magnetic susceptibility data were also collected in the Long lab for **1-Tb** and **1-Dy** over a range of temperatures. Fitting of the data yields magnetic relaxation barriers of U_{eff} = 41.13(4) cm^{-1} for **1-Tb** and 14.95(8) cm^{-1} for **1-Dy**, significantly reduced from those of the parent outer-sphere complexes at 227.0(4) cm^{-1} (**2-Tb**)[4b] and 123 cm^{-1} (**2-Dy**),[4a] though within range of many terbium and dysprosium single-molecule magnets described in the literature.[1f] The much faster relaxation and smaller barriers observed for both compounds is a direct testimony to the influence of the competing antiferromagnetic coupling interaction on the energy landscape.

In order to probe relaxation at lower temperatures, variable-field magnetization measurements were carried out from 1.8 K. As anticipated, an open magnetic hysteresis loop is observed for **1-Tb**, which remains open to temperatures as high as 3.8 K (Figure 2.13 top). This maximum hysteresis temperature is only a fraction of that observed for **2-Tb** at 14 K (Figure 2.13 bottom),[4b] again emphasizing the lower moment and weaker overall coupling engineered by the bridging K^+ counterion in **1-Tb**. An interesting feature in the magnetic hysteresis of **1-Tb**, not observed for **2-Tb**, is the presence of two steps, one centered at zero field for all temperatures. Such drops in the magnetization indicate rapid magnetic relaxation likely due to tunneling of the magnetization.[23] Indeed, the energy separation between ground and first excited levels in **1-Gd** is on the order of the tunnel splitting in some molecular magnets.[24] However, detailed theoretical analysis will be necessary to validate these interpretations and fully understand the magnetic hysteresis behavior.

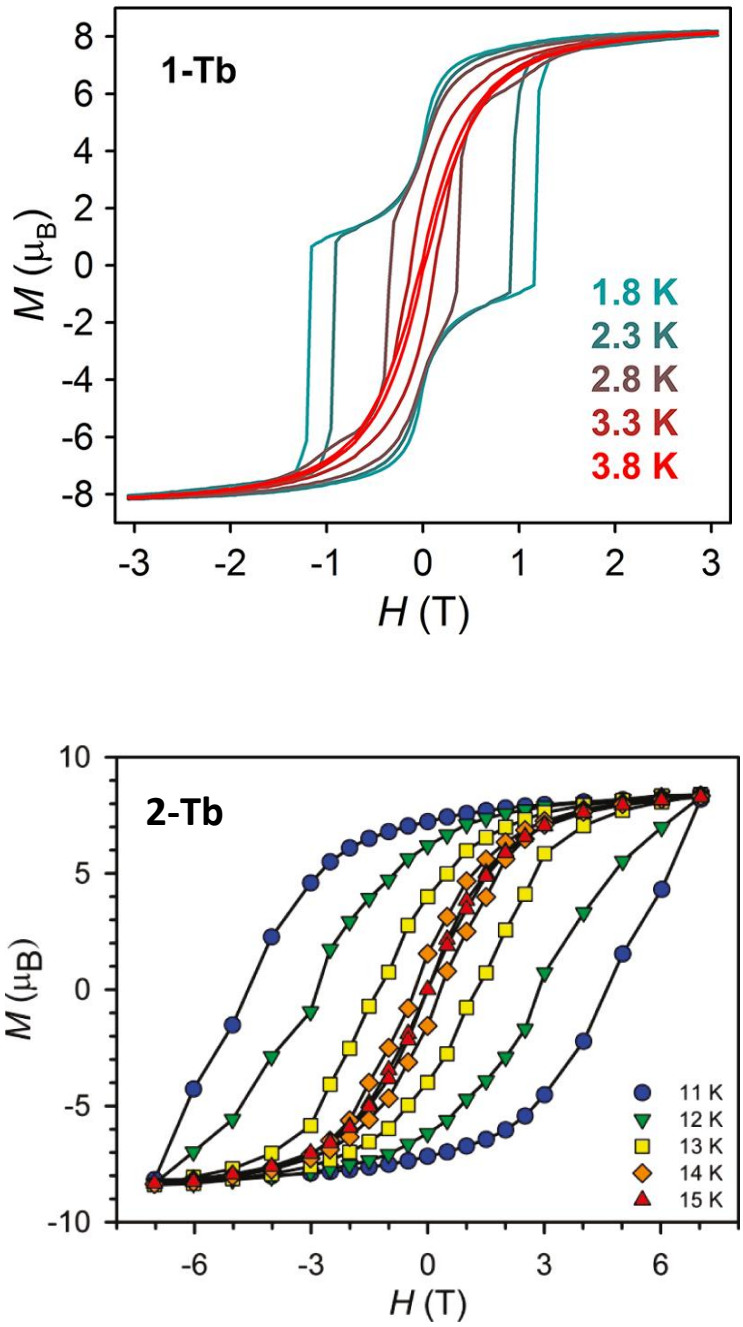

Figure 2.13. (Top) Variable-field magnetization data for {K[$(R_2N)_2$(THF)Tb]$_2$(μ_3-η^2:η^2-N_2)}, **1-Tb**, collected at a sweep rate of 1 mT/s and (bottom) [K(18-crown-6)(THF)$_2$]{[$(R_2N)_2$(THF)Tb]$_2$(μ-η^2:η^2-N_2)}, **2**-Tb,[4b] collected at a sweep rate of 0.9 mT/s.

Conclusions

The compounds $\{K[(R_2N)_2(THF)Ln]_2(\mu_3\text{-}\eta^2\text{:}\eta^2\text{:}\eta^2\text{-}N_2)\}$ (**1-Ln**; Ln = Gd, Tb, Dy; R = $SiMe_3$) featuring an inner-sphere K^+ counterion, were synthesized for comprehensive magnetic comparison with the previously reported single-molecule magnets $[K(18\text{-crown-}6)(THF)_2]\{[(R_2N)_2(THF)Ln]_2(\mu\text{-}\eta^2\text{:}\eta^2\text{-}N_2)\}$, **2-Ln**. Compounds **1-Ln** are less thermally stable than **2-Ln** and require shorter periods of crystallization before partial decomposition to products such as the $(N_2)^{2-}$ starting materials $[(R_2N)_2Ln(THF)]_2(\mu\text{-}\eta^2\text{:}\eta^2\text{-}N_2)$, **3-Ln**. Isolation of pure **1-Ln** was found to be significantly aided by crystal growth in the presence of a $Nd_2Fe_{13}B$ magnet adjacent to the crystallization vial, with **1-Ln** crystals forming predominantly on the side of the vial where the magnet was attached. This technique is not limited to radical-bridged dinuclear species, and has been found to be advantageous in promoting the crystallization of other complexes with large moments and anisotropy.

The compounds **1-Tb** and **1-Dy** are single-molecule magnets like the parent **2-Tb** and **2-Dy** compounds, but exhibit shorter relaxation times and much smaller relaxation barriers. Fitting of static magnetic susceptibility data for **1-Gd** reveals strong antiferromagnetic Gd-(N_2^{3-}) radical coupling that is the same strength as in the parent compound **2-Gd**, with $J \sim -27$ cm^{-1}. However, the folded Gd-(N_2^{3-})-Gd unit also introduces a small antiferromagnetic coupling interaction directly between Gd centers, which competes with the parallel alignment of Gd spins enforced by the antiferromagnetic Gd-(N_2^{3-}) radical coupling. The resulting energy spectrum of **1-Gd** consists of an $S = {}^9/_2$ ground state with a low-lying excited state $S = {}^{11}/_2$, and it is this absence of a well-isolated, higher-moment ground state that is likely the source of faster relaxation and smaller blocking temperatures for **1-Tb** and **1-Dy**. These results reveal the importance of a planar Ln-(N_2^{3-})-Ln unit to strong concerted exchange and very slow magnetic

relaxation[4] and perhaps more importantly highlight how a simple alkali metal such as potassium can be used to dramatically effect magnetic behavior.

Experimental

All syntheses and manipulations described below were conducted under nitrogen with rigorous exclusion of air and water using glovebox, Schlenk, and vacuum line techniques. Solvents were sparged with UHP argon and dried over columns containing Q-5 and molecular sieves. Potassium was washed with hexane and scraped to provide fresh surfaces before use. The compounds $[(R_2N)_2Ln(THF)]_2(\mu\text{-}\eta^2\text{:}\eta^2\text{-}N_2)$ (**3-Ln**; Ln = Tb,[9] Dy,[10] Gd[9]) were synthesized according to the literature method for the yttrium analog.[25] KC_8 was prepared according to the literature procedure.[26] $Nd_2Fe_{13}B$ magnets were obtained from United Nuclear Scientific Equipment and Supplies. IR samples were prepared as KBr pellets and analyzed using a Varian 1000 FT-IR system. Elemental analyses were either performed on a Perkin-Elmer Series II 2400 CHNS analyzer at the University of California, Irvine or by the Micro-Mass Facility at the University of California, Berkeley. Magnetic susceptibility measurements were performed using a Quantum Design MPMS2 SQUID magnetometer.

$\{K[(R_2N)_2(THF)Tb]_2(\mu_3\text{-}\eta^2\text{:}\eta^2\text{:}\eta^2\text{-}N_2)\}$ (1-Tb). This compound was synthesized by modification of a previously reported procedure.[25] **3-Tb** (300 mg, 0.27 mmol) was dissolved in THF (12 mL) in a nitrogen-filled glovebox to afford a pale blue solution, which was stored at −30 °C for ~1 h. A suspension of KC_8 (54 mg, 0.40 mmol) in THF (3 mL), that was also stored at −30 °C for approximately 1 h prior to use, was added dropwise to the cold pale blue solution with vigorous stirring. The reaction mixture immediately became orange, and formation of black insoluble material was observed. As soon as the addition was complete, the mixture was filtered

to remove the black solids, and the deep orange filtrate was concentrated to dryness under reduced pressure to yield a yellow powder. The powder was dissolved in a minimal amount of hexane in a vial which had a Grade N45 United Nuclear 3/4″ × 3/4″ × 1/8″ $Nd_2Fe_{13}B$ plate magnet attached to the outer wall using a rubber band. After 24 h at −30 °C, green crystals (230 mg, 73%) of **1-Tb** suitable for X-ray analysis grew on the side of the vial directly in contact with the magnet as well as on the bottom of the vial. IR: 2948s, 2895m, 1441w, 1245s, 994s, 867s, 832s, 770m, 751m, 663m, 606m, 547s cm^{-1}. Anal. Calcd for $C_{32}H_{88}KN_6O_2Si_8Tb_2 \bullet 0.5C_6H_{14}$, (**1-Tb** • $0.5C_6H_{14}$): C, 34.60; H, 7.97; N, 6.92. Found: C, 34.18; H, 7.98; N, 6.61.

{K[$(R_2N)_2$(THF)Dy]$_2$(μ_3-η^2:η^2:η^2-N_2)} (1-Dy). Following the procedure for **1-Tb**, **3-Dy** (300 mg, 0.26 mmol) was dissolved in THF (12 mL) to afford a green solution, which was treated with a KC_8 (50 mg, 0.37 mmol) suspension at −30 °C. After the mixture was filtered, removal of solvent from the red/orange filtrate afforded an orange powder, which was dissolved in a minimal amount of hexane for crystallization in the presence of a $Nd_2Fe_{13}B$ magnet. After 48 h at −30 °C, orange crystals (220 mg, 71%) of **1-Dy** suitable for X-ray analysis were obtained on the side of the vial directly in contact with the magnet and on the bottom of the vial. IR: 2946s, 2895s, 1443w, 1247s, 1001m, 876m, 841m, 769m, 750m, 663m, 548m cm^{-1}. Anal. Calcd for $C_{32}H_{88}KN_6O_2Si_8Dy_2 \bullet 0.5C_6H_{14}$ (**1-Dy** • $0.5C_6H_{14}$): C, 34.40; H, 7.92; N, 6.88. Found: C, 34.38; H, 8.18; N, 6.74.

{K[$(R_2N)_2$(THF)Gd]$_2$(μ_3-η^2:η^2:η^2-N_2)} (1-Gd). Following the procedure for **1-Tb**, **3-Gd** (300 mg, 0.27 mmol) was dissolved in THF (12 mL) to afford an aqua blue solution that was treated with a KC_8 (53 mg, 0.40 mmol) suspension at −30 °C. After the mixture was filtered, removal of solvent from the dark orange filtrate afforded a yellow-orange powder, which was dissolved in a minimal amount of pentane and crystallized in a vial with a $Nd_2Fe_{13}B$ magnet

attached to the side. After 24 h at −30 °C, orange X-ray quality crystals of **1-Gd** (120 mg, 38%) were obtained on the side of the vial directly in contact with the magnet and on the bottom of the vial. IR: 2947s, 2895s, 1442w, 1245s, 1010m, 869m, 767m, 751m, 663m, 603m, 538m cm^{-1}. Anal. Calcd for $C_{32}H_{88}KN_6O_2Si_8Gd_2 \bullet 0.5C_5H_{12}$ (**1-Gd** • $0.5C_5H_{12}$): C, 34.70; H, 7.99; N, 6.94. Found: C, 34.64; H, 7.63; N, 7.06.

X-ray Data Collection, Structure Solution and Refinement for {K[$(R_2N)_2$(THF)Tb]$_2$(μ_3-η^2:η^2:η^2-N_2)}, 1-Tb. A green crystal of approximate dimensions 0.14 x 0.14 x 0.20 mm was mounted on a glass fiber and transferred to a Bruker SMART APEX II diffractometer. The APEX2[27] program package was used to determine the unit-cell parameters and for data collection (30 sec/frame scan time for a sphere of diffraction data). The raw frame data was processed using SAINT[28] and SADABS[29] to yield the reflection data file. Subsequent calculations were carried out using the SHELXTL[30] program. The diffraction symmetry was 2/*m* and the systematic absences were consistent with the monoclinic space group $P2_1/n$ that was later determined to be correct. The structure was solved by direct methods and refined on F^2 by full-matrix least-squares techniques.[31] The analytical scattering factors[32] for neutral atoms were used throughout the analysis. Hydrogen atoms were included using a riding model. There was one-half molecule of toluene solvent (located about an inversion center) present per formula unit. The toluene was disordered and included using partial site-occupancy-factors and isotropic thermal parameters. The hydrogen atoms associated with the disordered solvent were not included in the refinement. At convergence, wR2 = 0.0585 and Goof = 1.029 for 504 variables refined against 12655 data (0.78Å), R1 = 0.0252 for those data with $I > 2.0\sigma(I)$. Details are given in Table 2.2.

X-ray Data Collection, Structure Solution and Refinement for {K[$(R_2N)_2$(THF)Dy]$_2$(μ_3-η^2:η^2:η^2-N_2)}, 1-Dy. An orange crystal of approximate dimensions 0.051 x 0.139 x 0.196 mm was mounted on a glass fiber and transferred to a Bruker SMART APEX II diffractometer. The APEX2[27] program package was used to determine the unit-cell parameters and for data collection (45 sec/frame scan time for a sphere of diffraction data). The raw frame data was processed using SAINT[28] and SADABS[29] to yield the reflection data file. Subsequent calculations were carried out using the SHELXTL[30] program. The diffraction symmetry was 2/*m* and the systematic absences were consistent with the monoclinic space group $P2_1/n$ that was later determined to be correct. The structure was solved by direct methods and refined on F^2 by full-matrix least-squares techniques.[31] The analytical scattering factors[32] for neutral atoms were used throughout the analysis. One half of what is probably a disordered hexane solvent molecule was present per formula unit. Hydrogen atoms were included using a riding model. At convergence, wR2 = 0.0826 and Goof = 1.015 for 496 variables refined against 13144 data (0.77 Å), R1 = 0.0389 for those 9397 data with $I > 2.0\sigma(I)$. Details are given in Table 2.2.

X-ray Data Collection, Structure Solution and Refinement for {K[$(R_2N)_2$(THF)Gd]$_2$(μ_3-η^2:η^2:η^2-N_2)}, 1-Gd. A yellow crystal of approximate dimensions 0.181 x 0.211 x 0.338 mm was mounted on a glass fiber and transferred to a Bruker SMART APEX II diffractometer. The APEX2[27] program package was used to determine the unit-cell parameters and for data collection (30 sec/frame scan time for a sphere of diffraction data). The raw frame data was processed using SAINT[28] and SADABS[29] to yield the reflection data file. Subsequent calculations were carried out using the SHELXTL[30] program. The diffraction symmetry was 2/*m* and the systematic absences were consistent with the monoclinic space group

$P2_1/n$ that was later determined to be correct. The structure was solved by direct methods and refined on F^2 by full-matrix least-squares techniques.[31] The analytical scattering factors[32] for neutral atoms were used throughout the analysis. One half of a disordered toluene solvent molecule was present per formula unit. Hydrogen atoms were included using a riding model. At convergence, wR2 = 0.0618 and Goof = 1.035 for 504 variables refined against 13113 data (0.77 Å), R1 = 0.0250 for those 11324 data with I > 2.0σ(I). Details are given in Table 2.2.

Table 2.2. Crystal data and structure refinement parameters for $\{K[(R_2N)_2(THF)Ln]_2(\mu_3\text{-}\eta^2\text{:}\eta^2\text{:}\eta^2\text{-}N_2)\}$ **1-Ln** where Ln = Gd, **1-Gd**; Tb, **1-Tb** or Dy, **1-Dy**.

	1-Gd • 0.5(C_7H_8)	**1-Tb** • 0.5(C_7H_8)	**1-Dy** • 0.5(C_6H_{14})
Empirical formula	$C_{35.5}H_{92}Gd_2KN_6O_2Si_8$	$C_{35.5}H_{92}KN_6O_2Si_8Tb_2$	$C_{35}H_{95}Dy_2KN_6O_2Si_8$
Formula weight	1213.47	1216.81	1220.98
Temperature (K)	143(2)	143(2)	143(2)
Space group	$P2_1/n$	$P2_1/n$	$P2_1/n$
a (Å)	12.4844(9)	12.4539(8)	12.4793(10)
b (Å)	21.3735(15)	21.4481(13)	21.5488(16)
c (Å)	22.3563(16)	22.3028(14)	22.2467(17)
α (°)	90	90	90
β (°)	104.9835(8)	104.9719(7)	105.0650(10)
γ (°)	90	90	90
Volume (Å^3)	5762.6(7)	5755.1(6)	5776.8(8)
Z	4	4	4
ρ_{calcd} (Mg/m^3)	1.399	1.404	1.404
μ (mm^{-1})	2.553	2.709	2.837
$R1^a$ [$I > 2\sigma(I)$ = 10615 data]	0.0250	0.0252	0.0389
$wR2^b$ (all data, 0.78 Å)	0.0618	0.0585	0.0826

$^a R1 = \Sigma||F_o|-|F_c|| / \Sigma|F_o|$. $^b wR2 = [\Sigma[w(F_o^2-F_c^2)^2] / \Sigma[w(F_o^2)^2]]^{1/}$

References

(1) (a) Ishikawa, N.; Sugita, M.; Ishikawa, T.; Koshihara, S.-y.; Kaizu, Y. *Journal of the American Chemical Society* **2003**, *125*, 8694. (b) AlDamen, M. A.; Clemente-Juan, J. M.; Coronado, E.; Martí-Gastaldo, C.; Gaita-Ariño, A. *Journal of the American Chemical Society* **2008**, *130*, 8874. (c) Jiang, S.-D.; Wang, B.-W.; Sun, H.-L.; Wang, Z.-M.; Gao, S. *Journal of the American Chemical Society* **2011**, *133*, 4730. (d) Baldoví, J. J.; Borrás-Almenar, J. J.; Clemente-Juan, J. M.; Coronado, E.; Gaita-Ariño, A. *Dalton Transactions* **2012**, *41*, 13705. (e) Chilton, N. F.; Langley, S. K.; Moubaraki, B.; Soncini, A.; Batten, S. R.; Murray, K. S. *Chemical Science.* **2013**, *4*, 1719. (f) Woodruff, D. N.; Winpenny, R. E.; Layfield, R. A. *Chemical Reviews* **2013**, *113*, 5110.

(2) Blagg, R. J.; Ungur, L.; Tuna, F.; Speak, J.; Comar, P.; Collison, D.; Wernsdorfer, W.; McInnes, E. J. L.; Chibotaru, L. F.; Winpenny, R. E. P. *Nature Chemistry* **2013**, *5*, 673.

(3) Sessoli, R.; Powell, A. K. *Coordination Chemistry Reviews* **2009**, *253*, 2328.

(4) (a) Rinehart, J. D.; Fang, M.; Evans, W. J.; Long, J. R. *Nature Chemistry* **2011**, *3*, 538. (b) Rinehart, J. D.; Fang, M.; Evans, W. J.; Long, J. R. *Journal of the American Chemical Society* **2011**, *133*, 14236.

(5) Demir, S.; Zadrozny, J. M.; Nippe, M.; Long, J. R. *Journal of the American Chemical Society* **2012**, *134*, 18546.

(6) Rajeshkumar, T.; Rajaraman, G. *Chemical Communications* **2012**, *48*, 7856.

(7) Evans, W. J.; Fang, M.; Zucchi, G.; Furche, F.; Ziller, J. W.; Hoekstra, R. M.; Zink, J. I. *Journal of the American Chemical Society* **2009**, *131*, 11195.

(8) Fang, M.; Bates, J. E.; Lorenz, S. E.; Lee, D. S.; Rego, D. B.; Ziller, J. W.; Furche, F.; Evans, W. *Inorganic Chemistry* **2011**, *50*, 1459.

(9) Evans, W. J.; Lee, D. S.; Rego, D. B.; Perotti, J. M.; Kozimor, S. A.; Moore, E. K.; Ziller, J. W. *Journal of the American Chemical Society* **2004**, *126*, 14574.

(10) Evans, W. J.; Zucchi, G.; Ziller, J. W. *Journal of the American Chemical Society* **2003**, *125*, 10.

(11) (a) Andres, U. *Magnetohydrodynamic & Magnetohydrostatic Methods of Mineral Separation*; John Wiley & Sons: New York, NY, **1976**. (b) Alminas, H. V.; Marceau, T. L.; Hoffman, J. D.; Bigelow, R. C. *A Laboratory-Scale Magnetohydrostatic Separator and its Application to Mineralogic Problems*; United States Government Printing Office: Washington, DC, **1984**.

(12) Arvidson, B. R.; Henderson, D. *Minerals Engineering* **1997**, *10*, 127.

(13) Ambashta, R. D.; Sillanpää, M. J. *Hazardous Materials* **2010**, *180*, 38.

(14) Latham, A. H.; Freitas, R. S.; Schiffer, P.; Williams, M. E. *Analytical Chemistry* **2005**, *77*, 5055.

(15) Mirica, K. A.; Shevkoplyas, S. S.; Phillips, S. T.; Gupta, M.; Whitesides, G. M. *Journal of the American Chemical Society* **2009**, *131*, 10049 and references therein.

(16) Atkinson, M. B. J.; Bwambok, D. K.; Chen, J.; Chopade, P. D.; Thuo, M. M.; Mace, C. R.; Mirica, K. A.; Kumar, A. A.; Myerson, A. S.; Whitesides, G. M. *Angewandte Chemie International Edition* **2013**, *125*, 10398.

(17) Yelamos, C.; Heeg, M. J.; Winter, C. H. *Inorganic Chemistry* **1998**, *37*, 3892.

(18) Pfirrmann, S.; Limberg, C.; Herwig, C.; Stober, R.; Ziemer, B. *Angewandte Chemie International Edition* **2009**, *48*, 3357.

(19) Smith, J. M.; Sadique, A. R.; Cundari, T. R.; Rodgers, K. R.; Lukat-Rodgers, G.; Lachicotte, R. J.; Flaschenriem, C. J.; Vela, J.; Holland, P. L. *Journal of the American Chemical Society* **2006**, *128*, 756.

(20) Evans, W. J.; Rego, D. B.; Ziller, J. W. *Inorganic Chemistry* **2006**, *45*, 3437.

(21) Evans, W. J.; Johnston, M. A.; Clark, R. D.; Anwander, R.; Ziller, J. W. *Polyhedron* **2001**, *20*, 2483.

(22) Benelli, C.; Gatteschi, D. *Chemical Reviews* **2002**, *102*, 2369.

(23) Gatteschi, D.; Sessoli, R. *Angewandte Chemie International Edition* **2003**, *42*, 268.

(24) del Barco, E.; Kent, A. D.; Hill, S.; North, J. M.; Dalal, N. S.; Rumberger, E. M.; Hendrickson, D. N.; Chakov, N.; Christou, G. J. *Low Temperature Physics* **2005**, *140*, 119.

(25) Evans, W. J.; Lee, D. S.; Ziller, J. W. *Journal of the American Chemical Society* **2004**, *126*, 454.

(26) Bergbreiter, D. E.; Killough, J. M. *Journal of the American Chemical Society* **1978**, *100*, 2126.

(27) APEX2 Version 2011.4-1, Bruker AXS, Inc.; Madison, WI 2011.

(28) SAINT Version 7.68a, Bruker AXS, Inc.; Madison, WI 2009.

(29) Sheldrick, G. M. SADABS, Version 2008/1, Bruker AXS, Inc.; Madison, WI 2008.

(30) Sheldrick, G. M. SHELXTL, Version 2008/4, Bruker AXS, Inc.; Madison, WI 2008.

(31) Sheldrick, G. M. SHELXL-2013/2. 2013.

(32) International Tables for Crystallography 1992, Vol. C., Dordrecht: Kluwer Academic Publishers.

CHAPTER 3

Chalcogen Reduction by $(N_2)^{2-}$ in the Bimetallic Yttrium Amide Complex $\{[(Me_3Si)_2N]_2(THF)Y\}_2(\mu\text{-}\eta^2\text{:}\eta^2\text{-}N_2)$ Leading to Co-crystallization of $(\mu\text{-}S_2)^{2-}$ and $(\mu\text{-}S)^{2-}$

Introduction[†]

Studies of rare earth reductive chemistry have provided a series of $(N_2)^{2-}$ and $(N_2)^{3-}$ complexes of the rare earth metals ligated by two bis(trimethylsilyl) ligands: $\{[(Me_3Si)_2N]_2Ln(THF)\}_2(\mu\text{-}\eta^2\text{:}\eta^2\text{-}N_2)$[1,2] and $K(THF)_x\{[(Me_3Si)_2N]_2Ln(THF)\}_2(\mu\text{-}\eta^2\text{:}\eta^2\text{-}N_2)$ (Ln = rare earth; x = 0, 6).[3,4] The latter complexes with Ln = Dy and Tb are of interest as single-molecule magnets,[4-6] and both sets of complexes function as reducing agents. Reductions of NO and O_2 by these complexes to form the $(NO)^{2-}$ complex, $\{[(Me_3Si)_2N]_2Y(THF)\}_2(\mu\text{-}\eta^2\text{:}\eta^2\text{-}NO)$,[7] the $(O_2)^{2-}$ complex, $\{[(Me_3Si)_2N]_2Y(THF)\}_2(\mu\text{-}\eta^2\text{:}\eta^2\text{-}O_2)$,[8] and the oxide, $\{[(Me_3Si)_2N]_2Y(THF)\}_2(\mu\text{-}O)$,[8] have been studied in efforts to increase the number of bimetallic complexes that could be precursors to interesting single-molecule magnets. This chapter presents the reduction chemistry of these reduced dinitrogen complexes with sulfur and selenium. The goal of this project was to expand the range of bridged bimetallic compounds and to determine if chalcogen congeners of the $(\mu\text{-}O_2)^{2-}$ and $(\mu\text{-}O)^{2-}$ bimetallic amide complexes could be made in this way. It was also of interest to determine if the bis(amide) rare earth reduction system could provide access to ligands like the $(\mu\text{-}S_3)^{2-}$ moiety isolated in the bimetallic bis(pentamethylcyclopentadienyl) complex $[(C_5Me_5)_2Sm]_2(\mu\text{-}\eta^1\text{:}\eta^3\text{-}S_3)$,[9] synthesized from $(C_5Me_5)_2Sm(THF)_2$ and sulfur, or more complicated lanthanide chalcogenides like the fascinating clusters derived from $Ln(EPh)_3$ and chalcogens (E = S, Se).[10-12]

[†]Portions of this chapter have been published: Corbey, J. F.; Fang, M.; Ziller, J. W.; Evans, W. J. *Inorg. Chem.* **2014**, *54*, 801.

Reduction of sulfur and selenium by $(N_2)^{2-}$ is observed, but, as reported here, the sulfur reaction is complicated by the fact that the $(\mu\text{-}S_2)^{2-}$and $(\mu\text{-}S)^{2-}$ complexes co-crystallize. Co-crystallization of similar ligands is a general problem in any area of chemistry that relies on X-ray crystallography for characterization. This has been particularly problematic in some inorganic systems where variable X-ray data due to different mixtures of complexes has been mistaken for "bond stretch isomerism".[13] Since $(S_2)^{2-}$ and S^{2-} ligands are of general interest in inorganic and particularly bioinorganic chemistry,[14-16] it is important to be aware of this co-crystallization possibility. Reduction of selenium to form $(Se_2)^{2-}$ and Se^{2-} analogs is reported for comparison. Isolation of a new aminotrisulfide ligand, $[S_3N(SiMe_3)_2]^{1-}$, is also described.

Results

Synthesis of Sulfur Products. Addition of elemental sulfur to a pale blue THF solution of the $(N_2)^{2-}$ complex $\{[(Me_3Si)_2N]_2Y(THF)\}_2(\mu\text{-}\eta^2\text{:}\eta^2\text{-}N_2)$, **1**, caused an immediate color change to bright green then yellow. Removal of solvent from the solution after 1 h and recrystallization from hexane yielded yellow crystals of a material designated as **2**. The ^{1}H NMR spectrum of **2** in benzene-d_6 contained two resonances of different intensities in the region associated with the $[N(SiMe_3)_2]^-$ ancillary ligands, 0.46 and 0.45 ppm, which suggested the presence of two different complexes. X-ray crystallographic analysis of the yellow crystals revealed a bimetallic entity containing two $\{[(Me_3Si)_2N]_2Y(THF)\}^{1+}$ units with three areas of electron density between the metal centers, Figure 3.1. A model for the crystallographic data for **2** with disulfide, $(S_2)^{2-}$, and monosulfide,

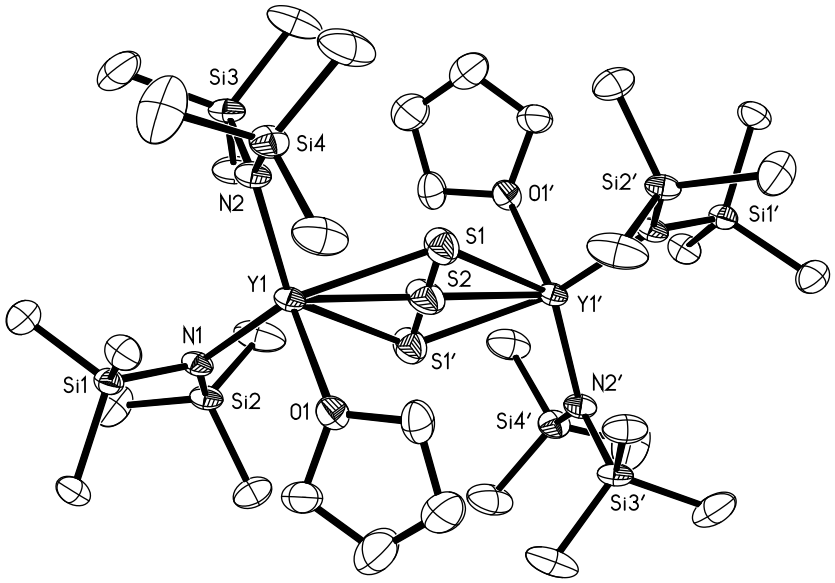

Figure 3.1. Thermal ellipsoid plot of **2** identified as a mixture of $\{[(Me_3Si)_2N]_2Y(THF)\}_2(\mu\text{-}\eta^2\text{:}\eta^2\text{-}S_2)$, **3**, and $\{[(Me_3Si)_2N]_2Y(THF)\}_2(\mu\text{-}S)$, **4**, drawn at the 50% probability level. Partial-site-occupancy of S1:S2 was modeled with an 8.6:1.4 mixture of $\{[(Me_3Si)_2N]_2Y(THF)\}_2(\mu\text{-}\eta^2\text{:}\eta^2\text{-}S_2)$, **3** and $\{[(Me_3Si)_2N]_2Y(THF)\}_2(\mu\text{-}S)$, **4**, respectively. Hydrogen atoms are omitted for clarity.

S^{2-}, bridging moieties, i.e. a mixture of $\{[(Me_3Si)_2N]_2Y(THF)\}_2(\mu\text{-}\eta^2\text{:}\eta^2\text{-}S_2)$, **3**, and $\{[(Me_3Si)_2N]_2Y(THF)\}_2(\mu\text{-}S)$, **4**, in an 8.6 to 1.4 ratio gave an acceptable refinement, eq 3.1.

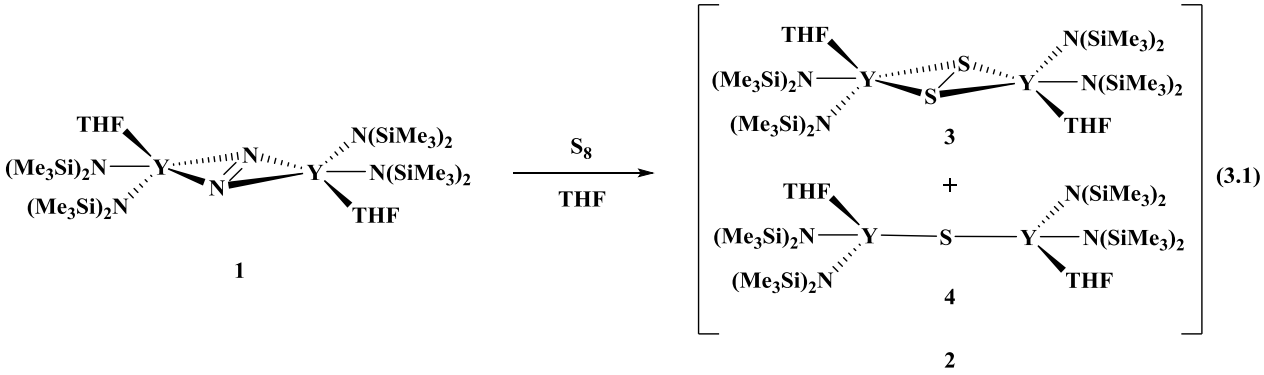

(3.1)

Varying the reaction time, temperature, sulfur equivalents, and crystallization solvent of the reaction in eq 3.1 did not lead to pure samples of either the disulfide, **3**, or the monosulfide species, **4**. A slight excess of sulfur [2.4 equiv of S per $(N_2)^{2-}$] consistently gave better yields of **2**. The ratio of the two $N(SiMe_3)_2$ NMR peaks for **3** and **4** varied from 1:1 to 4:1 in multiple reactions, but each batch of crystals examined refined to an approximate 9:1 mixture. Repeated crystallizations did not yield a mother liquor of just **4**, but instead led to other products (*vide infra*). Reactions using Ph_3PS as the sulfur source required heat to proceed and generated **4** as identified by NMR spectroscopy as well as the expected Ph_3P byproduct. However, decomposition of the $(N_2)^{2-}$ starting material also occurred during the heating process and **4** could not be isolated cleanly via this route.

Reactions were also performed using the $(N_2)^{3-}$ radical complex $K\{[(Me_3Si)_2N]_2(THF)Y\}_2(\mu_3\text{-}\eta^2\text{:}\eta^2\text{:}\eta^2\text{-}N_2)^2$ to see if the enhanced reducing power of the trianionic dinitrogen ligand could cleanly reduce sulfur to form a pure product. Addition of sulfur to $K\{[(Me_3Si)_2N]_2(THF)Y\}_2(\mu_3\text{-}\eta^2\text{:}\eta^2\text{:}\eta^2\text{-}N_2)$ produced the reduced sulfur products **3** and **4**, again as a mixture observed by NMR spectroscopy with roughly a 2:1 ratio of **3**:**4**. In addition, NMR evidence for the known $(N_2H_2)^{2-}$-containing compound $\{[(Me_3Si)_2N]_2(THF)Y\}_2(\mu\text{-}N_2H_2)$[17] as well as another $[N(SiMe_3)_2]^-$ -ligated product was also observed making this reaction more complicated than the reaction of sulfur with **1**.

However, addition of excess KC_8 to a THF solution of crystalline **2** causes the resonance at 0.46 ppm to diminish while the 0.45 ppm resonance remains (Figures 3.2 and 3.3). Crystallization of this sample from THF gave small amounts of colorless crystals of $\{[(Me_3Si)_2N]_2Y(THF)\}_2(\mu\text{-}S)$, **4**, Figure 3.4.

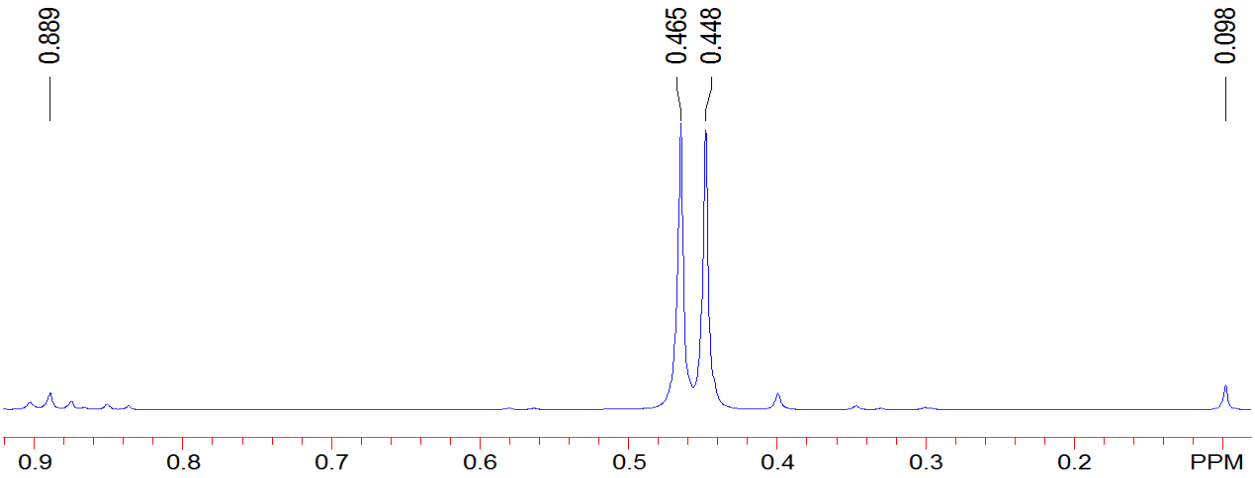

Figure 3.2. ^{1}H NMR spectrum of complex **2** containing a mixture of $\{[(Me_3Si)_2N]_2Y(THF)\}_2(\mu$-$\eta^2$:$\eta^2$-$S_2)$, **3**, and $\{[(Me_3Si)_2N]_2Y(THF)\}_2(\mu$-S), **4**, with amide resonances at 0.465 and 0.448 ppm, respectively.

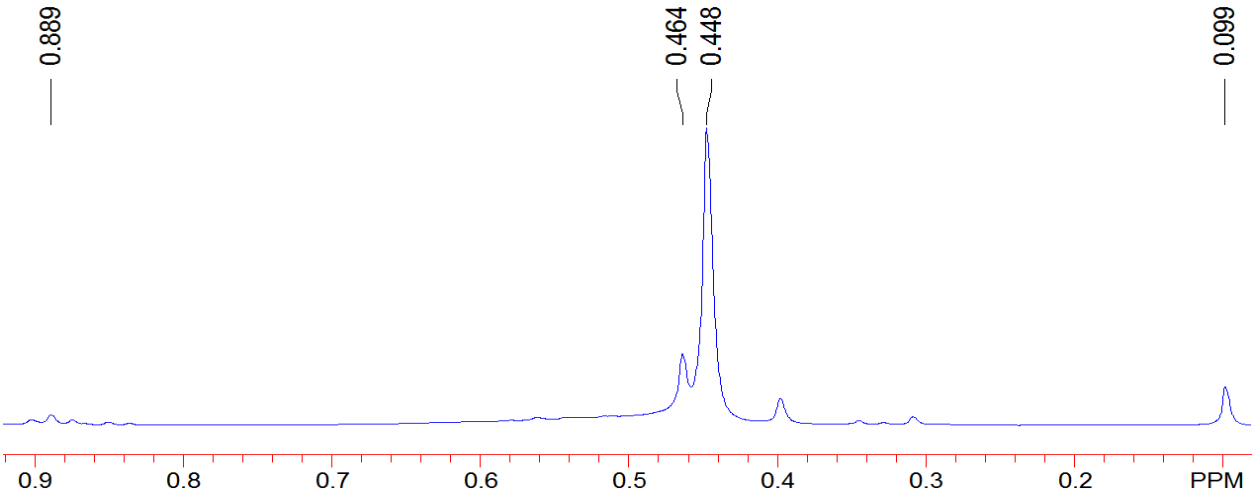

Figure 3.3. ^{1}H NMR spectrum of $\{[(Me_3Si)_2N]_2Y(THF)\}_2(\mu$-S), **4**, from reacting complex **2** with KC_8.

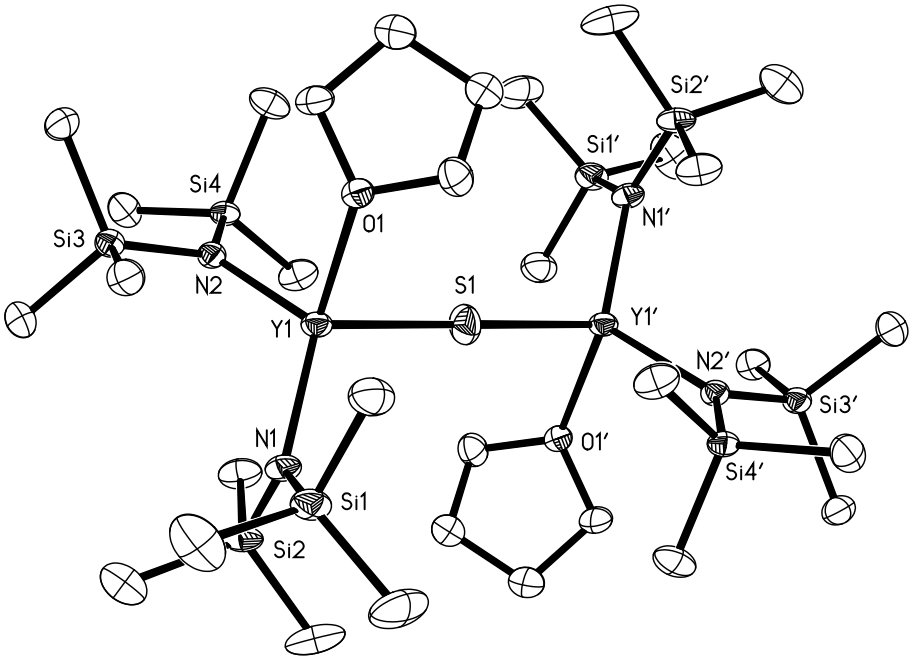

Figure 3.4. Thermal ellipsoid plot of $\{[(Me_3Si)_2N]_2Y(THF)\}_2(\mu\text{-S})$, **4**, drawn at the 50% probability level. Hydrogen atoms are omitted for clarity.

The ^1H NMR spectrum of these crystals contained only the 0.45 ppm resonance of the mixture found in **2**, and hence this resonance is assigned to **4**. Attempts to oxidize the S^{2-} component of **2** to form **3** using $AgBPh_4$ yielded NMR resonances consistent with the known cationic complex $\{[(Me_3Si)_2N]_2Y(THF)_2\}\{BPh_4\}$.[8] Addition of AgOTf to **2** resulted in isolation of the previously identified cyclic silver cluster, $Ag_4[N(SiMe_3)_2]_4$, as determined by X-ray crystallography.[18]

A second crystallization of the mother liquor of **2** yielded, in addition to more crystals of **2**, some colorless crystals that were analyzed by X-ray diffraction and found to be $[(Me_3Si)_2N]_2Y[\eta^2\text{-}S_3N(SiMe_3)_2](THF)$, **5**, Figure 3.5. Complex **5**, to our knowledge, contains

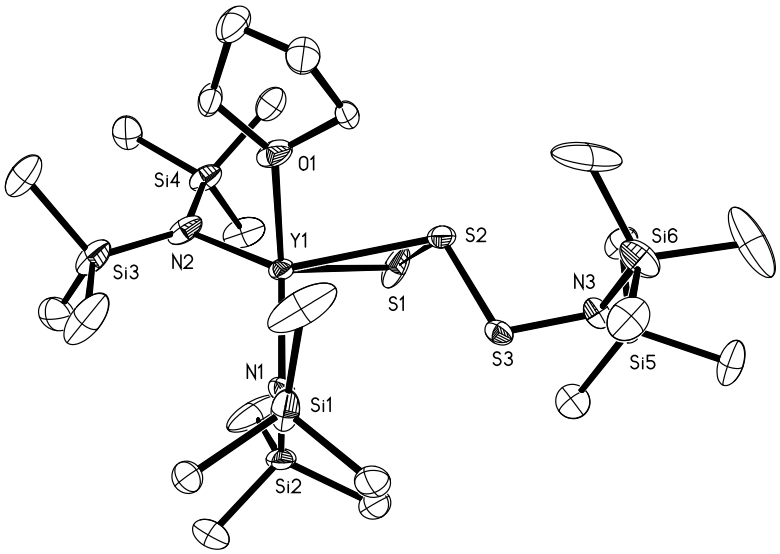

Figure 3.5. Thermal ellipsoid plot of $[(Me_3Si)_2N]_2Y[\eta^2\text{-}S_3N(SiMe_3)_2](THF)$, **5**, drawn at the 50% probability level. Hydrogen atoms are omitted for clarity.

the first example of the $[S_3N(SiMe_3)_2]^{1-}$ ligand. The closest examples of S_3NR_2 moieties of any kind in the crystallographic literature are organic compounds: a bis(fluorosilylamino)trisulfide, $[(^tBu_2FSi)NBu^t]SSS[^tBuN(SiF^tBu_2)]$, isolated in 1973 from sulfur and the lithium salt of the amine,[19] and the benzylidenimine trisulfide, (PhCHN)SSS(NCHPh), identified in 1991 from the reaction of sulfur with benzylamine in the presence of lead oxide.[20]

Synthesis of Selenium Products. In contrast to the reaction of the $(N_2)^{2-}$ complex **1** with elemental sulfur, two equiv of elemental selenium react cleanly with **1** to yield the selenium analog of **3**, namely the $(Se_2)^{2-}$ species $\{[(Me_3Si)_2N]_2Y(THF)\}_2(\mu\text{-}\eta^2\text{:}\eta^2\text{-}Se_2)$, **6**, Figure 3.6, eq 3.2. No contamination of a Se^{2-} complex analogous to **4** was observed in this reaction.

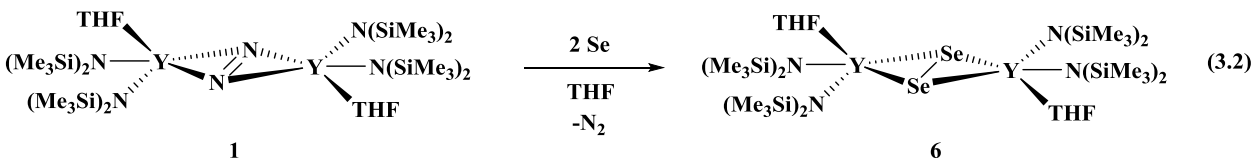

(3.2)

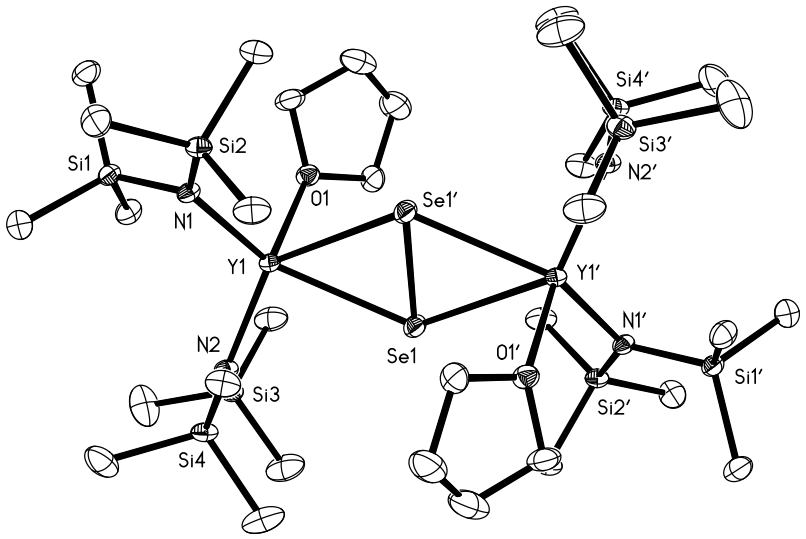

Figure 3.6. Thermal ellipsoid plot of $\{[(Me_3Si)_2N]_2Y(THF)\}_2(\mu\text{-}\eta^2\text{:}\eta^2\text{-}Se_2)$, **6**, drawn at the 50% probability level. Hydrogen atoms are omitted for clarity.

The selenium analog of **4** can also be synthesized by $(N_2)^{2-}$ reduction via **1** by reaction with one equiv of Ph_3PSe, eq 3.3. No heating is required for this reaction as was necessary for the sulfur analog, and the Se^{2-} complex $\{[(Me_3Si)_2N]_2Y(THF)\}_2(\mu\text{-Se})$, **7**, Figure 3.7, can be

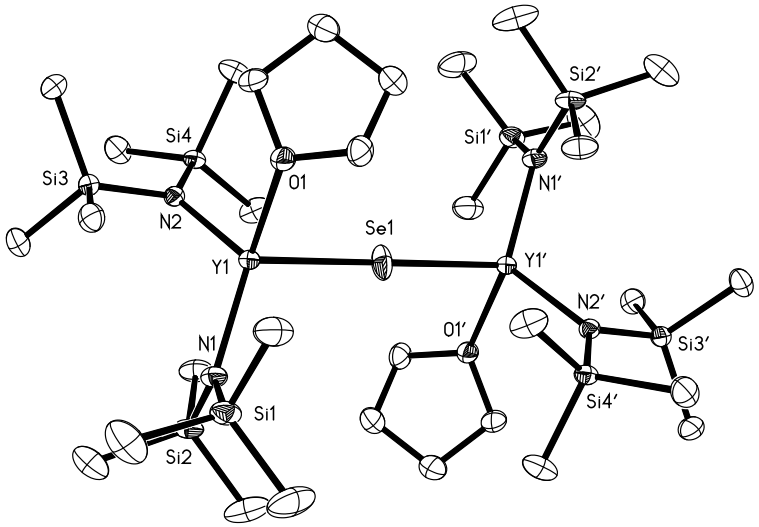

Figure 3.7. Thermal ellipsoid plot of $\{[(Me_3Si)_2N]_2Y(THF)\}_2(\mu\text{-Se})$, **7**, drawn at the 50% probability level. Hydrogen atoms are omitted for clarity.

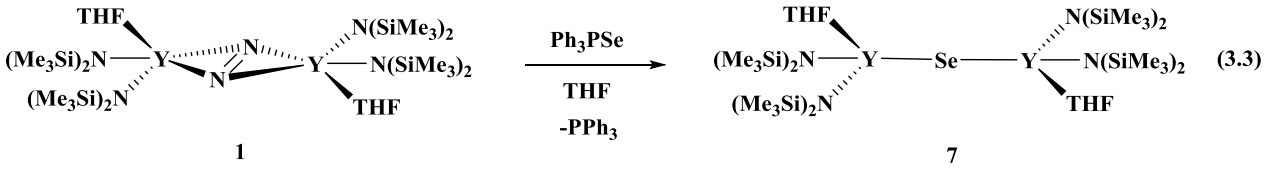

obtained as a pure crystalline product. Addition of KC_8 to the $(Se_2)^{2-}$ complex **6** yields the Se^{2-} complex **7**, eq 3.4, as determined by NMR spectroscopy. The addition of $AgBPh_4$ to **6** also parallels the sulfur reactivity and yields the known cationic complex $\{[(Me_3Si)_2N]_2Y(THF)_2\}\{BPh_4\}$, eq 3.5.[8]

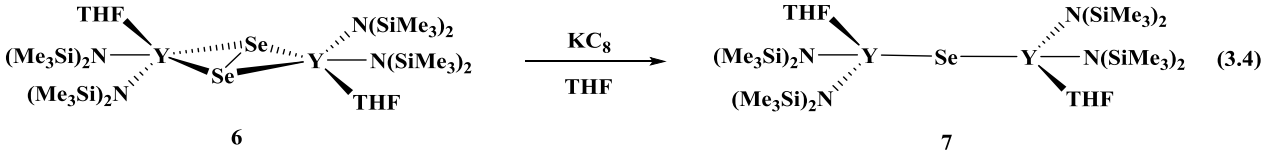

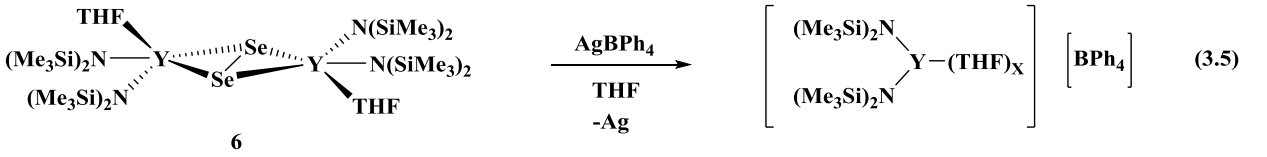

Structure. The structures of **2**, **4**, **5**, **6**, and **7** are compared in Table 3.1. Additional comparison with the oxygen analogs, $\{[(Me_3Si)_2N]_2Y(THF)\}_2(\mu\text{-}\eta^2\text{:}\eta^2\text{-}O_2)$, **8**, and $\{[(Me_3Si)_2N]_2Y(THF)\}_2(\mu\text{-}O)$, **9**, are presented in Table 3.2.[8] The $\{[(Me_3Si)_2N]_2Y(THF)\}^{1+}$ units are similar in all the complexes, both bimetallic and monometallic. This is clearly a flexible metal fragment that can bind a variety of ligands.

Table 3.1. Selected interatomic distances (Å) and angles (º) for complex **2**, $\{[(Me_3Si)_2N]_2Y(THF)\}_2(\mu\text{-}S)$, **4**, $[(Me_3Si)_2N]_2Y[\eta^2\text{-}S_3N(SiMe_3)_2](THF)$, **5**, $\{[(Me_3Si)_2N]_2Y(THF)\}_2(\mu\text{-}\eta^2\text{:}\eta^2\text{-}Se_2)$, **6**, and $\{[(Me_3Si)_2N]_2Y(THF)\}_2(\mu\text{-}Se)$, **7**, where E = S (**2**, **4**, **5**) or Se (**6, 7**).

	Y–E	Y–N	Y–O	N–Y–N	N–Y–E	Y–E–Y′
Complex **2:** $\{[(Me_3Si)_2N]_2Y(THF)\}_2(\mu\text{-}\eta^2\text{:}\eta^2\text{-}S_2)$, **3**/ $\{[(Me_3Si)_2N]_2Y(THF)\}_2(\mu\text{-}S)$, **4**	2.508(3) 2.705(1)	2.231(3) 2.238(3)	2.350(2)	116.36(11)	136.80(7) 90.74(8) 115.63(7) 112.13(8)	180.0 134.22(6)
$\{[(Me_3Si)_2N]_2Y(THF)\}_2(\mu\text{-}S)$, **4**	2.525(7)	2.221(2) 2.234(2)	2.353(2)	116.61(9)	113.39(7) 109.66(7)	180.0
$[(Me_3Si)_2N]_2Y[\eta^2\text{-}S_3N(SiMe_3)_2](THF)$, **5**	2.673(6) 2.840(6)	2.205(2) 2.231(2)	2.350(2)	119.71(7)	105.26(5) 103.76(5) 137.21(5) 99.03(5)	–
$\{[(Me_3Si)_2N]_2Y(THF)\}_2(\mu\text{-}\eta^2\text{:}\eta^2\text{-}Se_2)$, **6**	2.861(4) 2.911(4)	2.234(2) 2.236(2)	2.354(2)	115.58(8)	139.12(6) 89.91(6) 135.81(6) 93.98(5)	130.90(1)
$\{[(Me_3Si)_2N]_2Y(THF)\}_2(\mu\text{-}Se)$, **7**	2.654(2)	2.219(2) 2.229(2)	2.354(1)	116.93(6)	112.35(4) 109.09(4)	180.0

Table 3.2. Selected interatomic distances (Å) and angles (º) for the E^{2-} and $(E_2)^{2-}$ analogs of $\{[(Me_3Si)_2N]_2Y(THF)\}_2(\mu\text{-}E)$ and $\{[(Me_3Si)_2N]_2Y(THF)\}_2(\mu\text{-}\eta^2\text{:}\eta^2\text{-}E_2)$ where E = O, S, or Se.

		E–E	Y–E	Y–Y	E–Y–E′	Y–E–Y′
E^{2-}	$\{[(Me_3Si)_2N]_2Y(THF)\}_2(\mu\text{-}O)$, **9**	-	2.035(3)[a] 2.086(3)	4.091	-	166.23(14)
	$\{[(Me_3Si)_2N]_2Y(THF)\}_2(\mu\text{-}S)$, **4**	-	2.525(7)	5.050	-	180
	$\{[(Me_3Si)_2N]_2Y(THF)\}_2(\mu\text{-}Se)$, **7**	-	2.654(2)	5.309	-	180
$(E_2)^{2-}$	$\{[(Me_3Si)_2N]_2Y(THF)\}_2(\mu\text{-}\eta^2\text{:}\eta^2\text{-}O_2)$, **8**	1.535(3)	2.206(2) 2.240(2)	4.173	40.38(7)	139.62(7)
	$\{[(Me_3Si)_2N]_2Y(THF)\}_2(\mu\text{-}\eta^2\text{:}\eta^2\text{-}S_2)$, **3** (as a portion of complex **2**)	2.118(2) (S1–S1′)	2.705(1) (S1–Y1)	5.016	45.78(5) (S1–Y1–S1′)	134.22(6) (Y1–S1–Y1′)
	$\{[(Me_3Si)_2N]_2Y(THF)\}_2(\mu\text{-}\eta^2\text{:}\eta^2\text{-}Se_2)$, **6**	2.399(5)	2.861(4) 2.911(4)	5.250	49.10(1)	130.90(1)

[a]Oxygen is disordered in the structure.

The Y–S and Y–Se distances in the $\{[(Me_3Si)_2N]_2Y(THF)\}_2(\mu\text{-E})$ complexes **4** and **7** are consistent with the 0.14 Å difference in ionic radii between S^{2-} and Se^{2-} using the radii of Shannon.[21] A direct comparison with the oxygen analog, the O^{2-} complex, $\{[(Me_3Si)_2N]_2Y(THF)\}_2(\mu\text{-O})$,[8] **9,** is not possible because this structure contains a disordered oxide bridge.

Direct structural comparisons of the $(E_2)^{2-}$ series $\{[(Me_3Si)_2N]_2Y(THF)\}_2(\mu\text{-}\eta^2\text{:}\eta^2\text{-}E_2)$, where E = O, S, or Se, are complicated by the fact that the $(S_2)^{2-}$ structure is known only as the 86% component in a model of the co-crystallized mixture **2**. With this caveat, and using the Shannon O^{2-} radius that is 0.44 Å smaller than S^{2-},[21] the Y–E bond lengths follow the expected trends for the increasing size of O, S, and Se from the peroxide, **8**, to the disulfide, **3**, in complex **2**, to the diselenide, **6**. The E–Y–E′ angles also increase as expected as the atoms of the diatomic bridge get larger: **8**, 40.38(7)º; **3**, 45.78(5)º; and **6**, 49.10(1)º. An increase in Y···Y distances is also observed: **8**, 4.173; **3**, 5.016; and **6**, 5.250 Å. The 2.118(2) Å S(1)–S(1′) and 2.399(5) Å Se–Se distances in **2** and **6**, respectively, are consistent with other $(S_2)^{2-}$ and $(Se_2)^{2-}$ distances in the literature.[14,22-24]

In **5**, the $[\eta^2\text{-}S_3N(SiMe_3)_2]^{1-}$ anion ligates the $\{[(Me_3Si)_2N]_2Y(THF)\}^{1+}$ unit through two of the three sulfur atoms in the chain. The terminal sulfur, S(1), has the shorter Y–S distance, 2.673(6) Å, in comparison with the 2.840(6) Å length for Y–S(2). The 2.052(1) Å S(1)–S(2) distance is only slightly shorter than the 2.0823(8) Å S(2)–S(3) length and both are in the range defined by $[(^tBu_2FSi)NBu^t]SSS[^tBuN(SiF^tBu_2)]$, [2.102(1) Å][19] and (PhCHN)SSS(NCHPh), [2.051(1) Å].[20] The 1.704(2) Å S–N distance in **5** is also similar to those in these two organic complexes, 1.668(2) and 1.680(2) Å, in the former[14] and 1.661(3) Å in the latter.[19,20]

Three examples were found in the crystallographic literature in which an S_3 unit is bound η^2 to one metal and η^1 to another atom: $(C_5H_5)_2Ru_2(CO)S_5$,[25] $(C_5H_4{}^tBu)_3Nb_3S_{12}$[26] and $(C_5H_5)Ti(C_5H_5S_5)$.[27] The first two examples have an S_3 ligand bridging two metal centers in polymetallic complexes and the third example has a TiS_3C linkage formed by thermal rearrangement of $(C_5H_5)_2TiS_5$.[28] In all of these metal complexes, the S–S distance between the two sulfur atoms bound to the metal center is shorter than that observed in **5** (2.052(1) Å): Ru, 2.014(7) Å; Nb, 2.038 Å; Ti, 2.025(3) Å. The Nb complex shows a similar difference in metal-sulfur distances (2.481 and 2.600 Å, i.e. 0.119 Å) when compared to **5** (2.673(6) and 2.840(6) Å, i.e. 0.167 Å), but the two S–S distances in the $(S_3)^{2-}$ unit of the Nb complex are nearly the same (2.038 and 2.042 Å). In the Ru complex, the metal-sulfur distances are closer in length to one another, 2.255(4) and 2.362(6) Å, than **5** and the S–S distances are more disparate, 2.014(7) versus 2.110(5) Å.[25] The Ti complex has 2.358(3) and 2.474(3) Å Ti–S distances with a 2.025(3) Å S–S bond between the two coordinating sulfurs and a 2.061(3) Å S–S bond involving the third sulfur attached to the C_5H_5 ring. Hence, there is substantial variation in the coordination parameters of the η^2-S_3 units in the three previously known metal complexes and **5**.

Discussion

The $(N_2)^{2-}$ ligand in $\{[(Me_3Si)_2N]_2Y(THF)\}_2(\mu\text{-}\eta^2\text{:}\eta^2\text{-}N_2)$, **1**, is capable of reducing sulfur and selenium to make analogs of the $(O_2)^{2-}$ complex, $\{[(Me_3Si)_2N]_2Y(THF)\}_2(\mu\text{-}\eta^2\text{:}\eta^2\text{-}O_2)$, **8**, and the O^{2-} complex, $\{[(Me_3Si)_2N]_2Y(THF)\}_2(\mu\text{-}O)$, **9**.[8] The selenium complexes, **6** and **7**, constitute direct parallels with the oxides, but the sulfur system is more complicated because the two analogous complexes co-crystallize with both $\{[(Me_3Si)_2N]_2Y(THF)\}_2(\mu\text{-}\eta^2\text{:}\eta^2\text{-}S_2)$, **3**, and $\{[(Me_3Si)_2N]_2Y(THF)\}_2(\mu\text{-}S)$, **4**, in the same crystal. Co-crystallization of two similarly ligated complexes is well known,[13,29] but few reports involve sulfur. The closest examples found in the

literature involved side by side co-crystallization of two closely related sulfur complexes in the crystal lattice. The fulvalene (Fv) tungsten complexes of $(S_2)^{2-}$ and two $(SH)^{1-}$ ligands, $FvW_2(\mu\text{-}S_2)(CO)_6$ and $FvW_2(SH)_2(CO)_6$,[30] crystallize as two separate molecules in the same unit cell with both tungsten centers on the same side of the fulvalene moiety in the former complex and a trans arrangement of the tungsten atoms across the fulvalene in the latter. Bis(4-aminophenyl) disulfide, $(p\text{-}NH_2Ph)_2(\mu\text{-}S_2)$, crystallizes alongside 4-aminothiophenol, *p*-NH_2PhSH,[31] in the same unit cell. However, co-crystallization of the $S^{2-}/(S_2)^{2-}$ pair in complexes that overlay in all other components has not been reported to our knowledge. We are grateful to a reviewer for pointing out that in the nitrogen-anchored tris(aryloxide)-chelated uranium selenide system, < 7% of the bis$(Se)^{2-}$ bridged U^{V} complex, $\{[(^{Ad}ArO)_3N]U\}_2(\mu\text{-}Se)_2$, crystallizes with the U^{IV} $(Se_4)^{2-}$ complex, $\{[(^{Ad}ArO)_3N]U\}_2(\mu\text{-}\eta^3\text{:}\eta^3\text{-}Se_4)$, and the solvated analog of the latter complex, $\{[(^{Ad}ArO)_3N]U(THF)\}_2(\mu\text{-}\eta^2\text{:}\eta^2\text{-}Se_4)$, crystallizes with 5.5% of the $(Se_3)^{2-}$, complex,$\{[(^{Ad}ArO)_3N]U(THF)\}_2(\mu\text{-}Se_3)$.[29]

It is interesting to note that among all the bimetallic $\{[(Me_3Si)_2N]_2Y(THF)\}^{1+}$ complexes[3,8,17,32] including **2**, **4**, **6**, **7**, **8**, and **9**, only the S^{2-} and $(S_2)^{2-}$ complexes co-crystallize. One difference in the $(O_2)^{2-}$ complex **8** is that it was crystallized with a toluene of solvation which gives it quite different unit cell parameters from the O^{2-} complex **9**.[8] Attempts to obtain the $(S_2)^{2-}$ complex **4** in pure form by crystallizing **2** in the presence of toluene were unsuccessful. One difference between the **3**/**4** pair and the **8**/**9** pair is that **3** and **4** have similar Y···Y distances, 5.016 and 5.050 Å, respectively, while the distances for **8** and **9** are not as close, 4.091 and 4.173 Å, respectively. The **6**/**7** selenium pair are intermediate in this regard, 5.250 and 5.309 Å, respectively.

Sulfur is well known to adopt a variety of forms upon reduction including S^{2-}, $(S_2)^{2-}$ and $(S_3)^{2-}$ in lanthanide containing complexes.[9-12,14,33,34] Hence, the formation of **2-4** is not unexpected. However, other sulfur insertion chemistry occurs in this system as demonstrated by the isolation of $[(Me_3Si)_2N]_2Y[\eta^2\text{-}S_3N(SiMe_3)_2](THF)$, **5**. In this case, not only has sulfur been homologated to make an S_3 chain, but an N–S bond is also formed. Relatively few polysulfur amines have been crystallographically characterized. The route leading to the $[\eta^2\text{-}S_3N(SiMe_3)_2]^-$ ligand, the first of its kind to our knowledge, is unknown. It seems unlikely that sulfur would insert into a strong Y–N$[N(SiMe_3)_2]$ bond or that an $[N(SiMe_3)_2]^-$ ligand would attack $(S_2)^{2-}$ followed by S insertion. The ubiquitous $HN(SiMe_3)_2$, which is typically formed as a byproduct in reactions of rare earth complexes of bis(trimethylsilyl)amide ligands, could be involved in the reaction, but this does not explain the presence of three sulfur atoms.

Examination of the analogous selenium reactions reveals a pattern that differs from both the oxygen and sulfur congeners. Elemental selenium can be used to completely convert the $(N_2)^{2-}$ complex **1** to a $(Se_2)^{2-}$ complex $\{[(Me_3Si)_2N]_2Y(THF)\}_2(\mu\text{-}\eta^2\text{:}\eta^2\text{-}Se_2)$, **6**. While this is consistent with quantitative formation of the $(O_2)^{2-}$ complex $\{[(Me_3Si)_2N]_2Y(THF)\}_2(\mu\text{-}\eta^2\text{:}\eta^2\text{-}O_2)$, **8**, from O_2, the analogous sulfur reaction gives S^{2-} as well as $(S_2)^{2-}$. Ph_3PSe can be used to form the Se^{2-} complex, $\{[(Me_3Si)_2N]_2Y(THF)\}_2(\mu\text{-}Se)$, **7**, while similar oxygen and sulfur delivery reagents were unsuccessful routes to **9** and **4**, respectively.

Conclusion

The $(N_2)^{2-}$ ligand in $\{[(Me_3Si)_2N]_2Y(THF)\}_2(\mu\text{-}\eta^2\text{:}\eta^2\text{-}N_2)$, **1**, can effectively reduce both sulfur and selenium to make $(\mu\text{-}E)^{2-}$ and $(\mu\text{-}E_2)^{2-}$ complexes (E = S, Se) analogous to previously identified oxygen compounds, although Ph_3PSe is a better source for the Se^{2-} compound. The existence of this series demonstrates the coordinative flexibility of the

$\{[(Me_3Si)_2N]_2Y(THF)\}^{1+}$ cation for making bimetallic bridged species. The sulfur reactions provided the first example of co-crystallization of complexes of S^{2-} and $(S_2)^{2-}$ anions, which demonstrates that complexes of these two anions could be difficult to separate and could have very similar structures such that they could be mistaken for each other or a mixture of the two in metallosulfur chemistry. This pair of ions should be added to the list already identified through the bond stretch isomerism saga.[13] These studies also revealed the existence of the $[S_3N(SiMe_3)_2]^{1-}$ ligand and showed another way in which the $[N(SiMe_3)_2]^{1-}$ ligand can be more than an ancillary ligand.[3,35]

Experimental

All syntheses and manipulations described below were conducted under nitrogen or argon with rigorous exclusion of air and water using glovebox, Schlenk, and high-vacuum line techniques. Solvents were sparged with UHP argon and dried over columns containing Q-5 and molecular sieves. Benzene-d_6 was dried over sodium-potassium alloy, degassed using three freeze-pump-thaw cycles, and vacuum transferred before use. Potassium and sodium were washed with hexane and scraped to provide fresh surfaces before use. $\{[(Me_3Si)_2N]_2Y(THF)\}_2(\mu\text{-}\eta^2\text{:}\eta^2\text{-}N_2)$, **1**,[3] and KC_8[36] were prepared according to literature methods. ^1H (500 MHz) and ^{13}C (125 MHz) NMR spectra were obtained on a Bruker CRYO500 MHz spectrometer at 25 ºC in benzene-d_6 unless otherwise stated. IR samples were prepared as KBr pellets on a Varian 1000 FT-IR system. Elemental analyses were performed on a PerkinElmer Series II 2400 CHNS analyzer.

Reaction of $\{[(Me_3Si)_2N]_2Y(THF)\}_2(\mu\text{-}\eta^2\text{:}\eta^2\text{-}N_2)$, 1, with S_8. Addition of S_8 (12 mg, 0.047 mmol) to a stirred pale blue solution of **1** (150 mg, 0.15 mmol) in THF (10 mL) in a

nitrogen-filled glovebox caused an immediate color change to green. The solution became yellow after 20 min. After 1 h, the solvent was removed under reduced pressure to produce a yellow solid that was redissolved in a minimal amount of hexane and stored at −30 ºC. After 1 d, yellow crystals of a material designated as **2** (90 mg) were isolated. X-ray crystallography and NMR spectroscopy revealed these crystals to be a mixture of $\{[(Me_3Si)_2N]_2Y(THF)\}_2(\mu\text{-}\eta^2\text{:}\eta^2\text{-}S_2)$, **3**, and $\{[(Me_3Si)_2N]_2Y(THF)\}_2(\mu\text{-}S)$, **4**. ^{1}H NMR: δ 0.46 (s, 72H, N(Si*Me*$_3$)-**3**), 0.45 (s, 72H, N(Si*Me*$_3$)-**4**). ^{13}C NMR: δ 5.94 (s, N(Si*Me*$_3$)-**3**), 5.77 (s, N(Si*Me*$_3$)-**4**). An additional crop of colorless crystals were isolated from the concentrated mother liquor of **2** at −30 ºC after several weeks and identified as $[(Me_3Si)_2N]_2Y[\eta^2\text{-}S_3N(Me_3Si)_2](THF)$, **5**, by X-ray crystallography.

$\{[(Me_3Si)_2N]_2Y(THF)\}_2(\mu\text{-}S)$, 4. A yellow solution of **2** (160 mg) in THF (7 mL) was treated with KC_8 (13 mg, 0.010 mmol) and stirred. After 1 h, the reaction mixture was filtered to remove black solids. THF was removed under vacuum and the product was extracted with toluene (18 mL). The extract was centrifuged to remove pale insoluble material and the supernatant was concentrated to 2 mL and stored at −35 ºC to provide a small amount of colorless X-ray quality crystals (10 mg) of **4** after several days. ^{1}H NMR: δ 0.45 (s, 72H, N(Si*Me*$_3$)).

$\{[(Me_3Si)_2N]_2Y(THF)\}_2(\mu\text{-}\eta^2\text{:}\eta^2\text{-}Se_2)$, 6. Elemental Se (80 mg, 1.0 mmol) was added to a stirred solution of **1** (400 mg, 0.40 mmol) in THF (15 mL) and the reaction mixture became orange overnight. THF was removed under vacuum to yield orange solids which were dissolved in hexane (50 mL). The orange solution was stored at −30 ºC. Within 1 d, orange X-ray quality crystals of **6** were obtained (340 mg, 75%). ^{1}H NMR: δ 4.05 (m, 8H, THF), 1.32 (m, 8H, THF), 0.48 (s, 72H, N(Si*Me*$_3$)). ^{13}C NMR: δ 6.04 (s, N(Si*Me*$_3$)). IR: 2948s, 2896s, 1456m, 1245s,

977s, 867s, 775s, 662s, 610s cm^{-1}. Anal. Calcd for $\{[(Me_3Si)_2N]_2Y\}_2(\mu\text{-}\eta^2\text{:}\eta^2\text{-}Se_2)(THF)_{1.7}$, **6**•$(THF)_{-0.3}$: C, 33.63; H, 7.84; N, 5.09. Found: C, 33.45; H, 7.85; N, 4.80.

$\{[(Me_3Si)_2N]_2Y(THF)\}_2(\mu$-Se), 7. Ph_3PSe (18 mg, 0.050 mmol) was added to a stirred solution of **1** (50 mg, 0.050 mmol) in toluene (5 mL) and the stirred reaction mixture turned colorless overnight. The colorless solution was concentrated to 3 mL and stored at −30 ºC. After 3 d, colorless X-ray quality crystals of **7** were obtained (35 mg, 67%). ^{1}H NMR: δ 0.46 (s, 72H, N(SiMe_3)). ^{13}C NMR: δ 5.79 (s, N(SiMe_3)). The generation of Ph_3P is also observed by NMR spectroscopy. IR: 2949s, 2894s, 1444m, 1245s, 966s, 830s, 774s, 666s, 610s cm^{-1}. Anal. Calcd for $C_{32}H_{88}N_4O_2SeSi_8Y_2$, **7**: C, 36.87; H, 8.51; N, 5.37. Found: C, 36.44; H, 8.50; N, 5.25.

X-ray Data Collection, Structure Solution and Refinement for 2 identified as a mixture of $\{[(Me_3Si)_2N]_2Y(THF)\}_2(\mu\text{-}\eta^2\text{:}\eta^2\text{-}S_2)$, 3, and $\{[(Me_3Si)_2N]_2Y(THF)\}_2(\mu$-S), 4. A yellow crystal of approximate dimensions 0.301 x 0.286 x 0.243 mm was mounted on a glass fiber and transferred to a Bruker SMART APEX II diffractometer. The APEX2[37] program package was used to determine the unit-cell parameters and for data collection (15 sec/frame scan time for a sphere of diffraction data). The raw frame data was processed using SAINT[38] and SADABS[39] to yield the reflection data file. Subsequent calculations were carried out using the SHELXTL[40] program. There were no systematic absences nor any diffraction symmetry other than the Friedel condition. The centrosymmetric triclinic space group $P\bar{1}$ was assigned and later determined to be correct. The structure was solved by direct methods and refined on F^2 by full-matrix least-squares techniques. The analytical scattering factors[41] for neutral atoms were used throughout the analysis. The molecule is located on an inversion center. The bridging disulfide was disordered. S(1) and S(2) were included using multiple components with partial site-occupancy-factors (0.86:0.14). Hydrogen atoms were included using a riding model. At

convergence, wR2 = 0.1232 and Goof = 1.039 for 244 variables refined against 6272 data (0.75 Å), R1 = 0.0471 for those 5428 data with I > 2.0σ(I). Details are given in Table 3.3.

X-ray Data Collection, Structure Solution and Refinement for {[(Me$_3$Si)$_2$N]$_2$Y(THF)}$_2$(μ-S), 4. A colorless crystal of approximate dimensions 0.406 x 0.121 x 0.101 mm was mounted on a glass fiber and transferred to a Bruker SMART APEX II diffractometer. The APEX2[42] program package was used to determine the unit-cell parameters and for data collection (30 sec/frame scan time for a sphere of diffraction data). The raw frame data was processed using SAINT[43] and SADABS[39] to yield the reflection data file. Subsequent calculations were carried out using the SHELXTL[40] program. There were no systematic absences nor any diffraction symmetry other than the Friedel condition. The centrosymmetric triclinic space group $P\bar{1}$ was assigned and later determined to be correct. The structure was solved by direct methods and refined on F^2 by full-matrix least-squares techniques. The analytical scattering factors[41] for neutral atoms were used throughout the analysis. Hydrogen atoms were included using a riding model. The molecule was located on an inversion center. At convergence, wR2 = 0.1002 and Goof = 1.013 for 235 variables refined against 5926 data (0.77 Å), R1 = 0.0413 for those 4614 data with I > 2.0σ(I). Details are given in Table 3.3.

X-ray Data Collection, Structure Solution and Refinement for [(Me$_3$Si)$_2$N]$_2$Y[η^2-S$_3$N(Me$_3$Si)$_2$](THF), 5. A colorless crystal of approximate dimensions 0.367 x 0.135 x 0.058 mm was mounted on a glass fiber and transferred to a Bruker SMART APEX II diffractometer. The APEX2[37] program package was used to determine the unit-cell parameters and for data collection (15 sec/frame scan time for a sphere of diffraction data). The raw frame data was processed using SAINT[38] and SADABS[39] to yield the reflection data file. Subsequent calculations were carried out using the SHELXTL[40] program. There were no systematic

absences nor any diffraction symmetry other than the Friedel condition. The centrosymmetric triclinic space group $P\bar{1}$ was assigned and later determined to be correct. The structure was solved by direct methods and refined on F^2 by full-matrix least-squares techniques. The analytical scattering factors[41] for neutral atoms were used throughout the analysis. C(1), C(5), and the THF ligand, C(19)-C(22), were disordered and included using multiple components with partial site-occupancy-factors. Hydrogen atoms were included using a riding model. At convergence, wR2 = 0.0805 and Goof = 1.030 for 398 variables refined against 9881 data (0.73 Å), R1 = 0.0365 for those 8073 data with I > 2.0σ(I). Details are given in Table 3.3.

X-ray Data Collection, Structure Solution and Refinement for {[(Me$_3$Si)$_2$N]$_2$Y(THF)}$_2$(μ-η^2:η^2-Se$_2$), 6. An orange crystal of approximate dimensions 0.191 x 0.165 x 0.130 mm was mounted on a glass fiber and transferred to a Bruker SMART APEX II diffractometer. The APEX2[44] program package was used to determine the unit-cell parameters and for data collection (30 sec/frame scan time for a sphere of diffraction data). The raw frame data was processed using SAINT[38] and SADABS[39] to yield the reflection data file. Subsequent calculations were carried out using the SHELXTL[45] program. There were no systematic absences nor any diffraction symmetry other than the Friedel condition. The centrosymmetric triclinic space group $P\bar{1}$ was assigned and later determined to be correct. The structure was solved by direct methods and refined on F^2 by full-matrix least-squares techniques. The analytical scattering factors[41] for neutral atoms were used throughout the analysis. Hydrogen atoms were included using a riding model. The molecule was located about an inversion center (Z = 1). At convergence, wR2 = 0.0773 and Goof = 1.039 for 238 variables refined against 6329 data (0.74 Å), R1 = 0.0324 for those 5142 data with I > 2.0σ(I). Details are given in Table 3.3.

X-ray Data Collection, Structure Solution and Refinement for {[$(Me_3Si)_2N]_2Y(THF)\}_2(\mu$-Se), 7. A colorless crystal of approximate dimensions 0.218 x 0.276 x 0.316 mm was mounted in a cryoloop and transferred to a Bruker SMART APEX II diffractometer. The APEX2[37] program package was used to determine the unit-cell parameters and for data collection (25 sec/frame scan time for a sphere of diffraction data). The raw frame data was processed using SAINT[38] and SADABS[39] to yield the reflection data file. Subsequent calculations were carried out using the SHELXTL[40] program. There were no systematic absences nor any diffraction symmetry other than the Friedel condition. The centrosymmetric triclinic space group $P\bar{1}$ was assigned and later determined to be correct. The structure was solved using the coordinates of the sulfur analogue and refined on F^2 by full-matrix least-squares techniques. The analytical scattering factors[41] for neutral atoms were used throughout the analysis. Hydrogen atoms were included using a riding model. The molecule was located on an inversion center. At convergence, wR2 = 0.0696 and Goof = 1.047 for 235 variables refined against 6282 data (0.75 Å), R1 = 0.0278 for those 5647 data with $I > 2.0\sigma(I)$. Details are given in Table 3.3.

Table 3.3. Crystal data and structure refinement parameters for **2** determined to be a mixture of $\{[(Me_3Si)_2N]_2Y(THF)\}_2(\mu\text{-}\eta^2\text{:}\eta^2\text{-}S_2)$, **3**, and $\{[(Me_3Si)_2N]_2Y(THF)\}_2(\mu\text{-}S)$, **4**, $\{[(Me_3Si)_2N]_2Y(THF)\}_2(\mu\text{-}S)$, **4**, $[(Me_3Si)_2N]_2Y[\eta^2\text{-}S_3N(Me_3Si)_2](THF)$, **5**, $\{[(Me_3Si)_2N]_2Y(THF)\}_2(\mu\text{-}\eta^2\text{:}\eta^2\text{-}Se_2)$, **6** and $\{[(Me_3Si)_2N]_2Y(THF)\}_2(\mu\text{-}Se)$, **7**.

	2	**4**	**5**	**6**	**7**
Empirical formula	C_{32} H_{88} N_4 O_2 S_2 Si_8 Y_2	C_{32} H_{88} N_4 O_2 S Si_8 Y_2	C_{22} H_{62} N_3 O S_3 Si_6 Y	C_{32} H_{88} N_4 O_2 Se_2 Si_8 Y_2	C_{32} H_{88} N_4 O_2 Se Si_8 Y_2
Formula weight	1027.72	995.66	738.37	1121.52	1042.56
Temperature (K)	143(2)	143(2)	88(2)	133(2) K	143(2)
Space group	$P\bar{1}$	$P\bar{1}$	$P\bar{1}$	$P\bar{1}$	$P\bar{1}$
a (Å)	10.6928(8)	10.429(4)	8.8099(5)	10.8331(9)	10.4235(8)
b (Å)	12.0462(9)	12.160(4)	10.0494(6)	11.9995(10)	12.1854(10)
c (Å)	12.1372(9)	12.166(4)	23.8094(14)	12.0793(10)	12.1499(10)
α (°)	60.9538(8)	61.535(4)	101.0619(8)	61.5418(9)	61.9740(9)
β (°)	79.5414(9)	80.236(5)	90.9696(8)	80.0644(10)	80.5568(10)
γ (°)	88.4501(9)	89.078(5)	101.7946(8)	87.4348(10)	88.8205(10)
Volume (Å^3)	1340.63(17)	1332.9(8)	2021.6(2)	1358.5(2)	1340.96(19)
Z	1	1	2	1	1
ρ_{calcd} (Mg/m^3)	1.273	1.240	1.213	1.371	1.291
μ (mm^{-1})	2.440	2.414	1.794	3.671	3.039
$R1$[a]	0.0471	0.0413	0.0365	0.0324	0.0278
$wR2$[b]	0.1232	0.1002	0.0805	0.0773	0.0696

[a] $R1 = \Sigma||F_o|-|F_c|| / \Sigma|F_o|$. [b] $wR2 = [\Sigma[w(F_o^2-F_c^2)^2] / \Sigma[w(F_o^2)^2]]^{1/2}$

References

(1) Evans, W. J.; Lee, D. S.; Ziller, J. W. *Journal of the American Chemical Society* **2003**, *126*, 454.

(2) Evans, W. J.; Fang, M.; Zucchi, G. l.; Furche, F.; Ziller, J. W.; Hoekstra, R. M.; Zink, J. I. *Journal of the American Chemical Society* **2009**, *131*, 11195.

(3) Fang, M.; Bates, J. E.; Lorenz, S. E.; Lee, D. S.; Rego, D. B.; Ziller, J. W.; Furche, F.; Evans, W. J. *Inorganic Chemistry* **2011**, *50*, 1459.

(4) Meihaus, K. R.; Corbey, J. F.; Fang, M.; Ziller, J. W.; Long, J. R.; Evans, W. J. *Inorganic Chemistry* **2014**, *53*, 3099.

(5) Rinehart, J. D.; Fang, M.; Evans, W. J.; Long, J. R. *Nature Chemistry* **2011**, *3*, 538.

(6) Rinehart, J. D.; Fang, M.; Evans, W. J.; Long, J. R. *Journal of the American Chemical Society* **2011**, *133*, 14236.

(7) Evans, W. J.; Fang, M.; Bates, J. E.; Furche, F.; Ziller, J. W.; Kiesz, M. D.; Zink, J. I. *Nature Chemistry* **2010**, *2*, 644.

(8) Farnaby, J. H.; Fang, M.; Ziller, J. W.; Evans, W. J. *Inorganic Chemistry* **2012**, *51*, 11168.

(9) Evans, W. J.; Rabe, G. W.; Ziller, J. W.; Doedens, R. J. *Inorganic Chemistry* **1994**, *33*, 2719.

(10) Kornienko, A.; Moore, B. F.; Kumar, G. A.; Tan, M.-C.; Riman, R. E.; Brik, M. G.; Emge, T. J.; Brennan, J. G. *Inorganic Chemistry* **2011**, *50*, 9184.

(11) Moore, B. F.; Kumar, G. A.; Tan, M.-C.; Kohl, J.; Riman, R. E.; Brik, M. G.; Emge, T. J.; Brennan, J. G. *Journal of the American Chemical Society* **2010**, *133*, 373.

(12) Kornienko, A.; Emge, T. J.; Kumar, G. A.; Riman, R. E.; Brennan, J. G. *Journal of the American Chemical Society* **2005**, *127*, 3501.

(13) Parkin, G. *Accounts of Chemical Research* **1992**, *25*, 455.

(14) Zhang, Z.; Zhang, L.; Li, Y.; Hong, L.; Chen, Z.; Zhou, X. *Inorganic Chemistry* **2010**, *49*, 5715.

(15) Cheng, M.-L.; Li, H.-X.; Zhang, W.-H.; Ren, Z.-G.; Zhang, Y.; Lang, J.-P. *European Journal of Inorganic Chemistry* **2007**, *2007*, 1889.

(16) Goh, L. Y.; Hambley, T. W.; Robertson, G. B. *Organometallics* **1987**, *6*, 1051.

(17) Fang, M.; Lee, D. S.; Ziller, J. W.; Doedens, R. J.; Bates, J. E.; Furche, F.; Evans, W. J. *Journal of the American Chemical Society* **2011**, *133*, 3784.

(18) Hitchcock, P. B.; Lappert, M. F.; Pierssens, L. J. M. *Chemical Communications* **1996**, 1189.

(19) Klingebiel, U.; Pauer, F.; Sheldrick, G. M.; Stalke, D. *Chemische Berichte* **1991**, *124*, 2651.

(20) Barrick, J. C.; Calvo, C.; Olsen, F. P. *Canadian Journal of Chemistry* **1973**, *51*, 3697.

(21) Shannon, R. *Acta Crystallographica Section A* **1976**, *32*, 751.

(22) Evans, W. J.; Nyce, G. W.; Clark, R. D.; Doedens, R. J.; Ziller, J. W. *Angewandte Chemie International Edition* **1999**, *38*, 1801.

(23) Brown, J. L.; Wu, G.; Hayton, T. W. *Organometallics* **2012**, *32*, 1193.

(24) Fitzgerald, M.; Emge, T. J.; Brennan, J. G. *Inorganic Chemistry* **2002**, *41*, 3528.

(25) Brunner, H.; Janietz, N.; Wachter, J.; Nuber, B.; Ziegler, M. L. *Journal of Organometallic Chemistry* **1988**, *356*, 85.

(26) Brunner, H.; Meier, W.; Wachter, J.; Nuber, B.; Ziegler, M. L. *Journal of Organometallic Chemistry* **1990**, *381*, C7.

(27) Giolando, D. M.; Rauchfuss, T. B.; Wilson, S. R. *Journal of the American Chemical Society* **1984**, *106*, 6455.

(28) Tebbe, F. N.; Wasserman, E.; Peet, W. G.; Vatvars, A.; Hayman, A. C. *Journal of the American Chemical Society* **1982**, *104*, 4971.

(29) Franke, S. M.; Heinemann, F. W.; Meyer, K. *Chemical Science* **2014**, *5*, 942.

(30) Capps, K. B.; Whitener, G. D.; Bauer, A.; Abboud, K. A.; Wasser, I. M.; Vollhardt, K. P. C.; Hoff, C. D. *Inorganic Chemistry* **2002**, *41*, 3212.

(31) Vangala, V. R.; Desiraju, G. R.; Jetti, R. K. R.; Blaser, D.; Boese, R. *Acta Crystallographica Section C* **2002**, *58*, o635.

(32) Corbey, J. F.; Farnaby, J. H.; Bates, J. E.; Ziller, J. W.; Furche, F.; Evans, W. J. *Inorganic Chemistry* **2012**, *51*, 7867.

(33) Li, Y.; Pi, C.; Zhang, J.; Zhou, X.; Chen, Z.; Weng, L. *Organometallics* **2005**, *24*, 1982.

(34) Turcitu, D.; Nief, F.; Ricard, L. *Chemistry – A European Journal* **2003**, *9*, 4916.

(35) Korobkov, I.; Gambarotta, S. *Inorganic Chemistry* **2010**, *49*, 3409.

(36) Bergbreiter, D. E.; Killough, J. M. *Journal of the American Chemical Society* **1978**, *100*, 2126.

(37) APEX2 Version 2013.10-0, Bruker AXS, Inc.; Madison, WI 2013.

(38) SAINT Version 8.34a, Bruker AXS, Inc.; Madison, WI 2013.

(39) Sheldrick, G. M. SADABS, Version 2012/1, Bruker AXS, Inc.; Madison, WI 2012.

(40) Sheldrick, G. M. SHELXTL, Version 2013/4, Bruker AXS, Inc.; Madison, WI 2013.

(41) International Tables for Crystallography 1992, Vol. C., Dordrecht: Kluwer Academic Publishers.

(42) APEX2 Version 2011.4-1, Bruker AXS, Inc.; Madison, WI 2011.

(43) SAINT Version 7.68a, Bruker AXS, Inc.; Madison, WI 2009.

(44) APEX2 Version 2014.1-1, Bruker AXS, Inc.; Madison, WI 2014.

(45) Sheldrick, G. M. SHELXTL, Version 2014/2, Bruker AXS, Inc.; Madison, WI 2014.

CHAPTER 4

Crystallographic Characterization of a Second Molecular Example of the $(NO)^{2-}$ Radical: $\{[(Me_3Si)_2N]_2(THF)Tb\}_2(\mu\text{-}\eta^2\text{:}\eta^2\text{-NO})$

Introduction

The first molecular examples of the $(N_2)^{3-}$ radical anion were found in the bimetallic rare earth complexes $[K(THF)_6][A_2(THF)Ln]_2(\mu\text{-}\eta^2\text{:}\eta^2\text{-}N_2)$ and $\{K[A_2(THF)Ln]_2(\mu_3\text{-}\eta^2\text{:}\eta^2\text{:}\eta^2\text{-}N_2)\}$ (Ln = Dy, Y; A = $[OC_6H_3(^tBu)_2\text{-}2,6]^-$, $[N(SiMe_3)_2]^-$).[1] In the course of exploring the reactivity of this new form of reduced dinitrogen, it was found that $K\{[(Me_3Si)_2N]_2(THF)Y\}_2(\mu_3\text{-}\eta^2\text{:}\eta^2\text{:}\eta^2\text{-}N_2)$ can reduce nitric oxide to form yet another new reduced diatomic ion, namely the $(NO)^{2-}$ radical. This first example of $(NO)^{2-}$ was isolated as the bridging unit in the bimetallic yttrium complex $\{[(Me_3Si)_2N]_2(THF)Y\}_2(\mu\text{-}\eta^2\text{:}\eta^2\text{-NO})$, **1**, eq 4.1.[2]

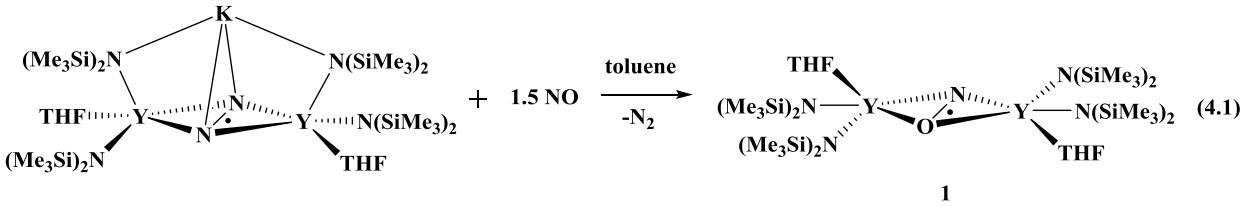

As exemplified in the literature and in previous chapters of this dissertation, the discovery that radical bridging ligands can couple unpaired spins of highly paramagnetic lanthanides has revolutionized the field of single-molecule magnets (SMMs).[3-9] With this in mind, it was of interest to synthesize the paramagnetic lanthanide analogs of the $(NO)^{2-}$ radical complex, **1**, in

order to compare their magnetic properties with those of the previously reported record breaking SMMs which contain the $(N_2)^{3-}$ radical bridging anion.[4]

Results and Discussion

Synthesis. In a similar fashion to the synthesis of **1**,[2] the Tb analog, {[$(Me_3Si)_2N$]$_2$(THF)Tb}$_2$(μ-η^2:η^2-NO), **2**, Figures 4.1 and 4.2, was made by reacting the $(N_2)^{3-}$ precursor K{[$(Me_3Si)_2N$]$_2$(THF)Tb}$_2$(μ_3-η^2:η^2:η^2-N_2)[8] with 1.5 equiv of nitric oxide, eq 4.2. A byproduct of this reaction is the $(N_2)^{2-}$ compound {[$(Me_3Si)_2N$]$_2$(THF)Tb}$_2$(μ-η^2:η^2-N_2), **3**,[2,10] which has similar solubility and crystallinity to **2** making isolation of pure samples challenging. Attempts were made to preferentially crystallize the more highly paramagnetic **2** away from the $(N_2)^{2-}$ byproduct **3** using an external magnetic field.[8] However, this technique was not particularly effective in this case. Due to the similar morphology and crystal colors of the $(NO)^{2-}$ species (**1** is very pale green, **2** is colorless) versus the pale blue $(N_2)^{2-}$ byproducts in each case, it is difficult, even when using a microscope to determine by eye if the crystalline batch is pure.[2] The elemental analysis data for **2** (C, 32.76; H, 7.53; N, 6.81) show that partial desolvation of THF occurs upon drying the sample prior to obtaining measurements, which is consistent with what was observed for compound **1**.[2] In comparing these data with the expected values for the $(N_2)^{2-}$ byproduct **3** (C, 33.96; H, 7.84; N, 7.43), it can be seen that the percent nitrogen and carbon in **2** are significantly lower than in **3**, consistent with an $(NO)^{2-}$ rather than an $(N_2)^{2-}$ moiety in samples of **2**.

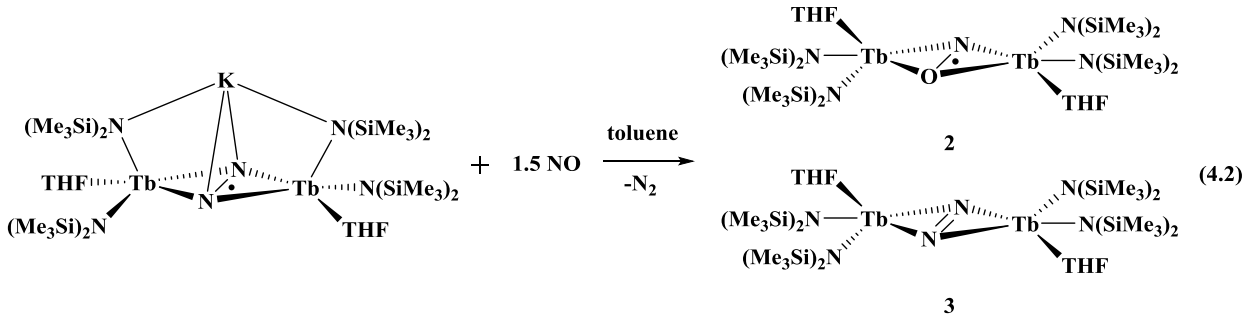

(4.2)

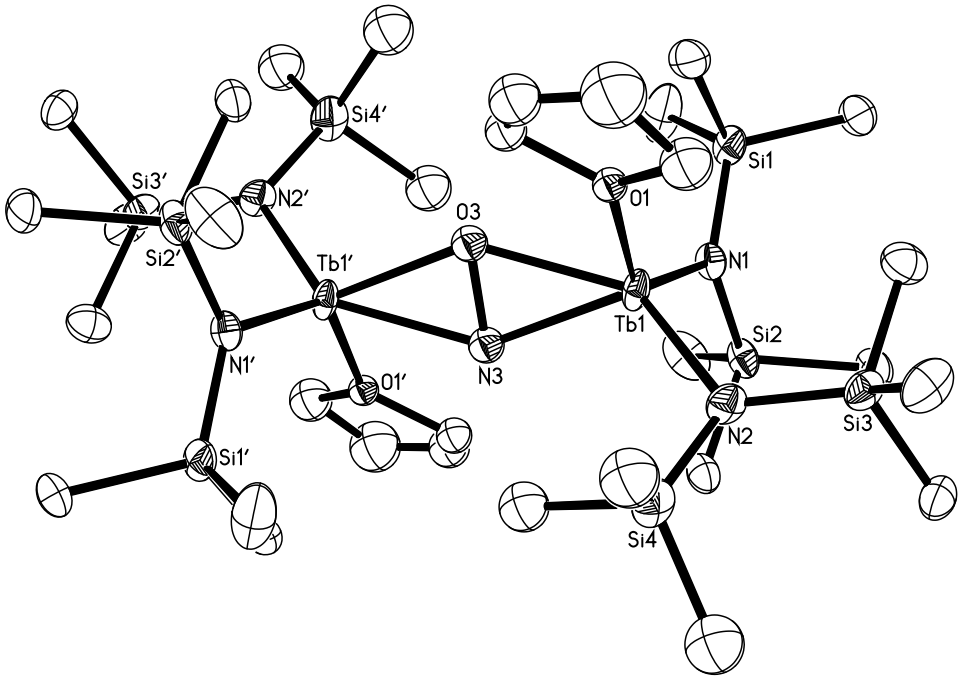

Figure 4.1. Thermal ellipsoid plot of $\{[(Me_3Si)_2N]_2(THF)Tb\}_2(\mu\text{-}\eta^2\text{:}\eta^2\text{-NO})$, **2**, drawn at the 30% probability level. Disorder in the ligands and the N3 and O3 positions is not shown. Hydrogen atoms and co-crystallized toluene have been omitted for clarity.

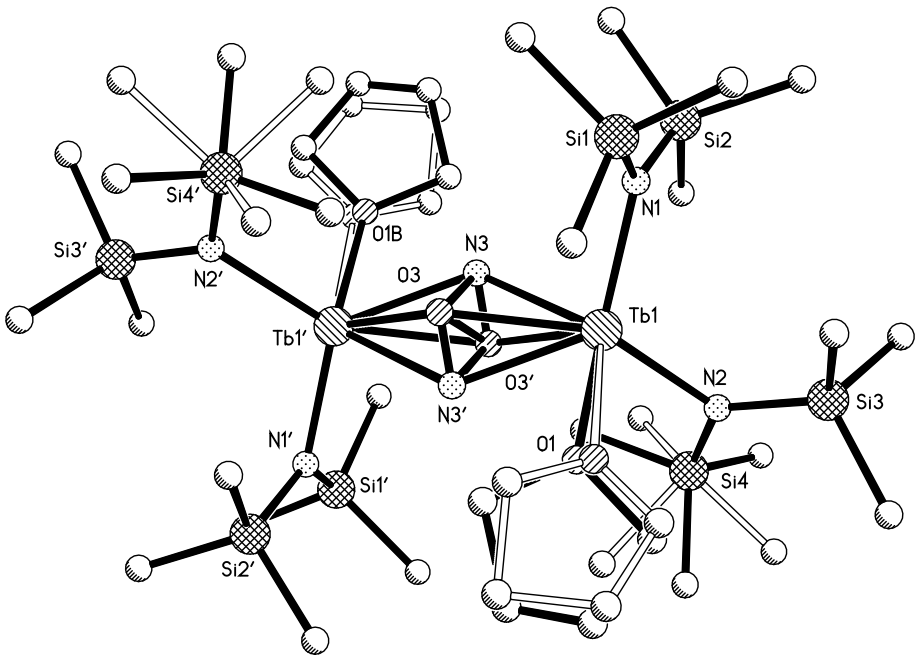

Figure 4.2. Crystal structure of $\{[(Me_3Si)_2N]_2(THF)Tb\}_2(\mu\text{-}\eta^2\text{:}\eta^2\text{-NO})$, **2**, displaying modeled disorder. Hydrogen atoms and co-crystallized toluene have been omitted for clarity.

Structural Analysis. $\{[(Me_3Si)_2N]_2(THF)Tb\}_2(\mu\text{-}\eta^2\text{:}\eta^2\text{-NO}) \bullet (C_7H_8)$, **2**, Figure 4.1, crystallizes in thetriclinic space group $P\bar{1}$, and the molecule is located about an inversion center. There is significant disorder in the ancillary ligands and the bridging diatomic ligand, which was successfully modeled using multiple components with partial site-occupancy-factors to give satisfactory refinement values (Table 4.2). The disordered plot is shown in Figure 4.2. The previously reported $\{[(Me_3Si)_2N]_2(THF)Y\}_2(\mu\text{-}\eta^2\text{:}\eta^2\text{-NO}) \bullet (THF)_2$, **1**, which crystallizes in the monoclinic space group *P*21/*c*, displays similar disorder in the diatomic bridging unit which is again located about an inversion center. This type of disorder is common for heterodiatomic ligands in otherwise symmetric environments.[11] As a result, the N–O distance in **1** is reported to have values ranging from 1.346(5) to 1.390(4) Å depending on the crystallographic model employed.[2] The N–O distances in **2** are 1.084(8) Å and 1.497(8) Å. The former is shorter than

that in free nitric oxide[12] and the latter is longer than the typical 1.44 to 1.47 Å distances[13] expected for an N–O single bond. These unreasonable distances are likely an artifact of the disorder model. The relatively high standard deviations associated with these bond lengths could be a consequence of the significant disorder throughout the molecular structure and makes subsequent conclusions regarding these distances problematic. Further spectroscopic scrutiny was employed to ascertain the identity of the bridging diatomic ligand in **2**.

Spectroscopic Studies. The highly paramagnetic and anisotropic nature of Tb^{3+} complexes in general precluded the use of NMR and EPR spectroscopies in the characterization of **2**.[14] The IR spectrum of **2** did not contain absorptions analogous to the two weak peaks found in samples of **1** at 1509 and 1382 cm^{-1}, which might be attributed to an N–O bond. As a more useful method for examining the presence of an N–N bond, Raman data were also collected on **2**, with assistance from Megan Fieser, and this spectrum is compared in Figure 4.3 to the previously reported spectral data for **1** as well as the ^{15}N-labeled analog of **1**.[2] Raman data on the suspected byproduct **3** and the $(N_2)^{3-}$ starting material for the reaction in eq 4.2, $K\{[(Me_3Si)_2N]_2(THF)Tb\}_2(\mu_3\text{-}\eta^2\text{:}\eta^2\text{:}\eta^2\text{-}N_2)$, were also collected and are shown in Figure 4.4.

The previously reported Raman spectrum of **1** displays a weak feature at 951 cm^{-1}, Figure 8.3 (top), which was assigned to the N–O bond using isotopic labeling studies.[2] As can be seen in the Raman spectrum of **2**, Figure 4.3 (bottom), the closest peak to that observed for **1** is significantly shifted at 917 cm^{-1}. This is a more drastic shift than would be expected simply due to the differing metal types of Y versus Tb, which would only be expected to cause shifts of a few wavenumbers.[1] Consequently, isotopic labeling studies will ultimately need to be performed to determine whether a band associated with the N–O bond is present in measurements of **2**. While an obvious peak associated with the N–O bond cannot be located in

the Raman spectrum of **2**, there is a band at 1430 cm^{-1}, which is very close to the 1428 cm^{-1} band assigned to the N–N bond in the byproduct **3**, suggesting the presence of **3** in crystalline samples of **2**. There is, however, no evidence of the starting material $K\{[(Me_3Si)_2N]_2(THF)Tb\}_2(\mu_3\text{-}\eta^2\text{:}\eta^2\text{:}\eta^2\text{-}N_2)$, whose N–N vibrational mode can be observed at 996 cm^{-1}, Figure 4.4 (bottom). It should also be noted that the $(N_2)^{3-}$ reagent $K\{[(Me_3Si)_2N]_2(THF)Tb\}_2(\mu_3\text{-}\eta^2\text{:}\eta^2\text{:}\eta^2\text{-}N_2)$ is highly reactive and has been known to thermally decompose into the neutral species **3**.[8] A comparison of the relevant Raman vibrational frequencies for **1** and **2** as well as their respective $(N_2)^{3-}$ precursors and the $(N_2)^{2-}$ byproducts can be found in Table 4.1.

Table 4.1. Raman vibrational frequencies associated with the diatomic bridging ligands in $\{[(Me_3Si)_2N]_2(THF)Y\}_2(\mu\text{-}\eta^2\text{:}\eta^2\text{-NO})$, **1**,[2] $\{[(Me_3Si)_2N]_2(THF)Tb\}_2(\mu\text{-}\eta^2\text{:}\eta^2\text{-NO})$, **2**, $\{[(Me_3Si)_2N]_2(THF)Y\}_2(\mu\text{-}\eta^2\text{:}\eta^2\text{-}N_2)$,[1] $\{[(Me_3Si)_2N]_2(THF)Tb\}_2(\mu\text{-}\eta^2\text{:}\eta^2\text{-NO})$, **3**, $\{[(Me_3Si)_2N]_2(THF)Y\}_2(\mu_3\text{-}\eta^2\text{:}\eta^2\text{:}\eta^2\text{-}N_2)K$[1] and $\{[(Me_3Si)_2N]_2(THF)Tb\}_2(\mu_3\text{-}\eta^2\text{:}\eta^2\text{:}\eta^2\text{-}N_2)K$.

Compound	**Raman Shift (cm^{-1})**
$\{[(Me_3Si)_2N]_2(THF)Y\}_2(\mu\text{-}\eta^2\text{:}\eta^2\text{-NO})$, **1**	951
$\{[(Me_3Si)_2N]_2(THF)Tb\}_2(\mu\text{-}\eta^2\text{:}\eta^2\text{-NO})$, **2**	917, 1430
$\{[(Me_3Si)_2N]_2(THF)Y\}_2(\mu\text{-}\eta^2\text{:}\eta^2\text{-}N_2)$[1]	1425
$\{[(Me_3Si)_2N]_2(THF)Tb\}_2(\mu\text{-}\eta^2\text{:}\eta^2\text{-NO})$, **3**	1428
$K\{[(Me_3Si)_2N]_2(THF)Y\}_2(\mu_3\text{-}\eta^2\text{:}\eta^2\text{:}\eta^2\text{-}N_2)$[1]	989
$K\{[(Me_3Si)_2N]_2(THF)Tb\}_2(\mu_3\text{-}\eta^2\text{:}\eta^2\text{:}\eta^2\text{-}N_2)$	996

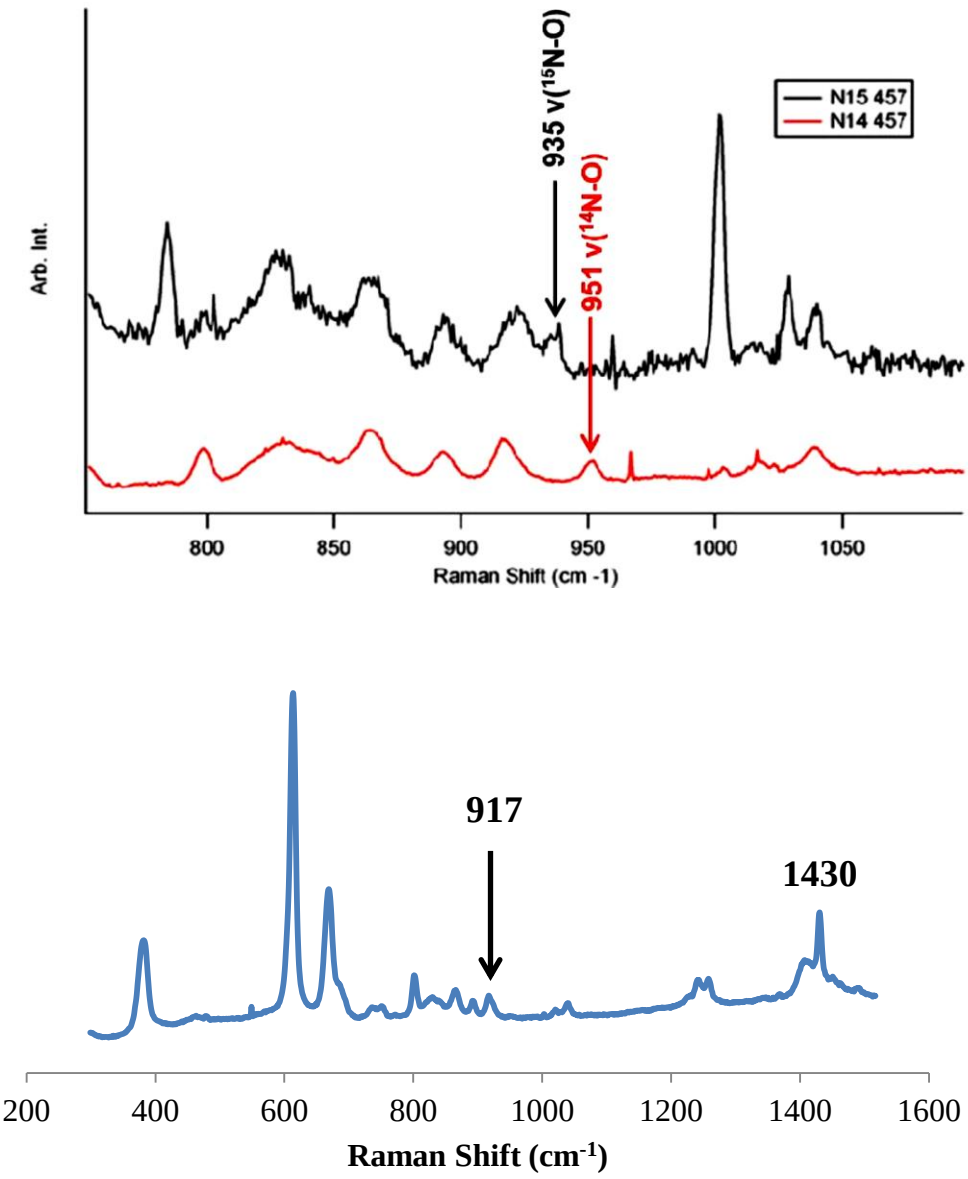

Figure 4.3. Raman spectra of (top) the previously reported $\{[(Me_3Si)_2N]_2(THF)Y\}_2(\mu\text{-}\eta^2\text{:}\eta^2\text{-NO})$, **1**, as well as its ^{15}N labeled analogue[2] compared to (bottom) crystalline samples of $\{[(Me_3Si)_2N]_2(THF)Tb\}_2(\mu\text{-}\eta^2\text{:}\eta^2\text{-NO})$, **2**.

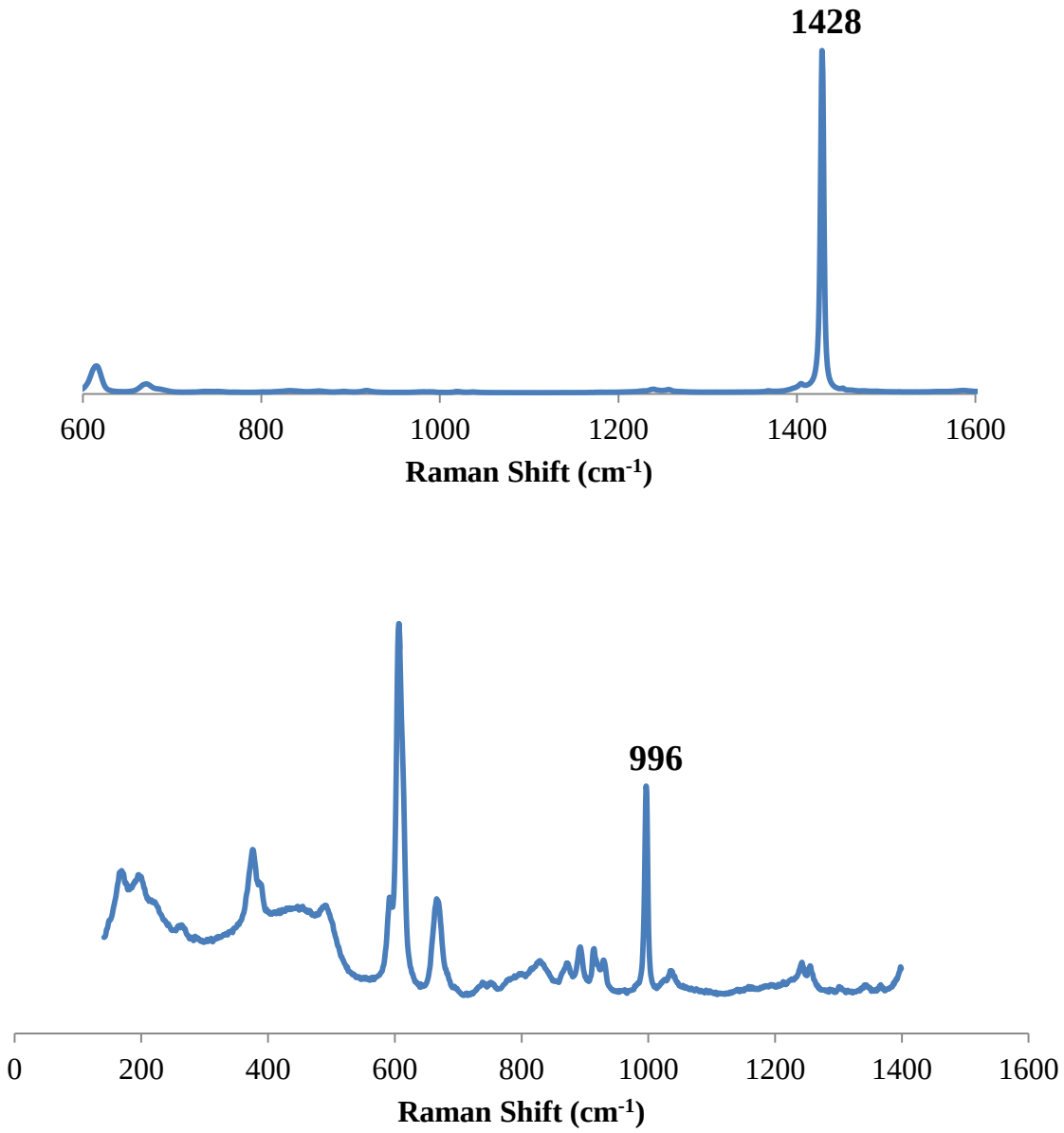

Figure 4.4. Raman spectra of (top) crystalline samples of $\{[(Me_3Si)_2N]_2(THF)Tb\}_2(\mu\text{-}\eta^2\text{:}\eta^2\text{-}N_2)$, **3**, and (bottom) crystalline samples of $K\{[(Me_3Si)_2N]_2(THF)Tb\}_2(\mu_3\text{-}\eta^2\text{:}\eta^2\text{:}\eta^2\text{-}N_2)$, the starting reagent in eq 4.2.[8]

Preliminary Magnetic Measurements. Direct current magnetic susceptibility measurements were performed by Katie Meihaus in the laboratory of Professor Jeffrey Long at

the University of California, Berkeley on samples of **2** which were determined by elemental analysis, also obtained at UC Berkeley, to have one toluene molecule per formula unit (C, 38.22; H, 7.89; N, 5.71) which is consistent with the crystallographic data. When compared with the elemental analysis values expected for **3** and including one toluene per molecular formula (C, 38.28; H, 7.91; N, 6.87), again, the percent nitrogen is significantly lower in **2** than in **3**. This is consistent with the presence of $(NO)^{2-}$ rather than $(N_2)^{2-}$ in samples of **2**. However, the magnetic susceptibility data for **2**, shown in Figure 4.5 (blue circles), do not indicate strong magnetic coupling of the Tb centers as would be expected through a radical bridging diatomic ligand.[3,4] Rather, the $\chi_M T$ versus T data looks very reminiscent of the simple paramagnet $\{[(Me_3Si)_2N]_2(THF)Tb\}_2(\mu\text{-}\eta^2\text{:}\eta^2\text{-}N_2)$, **3**, compared in Figure 4.5 (green circles). Indeed, ac magnetic susceptibility measurements on samples of **2** were found to undergo fast magnetic relaxation, even in the presence of an applied dc field. Hence, no evidence of strong magnetic coupling via an $(NO)^{2-}$ ligand was obtainable with this sample.

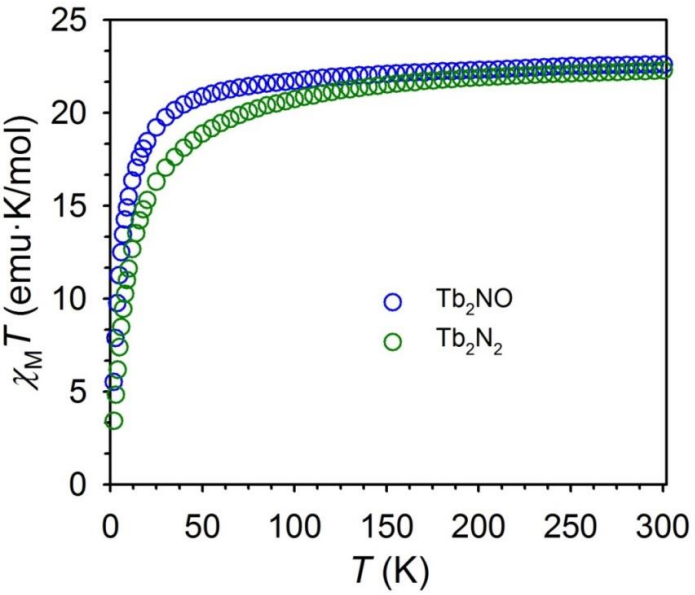

Figure 4.5. Plot of the product of the molar magnetic susceptibility and temperature ($\chi_M T$) as a function of temperature (T) for **2** (blue circles) and **3** (green circles).

[NO][BF_4]. Due to the difficulty in isolating pure samples of **2** via the reaction shown in eq 8.2, it was of interest to determine if the $(NO)^{2-}$ complexes **1** and **2** could be synthesized by other routes. One of the routes explored involves addition of the nitrosonium salt [NO][BF_4] to the $(N_2)^{3-}$ precursor K{[$(Me_3Si)_2N$]$_2$(THF)Ln}$_2$(μ_3-η^2:η^2:η^2-N_2) used above. Reactions were first pursued with Ln = Y, because its nuclear spin of I = ½ makes EPR and NMR useful spectroscopic techniques in characterizing the products of these reactions. Upon addition of the colorless nitrosonium salt to an intense yellow solution of K{[$(Me_3Si)_2N$]$_2$(THF)Y}$_2$(μ_3-η^2:η^2:η^2-N_2) in diethyl ether, the reaction solution became colorless. A preliminary EPR spectrum of this crude reaction solution is shown in Figure 4.6 (top). Although this spectrum vaguely resembles an unresolved triplet of triplets, which would be expected for radical coupling to two nuclear spin I = ½ ^{89}Y atoms and one I = 1 ^{14}N atom, it looks very different from the well-resolved spectrum previously reported for **1** shown in Figure 4.6 (bottom).[2] Additionally, pale blue crystals of the $(N_2)^{2-}$ byproduct {[$(Me_3Si)_2N$]$_2$(THF)Y}$_2$(μ-η^2:η^2-N_2) were isolated from the reaction with [NO][BF_4] as identified by X-ray crystallography.

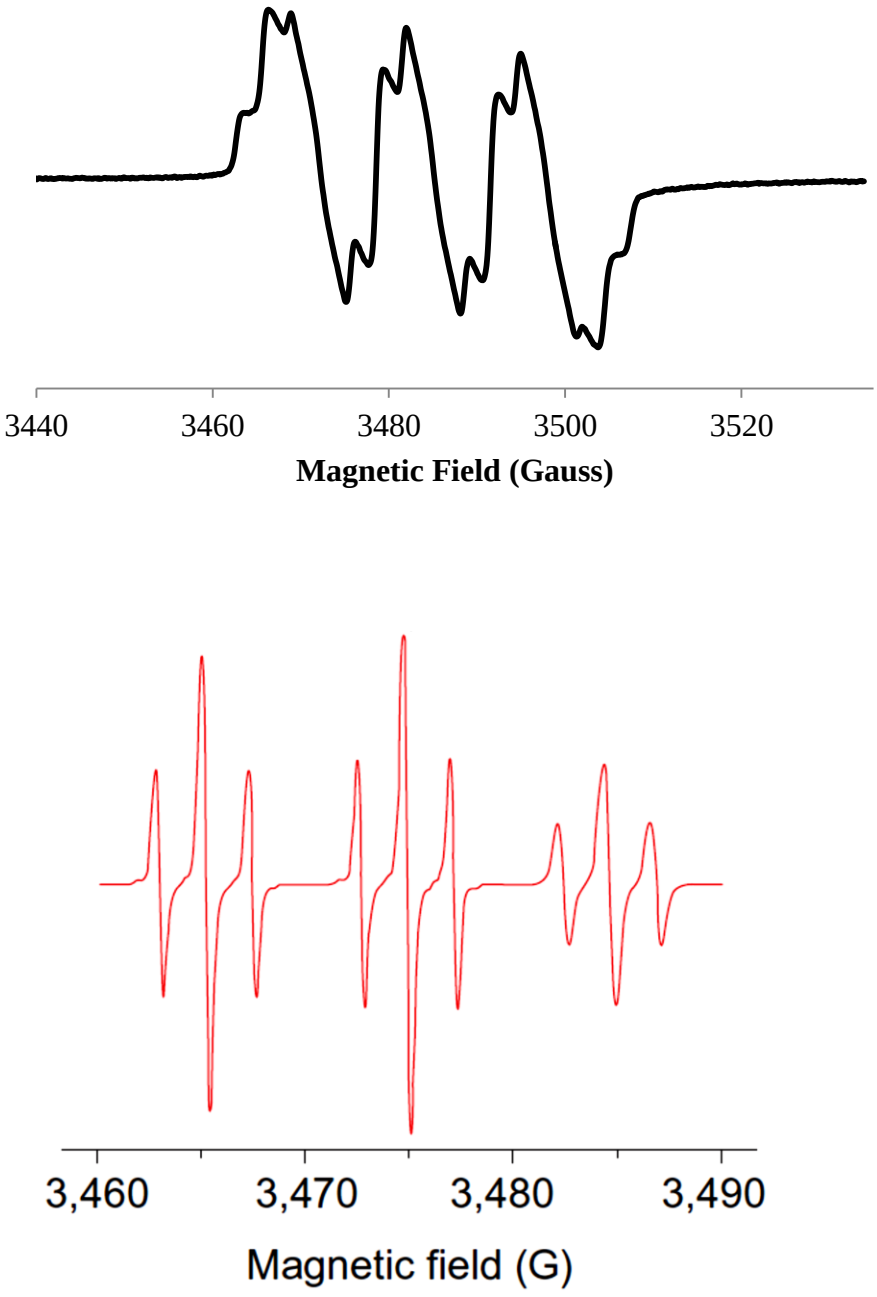

Figure 4.6. (Top) Resulting EPR spectrum after addition of $[NO][BF_4]$ to $K\{[(Me_3Si)_2N]_2(THF)Y\}_2(\mu_3\text{-}\eta^2\text{:}\eta^2\text{:}\eta^2\text{-}N_2)$ and (bottom) the previously reported EPR spectrum for **1**.[2]

Conclusion

X-ray crystallographic data and elemental analysis suggest that the Tb analog of the first $(NO)^{2-}$-containing complex $\{[(Me_3Si)_2N]_2(THF)Y\}_2(\mu\text{-}\eta^2\text{:}\eta^2\text{-NO})$, **1**, has been synthesized via similar methods making $\{[(Me_3Si)_2N]_2(THF)Tb\}_2(\mu\text{-}\eta^2\text{:}\eta^2\text{-NO})$, **2**, the second crystallographically characterized example of an $(NO)^{2-}$ radical-containing complex. However, magnetic susceptibility data on samples of **2** did not show SMM behavior, and the presence of the $(N_2)^{2-}$ byproduct, namely $\{[(Me_3Si)_2N]_2(THF)Tb\}_2(\mu\text{-}\eta^2\text{:}\eta^2\text{-}N_2)$, **3**, was observable by Raman spectroscopy. These results exemplify the importance of acquiring additional characterization data to support X-ray crystallographic findings.

Experimental

All syntheses and manipulations described below were conducted under nitrogen or argon with rigorous exclusion of air and water using glovebox, Schlenk, and high-vacuum line techniques. Solvents were sparged with UHP argon and dried over columns containing Q-5 and molecular sieves. Potassium and sodium were purchased from Aldrich, washed with hexanes, and scraped to provide fresh surfaces before use. $[NO][BF_4]$ was purchased from Sigma Aldrich and used as received. $K\{[(Me_3Si)_2N]_2(THF)Ln\}_2(\mu_3\text{-}\eta^2\text{:}\eta^2\text{:}\eta^2\text{-}N_2)$ (Ln = Tb,[8] Y[1]) were synthesized according to the literature. IR samples were prepared as KBr pellets on a Varian 1000 FT-IR system. EPR spectra were collected using a Bruker EMX spectrometer equipped with an ER041XG microwave bridge. Elemental analyses were performed on a PerkinElmer Series II 2400 CHN analyzer. Raman experiments were performed on crystalline samples in a quartz cell sealed with a Teflon stopcock with a Renishaw inVia confocal Raman microscope using 532 nm laser excitation (laser power 10%, laser focus 50% at 200 s exposure) and a 5 X

objective lens. Magnetic susceptibility measurements were collected using a Quantum Design MPMS2 SQUID magnetometer.

{[(Me$_3$Si)$_2$N]$_2$(THF)Tb}$_2$(μ-η^2:η^2-NO), 2. Following previously reported procedures,[2] in a nitrogen-filled glovebox, K{[(Me$_3$Si)$_2$N]$_2$(THF)Tb}$_2$(μ_3-η^2:η^2:η^2-N$_2$) (100 mg, 0.08 mmol) was dissolved in toluene (6 mL) to yield a yellow/orange solution which was transferred to a sealable 50 mL Schlenk flask equipped with a greaseless stopcock and a Teflon stirbar. The flask was connected to a high-vacuum line and N_2 was removed using 3 freeze-pump-thaw cycles. NO (1.5 equiv) was transferred to the flask while the solution was frozen at −196 ºC. The frozen solution was allowed to melt at −78 ºC and then warmed to room temperature with vigorous stirring during which time the solution changed from intense yellow to pale yellow. Excess NO was removed from the reaction flask under reduced pressure and the solution was transferred to an argon-filled glovebox, concentrated to 1 mL and stored at −35 ºC. After 2 days, colorless X-ray quality crystals of **2** (20 mg, 21%) were isolated. Partial desolvation of THF occurred when the crystals were dried under reduced pressure. IR: 2948s, 2895s, 2185w, 2128w, 1434m, 1247s, 1184w, 992s, 843s, 771m, 667m, 605m cm^{-1}. Anal. Calcd for $C_{24}H_{72}N_5OSi_8Tb_2$ • (-0.6THF), **2** • (-0.6THF): C, 32.61; H, 7.69; N, 6.42; found: C, 32.76; H, 7.53; N, 6.81.

Reaction with [NO][BF$_4$]. To a stirred yellow diethyl ether solution (6 mL) of K{[(Me$_3$Si)$_2$N]$_2$(THF)Y}$_2$(μ_3-η^2:η^2:η^2-N$_2$) (10 mg, 0.01 mmol) was added an ether suspension of [NO][BF$_4$] (1.3 mg, 0.01 mmol) which caused the solution to turn colorless over 5 min. Formation of white precipitate was observed and an EPR spectrum of the crude mixture was obtained. This reaction was repeated with 40 mg K{[(Me$_3$Si)$_2$N]$_2$(THF)Y}$_2$(μ_3-η^2:η^2:η^2-N$_2$) (0.04 mmol) and 5 mg [NO][BF$_4$] (0.04 mmol) from which pale blue crystals of

{[$(Me_3Si)_2N]_2(THF)Y\}_2(\mu$-$\eta^2$:$\eta^2$-$N_2$) were isolated after centrifugation and identified by X-ray crystallography.

X-ray Data Collection, Structure Solution and Refinement for {[$(Me_3Si)_2N]_2(THF)Tb\}_2(\mu$-$\eta^2$:$\eta^2$-NO), 2. A colorless crystal of approximate dimensions 0.603 x 0.332 x 0.246 mm was mounted in a loop and transferred to a Bruker SMART APEX II diffractometer. The APEX2[15] program package was used to determine the unit-cell parameters and for data collection (15 sec/frame scan time for a sphere of diffraction data). The raw frame data was processed using SAINT[16] and SADABS[17] to yield the reflection data file. Subsequent calculations were carried out using the SHELXTL[18] program. There were no systematic absences nor any diffraction symmetry other than the Friedel condition. The centrosymmetric triclinic space group $P\bar{1}$ was assigned and later determined to be correct. The structure was solved by direct methods and refined on F^2 by full-matrix least-squares techniques. The analytical scattering factors[19] for neutral atoms were used throughout the analysis. Hydrogen atoms were included using a riding model. O(1), C(10), C(11), C(12), C(13), C(14), C(15), and C(16) were disordered and included using multiple components with partial site-occupancy-factors. There was one disordered toluene molecule of solvation per formula unit, and the molecule was located about an inversion center. At convergence, wR2 = 0.0848 and Goof = 1.056 for 281 variables refined against 6897 data (0.75Å), R1 = 0.0326 for those 6238 data with $I > 2.0\sigma(I)$. Details are given in Table 4.2.

Table 4.2. Crystal data and structure refinement parameters for $\{[(Me_3Si)_2N]_2(THF)Tb\}_2(\mu$-$\eta^2$:$\eta^2$-NO), **2**

	2 • (C_7H_8)
Empirical formula	$C_{32}H_{88}N_5O_3Si_8Tb_2 \bullet (C_7H_8)$
Formula weight	1225.76
Temperature (K)	143(2)
Space group	$P\bar{1}$
a (Å)	11.6498(13)
b (Å)	12.3412(13)
c (Å)	12.8812(14)
α (°)	101.9289(12)
β (°)	110.0435(12)
γ (°)	110.1914(12)
Volume (Å^3)	1517.9(3)
Z	1
ρ_{calcd} (Mg/m^3)	1.341
μ (mm^{-1})	2.502
$R1^a$ [$I > 2\sigma(I)$]	0.0326
$wR2^b$	0.0848

$^aR1 = \Sigma||F_o|-|F_c|| / \Sigma|F_o|$. $^bwR2 = [\Sigma[w(F_o^2-F_c^2)^2] / \Sigma[w(F_o^2)^2]]^{1/2}$

References

(1) Evans, W. J.; Fang, M.; Zucchi, G. l.; Furche, F.; Ziller, J. W.; Hoekstra, R. M.; Zink, J. I. *Journal of the American Chemical Society* **2009**, *131*, 11195.

(2) Evans, W. J.; Fang, M.; Bates, J. E.; Furche, F.; Ziller, J. W.; Kiesz, M. D.; Zink, J. I. *Nature Chemistry* **2010**, *2*, 644.

(3) Rinehart, J. D.; Fang, M.; Evans, W. J.; Long, J. R. *Nature Chemistry* **2011**, *3*, 538.

(4) Rinehart, J. D.; Fang, M.; Evans, W. J.; Long, J. R. *Journal of the American Chemical Society* **2011**, *133*, 14236.

(5) Demir, S.; Nippe, M.; Gonzalez, M. I.; Long, J. R. *Chemical Science* **2014**, *5*, 4701.

(6) Demir, S.; Zadrozny, J. M.; Nippe, M.; Long, J. R. *Journal of the American Chemical Society* **2012**, *134*, 18546.

(7) Woodruff, D. N.; Winpenny, R. E. P.; Layfield, R. A. *Chemical Reviews* **2013**, *113*, 5110.

(8) Meihaus, K. R.; Corbey, J. F.; Fang, M.; Ziller, J. W.; Long, J. R.; Evans, W. J. *Inorganic Chemistry* **2014**, *53*, 3099.

(9) Demir, S.; Jeon, I.-R.; Long, J. R.; Harris, T. D. *Coordination Chemistry Reviews* **2015**, *289–290*, 149.

(10) Evans, W. J.; Lee, D. S.; Rego, D. B.; Perotti, J. M.; Kozimor, S. A.; Moore, E. K.; Ziller, J. W. *Journal of the American Chemical Society* **2004**, *126*, 14574.

(11) Černák, J.; Orendáč, M.; Potočňák, I.; Chomič, J.; Orendáčová, A.; Skoršepa, J.; Feher, A. *Coordination Chemistry Reviews* **2002**, *224*, 51.

(12) Archer, S. *The FASEB Journal* **1993**, *7*, 349.

(13) Allen, F. H.; Kennard, O.; Watson, D. G.; Brammer, L.; Orpen, A. G.; Taylor, R. *Journal of the Chemical Society, Perkin Transactions 2* **1987**, S1.

(14) MacDonald, M. R.; Bates, J. E.; Ziller, J. W.; Furche, F.; Evans, W. J. *Journal of the American Chemical Society* **2013**, *135*, 9857.

(15) APEX2 Version 2011.4-1, Bruker AXS, Inc.; Madison, WI 2011.

(16) SAINT Version 7.68a, Bruker AXS, Inc.; Madison, WI 2009.

(17) Sheldrick, G. M. SADABS, Version 2008/1, Bruker AXS, Inc.; Madison, WI 2008.

(18) Sheldrick, G. M. SHELXTL, Version 2014/7, Bruker AXS, Inc.; Madison, WI 2008.

(19) International Tables for Crystallography 1992, Vol. C., Dordrecht: Kluwer Academic Publishers.

CHAPTER 5

Isolation and Structure of the Bis(allyl) and Bis(ammonia) Pentamethylcyclopentadienyl Dysprosium Complexes, $(C_5Me_5)Dy(C_3H_5)_2(THF)$ and $[(C_5Me_5)_2Dy(NH_3)_2][BPh_4]$, from the Synthesis of $[(C_5Me_5)_2Dy][(\mu\text{-}Ph)_2BPh_2]$

Introduction

The unsolvated metallocene cations, $[(C_5Me_5)_2Ln][(\mu\text{-}Ph)_2BPh_2]$,[1-10] are commonly used as precursors to a variety of highly reactive organometallic lanthanide complexes such as $(C_5Me_5)_2LnR$ [R = C_5Me_5,[6] $CH(SiMe_3)_2$,[1] CH_2SiMe_3,[11] CH_2CMe_3,[11] Me,[4,11] and N_3[11]], since the $(BPh_4)^-$ anion is loosely ligated and easily displaced. In the presence of some coordinating substrates, these unsolvated metallocene cations can also be used to synthesize bimetallic species such as $[(C_5Me_5)_2(THF)Ln]_2(\mu\text{-}\eta^2\text{:}\eta^2\text{-}N_2)$[5] and $\{(C_5Me_5)_2Ln[\mu\text{-}N(SiMe_3)NC]\}_2$[7] as well as radical complexes such as $\{[(C_5Me_5)_2Ln]_2(phz)\}\{BPh_4\}$.[8,11] In contrast, solvated cations such as $[(C_5Me_5)_2Ln(THF)_2][BPh_4]$[12,13] are less reactive and often fail to provide the desired products described above.[1,11]

The unsolvated metallocene cations are prepared according to equations 5.1-5.4[1-9,11] starting from $LnCl_3$ that is obtained by desolvation of $LnCl_3(H_2O)_x$ in the presence of NH_4Cl.[14-19] This synthesis has been carried out repeatedly for all of the rare earths except Pm and Eu.[1-10] In the course of executing these reactions with Ln = Dy, two new complexes were isolated. These complexes were not identified by NMR spectroscopy due to the paramagnetism of Dy^{3+}, μ = 10.5 μ_B, but X-ray crystallography unequivocally revealed their identity. The discovery and structural

characterization of these two complexes demonstrates the subtleties that can exist in organolanthanide reaction chemistry even in heavily investigated reactions.

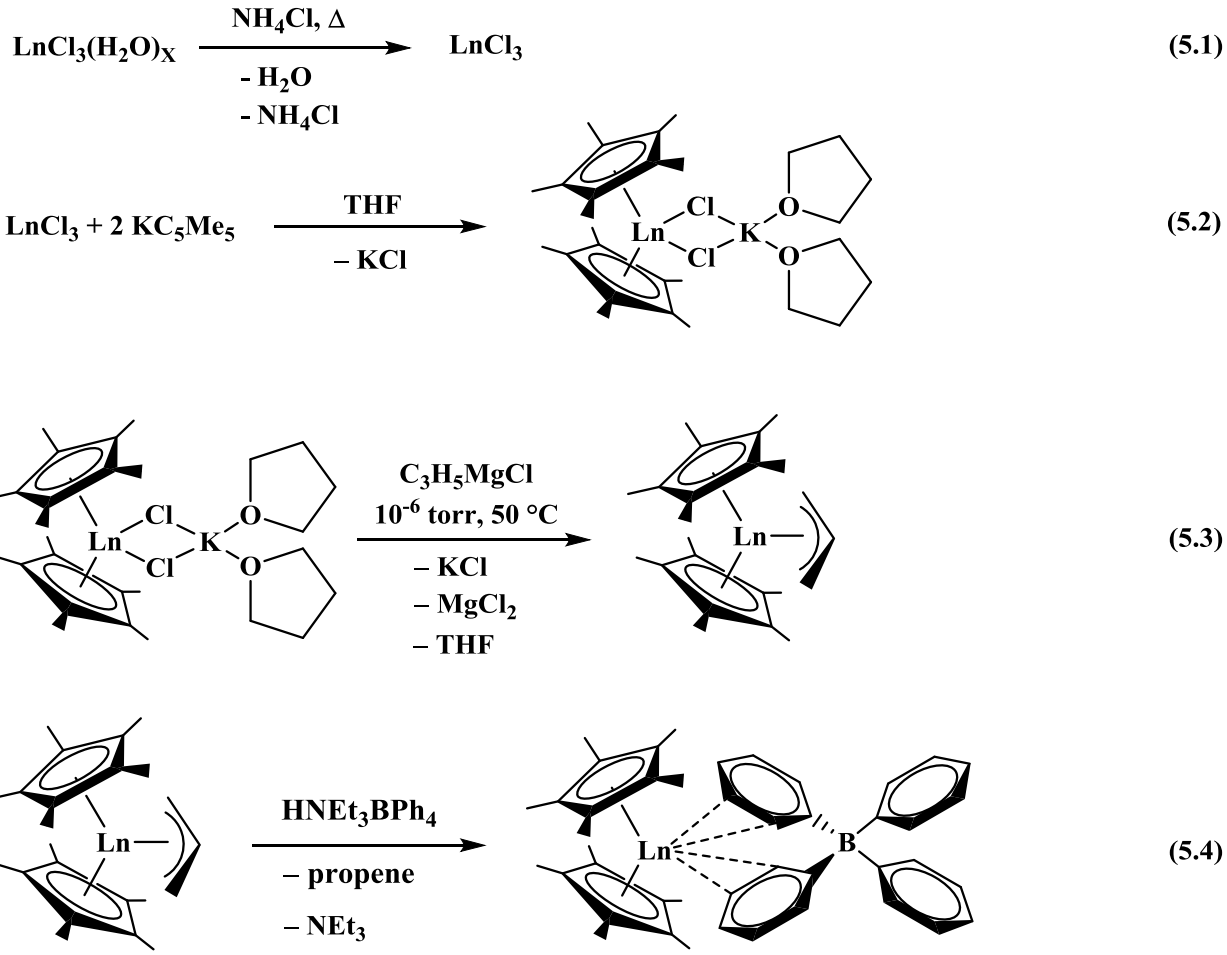

Results and Discussion

$[(C_5Me_5)_2Dy(NH_3)_2][BPh_4]$, 1. The reaction of $(C_5Me_5)_2Dy(C_3H_5)$ with Et_3NHBPh_4 in the absence of coordinating solvent is expected to produce $[(C_5Me_5)_2Dy][(\mu\text{-}Ph)_2BPh_2]$ (eq 5.4). However, in the preparation of one large batch on a 2 g scale, recrystallization of the isolated product yielded colorless crystals of $[(C_5Me_5)_2Dy(NH_3)_2][BPh_4]$, **1** (Figure 5.1). These crystals could be grown from toluene and benzene in gloveboxes containing coordinating and

noncoordinating solvents at room temperature and at −30 °C. While the bis(solvated) metallocene cations of THF,[12,13] tetrahydrothiophene (THT),[20] pyridine,[11] acetone,[11] and $OPPh_3$[11] have been crystallographically characterized, to our knowledge, this is the first ammonia adduct. The exact source of NH_3 is unknown. However, the NH_4Cl used to dehydrate $DyCl_3(H_2O)_x$ (eq 5.1) is a possible source. If the excess NH_4Cl was not completely separated by sublimation from the $DyCl_3$, it could have gotten carried along in the synthesis and subsequently provide the NH_3 ligands. However, the NH_3 source would need to survive several synthetic steps (eq 5.2-5.4) to be present in the cation. Elemental analysis of the $DyCl_3$ obtained after the drying process showed no evidence of nitrogen present.

Structural Discussion. Complex **1** has an overall structure like that of many bis(pentamethylcyclopentadienyl) metallocenes. Two additional ligands are attached to the metal to give an eight coordinate complex. The closest ammonia-ligated compounds in the literature for comparison are $(C_5Me_5)_2Yb(SPh)(NH_3)$,[21] $(C_5Me_5)_2Yb(TePh)(NH_3)$,[22] and $(C_5Me_5)_2Yb(THF)(NH_3)$.[23] The 2.476(3) and 2.466(3) Å Dy–N distances in **1** are comparable to the 2.428(3) and 2.45(1) Å distances in $(C_5Me_5)_2Yb(SPh)(NH_3)$[21] and $(C_5Me_5)_2Yb(TePh)(NH_3)$,[22] respectively, when the 0.042 Å difference in 8-coordinate ionic radii is considered.[24] The Dy–N distances in **1** also compare well with the 2.55(3) Å distance in $(C_5Me_5)_2Yb(THF)(NH_3)$[23] considering that 8-coordinate Yb^{2+} has an ionic radius 0.113 Å larger than Dy^{3+}.[24] The 140.2° (ring centroid)–Dy–(ring centroid) angle in **1** is larger than the 135-137° angles in $(C_5Me_5)_2Yb(SPh)(NH_3)$,[21] $(C_5Me_5)_2Yb(TePh)(NH_3)$,[22] and $(C_5Me_5)_2Yb(THF)(NH_3)$[23] and probably reflects the small steric demand of two NH_3 ligands compared to the other compounds.

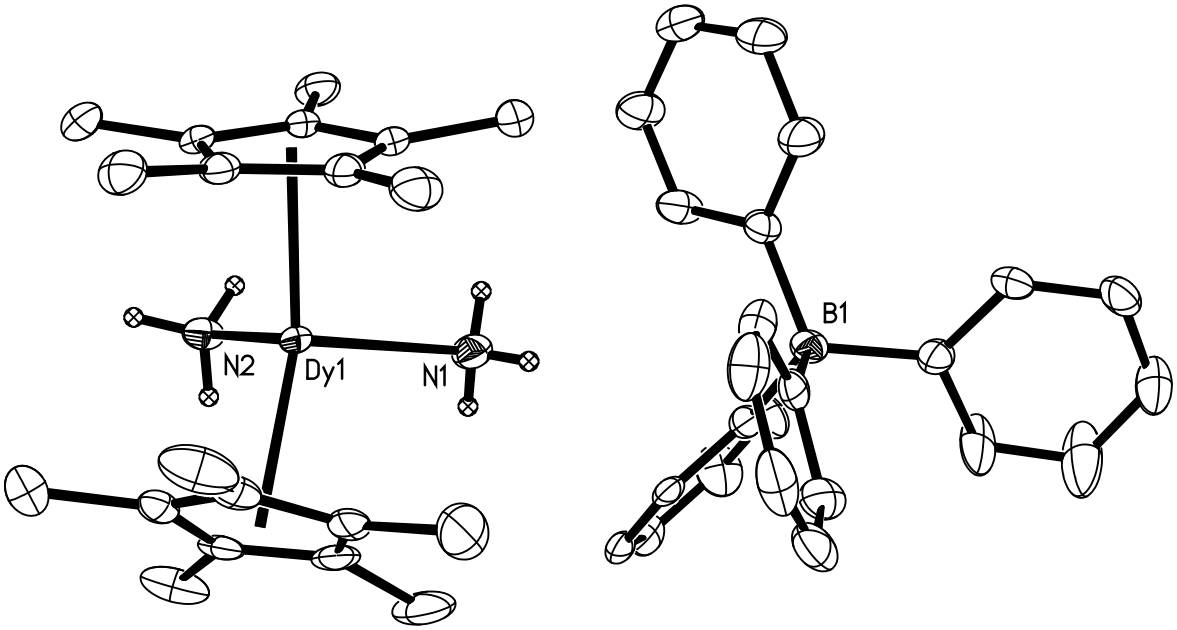

Figure 5.1. Thermal ellipsoid plot of $[(C_5Me_5)_2Dy(NH_3)_2][BPh_4]$, **1**, drawn at the 50% probability level. All hydrogens except those belonging to the NH_3 ligands have been omitted for clarity.

$(C_5Me_5)Dy(C_3H_5)_2(THF)$, 2. In an attempt to understand the source of the bis(ammonia) product, the precursors, $(C_5Me_5)_2DyCl_2K(THF)_2$ and $(C_5Me_5)_2Dy(C_3H_5)$ were remade from the same batch of $DyCl_3$ as previously used. The reaction of $(C_5Me_5)_2DyCl_2K(THF)_2$ with one equiv of the allyl-Grignard reagent $(C_3H_5)MgCl$ gave mainly the expected product in eq 5.3, $(C_5Me_5)_2Dy(C_3H_5)$, but single crystals of $(C_5Me_5)Dy(C_3H_5)_2(THF)$, **2**, were also isolated. The latter complex was identified by X-ray crystallography, Figure 5.2.

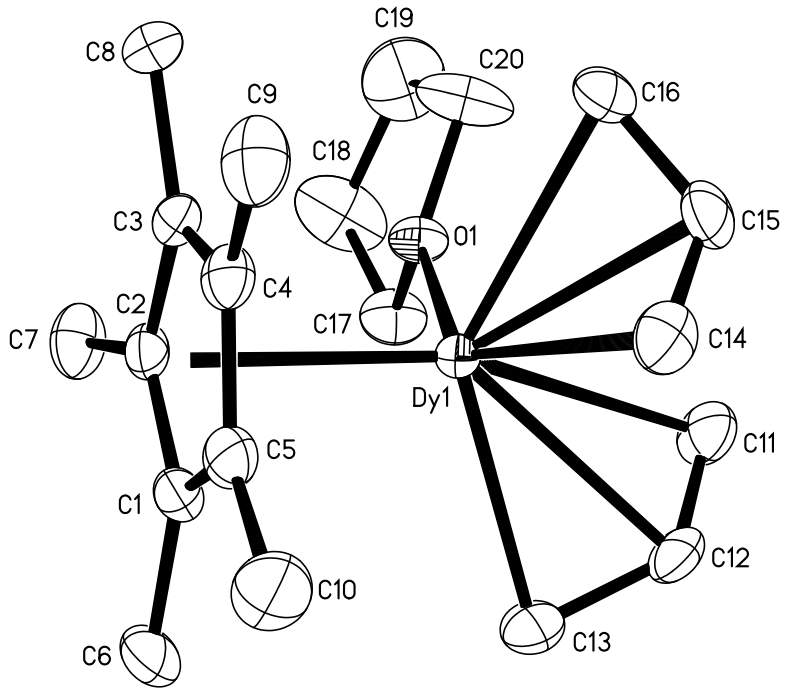

Figure 5.2. Thermal ellipsoid plot of $(C_5Me_5)Dy(C_3H_5)_2(THF)$, **2**, drawn at the 50% probability level. Hydrogen atoms have been omitted for clarity.

The crystal data for **2** show that this complex contains one η^5-cyclopentadienyl group and two η^3-allyl ligands. Rare earth complexes containing a single C_5Me_5 ring are much less common than the bis(pentamethylcyclopentadienyl) metallocenes, and those with two allyl ligands are particularly rare. Only two examples are in the literature to our knowledge: $(C_5Me_5)Sc(C_3H_5)_2$[25] and $(C_5Me_5)Nd(C_3H_5)_2(dioxane)$.[26]

The origin of the crystals of **2** is unknown. From reactions of $(C_5Me_5)_2DyCl_2K(THF)_2$ with two equiv of $(C_3H_5)MgCl$, only crystals of $(C_5Me_5)_2Dy(C_3H_5)$ were obtained. Ligand redistribution is common in the chemistry of lanthanide complexes of small cyclopentadienyl ligands,[27-29] but it is not common in pentamethylcyclopentadienyl systems, since $(C_5Me_5)_3Dy$[30] is so sterically crowded that it is not a viable ligand redistribution product. Attempts to make **2** by

addition of excess $(C_3H_5)MgCl$ to $(C_5Me_5)_2Dy(C_3H_5)$ were unsuccessful. Evidently, however, under some crystallization conditions, **2** can be isolated, even when $(C_5Me_5)_2Dy(C_3H_5)$ is the main product and is the only product isolated from further recrystallizations of the same batch.

Structural Discussion. The structure of $(C_5Me_5)Dy(C_3H_5)_2(THF)$, **2**, is compared with that of compositionally similar $(C_5Me_5)Nd(C_3H_5)_2(dioxane)$[26] and with $(C_5Me_5)_2Dy(C_3H_5)$[8,9] in Table 5.1. The bond distances in **2** are similar to those in $(C_5Me_5)Nd(C_3H_5)_2(dioxane)$. In both cases, the shortest Ln–C(allyl) distances are those of the carbon closest to the neighboring allyl ligand. Both **2** and $(C_5Me_5)Nd(C_3H_5)_2(dioxane)$ have typical Ln–C(allyl) distances that usually involve one short and two longer bond lengths. Interestingly, the Dy–C(allyl) distances in **2** are uniformly larger than those in $(C_5Me_5)_2Dy(C_3H_5)$ which has all Ln–C(allyl) about the same.

Table 5.1. Comparison of selected bond lengths (Å) of $(C_5Me_5)_2Dy(C_3H_5)$,[8,9] $(C_5Me_5)Dy(C_3H_5)_2(THF)$, **2**, and $(C_5Me_5)Nd(C_3H_5)_2(dioxane)$,[26] where Cnt = (C_5Me_5) ring-centroid and C(allyl) refers to C atoms of the allyl ligands.

	Ln–Cnt	Ln–C(allyl)
$(C_5Me_5)_2Dy(C_3H_5)$[8,9]	2.374 2.359	2.602(3), 2.613(3), 2.596(3)
$(C_5Me_5)Dy(C_3H_5)_2(THF)$, **2**	2.384	C(11): 2.749(3), C(12): 2.642(3), C(13): 2.508(3) C(14): 2.686(3), C(15): 2.647(3), C(16): 2.582(3)
$(C_5Me_5)Nd(C_3H_5)_2(dioxane)$[26]	2.497	2.79(1), 2.78(1), 2.651(9) 2.75(1), 2.69(1), 2.669(9)

Conclusion

The isolation of $[(C_5Me_5)_2Dy(NH_3)_2][BPh_4]$, **1**, and $(C_5Me_5)Dy(C_3H_5)_2(THF)$, **2**, demonstrates that even in well-established synthetic routes to commonly used materials, unexpected new products can be obtained. In these highly paramagnetic systems, X-ray crystallography was instrumental in identifying these products.

Experimental

The syntheses and manipulations described below were conducted under nitrogen or argon with rigorous exclusion of air and water by Schlenk, vacuum line, and glovebox techniques. Solvents were sparged with UHP argon and dried over columns containing Q-5 and molecular sieves. $DyCl_3$ was dried according to literature procedures by heating a mixture of the hydrated chloride with an excess of NH_4Cl.[14-19] $K[N(SiMe_3)_2]$ (Aldrich, 95%) was purified via toluene extraction before use. C_5Me_5H was dried over molecular sieves and degassed using three freeze-pump-thaw cycles. KC_5Me_5 was synthesized by deprotonation of C_5Me_5H with $K[N(SiMe_3)_2]$. The methods described below are general procedures used to produce the known intermediates in eqs 5.1-5.4,[4] but are given here to show precisely the reactions that led to the isolation of $(C_5Me_5)Dy(C_3H_5)_2(THF)$ and $[(C_5Me_5)_2Dy(NH_3)_2][BPh_4]$.

$(C_5Me_5)_2DyCl_2K(THF)_2$.[8,9] In a nitrogen-filled glovebox, KC_5Me_5 (2.9 g, 16.8 mmol) was added to a stirred THF slurry of $DyCl_3$ (2.4 g, 8.8 mmol) over 20 min to yield an opaque mixture. After 2 d, the reaction mixture was centrifuged to remove white solids, the pale yellow supernatant was filtered, and the solvent was removed under reduced pressure. The solid was washed with toluene and hexane and dried to produce $(C_5Me_5)_2DyCl_2K(THF)_2$ as an off-white solid (3.2 g, 62% yield).

$(C_5Me_5)_2Dy(C_3H_5)$.[8,9] Addition of $(C_3H_5)MgCl$ (2.7 mL, 5.2 mmol) in THF to a pale yellow solution of $(C_5Me_5)_2DyCl_2K(THF)_2$ (3.2 g, 5.2 mmol) in toluene (175 mL) caused an immediate color change to bright yellow. After the mixture was stirred overnight, solvent was removed under reduced pressure to yield a tacky yellow-orange solid. Extraction of the solvent with 10:1 hexane/dioxane overnight generated a white precipitate that was separated by centrifugation. Removal of solvent from the yellow supernatant gave $(C_5Me_5)_2Dy(C_3H_5)(THF)_X$ as a yellow-orange solid which was transferred to a sublimation tube equipped with a sealable Teflon adapter and desolvated by exposure to vacuum (1 ×10-6 Torr) for 5 d. The apparatus was brought into a nitrogen-filled glovebox free of coordinating solvents. Extraction into hexanes and evaporation provided $(C_5Me_5)_2Dy(C_3H_5)$ (1.53 g, 62% yield) as a bright orange solid. Crystals of $(C_5Me_5)_2Dy(C_3H_5)$ can be grown from hexane at –30 °C.

$[(C_5Me_5)_2Dy][(\mu\text{-}Ph)_2BPh_2]$.[9] Addition of $(C_5Me_5)_2Dy(C_3H_5)$ (1.2 g, 2.6 mmol) to Et_3NHBPh_4 (1.04 g, 2.5 mmol) in toluene (15 mL) produced a cloudy orange mixture that was stirred overnight. The mixture was filtered and the collected solids were washed with toluene and hexane and dried to yield a pale yellow solid (1.82 g, 98% if $[(C_5Me_5)_2Dy][(\mu\text{-}Ph)_2BPh_2]$).

$[(C_5Me_5)_2Dy(NH_3)_2][BPh_4]$, 1. Recrystallization of the yellow solid described above from hot toluene yielded colorless crystals identified by X-ray crystallography to be $[(C_5Me_5)_2Dy(NH_3)_2][BPh_4]$, **1** (Figure 5.1). Attempts to reproduce this result using a different batch of intermediates starting with the same $DyCl_3$ source only yielded pale yellow crystals of the known unsolvated cation $[(C_5Me_5)_2Dy][(\mu\text{-}Ph)_2BPh_2]$.[9,30]

$(C_5Me_5)Dy(C_3H_5)_2(THF)$, 2. In an attempt to understand how the bis(ammonia) product $[(C_5Me_5)_2Dy(NH_3)_2][BPh_4]$ had formed, the allyl precursor $(C_5Me_5)_2Dy(C_3H_5)$, was remade from the same $DyCl_3$ batch as described above. However this time, crystallization of

$(C_5Me_5)_2Dy(C_3H_5)$ from cold hexane before desolvation under vacuum yielded a mixture of yellow and orange crystals. X-ray crystallography identified the yellow crystals as the bis(allyl) THF solvate $(C_5Me_5)Dy(C_3H_5)_2(THF)$, **2**, (Figure 5.2) and the orange crystals as the known mono(allyl) unsolvated species $(C_5Me_5)_2Dy(C_3H_5)$. Subsequent attempts to isolate crystals of the bis(allyl) product **2** under various conditions only yielded the known mono(allyl) $(C_5Me_5)_2Dy(C_3H_5)$.

X-ray Data Collection, Structure Solution and Refinement for $[(C_5Me_5)_2Dy(NH_3)_2][BPh_4]$, 1. A colorless crystal of approximate dimensions 0.053 x 0.157 x 0.426 mm was mounted on a glass fiber and transferred to a Bruker SMART APEX II diffractometer. The APEX2[31] program package was used to determine the unit-cell parameters and for data collection (10 sec/frame scan time for a sphere of diffraction data). The raw frame data was processed using SAINT[32] and SADABS[33] to yield the reflection data file. Subsequent calculations were carried out using the SHELXTL[34] program. There were no systematic absences nor any diffraction symmetry other than the Friedel condition. The centrosymmetric triclinic space group $P\bar{1}$ was assigned and later determined to be correct. The structure was solved by direct methods and refined on F^2 by full-matrix least-squares techniques. The analytical scattering factors[35] for neutral atoms were used throughout the analysis. Hydrogen atoms were included using a riding model. Carbon atoms C(17), C(31)-C(40), C(54) and C(55) were disordered and included using multiple components with partial site-occupancy-factors. At convergence, wR2 = 0.0791 and Goof = 1.073 for 941 variables refined against 20304 data (0.75Å), R1 = 0.0386 for those 16659 data with $I > 2.0\sigma(I)$. Details are given I Table 5.2.

X-ray Data Collection, Structure Solution and Refinement for $(C_5Me_5)Dy(C_3H_5)_2(THF)$, 2. A yellow crystal of approximate dimensions 0.223 x 0.200 x

0.115 mm was mounted on a glass fiber and transferred to a Bruker SMART APEX II diffractometer. The APEX2[36] program package was used to determine the unit-cell parameters and for data collection (15 sec/frame scan time for a sphere of diffraction data). The raw frame data was processed using SAINT[37] and SADABS[33] to yield the reflection data file. Subsequent calculations were carried out using the SHELXTL[34] program. There were no systematic absences nor any diffraction symmetry other than the Friedel condition. The centrosymmetric triclinic space group $P\bar{1}$ was assigned and later determined to be correct. The structure was solved by direct methods and refined on F^2 by full-matrix least-squares techniques. The analytical scattering factors[35] for neutral atoms were used throughout the analysis. Hydrogen atoms were included using a riding model. At convergence, wR2 = 0.0601 and Goof = 1.083 for 204 variables refined against 4354 data (0.74 Å), R1 = 0.0231 for those 4119 data with $I > 2.0\sigma(I)$. Details are given I Table 5.2.

Table 5.2. Crystallographic details for $[(C_5Me_5)_2Dy(NH_3)_2][BPh_4]$, **1**, and $(C_5Me_5)Dy(C_3H_5)_2(THF)$, **2**.

	$[(C_5Me_5)_2Dy(NH_3)_2][BPh_4]$, **1**	$(C_5Me_5)Dy(C_3H_5)_2(THF)$, **2**
Empirical formula	$C_{44}H_{56}BDyN_2 \bullet \frac{1}{2}(C_7H_8)$	$C_{20}H_{33}DyO$
Formula weight	832.28	451.96
Temperature (K)	100(2)	143(2)
Space group	$P\bar{1}$	$P\bar{1}$
a, *b*, *c* (Å)	10.144(1), 14.219(2), 28.976(3)	8.564(9), 8.864(9), 13.114(1)
α, *β*, *γ* (°)	81.269(6), 84.862(6), 80.791(6)	84.979(1), 76.620(1), 80.143(1)
Volume ($Å^3$)	4068.5(8)	952.91(17)
Z	4	2
ρ_{calcd} (Mg/m^3)	1.359	1.575
Radiation type	Mo *K α*	Mo *K α*
μ (mm^{-1})	1.871	3.921
Crystal size (mm^3)	0.426 x 0.157 x 0.053	0.223 x 0.200 x 0.115
Diffractometer	Bruker SMART APEX II	Bruker SMART APEX II
Absorption correction	Semi-empirical from equivalents (SADABS, 2012, Bruker)	Numerical (SADABS, 2012, Bruker)
T_{min}, T_{max}	0.6425, 0.7457	0.5445, 0.8087
No. of measured, independent, and observed [I>2sigma(I)] reflections	131157, 20304, 16659	10865, 4354, 4119
R_{int}	0.0521	0.0263
$R1$,[a] $wR2$[b]	0.0386, 0.0791	0.0231, 0.0587
No. of reflections	20304	4354
No. of parameters	941	204
H-atom treatment	H-atom parameters constrained	H-atom parameters constrained

[a] $R1 = \Sigma||F_o|-|F_c|| / \Sigma|F_o|$. [b] $wR2 = [\Sigma[w(F_o^2-F_c^2)^2] / \Sigma[w(F_o^2)^2]]^{1/2}$

References

(1) Evans, W. J; Seibel, C. A.; Ziller, J. W. *Journal of the American Chemical Society* **1998**, *120*, 6745.

(2) Evans, W. J.; Lee, D. S.; Lie, C.; Ziller, J. W. *Angewandte Chemie International Edition* **2004**, *43*, 5517.

(3) Evans, W. J.; Perotti, J. M.; Kozimor, S. A.; Champagne, T. M.; Davis, B. L.; Nyce, G. W.; Fujimoto, C. H.; Clark, R. D.; Johnston, M. A.; Ziller, J. W. *Organometallics* **2005**, *24*, 3916.

(4) Evans, W. J.; Perotti, J. M.; Ziller, J. W. *Journal of the American Chemical Society* **2005**, *127*, 3894.

(5) Evans, W. J.; Lee, D. S.; Ziller, J. W.; Kaltsoyannis, N. *Journal of the American Chemical Society* **2006**, *128*, 14176.

(6) Evans, W. J.; Davis, B. L.; Champagne, T. M.; Ziller, J. W. *Proceedings of the National Academy of Sciences* **2006**, *103*, 12678.

(7) Evans, W. J.; Montalvo, E.; Champagne, T. M.; Ziller, J. W.; DiPasquale, A. G.; Rheingold, A. L. *Journal of the American Chemical Society* **2007**, *130*, 16.

(8) Corbey, J. F. M., Thomas J.; Fieser, Megan E.; Ziller, Joseph W.; Evans, William J. *unpublished results* **2012**.

(9) Demir, S.; Zadrozny, J. M.; Nippe, M.; Long, J. R. *Journal of the American Chemical Society* **2012**, *134*, 18546.

(10) Demir, S.; Zadrozny, J. M.; Long, J. R. *Chemistry – A European Journal* **2014**, *20*, 9524.

(11) MacDonald, M. R.; Ziller, J. W.; Evans, W. J. *Inorganic Chemistry* **2011**, *50*, 4092.

(12) Evans, W. J.; Ulibarri, T. A.; Chamberlain, L. R.; Ziller, J. W.; Alvarez, D. *Organometallics* **1990**, *9*, 2124.

(13) Schumann, H.; Winterfeld, J.; Keitsch, M. R.; Herrmann, K.; Demtschuk, J. *Zeitschrift für anorganische und allgemeine Chemie* **1996**, *622*, 1457.

(14) Taylor, M. D.; Carter, C. P. *Journal of Inorganic and Nuclear Chemistry* **1962**, *24*, 387.

(15) Taylor, M. D. *Chemical Reviews* **1962**, *62*, 503.

(16) J. Burgess, J. K. *Advances in Inorganic Chemistry and Radiochemistry* **1981**, *24*, 57.

(17) Brown, D. *Halides of the lanthanides and actinides, Chap. 3*; Wiley-lnterscience: New York, 1968.

(18) Meyer, G. *Inorganic Synthesis* **1989**, *25*, 146.

(19) (Ed.), F. T. E.; Georg Thieme: Stuttgart, 1997.

(20) Heeres, H. J.; Meetsma, A.; Teuben, J. H. *Journal of Organometallic Chemistry* **1991**, *414*, 351.

(21) Zalkin, A.; Henly, T. J.; Andersen, R. A. *Acta Crystallographica Section C* **1987**, *43*, 233.

(22) Berg, D. J.; Andersen, R. A.; Zalkin, A. *Organometallics* **1988**, *7*, 1858.

(23) Wayda, A. L.; Dye, J. L.; Rogers, R. D. *Organometallics* **1984**, *3*, 1605.

(24) Shannon, R. *Acta Crystallographica Section A* **1976**, *32*, 751.

(25) Yu, N.; Nishiura, M.; Li, X.; Xi, Z.; Hou, Z. *Chemistry – An Asian Journal* **2008**, *3*, 1406.

(26) Taube, R.; Maiwald, S.; Sieler, J. *Journal of Organometallic Chemistry* **2001**, *621*, 327.

(27) Mueller, T. J.; Fieser, M. E.; Ziller, J. W.; Evans, W. J. *Chemical Science* **2011**, *2*, 1992.

(28) Lorenz, S. E.; Schmiege, B. M.; Lee, D. S.; Ziller, J. W.; Evans, W. J. *Inorganic Chemistry* **2010**, *49*, 6655.

(29) Evans, W. J.; Lorenz, S. E.; Ziller, J. W. *Inorganic Chemistry* **2009**, *48*, 2001.

(30) Mueller, T. J. *Dissertation* **2011**, 208.

(31) APEX2 Version 2013.6-2, Bruker AXS, Inc.; Madison, WI 2013.

(32) SAINT Version 8.31b, Bruker AXS, Inc.; Madison, WI 2012.

(33) Sheldrick, G. M. SADABS, Version 2012/1, Bruker AXS, Inc.; Madison, WI 2012.

(34) Sheldrick, G. M. SHELXTL, Version 2013/3, Bruker AXS, Inc.; Madison, WI 2013.

(35) International Tables for Crystallography 1992, Vol. C., Dordrecht: Kluwer Academic Publishers.

(36) APEX2 Version 2011.4-1, Bruker AXS, Inc.; Madison, WI 2011.

(37) SAINT Version 7.68a, Bruker AXS, Inc.; Madison, WI 2009.

CHAPTER 6

Slow Magnetic Relaxation in the Radical-Bridged Bimetallic Rare Earth Complexes $\{[(C_5Me_5)_2Ln]_2(phz)\}\{BPh_4\}$ (Ln = Dy, Tb; phz = phenazine)

Introduction

The discovery that bridging radical-containing ligands can facilitate very strong exchange coupling in bimetallic rare earth systems has stimulated intense interest in the field of single-molecule magnets (SMMs) to synthesize more examples of radical-bridged complexes.[1-4] Initiating this awareness were the $(N_2)^{3-}$ radical species, [K(18-crown-6)$(THF)_2$][{[$(Me_3Si)_2N]_2$(THF)Ln}$_2$(μ-η^2:η^2-N_2)] (Ln = Dy, Tb), which function as excellent SMMs. In this system, the Tb analog demonstrated the highest blocking temperature of any SMM to date[2] and the Gd analog displayed the strongest magnetic exchange coupling ever observed for a Gd compound.[1] In this $(N_2)^{3-}$ series, the strong coupling is thought to be a result of direct overlap of the diffuse radical ligand orbitals on the N_2 bridge with the 4f orbitals of each lanthanide center.[5] It is of interest to modify the ancillary ligands and the bridging radical ligand to understand more about what makes this type of system ideal for single-molecule magnetism.

The Evans group has reported a phenazine (phz) radical bridged complex with diamagnetic yttrium, namely $\{[(C_5Me_5)_2Y]_2(\mu\text{-phz})\}\{BPh_4\}$, **1**, synthesized by combining 2 equiv of the cationic precursor $[(C_5Me_5)_2Y][(\mu\text{-}Ph)_2BPh_2]$ with 1 equiv of phenazine in benzene which reacts over 2 d as shown in eq 6.1.[6] This complex is reported to be the first rare earth species containing the radical $(phz)^{\bullet-}$ moiety.

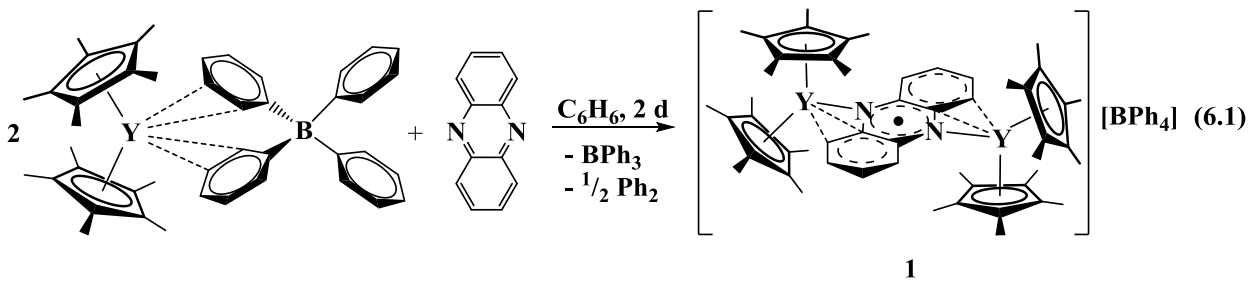

(6.1)

1

initial reactions. The paramagnetic lanthanide analogs using Tb, Dy and Gd were targeted to analyze their magnetic properties for comparison with the previously reported radical $(N_2)^{3-}$ bridged SMMs. 2,2′-Bipyrimidine (bpym) was another bridging ligand of interest in these systems and reactions including this ligand are described below. Around this same time, our collaborators in the Long group at the University of California, Berkeley reported a series of radical-bridged 2,2′-bipyrimidine (bpym) bimetallic rare earth complexes, $\{[(C_5Me_5)_2Ln]_2(\mu\text{-bpym})\}\{BPh_4\}$, where Ln = Gd, Dy, or Tb, unaware we were also working with the same system. The reported $(bpym)^{\bullet-}$ radical complexes display desirable magnetic coupling and magnetic hysteresis up to 7 K at an average sweep rate of 0.002 T/s when Ln = Dy.[3] This can be compared to the magnetic hysteresis observed for $[\{[(Me_3Si)_2N]_2(THF)Dy\}_2(\mu\text{-}\eta^2\text{:}\eta^2\text{-}N_2)]^-$ at temperatures as high as 8 K at an average sweep rate of 0.08 T/s. In the case of the 2,2′-bipyrimidine radical-bridged complexes, the Tb analog, which ceases to display remnant magnetization at temperatures above 2 K, does not possess better magnetic properties than the Dy analog. This is in contrast to what is observed in the $(N_2)^{3-}$ radical-bridged series for which the Tb analog demonstrates the strongest magnetic properties and maintains magnetic hysteresis at temperatures as high as 14 K with an average sweep rate of 0.0009 T/s.[2] Regardless, the series of $(bpym)^{\bullet-}$ complexes represents a good comparison to the $(phz)^{\bullet-}$ complexes described here.

Results

Synthesis. Phenazine Bridge. The paramagnetic lanthanide analogs of **1**, namely $\{[(C_5Me_5)_2Ln]_2(\mu\text{-phz})\}\{BPh_4\}$ (Ln = Dy, **2**; Tb, **3**), Fig. 6.1, can be synthesized by an analogous route[6] to **1** by reacting 2 equiv of $[(C_5Me_5)_2Ln][(\mu\text{-Ph})_2BPh_2]$ with 1 equiv of phenazine over 2 d. However, unlike $[(C_5Me_5)_2Y][(\mu\text{-Ph})_2BPh_2]$, which is fully soluble in benzene, $[(C_5Me_5)_2Ln][(\mu\text{-Ph})_2BPh_2]$ (Ln = Tb, Dy) were only partially soluble in benzene, even with heating. This made it challenging to isolate the radical dimeric species in yields greater than 20%.

A new route to synthesizing **1**-**3** was devised in which 1 equiv of KC_8 is added to the reaction mixture to produce $KBPh_4$ and graphite as byproducts, eq 6.2. While this new route significantly decreases the reaction time from 2 days to a few hours, initial experiments do not indicate a noticeable increase in product yields. The same is true when the phenazine radical is first isolated as a potassium salt ("K(phz)") from a THF solution then used as a reagent to generate the bridging species **1**-**3**, eq 4.2. Interestingly, crystals of **2** and **3** can be isolated using an external $Nd_2Fe_{13}B$ magnet as has been observed for other highly paramagnetic lanthanide complexes.[7]

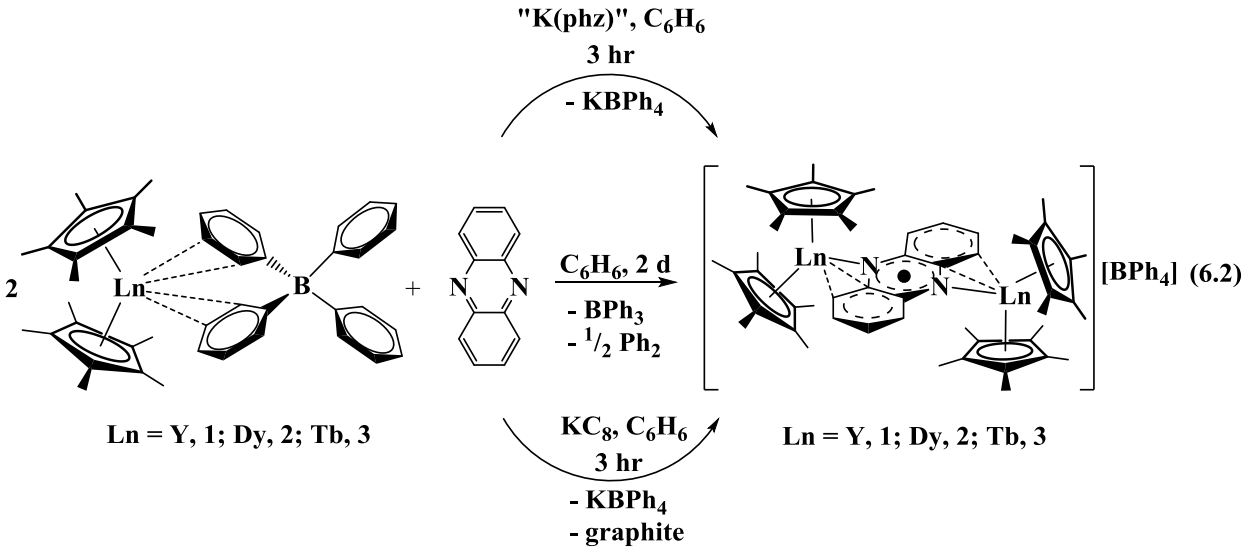

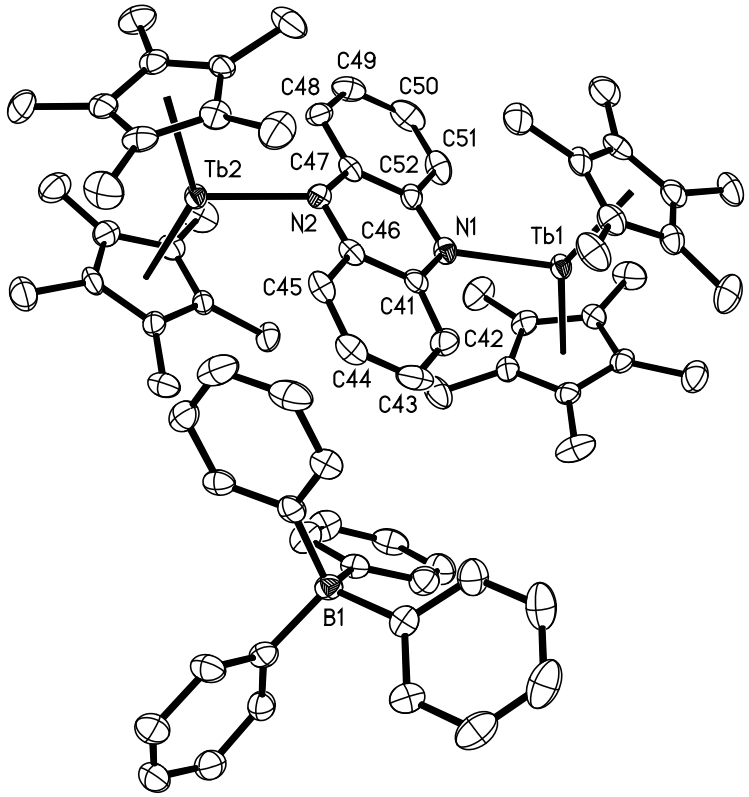

Figure 6.1. Thermal ellipsoid plot of $\{[(C_5Me_5)_2Tb]_2(\mu\text{-phz})\}\{BPh_4\}\bullet 5(C_6H_6)$, **3•5($C_6H_6$)**, drawn at the 50% probability level. Hydrogen atoms and cocrystallized solvent molecules have been omitted for clarity.

In light of the reported synthesis for the bpym analogs,[3] these reactions with phz were attempted in THF. Unlike the reactions with bpym, for which the authors report a color change simply upon addition of bpym to a colorless THF solution of $[(C_5Me_5)_2Ln][(\mu\text{-}Ph)_2BPh_2]$, there was no noticeable reaction of phz with $[(C_5Me_5)_2Ln][(\mu\text{-}Ph)_2BPh_2]$ when test reactions were performed with the Y analog. It is known that THF solvation of the unsolvated $[(C_5Me_5)_2Ln][(\mu\text{-}Ph)_2BPh_2]$ cationic species drastically reduces the reactivity of these complexes,[8] so it is not surprising that phz, which has only one donor nitrogen atom that can bind per metal ion, would not be able to displace multiple THF molecules binding the metal ion. Further, when 1 equiv of KC_8 is then added to a 2:1 solution of what is now $[(C_5Me_5)_2Y(THF)_2][BPh_4]$ and phz, the result is a dark red solution whose NMR spectrum is consistent with the known $(phz)^{2-}$ complex $[(C_5Me_5)_2Y]_2(\mu\text{-phz})$ identified as a decomposition product of **1** along with 5,10-dihydrophenazine.[6]

Several attempts to synthesize the Gd analog of **1** directly from the routes described for **1**-**3** above were pursued. However, the only product isolated from these reactions was 5,10-dihydrophenazine (as determined by X-ray crystallography[9]), a reported decomposition product of **1**.[6] Another route to obtaining the $(phz)^{\bullet-}$ complex would be to first synthesize the $(phz)^{2-}$-bridged species and then oxidize it. While the Y analog of the $(phz)^{2-}$ complex $[(C_5Me_5)_2Y]_2(\mu\text{-phz})$ was reported as another decomposition product of **1**,[6] the Gd analog was not known. Indeed, the reaction of 2 equiv of $[(C_5Me_5)_2Gd][(\mu\text{-}Ph)_2BPh_2]$ with 2 equiv of KC_8 and 1 equiv of phenazine in THF, yields the $(phz)^{2-}$ species $[(C_5Me_5)_2Gd]_2(\mu\text{-phz})$, **4**, Fig 6.2. Attempts to oxidize **4** using $AgBPh_4$ to generate the $(phz)^{\bullet-}$ analog were unsuccessful.

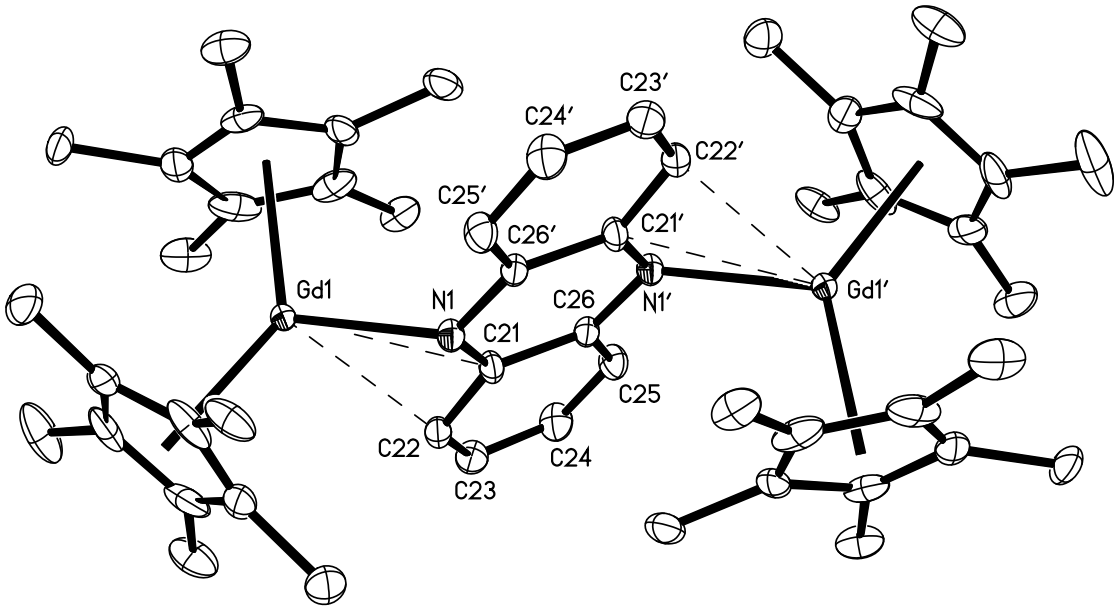

Figure 6.2. Thermal ellipsoid plot of $[(C_5Me_5)_2Gd]_2(\mu\text{-phz})$, **4**, drawn at the 50% probability level. Hydrogen atoms and cocrystallized solvent molecules have been omitted for clarity. Disorder in the methyl substituents of the cyclopentadienyl ligands has also been omitted.

2,2′-Bipyrimidine. Reactions of 2,2′-bipyrimidine with $[(C_5Me_5)_2Y][(\mu\text{-Ph})_2BPh_2]$ were also explored. Following an analogous procedure to the phenazine reactions above to target a $(bpym)^{\bullet-}$ radical-bridged complex, 2 equiv of $[(C_5Me_5)_2Y][(\mu\text{-Ph})_2BPh_2]$ were reacted with 1 equiv of 2,2′-bipyrimidine in benzene. This immediately generates an orange solution that produces a black precipitate within minutes which was insoluble in THF and unidentifiable. However, since BPh_3 is observed as a byproduct by NMR spectroscopy, this suggested a reduction occurred. The same result was observed when the Tb analog $[(C_5Me_5)_2Tb][(\mu\text{-Ph})_2BPh_2]$ was used. If instead, the Y cationic complex $[(C_5Me_5)_2Y][(\mu\text{-Ph})_2BPh_2]$ is reacted with 2,2′-bipyrimidine in a 1:1 ratio in THF, the neutral adduct $[(C_5Me_5)_2Y(bpym)][BPh_4]$, **5**, can be isolated as orange crystals, eq 6.3, Fig. 6.3. This neutral bpym adduct is likely the Y analog of the orange intermediate that Long and coworkers reported observing before addition of

KC_8 to form the $(bpym)^{\bullet-}$ radical complexes $\{[(C_5Me_5)_2Ln]_2(\mu\text{-bpym})\}\{BPh_4\}$ of the Ln = Gd, Tb, and Dy analogs.[3]

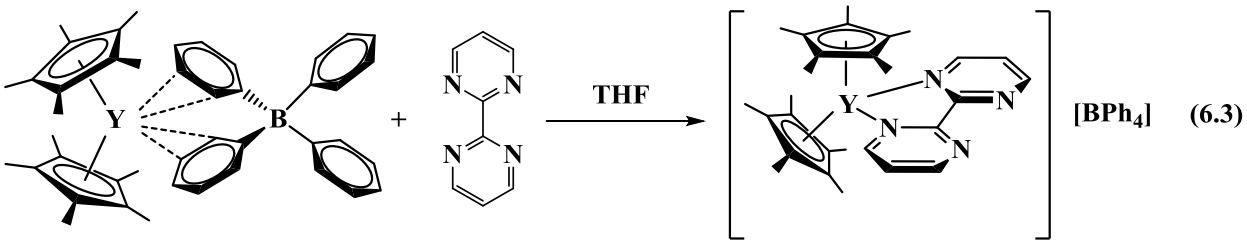

5

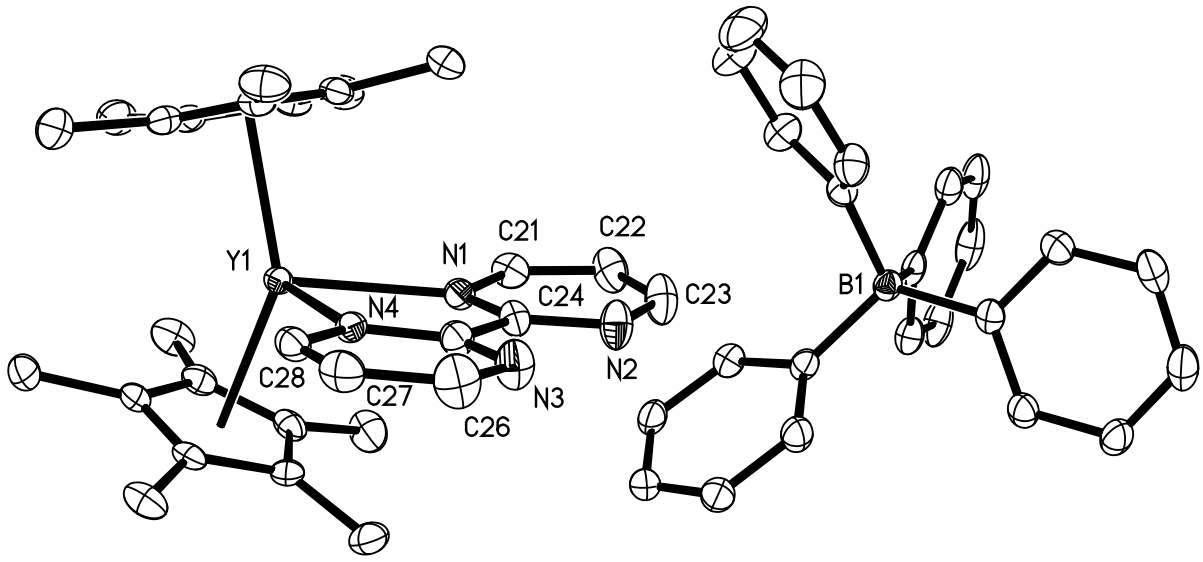

Figure 6.3. Thermal ellipsoid plot of $[(C_5Me_5)_2Y(bpym)][BPh_4]$, **5**, drawn at the 50% probability level. Hydrogen atoms and cocrystallized solvent molecules have been omitted for clarity.

Crystallographic Analysis. The crystal structure of the Dy complex $\{[(C_5Me_5)_2Dy]_2(\mu\text{-phz})\}\{BPh_4\}$, **2**, is isomorphous with the previously published Y analog **1**,[6] crystallizing in the orthorhombic space group $P2_12_12_1$ with one cocrystallized benzene molecule of solvation.

Interestingly, the Tb analog has been crystallographically characterized with two different triclinic unit cells, one for a refined structure containing five cocrystallized benzene molecules, **3•5(C_6H_6)**, and one for a structure containing none, **3**. The structure of **3•5(C_6H_6)**, with solvent molecules omitted, is shown in Figure 6.1 and is structurally similar to the Y and Dy analogs. As can be seen in Table 6.1, the number of cocrystallized solvent molecules does appear to affect the metrical parameters within the dimeric coordination complex. For example, the position of the bridging $(phz)^{\bullet-}$ ligand is significantly different between complex **3** and **3•5(C_6H_6)**. Although the Tb–N distances do not change drastically between these two crystallographic solutions, the distances from the metal centers to the carbon atoms nearest the nitrogen atoms as well as the next nearest carbon atoms vary significantly (see Table 4.1, Tb–C_α and Tb–C_β). This structural flexibility is also evidenced by the range of Ln–N–(phz plane) angles (155-163°) in **1-3**. Although there appears to be some variability in the position of the bridging $(phz)^{\bullet-}$ between the two rare earth centers in **1-3**, the Ln–Cnt distances and angles stay relatively constant and consistent with what is observed for rare earth metallocene complexes containing metals of ionic radii between 1.07 and 1.10 Å and pentamethylcyclopentadienyl ligands.[8,10,11]

Complex **4**, Fig 6.2, is structurally similar to the previously reported Y analog $[(C_5Me_5)_2Y]_2(\mu\text{-phz})$.[6] However, in this case, the Gd analog **4** cocrystallizes with a toluene molecule of solvation while the Y analog cocrystallizes with one benzene molecule, so they are not isomorphous. Despite the larger ionic radius of Gd compared to Dy, Tb and Y, the distances from Gd to the atoms comprising the central ring of phenazine in **4** (Gd–N and Gd–C_α) are noticeably shorter than the analogous distances in **1-3**. This is consistent with the more anionic $(phz)^{2-}$ ligand versus $(phz)^{1-}$. Associated with the short Gd–(phz) distances in **4** is a smaller Cnt–Gd–Cnt angle of 136.5° compared to 142-144° in **1-3**. This is consistent with what is

observed for $[(C_5Me_5)_2Y]_2(\mu$-phz) (Cnt–Y–Cnt = 137.0°) when compared to its $(phz)^{1-}$ analog **1** (Cnt–Y–Cnt = 142.4, 142.8°).[6] As an effect, the tilt of the phenazine bridging in **4** and $[(C_5Me_5)_2Y]_2(\mu$-phz) (Ln–N–(phz plane) = 135.2° and 144.5°, respectively) is more drastic than in the $(phz)^{1-}$-containing species (Ln–N–(phz plane) = 155-163°).

Table 6.1. Selected bond lengths (Å) and angles (deg) in complexes **1-4** and $[(C_5Me_5)_2Y]_2$(phz).[6]

Compound	Ln–Cnt	Ln–N	Ln–C_α [a]	Ln–C_β [b]	Cnt–Ln–Cnt	Ln–N–(phz plane)[c]
$\{[(C_5Me_5)_2Y]_2(\mu$-phz)$\}\{BPh_4\}\bullet(C_6H_6)$, **1**[6]	2.318	2.358(2)	3.062(2)	3.028(2)	142.8	160.9
	2.325	2.355(2)	3.060(2)	3.028(2)	142.4	159.9
	2.320					
	2.326					
$\{[(C_5Me_5)_2Dy]_2(\mu$-phz)$\}\{BPh_4\}\bullet(C_6H_6)$, **2**	2.325	2.369(2)	3.066(3)	3.026(3)	143.1	156.8
	2.333	2.369(2)	3.064(3)	3.020(3)	142.7	155.5
	2.326					
	2.335					
$\{[(C_5Me_5)_2Tb]_2(\mu$-phz)$\}\{BPh_4\}$, **3**	2.358	2.405(2)	3.109(2)	3.053(3)	142.8	158.5
	2.346	2.375(2)	3.223(2)	3.323(3)	143.2	158.4
	2.333					
	2.350					
$\{[(C_5Me_5)_2Tb]_2(\mu$-phz)$\}\{BPh_4\}\bullet5(C_6H_6)$, **3•5($C_6H_6$)**	2.341	2.370(4)	3.312(7)	3.522(8)	143.9	162.8
	2.338	2.360(4)	3.371(7)	3.619(8)	142.7	155.7
	2.347					
	2.348					
$[(C_5Me_5)_2Gd]_2(\mu$-phz)$\bullet(C_7H_8)$, **4**	2.412	2.346(2)	2.843(2)	2.816(2)	136.5	135.2
	2.393					
$[(C_5Me_5)_2Y]_2(\mu$-phz)$\bullet(C_6H_6)$[6]	2.366	2.298(1)	2.817(2)	2.785(2)	137.0	144.5
	2.346					

[a] C_α = C41, C47 for **1**,[6] **2•5(C_6H_6)** and **3**; C23, C49 for **2**; C21 for $[(C_5Me_5)_2Y]_2(\mu$-phz)[6] and **4**. [b] C_β = C42, C48 for **1**,[6] **2•5(C_6H_6)** and **3**; C24, C48 for **2**; C22 for $[(C_5Me_5)_2Y]_2(\mu$-phz)[6] and **4**. [c] Plane is defined by the 6 atoms in the central ring of phenazine.

As can be seen in Table 6.2, the metrical parameters pertaining to the monometallic (bpym) species **5** are very similar to the analogous features in the bimetallic $(bpym)^{\bullet-}$ complexes $\{[(C_5Me_5)_2Ln]_2(\mu$-bpym)$\}\{BPh_4\}$ (Ln = Dy, Tb). An interesting difference is the slight torsion between the rings of the neutral bpym ligand in **5** which is absent in the reduced bpym species.

While no literature examples of monometallic rare earth 2,2′-bipyrimidine metallocenes could be found, 2,2′-bipyridyl (bipy) rare earth metallocenes have been reported and are comprable (*vide infra*). The dihedral angles between the bpym rings in **5** are similar to analogous angles observed for the bipy Yb^{2+} metallocene complexes $(C_5Me_5)_2Yb(bipy)$ (3°) and $[(C_5Me_5)_2Yb(bipy)][(C_5Me_5)_2YbCl_2]$ (8°) reported by Andersen and coworkers.[12] The authors state that greater torsion of the bound rings indicates ligand neutrality. This can be compared to the Sm^{3+} analog, $(C_5Me_5)_2Sm(bipy)$, reported by Evans and coworkers in which the dihedral angle is only 1°.[13] This conclusion is also consistent with what is observed for the neutral bpym complex **5**, which demonstrates slight torsion between bpym rings versus the reduced $(bpym)^{1-}$ complexes $\{[(C_5Me_5)_2Ln]_2(\mu\text{-bpym})\}\{BPh_4\}$ (Ln = Dy, Tb) which show zero torsion of the aromatic rings.

Table 6.2. Selected bond lengths (Å) and angles (deg) in **5** and $\{[(C_5Me_5)_2Ln]_2(\mu\text{-bpym})\}\{BPh_4\}$ (Ln = Dy, Tb).[3]

Compound	Ln–Cnt[a]	Ln–N	Cnt–Ln–Cnt	Dihedral Angle Between (bpym) Rings
$[(C_5Me_5)_2Y](bpym)][BPh_4]$, **5**	2.336	2.416(2)	142.5	5
	2.325	2.435(2)	143.3	7
	2.330	2.421(2)		
	2.348	2.430(2)		
$\{[(C_5Me_5)_2Dy]_2(\mu\text{-bpym})\}\{BPh_4\}$[3]	2.350	2.427(5)	141.5	0
	2.326			
$\{[(C_5Me_5)_2Tb]_2(\mu\text{-bpym})\}\{BPh_4\}$[3]	2.408	2.434(5)	139.5	0
	2.366			

[a] There were two unique molecules in the assymmetric unit of **5**.

Preliminary Magnetic Studies. Preliminary magnetic measurements of **2** and **3**, performed by Dr. Selvan Demir in the laboratory of Professor Jeffrey R. Long at the University of California, Berkeley, indicate that both of these complexes possess SMM properties. Figure

6.4 shows preliminary temperature-dependent dc magnetic susceptibility data for **2** between 1.8 and 300 K. The room temperature $\chi_M T$ value for the Dy analog **2** is 28.9 cm^3K/mol, indicated by the black line in Figure 6.4. This can be compared to the room temperature $\chi_M T$ value of 27.4 cm^3K/mol for $\{[(C_5Me_5)_2Dy]_2(\mu\text{-bpym})\}\{BPh_4\}$.[3] As the temperature decreases, there is a shallow minimum in $\chi_M T$ that can be observed at 125 K followed by a rise in $\chi_M T$ which obtains a maximum value at 18K, surpassing the maximum $\chi_M T$ observed in the the $(bpym)^{\bullet-}$ analog, suggestive of antiferromagnetic coupling between the radical bridging ligand and the lanthanide ions as has been previously observed in other radical containing SMMs.[1-3,7,14] At lower temperatures, the $\chi_M T$ decreases dramatically, indicative of magnetic blocking of the magnetization as has also been reported in the above mentioned references. Since the Gd analog of **2** and **3** could not be isolated, quantitative analysis of the strength of magnetic exchange coupling in these $(phz)^{\bullet-}$-bridged complexes is not reported here.

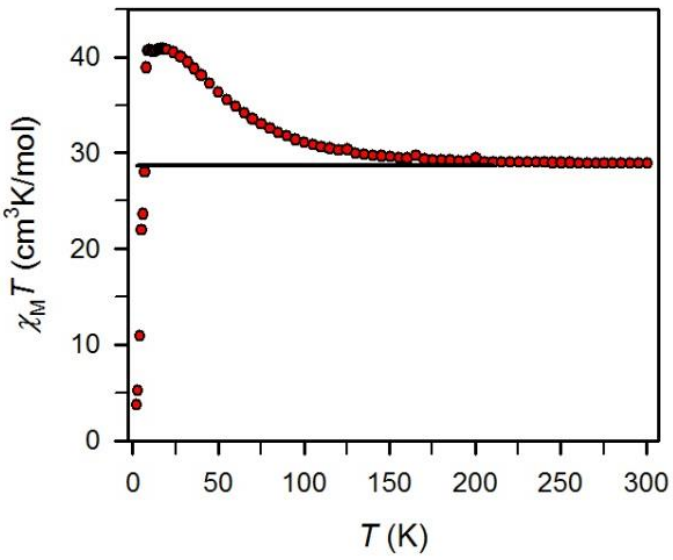

Figure 6.4. Variable-temperature dc magnetic susceptibility data for $\{[(C_5Me_5)_2Dy]_2(\mu\text{-phz})\}\{BPh_4\}$, **2**. The black line represents the theoretical room temperature $\chi_M T$ value.

Ac magnetic susceptibility data were collected for **2** and **3** over a range of temperatures, and plots of the out-of-phase component (χ_M'') are show in Figure 6.5 collected under zero applied field. Two distinct sets of peaks for each complex can be seen in these ac data indicating the presence of a second temperature dependent, magnetically relevant species in each sample. For **2** (Fig 6.5 top), fitting to the five peaks at higher frequencies (8-12 K) yields a relaxation barrier of U_{eff} = 59 cm^{-1} (τ_0 = 3.53 x 10^{-7} s). However, fitting to the three peaks at lower frequencies (10-12 K) yields a much higher relaxation barrier of U_{eff} = 100 cm^{-1} (τ_0 = 3.87 x 10^{-7} s), suggesting that one of the species in the sample can achieve a barrier to relaxation that is nearly twice that of the other paramagnetic contaminant. A similar scenario is observed in the case of the Tb analog **3** (Fig 6.5 bottom) for which two relaxation barriers can again be extracted, one at 61 cm^{-1} and another at 109 cm^{-1}. These values can be compared to those reported for the $(bpym)^{\bullet-}$ complexes of Dy (U_{eff} = 87.8(3) cm^{-1}, τ_0 = 1.03(4) × 10^{-7} s) and Tb (U_{eff} = 44(2) cm^{-1}, τ_0 = 4(1) × 10^{-8} s), respectively. The fact that samples of **2** and **3** possess higher barriers to relaxation than their $(bpym)^{\bullet-}$ analogs suggests $(phz)^{\bullet-}$ may be a better bridging ligand to enhance SMM properties than $(bpym)^{\bullet-}$, however, the presence of a second complex of interest in samples of **2** and **3** complicates this analysis. Possible explanations for the apparent presence of two species in samples of **2** and **3** are addressed in the Discussion section below.

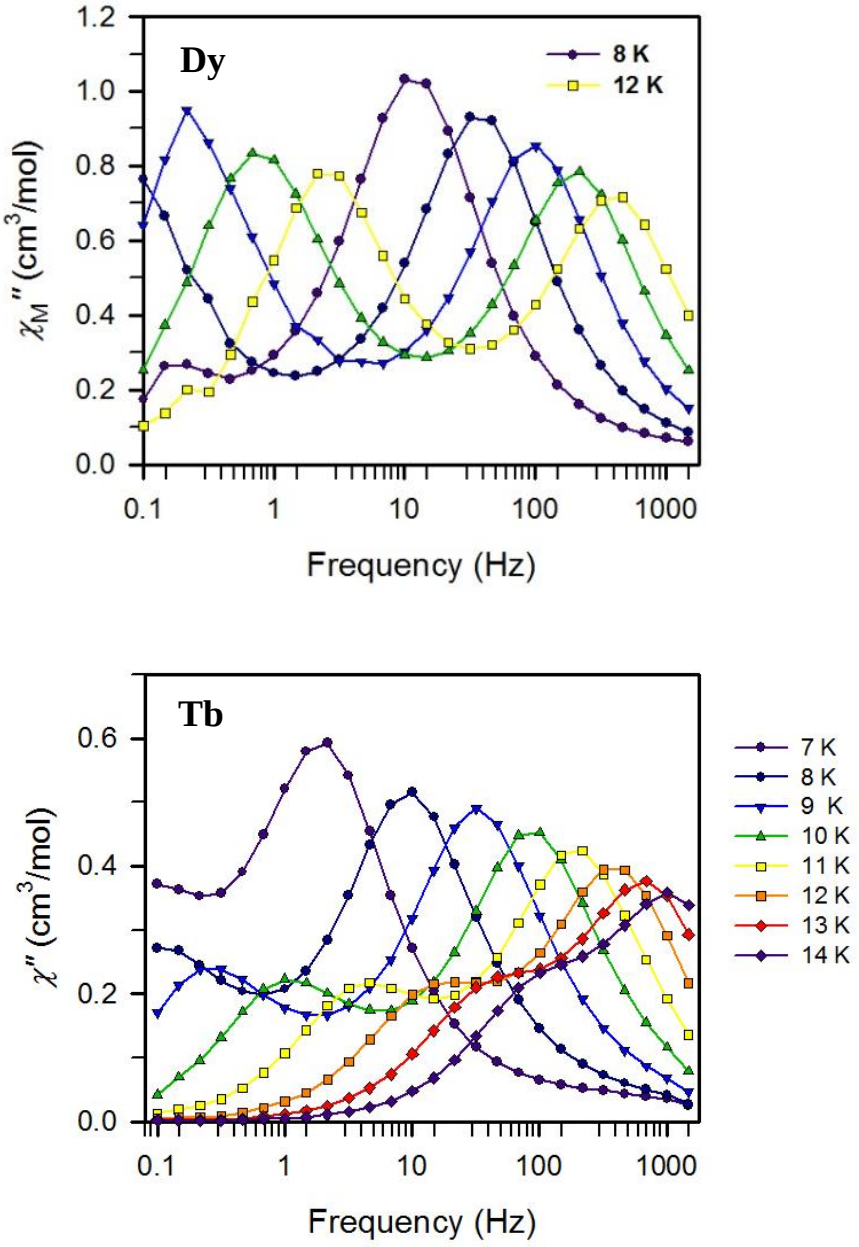

Figure 6.5. Out-of-phase (χ_M'') components of the ac magnetic susceptibility under zero applied dc field for (top) {[$(C_5Me_5)_2Dy]_2(\mu$-phz)}{BPh_4}, **2**, from 8 K (purple circles) to 12 K (yellow squares) and (bottom) {[$(C_5Me_5)_2Tb]_2(\mu$-phz)}{BPh_4}, **3**, from 7 K (purple circles) to 14K (purple diamonds). Solid lines represent fits to the data.

Magnetic hysteresis measurements were obtained for the Dy analog **2**, Figure 6.6. Complex **2** displays a waist-constricted hysteresis loop at temperatures as high as 8 K for this preliminary data. The apparent step at zero applied field (H = 0) suggests tunneling of the magnetization. This feature is similar to what is reported in the hysteresis data for $\{[(C_5Me_5)_2Dy]_2(\mu\text{-bpym})\}\{BPh_4\}$ which displays remnant magnetization up to temperatures as high as 6.5 K.[3] At the time of publication in 2012, there were said to be only four molecular complexes that displayed higher blocking temperatures than $\{[(C_5Me_5)_2Dy]_2(\mu\text{-bpym})\}\{BPh_4\}$. The bridging $(phz)^{\bullet-}$ analog can now be added to this list.

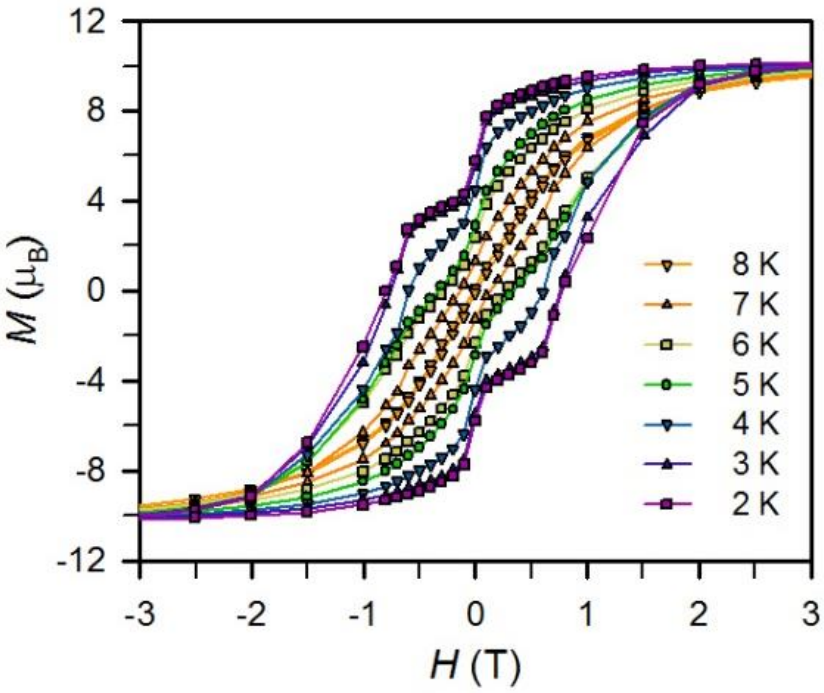

Figure 6.6. Variable-field magnetization (M) data for $\{[(C_5Me_5)_2Dy]_2(\mu\text{-phz})\}\{BPh_4\}$, **2**, collected from 2 to 8 K.

Discussion

Unlike the reaction of phenazine (phz) with $[(C_5Me_5)_2Ln][(\mu\text{-}Ph)_2BPh_2]$ in benzene, which requires days to go to completion, 2,2′-bipyrimidine (bpym) reacts immediately with $[(C_5Me_5)_2Ln][(\mu\text{-}Ph)_2BPh_2]$ in benzene to generate a transient orange solution that goes on to form insoluble black solids within minutes. It is likely that the short-lived orange species in the latter reaction is the crystallographically characterized neutral bpym complex **5**. It makes sense that bpym demonstrates higher reactivity due to its multiple donor atoms and tendency to take on a multidentate binding mode. Differences in reactivity are also observed for the THF solvated cationic precursors $[(C_5Me_5)_2Ln(THF)_2][BPh_4]$ (Ln = Y, Dy, Tb, Gd) when reacted with either phz or bpym in the presence of KC_8. In the case of phz, reduction of 1 equiv of phz by 1 equiv of KC_8 in the presence of 2 equiv of $[(C_5Me_5)_2Y(THF)_2][BPh_4]$ yields mostly the doubly reduced $(phz)^{2-}$ species $[(C_5Me_5)_2Y]_2(\mu\text{-phz})$ as identified by NMR spectroscopy.[6] Conversely, when the same reaction is performed with bpym in place of phz, the radical bridged $\{[(C_5Me_5)_2Ln]_2(\mu\text{-bpym})\}\{BPh_4\}$ complexes can be isolated in greater than 50% crystalline yields.[3] Due to the relative ease with which phenazine can be reduced, it makes sense that $(phz)^{1-}$ would be more susceptible to reduction when compared with $(bpym)^{1-}$, which is expected to have a much larger reduction potential.

While the bpym radical complexes are easier synthetically to work with, the phz radical species **2** and **3** demonstrate higher barriers to relaxation based on preliminary ac magnetic susceptibility measurements. However, these same data also indicate the presence of a second species in crystalline samples of **2** and **3** which contributes a second set of signals in the dynamic susceptibility data. The source of this second relaxation process is still unclear. However, based on the variability of crystalline forms exemplified in the X-ray data of **3**, it is conceivable that the $(phz)^{\bullet-}$ bridge could take on slightly different positions depending on the crystalline structure

which could cocrystallize in the same sample batch, a property that has been observed in other bimetallic rare earth species.[15,16] It should also be noted that the cationic precursors to the bridging $(phz)^{\bullet-}$ complexes as well as the $(bpym)^{\bullet-}$ complexes, namely $[(C_5Me_5)_2Ln][(\mu\text{-}Ph)_2BPh_2]$, have been shown to display high spin-relaxation barriers themselves (U_{eff} = 221 cm^{-1} for Ln = Tb and U_{eff} = 314 cm^{-1} for Ln = Dy), however, these complexes display closed hysteresis loops at zero field.[17]

Although the purity of these samples was verified by elemental analysis and the number of solvent molecules per dimeric unit was determined before magnetic measurements were obtained, these values do not vary substantially upon incorporation of a small percentage of a possible $[(C_5Me_5)_2Ln][(\mu\text{-}Ph)_2BPh_2]$ contaminant. For example, for **3** containing no cocrystallized solvent molecules, the elemental analysis values are predicted to be C, 67.87; H, 8.14; N, 1.88. After incorporating ¼ $[(C_5Me_5)_2Tb][(\mu\text{-}Ph)_2BPh_2]$ for every molecule of **3** into the calculated values, the elemental analysis is still a match within the detection limit of the instrument (C, 68.17; H, 7.98; N, 1.67). Therefore, the starting material $[(C_5Me_5)_2Ln][(\mu\text{-}Ph)_2BPh_2]$ cannot be ruled out as the possible magnetic contaminant, since these complexes have similar solubility and crystallinity to their $(phz)^{1-}$ products. It is also possible that even if a relatively small percentage of crystals had a different morphology or phz ligand position, this could perturb the magnetic data obtained by the highly sensitive SQUID magnetometer. Unlike the rigid bpym unit which can bind both metal centers in a bidentate fashion, the position of the phz bridge is more variable as demonstrated by the X-ray crystallographic data shown in Table 4.1 above. A different angle of the phz ligand with respect to the metal centers could lead to different magnetic relaxation pathways. Ultimately, solution magnetic measurements on **2** and **3** will need to be pursued to ensure the uniformity of the magnetic environment.

Conclusion

The Dy and Tb analogs of $\{[(C_5Me_5)_2Ln]_2(\mu\text{-phz})\}\{BPh_4\}$ can indeed be synthesized via a similar route to the previously reported Y analog.[6] However, in the course of this study, it was found that addition of KC_8 to the initial reaction conditions drastically decreases the reaction time from 2 d to 3 hrs. Preliminary magnetic measurements indicate there are two unique magnetic relaxation processes occurring in samples of **2** and **3** suggesting the presence of multiple species or multiple magnetic environments. However, despite their complicated magnetic characteristics, **2** and **3** demonstrate high relaxation barriers and blocking temperatures when compared with other SMMs in the field.[18]

Experimental

All syntheses and manipulations described below were conducted under nitrogen or argon with rigorous exclusion of air and water using glovebox, Schlenk, and high-vacuum line techniques. Solvents were sparged with UHP argon and dried over columns containing Q-5 and molecular sieves. KC_8[19] and $[(C_5Me_5)_2Ln][(\mu\text{-Ph})_2BPh_2]$[8] (Ln = Tb, Dy, or Gd) were prepared according to literature procedures. $Nd_2Fe_{13}B$ magnets were obtained from United Nuclear Scientific Equipment and Supplies. ^1H and ^{13}C NMR spectra were obtained on a Bruker CRYO500 MHz spectrometer at 25 ºC. IR samples were prepared as KBr pellets on a Varian 1000 FT-IR system. Elemental analyses were performed on a PerkinElmer Series II 2400 CHN analyzer. Magnetic susceptibility measurements were collected using a Quantum Design MPMS2 SQUID magnetometer. Magnetic samples were prepared in quartz tubes as powders restrained in eicosane to prevent crystallite torqueing and provide good thermal contact between the sample and the bath. Tubes were fitted with sealable adapters, evacuated on a Schlenk line, and flame sealed under vacuum.

{[(C_5Me_5)$_2$Dy]$_2$(phz)}{BPh_4}, 2. In a nitrogen-filled glovebox, KC_8 (13 mg, 0.1 mmol) was added to a benzene solution (18 mL) containing phenazine (18 mg, 0.1 mmol) and [(C_5Me_5)$_2$Tb][(μ-Ph)$_2$$BPh_2$] (150 mg, 0.2 mmol) and color changes from yellow/orange to brown to dark green were observed over 1 min. The reaction mixture was left to stir 2 hr, then was centrifuged to remove white and black solids. The dark green supernatant was concentrated to 8 mL under reduced pressure with heating and hexane was slowly diffused into the solution over 1 d to yield **3** as dichroic dark green/purple X-ray quality crystals (20 mg, 12%) which grow near the $Nd_2Fe_{13}B$ magnet attached to the side of the vial. IR: 3055w, 2963m, 2909m, 2857m, 1603w, 1515w, 1479m, 1430m, 1380w, 1326w, 1299w, 1261w, 1152w, 1030w, 901w, 842w, 734s, 705s, 686m, 612s cm^{-1}. Anal. Calcd for $C_{68}H_{88}BN_2Dy_2$ • (C_6H_6), **2 • (C_6H_6)**: C, 66.86; H, 6.50; N, 2.05. Found: C, 66.82; H, 6.83; N, 2.37.

{[(C_5Me_5)$_2$Tb]$_2$(phz)}{BPh_4}, 3. Following procedures previously reported,[6] in a nitrogen-filled glovebox, benzene (8 mL) was added to [(C_5Me_5)$_2$Tb][(μ-Ph)$_2$$BPh_2$] (50 mg, 0.07 mmol) to make a cloudy, yellow mixture. While stirring, a benzene solution of phenazine (6 mg, 0.03 mmol) was added and after stirring for 1 hr, the solution began to turn light green. The solution was stirred for 2 d, during which time it became very dark green. After the solvent was removed under vacuum, the resulting green/brown solids were washed with hexane and dried under reduced pressure. The solids were then redissolved in benzene (4 mL) and hexane was slowly diffused into the solution over 2 d to yield **3** as dichroic dark green/purple X-ray quality crystals (10 mg, 17%) which grow near the $Nd_2Fe_{13}B$ magnet attached to the side of the vial. IR: 3033m, 2908s, 2859s, 2298w, 1580w, 1532m, 1429m, 1381w, 1326m, 1261w, 1152w, 1021w, 899w, 824w, 732s, 703s, 679s, 613m cm^{-1}. Anal. Calcd for $C_{76}H_{92}BN_2Tb_2$ • (C_6H_6), **3** • (C_6H_6): C, 68.38; H, 6.86; N, 1.94. Found: C, 68.39; H, 6.66; N, 1.88.

$[(C_5Me_5)_2Gd]_2(phz)$, 4. A dark magenta THF (3 mL) suspension of phenazine (6 mg, 0.03 mmol) and KC_8 (9 mg, 0.07 mmol) was added dropwise to a colorless THF solution of $[(C_5Me_5)_2Gd(THF)_2][BPh_4]$ (50 mg, 0.07 mmol) and the dark reaction mixture was left to stir 20 min. Centrifugation removed black and white solids and the dark red supernatant was filtered and solvent was removed under reduced pressure. The red solids were dissolved in toluene (3 mL) and stored at −35 °C in a vial with a $Nd_2Fe_{13}B$ magnet attached to the side. After 1 d, dark red X-ray quality crystals were obtained.

$[(C_5Me_5)_2Y](bpym)][BPh_4]$, 5. A THF solution (2 mL) of 2,2′-bipyrimidine (bpym) (8 mg, 0.05 mmol) was added dropwise to a colorless THF solution (4 mL) of $[(C_5Me_5)_2Y(THF)_2][BPh_4]$ (34 mg, 0.05 mmol) to yield an orange solution which was stirred for 30 min then stored at −35 °C. After 1 d, orange X-ray quality crystals were obtained.

X-ray Data Collection, Structure Solution and Refinement for $\{[(C_5Me_5)_2Dy]_2(phz)\}\{BPh_4\}$, 2. A dark green crystal of approximate dimensions 0.451 x 0.285 x 0.113 mm was mounted on a glass fiber and transferred to a Bruker SMART APEX II diffractometer. The APEX2[20] program package was used to determine the unit-cell parameters and for data collection (20 sec/frame scan time for a sphere of diffraction data). The raw frame data was processed using SAINT[21] and SADABS[22] to yield the reflection data file. Subsequent calculations were carried out using the SHELXTL[23] program. The diffraction symmetry was *mmm* and the systematic absences were consistent with the orthorhombic space group $P2_12_12_1$ that was later determined to be correct. The structure was solved by direct methods and refined on F^2 by full-matrix least-squares techniques. The analytical scattering factors[24] for neutral atoms were used throughout the analysis. Hydrogen atoms were included using a riding model. At convergence, wR2 = 0.0374 and Goof = 1.020 for 804 variables refined against 16610 data

(0.75 Å), R1 = 0.0175 for those 15940 data with I > 2.0σ(I). The absolute structure was assigned by refinement of the Flack parameter.[25] Details are given in Table 6.3.

X-ray Data Collection, Structure Solution and Refinement for {[$(C_5Me_5)_2Tb]_2$(phz)}{BPh_4}, 3. A green crystal of approximate dimensions 0.459 x 0.280 x 0.276 mm was mounted on a glass fiber and transferred to a Bruker SMART APEX II diffractometer. The APEX2[26] program package was used to determine the unit-cell parameters and for data collection (10 sec/frame scan time for a sphere of diffraction data). The raw frame data was processed using SAINT[27] and SADABS[28] to yield the reflection data file. Subsequent calculations were carried out using the SHELXTL[29] program. There were no systematic absences nor any diffraction symmetry other than the Friedel condition. The centrosymmetric triclinic space group $P\bar{1}$ was assigned and later determined to be correct. The structure was solved by direct methods and refined on F^2 by full-matrix least-squares techniques. The analytical scattering factors[24] for neutral atoms were used throughout the analysis. There were two half molecules per asymetric unit, each located about an inversion center. Hydrogen atoms were included using a riding model. At convergence, wR2 = 0.0561 and Goof = 1.051 for 754 variables refined against 15550 data (0.75 Å), R1 = 0.0257 for those 13820 data with I > 2.0σ(I). Details are given in Table 6.3.

X-ray Data Collection, Structure Solution and Refinement for {[$(C_5Me_5)_2Tb]_2$(μ-phz)}{BPh_4} • 5(C_6H_6), 3 • 5(C_6H_6). A green crystal of approximate dimensions 0.27 x 0.25 x 0.11 mm was mounted on a glass fiber and transferred to a Bruker SMART APEX II diffractometer. The APEX2[30] program package was used to determine the unit-cell parameters and for data collection (35 sec/frame scan time for a sphere of diffraction data). The raw frame data was processed using SAINT[21] and SADABS[22] to yield the reflection data file. Subsequent

calculations were carried out using the SHELXTL[23] program. There were no systematic absences. The noncentrosymmetric triclinic space group *P*1 was assigned and later determined to be correct. The structure was solved by direct methods and refined on F^2 by full-matrix least-squares techniques. The analytical scattering factors[24] for neutral atoms were used throughout the analysis. Hydrogen atoms were included using a riding model. There were five molecules of benzene solvent present. One of the solvent molecules exhibited rotational disorder and was included using multiple components with partial site-occupancy-factors. At convergence, wR2 = 0.0605 and Goof = 1.033 for 1015 variables refined against 19278 data (0.75 Å), R1 = 0.0254 for those 17991 data with $I > 2.0\sigma(I)$. The structure was refined as a racemic twin with BASF = 0.275(5). Details are given in Table 6.3.

X-ray Data Collection, Structure Solution and Refinement for $[(C_5Me_5)_2Gd]_2(phz)$, 4. A red crystal of approximate dimensions 0.216 x 0.080 x 0.048 mm was mounted on a glass fiber and transferred to a Bruker SMART APEX II diffractometer. The APEX2[30] program package was used to determine the unit-cell parameters and for data collection (25 sec/frame scan time for a sphere of diffraction data). The raw frame data was processed using SAINT[21] and SADABS[28] to yield the reflection data file. Subsequent calculations were carried out using the SHELXTL[29] program. There were no systematic absences nor any diffraction symmetry other than the Friedel condition. The centrosymmetric triclinic space group $P\bar{1}$ was assigned and later determined to be correct. The structure was solved by direct methods and refined on F^2 by full-matrix least-squares techniques. The analytical scattering factors[24] for neutral atoms were used throughout the analysis. Hydrogen atoms were included using a riding model. The molecule was situated about an inversion center. There was one toluene molecule of solvation present per formula unit. C(6), C(7), C(8), C(9), C(10), C(16), C(17), C(18), C(19), and C(20)

were disordered and included using multiple components with partial site-occupancy-factors. At convergence, wR2 = 0.0476 and Goof = 1.060 for 408 variables refined against 6049 data (0.74 Å), R1 = 0.0196 for those 5654 data with I > 2.0σ(I). Details are given in Table 6.3.

X-ray Data Collection, Structure Solution and Refinement for $[(C_5Me_5)_2Y](bpym)][BPh_4]$, 5. An orange crystal of approximate dimensions 0.362 x 0.286 x 0.114 mm was mounted on a glass fiber and transferred to a Bruker SMART APEX II diffractometer. The APEX2[30] program package was used to determine the unit-cell parameters and for data collection (20 sec/frame scan time for a sphere of diffraction data). The raw frame data was processed using SAINT[21] and SADABS[28] to yield the reflection data file. Subsequent calculations were carried out using the SHELXTL[29] program. There were no systematic absences nor any diffraction symmetry other than the Friedel condition. The centrosymmetric triclinic space group $P\bar{1}$ was assigned and later determined to be correct. The structure was solved by direct methods and refined on F^2 by full-matrix least-squares techniques. The analytical scattering factors[24] for neutral atoms were used throughout the analysis. Hydrogen atoms were included using a riding model. There was one THF of solvation present per formula unit, and there were two molecules present in the asymmetric unit. At convergence, wR2 = 0.0968 and Goof = 1.023 for 1155 variables refined against 22964 data (0.75 Å), R1 = 0.0424 for those 18097 data with I > 2.0σ(I). Details are given in Table 6.3.

Table 6.3. Crystal data and structure refinement parameters for {[$(C_5Me_5)_2Dy]_2(\mu$-phz)}{BPh_4}, **2**, {[$(C_5Me_5)_2Tb]_2(\mu$-phz)}{BPh_4}, **3**, {[$(C_5Me_5)_2Tb]_2(\mu$-phz)}{BPh_4} • 5(C_6H_6), **3 • 5(C_6H_6)**, [$(C_5Me_5)_2Gd]_2(\mu$-phz), **4** and [$(C_5Me_5)_2Y$](bpym)][BPh_4], **5**.

	2 • (C_6H_6)	**3**	**3** • 5(C_6H_6)	**4** • (C_7H_8)	**5** • (OC_4H_8)
Empirical formula	$C_{76}H_{88}BDy_2N_2$• (C_6H_6)	$C_{76}H_{88}BN_2Tb_2$	$C_{76}H_{88}BN_2Tb_2$ • 5(C_6H_6)	$C_{52}H_{68}Gd_2N_2$• (C_7H_8)	$C_{52}H_{56}BN_4Y$• (OC_4H_8)
Formula weight	1443.40	1358.13	1748.67	1127.71	908.83
Temperature (K)	88(2)	88(2)	143(2)	88(2)	88(2)
Space group	$P2_12_12_1$	$P\bar{1}$	$P1$	$P\bar{1}$	$P\bar{1}$
a (Å)	13.6171(5)	10.3454(9)	10.6084(16)	10.4383(6)	10.5753(4)
b (Å)	18.4939(7)	12.3734(11)	15.029(2)	11.0425(6)	17.8412(6)
c (Å)	27.1520(11)	25.318(2)	16.183(2)	11.3742(6)	26.1755(9)
α (°)	90	97.7770(11)	64.4758(16)	80.6980(10)	101.8063(4)
β (°)	90	95.8778(11)	71.4954(16)	77.0340(10)	94.8224(5)
γ (°)	90	95.9838(11)	82.3321(16)	85.5200(10)	90.6138(5)
Volume (Å^3)	6837.8(5)	3171.2(5)	2207.9(6)	1259.62(12)	4815.1(3)
Z	4	2	1	1	4
ρ_{calcd} (Mg/m^3)	1.402	1.422	1.315	1.487	1.254
μ (mm^{-1})	2.214	2.256	1.637	2.649	1.255
$R1^a$ [$I > 2\sigma(I)$]	0.0175	0.0257	0.0254	0.0196	0.0424
$wR2^b$	0.0374	0.0561	0.0605	0.0476	0.0968

$^aR1 = \Sigma||F_o|-|F_c|| / \Sigma|F_o|$. $^bwR2 = [\Sigma[w(F_o^2-F_c^2)^2] / \Sigma[w(F_o^2)^2]]^{1/2}$

References

(1) Rinehart, J. D.; Fang, M.; Evans, W. J.; Long, J. R. *Nature Chemistry* **2011**, *3*, 538.

(2) Rinehart, J. D.; Fang, M.; Evans, W. J.; Long, J. R. *Journal of the American Chemical Society* **2011**, *133*, 14236.

(3) Demir, S.; Zadrozny, J. M.; Nippe, M.; Long, J. R. *Journal of the American Chemical Society* **2012**, *134*, 18546.

(4) Woodruff, D. N.; Winpenny, R. E. P.; Layfield, R. A. *Chemical Reviews* **2013**, *113*, 5110.

(5) Rajeshkumar, T.; Rajaraman, G. *Chemical Communications* **2012**, *48*, 7856.

(6) MacDonald, M. R.; Ziller, J. W.; Evans, W. J. *Inorganic Chemistry* **2011**, *50*, 4092.

(7) Meihaus, K. R.; Corbey, J. F.; Fang, M.; Ziller, J. W.; Long, J. R.; Evans, W. J. *Inorganic Chemistry* **2014**, *53*, 3099.

(8) Evans, W. J.; Seibel, C. A.; Ziller, J. W. *J. Am. Chem. Soc.* **1998**, *120*, 6745.

(9) Thalladi, V. R.; Smolka, T.; Gehrke, A.; Boese, R.; Sustmann, R. *New Journal of Chemistry* **2000**, *24*, 143.

(10) Evans, W. J.; Lee, D. S.; Ziller, J. W.; Kaltsoyannis, N. *Journal of the American Chemical Society* **2006**, *128*, 14176.

(11) Evans, W. J.; Davis, B. L.; Champagne, T. M.; Ziller, J. W. *Proceedings of the National Academy of Sciences* **2006**, *103*, 12678.

(12) Schultz, M.; Boncella, J. M.; Berg, D. J.; Tilley, T. D.; Andersen, R. A. *Organometallics* **2002**, *21*, 460.

(13) Evans, W. J.; Drummond, D. K. *Journal of the American Chemical Society* **1989**, *111*, 3329.

(14) Demir, S.; Nippe, M.; Gonzalez, M. I.; Long, J. R. *Chemical Science* **2014**, *5*, 4701.

(15) Liu, S.-S.; Gao, S.; Ziller, J. W.; Evans, W. J. *Dalton Transactions* **2014**, *43*, 15526.

(16) Corbey, J. F.; Fang, M.; Ziller, J. W.; Evans, W. J. *Inorganic Chemistry* **2014**.

(17) Demir, S.; Zadrozny, J. M.; Long, J. R. *Chemistry – A European Journal* **2014**, *20*, 9524.

(18) Rinehart, J. D.; Long, J. R. *Chemical Science* **2011**, *2*, 2078.

(19) Bergbreiter, D. E.; Killough, J. M. *Journal of the American Chemical Society* **1978**, *100*, 2126.

(20) APEX2 Version 2012.4-0, Bruker AXS, Inc.; Madison, WI 2012.

(21) SAINT Version 7.68a, Bruker AXS, Inc.; Madison, WI 2009.

(22) Sheldrick, G. M. SADABS, Version 2008/1, Bruker AXS, Inc.; Madison, WI 2008.

(23) Sheldrick, G. M. SHELXTL, Version 2008/4, Bruker AXS, Inc.; Madison, WI 2008.

(24) International Tables for Crystallography 1992, Vol. C., Dordrecht: Kluwer Academic Publishers.

(25) Flack, H. D. Acta. Cryst., A39, 876-881, 1983.

(26) APEX2 Version 2013.6-2, Bruker AXS, Inc.; Madison, WI 2013.

(27) SAINT Version 8.32b, Bruker AXS, Inc.; Madison, WI 2012.

(28) Sheldrick, G. M. SADABS, Version 2014/5, Bruker AXS, Inc.; Madison, WI 2014.

(29) Sheldrick, G. M. SHELXTL, Version 2014/7, Bruker AXS, Inc.; Madison, WI 2014.

(30) APEX2 Version 2011.4-1 Bruker AXS, Inc.; Madison, WI 2011.

CHAPTER 7

Synthesis and Structure of Nitrile-Solvated Rare Earth Metallocene Cations

$[Cp_2Ln(NCR)_3][BPh_4]$ ($Cp = C_5Me_5, C_5H_4SiMe_3$; R = Me, ^{t}Bu, Ph)

Introduction

One of the remarkable advances in actinide metallocene chemistry has been the discovery that, under some circumstances, the bent metallocene geometry found in every $(C_5Me_5)_2AnX_nL_m$ complex (An = actinide; X = anionic ligand; L = neutral ligand; n = 1,2; m = 0-2) since this class was first reported in 1978,[1] could be converted to a structure in which the two cyclopentadienyl planes are parallel. This was accomplished simply by adding acetonitrile (MeCN) to the tetravalent uranium complexes $(C_5Me_5)_2UX_2$ (X = I, OTf)[2] or by adding $HNEt_3BPh_4$ to $(C_5Me_5)_2UMe_2$ in MeCN, eq 7.1.[3] Metallocenes with parallel C_5Me_5 planes could also

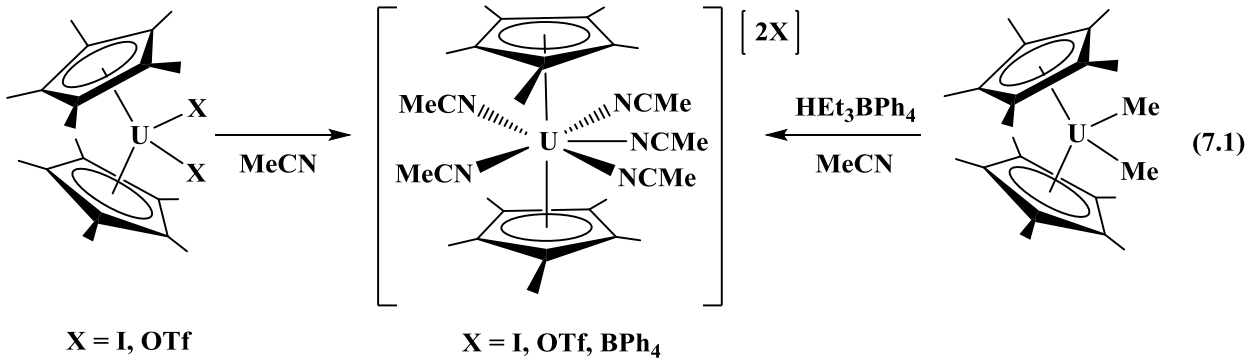

be obtained by addition of NEt_4CN to the uranium metallocene $(C_5Me_5)_2U(OTf)_2$, eq 7.2.[4] In eq 7.2, the linear penta-cyanide complex is said to be in equilibrium with the bent tri-cyanide

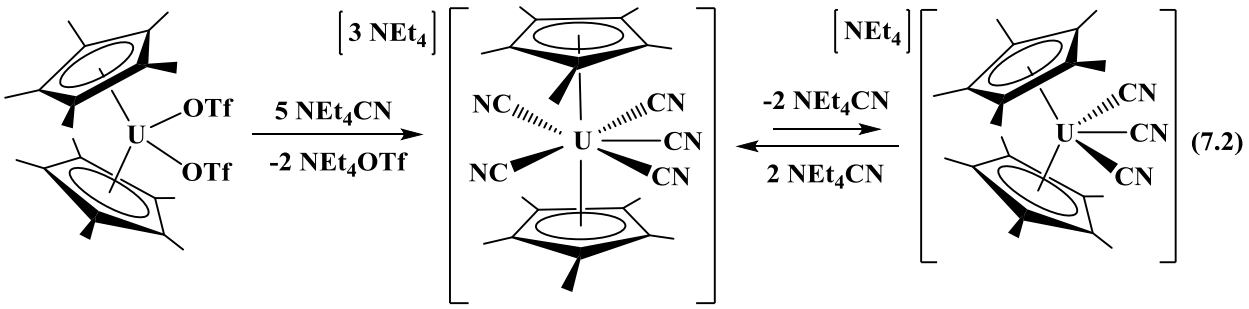

(7.2)

analog.[4] Detailed studies of the bent versus linear geometries for the uranium C_5Me_5 metallocenes showed that the structures were highly dependent on reaction conditions, and parallel plane structures were favored for U^{4+} and U^{5+}, but not U^{3+}.[3,5] The similarity of $(C_5Me_5)_2UI(NCMe)_2$ to $(C_5Me_5)_2CeI(NCMe)_2$ suggested that parallel plane C_5Me_5 metallocenes were not favored with Ln^{3+} complexes.[3] Although there have been numerous reports of f element cyclooctatetraene (COT)-containing complexes with parallel ring geometries,[6-16] as well as nearly parallel geometries obtained with $(COT)Ln(C_5Me_5)$ systems,[17-23] the present study focuses only on bis(pentamethylcyclopentadienyl) complexes.

Since an extensive series of rare metallocene cations of the formula $[(C_5Me_5)_2Ln][(\mu\text{-}Ph)_2BPh_2]$ are available[24,25] and contain labile BPh_4 anions, it was of interest to determine how nitrile coordination would affect their structure. Formation of bent metallocene base adducts of the cations $[(C_5Me_5)_2LnL_2][BPh_4]$ are known for L = $OPPh_3$,[26] tetrahydrothiophene,[27] THF,[28] py,[29] acetone,[29] and NH_3,[30] but the effect of coordination of cylindrical nitriles was unknown. If

linear metallocenes could be obtained with bis(pentamethylcyclopentadienyl) complexes with highly paramagnetic lanthanides, it would provide a new class of metallocenes with axial symmetry that could be valuable in the area of single-molecule magnetism.[6,7,31]

Although no linear metallocenes had been observed for +3 metal complexes of the f elements with two C_5Me_5 ligands, the use of the $(BPh_4)^{1-}$ precursors had not been examined. Reported here are the structures of products of adding nitriles to $[(C_5Me_5)_2Ln][(\mu\text{-}Ph)_2BPh_2]$ as well as to the Me_3Si-substituted cyclopentadienyl system $[(C_5H_4SiMe_3)_2Y(THF)_2][BPh_4]$.[32,33] Since the key point of comparison is the bent versus linear structure, and since both structures would have the same NMR spectral pattern when observable in the systems with lower magnetic moments, X-ray crystallographic data were essential to evaluate the differences in rare earth versus actinide chemistry.

Results

The bent metallocene cationic complexes $[(C_5Me_5)_2Ln][(\mu\text{-}Ph)_2BPh_2]$,[25] **1-Ln** (Ln = Gd, La, Y) were reacted in toluene with excess acetonitrile (MeCN) to produce $[(C_5Me_5)_2Ln(NCMe)_3][BPh_4]$, **2-Ln** (Ln = ; La, Gd, Y), eq 7.3, as determined by NMR

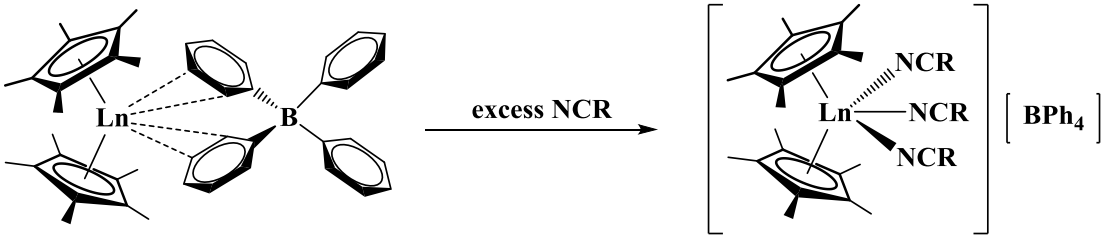

(7.3)

1-Ln

Ln = Y, La, Gd

R = Me, 2-Ln; La, Gd, Y

^{t}Bu, 3-Y

Ph, 4-Ln; La, Gd

spectroscopy (**2-La** and **2-Y**), elemental analysis (each **2-Ln**), and X-ray crystallography (**2-Gd** and **2-Y**), Figure 7.1. For **2-La**, THF was required in order to isolate crystals for characterization, and this resulted in crystals of $[(C_5Me_5)_2La(NCMe)_2(THF)][BPh_4]$, **5-La**, Figure 7.2. Although excess nitrile is used in these reactions, it appears that only three neutral ligands bind the trivalent rare earth center in the isolated products, even in the case of the largest rare earth metal La.

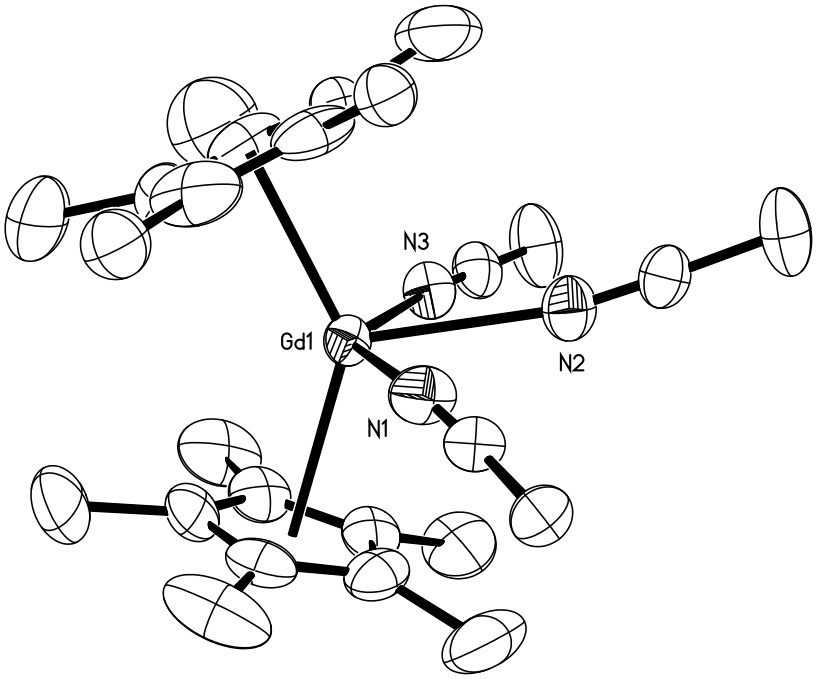

Figure 7.1. Thermal ellipsoid plot of the cation of $[(C_5Me_5)_2Gd(NCMe)_3][BPh_4]$, **2-Gd**, drawn at the 50% probability level. Hydrogen atoms and cocrystallized solvent molecules are omitted for clarity.

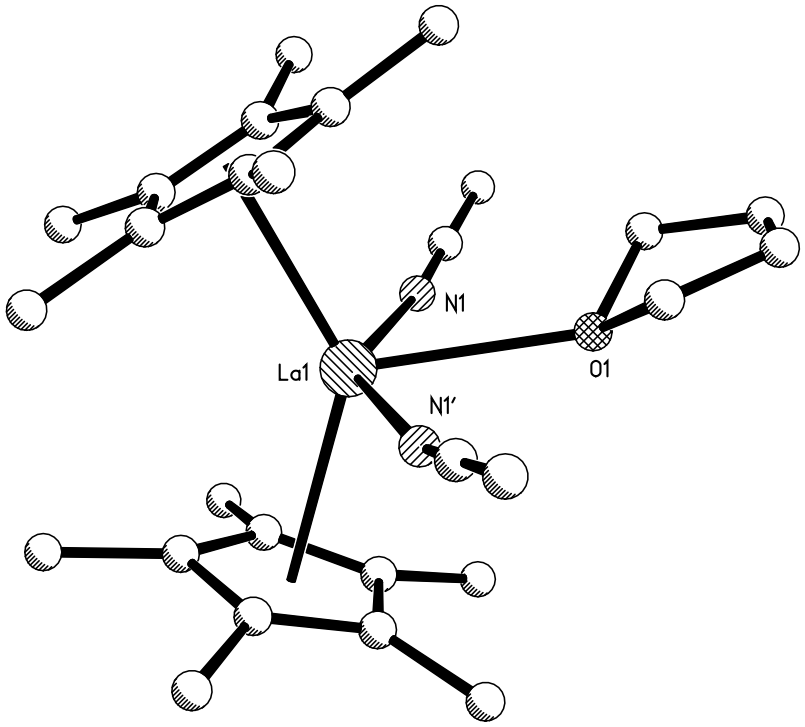

Figure 7.2. Crystal structure of the cation of $[(C_5Me_5)_2La(NCMe)_2(THF)][BPh_4]$, **5-La**, grown from a toluene/THF solution of $[(C_5Me_5)_2La(NCMe)_3][BPh_4]$, **2-La**. Hydrogen atoms and co-crystallized solvent molecules are omitted for clarity.

Similar products are obtained when *tert*-butylnitrile (^{t}BuCN) and benzonitrile (PhCN) are used in place of MeCN, eq 7.3. Addition of excess ^{t}BuCN to a toluene slurry of **1-Y** yields $[(C_5Me_5)_2Y(NC^tBu)_3][BPh_4]$, **3-Y**, as determined by elemental analysis and X-ray crystallography, Figure 7.3. Analogously, excess PhCN can be added to **1-La** and **1-Gd** in toluene to generate yellow solutions from which X-ray quality crystals of $[(C_5Me_5)_2Ln(NCPh)_3][BPh_4]$ (Ln = La, **4-La**; Gd; **4-Gd**) were obtained, Figure 7.4. As found in the MeCN complexes above, three nitrile ligands bind the metal centers. This can be compared with the previously reported Sm^{2+} complex $(C_5Me_5)_2Sm(NC^tBu)_2$,[34] crystallized from reaction of $(C_5Me_5)_2Sm(THF)_2$ with 2 equiv of ^{t}BuCN in toluene.

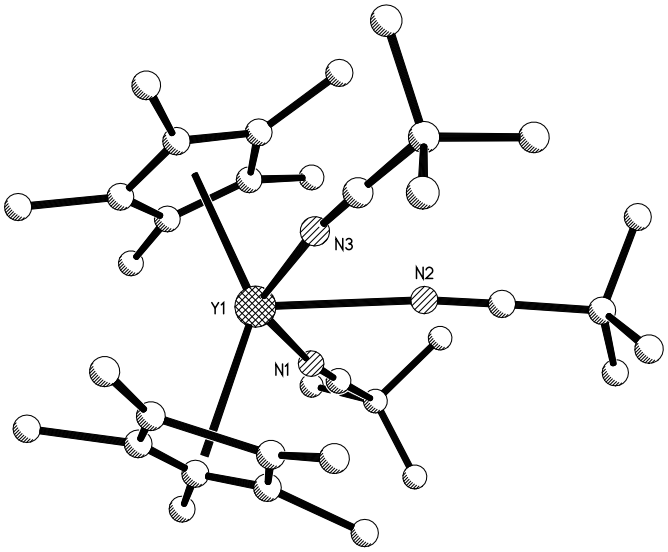

Figure 7.3. Crystal structure of the cation of $[(C_5Me_5)_2Y(NC^tBu)_3][BPh_4]$, **3-Y**. Hydrogen atoms and co-crystallized solvent molecules are omitted for clarity. Disorder in the ligands has also been omitted.

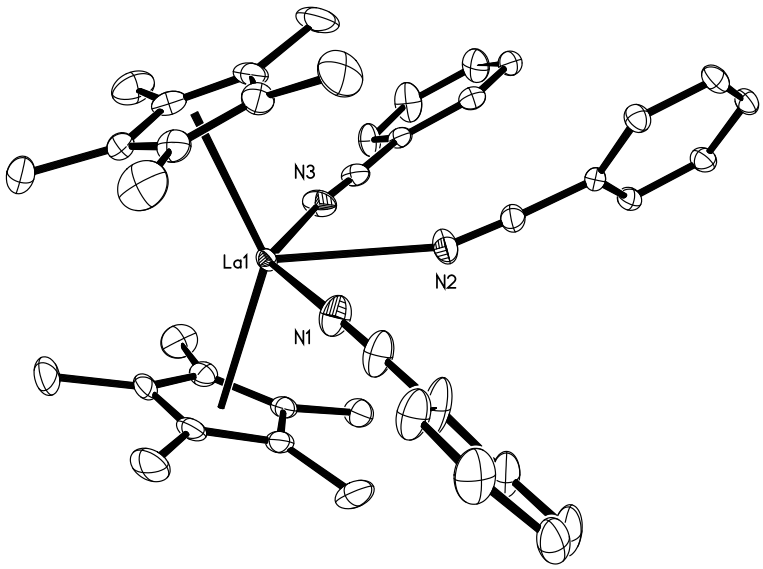

Figure 7.4. Thermal ellipsoid plot of the cation of $[(C_5Me_5)_2La(NCPh)_3][BPh_4]$, **4-La**, drawn at the 30% probability level. Hydrogen atoms and co-crystallized solvent molecules are omitted for clarity. Disorder in one of the six-membered rings has also been omitted. **4-Gd** is isomorphous with **4-La**.

In an effort to reduce the electron donating capabilities of the cyclopentadienyl ligand and perhaps enhance the Lewis acidity of the rare earth center, the less electron donating and less sterically demanding $(C_5H_4SiMe_3)^{1-}$ ligand was used in place of $(C_5Me_5)^{1-}$. $[(C_5H_4SiMe_3)_2Y(THF)_2][BPh_4]$[33] was synthesized and reacted with excess MeCN to generate $[(C_5H_4SiMe_3)_2Y(NCMe)_3][BPh_4]$, **6-Y**, Figure 7.5. Although there are already two THF molecules bound to Y in the cationic metallocene precursor, the use of excess nitriles in toluene leads to displacement of both the THF ligands. Despite the decreased steric hindrance and electron donating capabilities of $(C_5H_4SiMe_3)^{1-}$ compared to $(C_5Me_5)^{1-}$, only three MeCN ligands are found to bind the Y center.

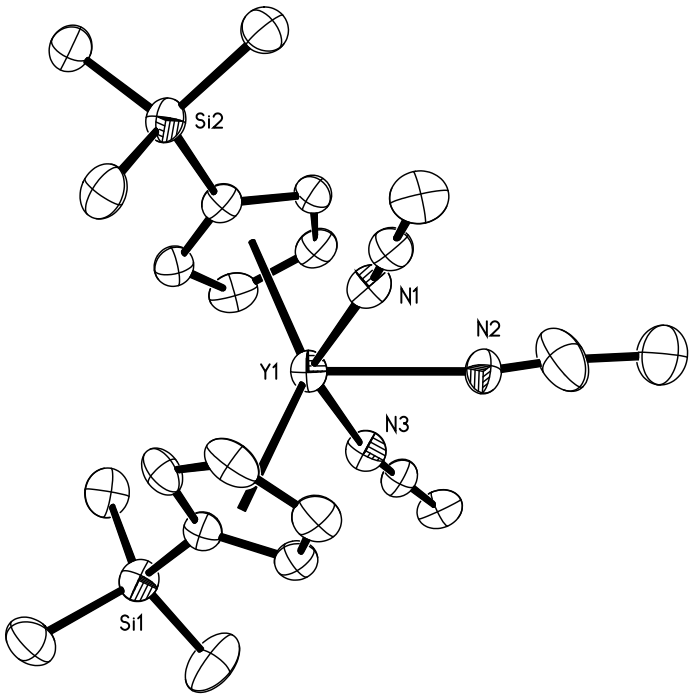

Figure 7.5. Thermal ellipsoid plot of the cation of $[(C_5H_4SiMe_3)_2Y(NCMe)_3][BPh_4]$, **6-Y**, drawn at the 50% probability level. Hydrogen atoms and co-crystallized solvent molecules are omitted for clarity.

Crystallographic Analysis. A comparison of the metrical parameters for **2-Gd**, **4-La**, **4-Gd,** and **6-Y** is presented in Table 7.1. Although X-ray crystallographic data were obtained for **2-Y**, **3-Y** and **5-La**, these data were only of high enough quality to establish connectivity in these structures. For **2-Gd**, **4-La**, and **4-Gd**, the similarity of the distances in all three complexes is evident from the table, which includes distances for **4-La** adjusted for the 0.109 Å difference in the 9-coordinate ionic radii of Gd^{3+} and La^{3+}.[35] The Ln–(C_5Me_5 ring centroid) distances and angles are consistent with other known $(C_5Me_5)^{1-}$ rare earth metallocene cationic complexes in the literature.[24,25,29] However, unlike the uranium metallocene reported by Ephritikhine and coworkers, in which the two $(C_5Me_5)^{1-}$ ligands take on a linear geometry upon coordination of MeCN,[2] the rare earth metallocenes maintain their bent geometry, with Cnt–Ln–Cnt angles of 136-140°, very similar to the angles observed in their **1-Ln** precursors.[24]

The average Y–Cnt distance of 2.354 Å in **6-Y** is slightly longer than that of its bis(THF) precursor $[(C_5H_4SiMe_3)_2Y(THF)_2][BPh_4]$ which has an average Y–Cnt distance of 2.271 Å.[32] For comparison, the difference in Shannon ionic radii for nine and eight coordinate Y^{3+} is 0.056 Å.[35] Adjustments to the parameters of **6-Y** to account for the 0.032 Å difference in the ionic radii of Gd^{3+} and Y^{3+} are also included in Table 7.1. Despite a different number of ligands, the Cnt–Y–Cnt angle in **6-Y** of 136.8° is essentially identical to the average analogous angle in $[(C_5H_4SiMe_3)_2Y(THF)_2][BPh_4]$ of 136.6°.

Table 7.1. Selected bond lengths (Å) and angles (deg) in $[(C_5Me_5)_2Gd(NCMe)_3][BPh_4]$, **2-Gd**, $[(C_5Me_5)_2La(NCPh)_3][BPh_4]$, **4-La**, $[(C_5Me_5)_2Gd(NCPh)_3][BPh_4]$, **4-Gd** and $[(C_5H_4SiMe_3)_2Y(NCMe)_3][BPh_4]$, **6-Y** where Cnt = ring centroid**.** For comparison, the distances for **4-La** and **6-Y** adjusted for the difference in ionic radii with Gd are given as **4-La*** and **6-Y***.

Compound	Ln–Cnt	Ln–N	Cnt–Ln–Cnt
2-Gd[a]	2.411, 2.406	2.488(6), 2.500(6), 2.545(6)	137.5
	2.416, 2.410	2.484(6), 2.501(6), 2.577(6)	137.2
	2.428, 2.410	2.485(6), 2.489(6), 2.533(7)	139.3
	2.428, 2.418	2.494(5), 2.504(5), 2.567(6)	138.7
4-Gd	2.396, 2.407	2.489(3), 2.509(3), 2.553(3)	139.1
4-La*	2.407, 2.421	2.517(2), 2.543(3), 2.588(2)	-
6-Y*	2.391, 2.381	2.470(4), 2.473(4), 2.498(4)	-
4-La	2.516, 2.530	2.626(2), 2.652(3), 2.697(2)	139.0
6-Y	2.359, 2.349	2.438(4), 2.441(4), 2.466(4)	136.8

[a] There were four unique molecules in the asymmetric unit of **2-Gd.**

IR Spectroscopy. The ν(C≡N) stretching frequencies for the MeCN-ligated complexes, **2-Y**, **2-Gd**, and **2-La**, are observed at 2272, 2270 and 2265 cm^{-1}, respectively. These are similar to the IR bands reported for the linear metallocene $[(C_5Me_5)_2U(NCMe)_5][BPh_4]$ at 2269 and 2262 cm^{-1}.[3] These absorptions are higher in energy than that of free MeCN (2254 cm^{-1})[36] which is consistent with the ligand acting primarily as a σ-donor to the metal.[3,37] The C≡N stretch in the ^{t}BuCN analog **3-Y** is observed at 2260 cm^{-1} which is consistent with other rare earth ^{t}BuCN adducts in the literature[38] and again higher in energy than free ^{t}BuCN (2235 cm^{-1}). The PhCN ligated species **4-Gd** and **4-La** display strong features in the IR spectrum at 2248 and 2243 cm^{-1}, respectively, again above the value of the free ligand, 2231 cm^{-1}.[36,39,40] In the $C_5H_4SiMe_3$-substituted MeCN adduct **6-Y**, ν(C≡N) is observed at 2272 cm^{-1}. Since this is identical to what

is observed for the C_5Me_5 analog **2-Y**, this suggests that the less electron donating $C_5H_4SiMe_3$ does not affect the C≡N bond of the nitrile ligand.

Discussion

While addition of excess MeCN to the U^{4+} bent metallocene complexes $(C_5Me_5)_2UX_2$ (X = I, OTf) yields the linear metallocene penta-nitrile adducts $[(C_5Me_5)_2U(NCMe)_5][X_2]$, similar addition of nitrile to the Ln^{3+} bent metallocene complexes $[(C_5Me_5)_2Ln][(\mu\text{-}Ph)_2BPh_2]$, **1-Ln** (Ln = Y, La, Gd), yields only the tri-nitrile adducts $[(C_5Me_5)_2Ln(NCR)_3][BPh_4]$ (R = Me, **2**; *t*Bu, **3**; Ph, **4**) which retain the bent geometry of the metallocene unit. Even in the case of La^{3+}, which has a larger ionic radius (1.216 Å)[35] than U^{4+} (1.05 Å),[35] only three neutral donors were found to bind to the metal center. This suggests this difference in reactivity and structure is not a consequence of steric hindrance.

Since 9-coordinate U^{4+} has a 3.8 charge-to-radius ratio, which is larger than that of any of the trivalent rare earth ions with the same coordinate value, 2.5-3.4, it is a stronger Lewis acid and more prone to accept additional Lewis bases in the same bis(pentamethylcyclopentadienyl) metallocene environment. Examination of a less electron donating cyclopentadienyl ligand, namely $(C_5H_4SiMe_3)^{1-}$, does not appear to significantly affect the electronic or steric capabilities of the rare earth, yttrium, to bind more than three nitrile donors at a time.

Conclusion

The bent metallocene cations, $[(C_5Me_5)_2Ln][(\mu\text{-}Ph)_2BPh_2]$, **1-Ln** (Ln = Y, La, Gd) and $[(C_5H_4SiMe_3)_2Y(THF)_2][BPh_4]$, readily add nitriles such as MeCN, ^{t}BuCN, and PhCN to form tri-nitrile complexes, $[(C_5R_5)_2Ln(NCR)_3][BPh_4]$, that display bent metallocene structures. This is

consistent with reported observations for U^{3+} metallocenes, and no evidence for formation of higher coordinate complexes with a linear metallocene unit was found in contrast to results obtained with U^{4+} and U^{5+}.

Experimental Details

All manipulations and syntheses described below were conducted with the rigorous exclusion of air and water using standard Schlenk line and glovebox techniques under a dinitrogen atmosphere. Solvents were sparged with UHP argon and dried by passage through columns containing Q-5 and molecular sieves prior to use. Deuterated NMR solvents were dried over NaK alloy, degassed by three freeze-pump-thaw cycles, and vacuum transferred before use. Acetonitrile, *t*-butyl nitrile and benzonitrile were dried over molecular sieves and degassed by three freeze-pump-thaw cycles. $[(C_5Me_5)_2Ln][(\mu\text{-}Ph)_2BPh_2]$, **1**, (Ln = Y, **1-Y**; La, **1-La**; Gd, **1-Gd**) were synthesized according to the literature procedure.[24,25] $[(C_5H_4SiMe_3)_2Y(THF)_2][BPh_4]$[33] was prepared from $[(C_5H_4SiMe_3)_2]_3Y$[41] and HEt_3NBPh_4. The $Nd_2Fe_{14}B$ magnets used in the crystallizations were obtained from United Nuclear Scientific Equipment and Supplies. ^1H NMR spectra were recorded on Bruker GN500 or CRYO500 MHz spectrometers (^{13}C NMR at 126 MHz) at 298 K unless otherwise stated and referenced internally to residual protio-solvent resonances. IR samples were prepared as KBr pellets on a Varian 1000 FT-IR system. Elemental analyses were conducted on a Perkin-Elmer 2400 Series II CHNS elemental analyzer.

$[(C_5Me_5)_2Gd(NCMe)_3][BPh_4]$, 2-Gd. Toluene (5 mL) was added to **1-Gd** (50 mg, 0.059 mmol) to make a cloudy pale yellow mixture to which was added an excess of MeCN (~0.5 mL, 10 mmol) dropwise until the solution became colorless and transparent. Solvent was

removed from the solution to yield **2-Gd** as a white solid (54 mg, 90%). IR: 3053m, 2979m, 2918s, 2857m, 2300w, 2270m, 1578w, 1480m, 1427m, 1265w, 1181w, 1148w, 1030w, 849w, 732s, 707s, 607m cm^{-1}. Anal. Calcd for $C_{50}H_{59}N_3BGd$ • THF, **2-Gd • THF**: C, 68.84; H, 7.17; N, 4.46. Found: C, 68.63; H, 6.82; N, 4.00. X-ray quality crystals of **2-Gd** could be grown from a concentrated toluene solution with MeCN stored at −35 ºC.

$[(C_5Me_5)_2La(NCMe)_3][BPh_4]$, 2-La. Following the procedure for **2-Gd** above, MeCN (~1 mL, 20 mmol) was added to **1-La** (100 mg, 0.14 mmol) in toluene. The colorless transparent solution was stored at −35 ºC for several days and yielded colorless microcrystalline solids of **2-La** (30 mg, 25%). ^{1}H NMR (acentonitrile-d_3): δ 7.28 (br s, *o*-B*Ph*$_4$, 8H), 7.00 (t, $^3J_{HH}$ = 7.5 Hz, *m*-B*Ph*$_4$, 8H), 6.85 (t, $^3J_{HH}$ = 7.2 Hz, *p*-B*Ph*$_4$, 4H), 1.91 (s, C_5*Me*$_5$, 30H). ^{13}C NMR (acentonitrile-d_3): δ 136.7 (B*Ph*$_4$), 130.0 (B*Ph*$_4$), 126.6 (B*Ph*$_4$), 122.8 (C_5Me$_5$), 120.7 (B*Ph*$_4$), 11.2 (C_5Me$_5$). The ^{1}H and ^{13}C resonances of the MeCN ligands were not discernable due to exchange with CD_3CN. IR: 3056m, 2982m, 2920s, 2856m, 2297m, 2265s, 1578m, 1479m, 1428m, 1266m, 1182w, 1147w, 1066w, 1031m, 929w, 846w, 732s, 704s, 606m cm^{-1}. Anal. Calcd for $C_{50}H_{59}N_3BLa$, **2-La**: C, 70.51; H, 6.98; N, 4.93. Found: C, 69.92; H, 6.44; N, 5.42. To obtain X-ray quality crystals, THF (5 mL) was added to a concentrated mixture of **2-La** in toluene and MeCN. However, crystals of a THF substitution product, $[(C_5Me_5)_2La(NCMe)_2(THF)][BPh_4]$, **5-La**, were isolated. Although the crystallographic data confirm the structure, these data were not of high enough quality to discuss metrical parameters.

$[(C_5Me_5)_2Y(NCMe)_3][BPh_4]$, 2-Y. Following the procedure for **2-Gd** above, MeCN (~1 mL, 20 mmol) was added to **1-Y** (100 mg, 0.15 mmol) in toluene. After stirring the colorless transparent mixture for 5 min, a pale precipitate was observed. THF (~2 mL) was added dropwise to this mixture while stirring until the solution became colorless and transparent again.

The solution was stored at −35 ºC for several days and yielded colorless crystals of **2-Y** (95 mg, 74%). Although the crystallographic data confirm the structure of **2-Y**, these data were not of high enough quality to report metrical values. ^{1}H NMR (acentonitrile-d_3): δ 7.28 (br s, *o*-B*Ph*$_4$, 8H), 7.00 (t, $^{3}J_{HH}$ = 7.5 Hz, *m*-B*Ph*$_4$, 8H), 6.85 (t, $^{3}J_{HH}$ = 7.2 Hz, *p*-B*Ph*$_4$, 4H), 1.85 (s, C$_5$*Me*$_5$, 30H). ^{13}C NMR (acentonitrile-d_3): δ 136.8 (B*Ph*$_4$), 129.3 (B*Ph*$_4$), 126.6 (B*Ph*$_4$), 122.8 (B*Ph*$_4$), 117.8 (*C*$_5$Me$_5$), 11.7 (*C*$_5$Me$_5$). The ^{1}H and ^{13}C resonances of the MeCN ligands were not discernable due to exchange with CD_3CN. IR: 3052s, 2979s, 2909s, 2855s, 2723w, 2281m, 2272s, 1578m, 1478s, 1426s, 1379m, 1266w, 1181w, 1147m, 1065m, 1030m, 846m, 733s, 704s, 606s cm^{-1}. Anal. Calcd for $C_{50}H_{59}N_3BY$ • MeCN, **2-Y** • MeCN: C, 74.11; H, 7.42; N, 6.65. Found: C, 74.03; H, 7.63; N, 6.51.

[(C$_5$Me$_5$)$_2$Y(NC^{t}Bu)$_3$][BPh$_4$], 3-Y. Following the procedure for **2** above, excess ^{t}BuCN (~0.4 mL, 4 mmol) was added to **1-Y** (100 mg, 0.15 mmol) in toluene. After stirring the colorless transparent mixture for about 2 min, the reaction mixture became opaque with white precipitate. THF (~2 mL) was added until the solution became transparent again. **3-Y** was isolated as a fluffy white solid (122 mg, 86%) under reduced pressure. IR: 3121w, 3057m, 3035m, 2981s, 2931s, 2907s, 2861m, 2723w, 2260s, 1935w, 1875w, 1812w, 1580m, 1474s, 1459s, 1426m, 1371m, 1262w, 1235m, 1206w, 1132w, 1064w, 1031m, 843w, 733s, 704s, 612m cm^{-1}. Anal. Calcd for $C_{62}H_{86}N_3BY$, **3-Y**: C, 76.36; H, 8.36; N, 4.53. Found: C, 76.73; H, 8.52; N, 4.16. X-ray quality crystals were grown from a concentrated toluene/THF solution with *t*BuCN at −35 ºC.

[(C$_5$Me$_5$)$_2$Gd(NCPh)$_3$][BPh$_4$], 4-Gd. Following the procedure for **2** above, PhCN (~1 mL, 10 mmol) was added dropwise to a yellow toluene slurry (5 mL) of **1-Gd** (60 mg, 0.08 mmol) to make a transparent yellow solution. The solution was stored at −35 ºC in a vial with a

NdFeB magnet attached to the outside. After several days, X-ray quality crystals of **4-Gd** had formed near the magnet (41 mg, 25%). IR: 3051m, 2967m, 2895m, 2851m, 2248s, 1593m, 1578m, 1478m, 1445s, 1425m, 1333w, 1269w, 1260w, 1175w, 1139w, 1065w, 1023m, 998w, 925w, 842w, 758s, 733s, 705s, 683s, 612sm, 555s cm^{-1}. Anal. Calcd for $C_{65}H_{65}N_3BGd$ • MeCN, **4-Gd** • MeCN: C, 73.33; H, 6.25; N, 5.11. Found: C, 73.31; H, 5.79; N, 5.32.

$[(C_5Me_5)_2La(NCPh)_3][BPh_4]$, 4-La. As described above for **2** above, PhCN (~1 mL, 10 mmol) was added dropwise to an off-white toluene slurry (5 mL) of **1-La** (100 mg, 0.14 mmol) to make a transparent yellow solution which was stored at −35 ºC. After several days, X-ray quality crystals of **4-La** had formed (145 mg, 98%). IR: 3055m, 3003m, 2968m, 2901m, 2853m, 2721w, 2243s, 1957w, 1901w, 1595m, 1578m, 1479m, 1446s, 1427m, 1175m, 1153m, 1067w, 1025m, 998w, 924w, 851w, 757s, 742s, 714s, 687s, 627w, 601m cm^{-1}. Anal. Calcd for $C_{65}H_{65}N_3BLa$ • MeCN, **4-La** • MeCN: C, 74.58; H, 6.35; N, 5.19. Found: C, 74.76; H, 5.93; N, 5.14. X-ray quality crystals were grown at −35 ºC.

$[(C_5H_4SiMe_3)_2Y(NCMe)_3][BPh_4]$, 6-Y. Following the above procedures, MeCN (1.5 mL, 30 mmol) was added to a white slurry of $[(C_5H_4SiMe_3)_2Y(THF)_2][BPh_4]$ (83 mg, 0.09 mmol) in toluene. The solvent was removed from the colorless transparent mixture under reduced pressure to yield a tacky white solid. This was stirred in hexane (10 mL) for 30 min then dried under reduced pressure to yield **6-Y** as a white powder (66 mg, 85%). X-ray quality crystals could be grown from toluene/MeCN solutions at −35 ºC. ^{1}H NMR (acentonitrile-d_3): δ 7.27 (br s, *o*-B*Ph*$_4$, 8H), 6.99 (t, $^3J_{HH}$ = 7.4 Hz, *m*-B*Ph*$_4$, 8H), 6.84 (t, $^3J_{HH}$ = 7.2 Hz, *p*-B*Ph*$_4$, 4H), 6.30 (m, $C_5H_4SiMe_3$, 4H), 6.21 (m, $C_5H_4SiMe_3$, 4H), 0.19 (s, C_5H_4Si*Me*$_3$, 18H). ^{13}C NMR (acentonitrile-d_3): δ 166.7 (B*Ph*$_4$), 136.7 (B*Ph*$_4$), 126.6 (B*Ph*$_4$), 122.8 (B*Ph*$_4$), 121.6 (*C*$_5$H$_4$SiMe$_3$), 117.8 (*C*$_5$H$_4$SiMe$_3$), 112.8 (*C*$_5$H$_4$SiMe$_3$), 0.33 (C_5H_4Si*Me*$_3$). The ^{1}H and ^{13}C

resonances of the MeCN ligands were not discernable due to exchange with CD_3CN. IR: 3214m, 3054m, 2999m, 2984m, 2921m, 2304m, 2272m, 1948w, 1884w, 1821w, 1578m, 1479m, 1428m, 1392m, 1365m, 1250m, 1180m, 1151m, 1066w, 1042m, 1031m, 971w, 953w, 905m, 839s, 783m, 741s, 706s, 605m cm^{-1}. Anal. Calcd for $C_{46}H_{55}N_3BY$ • ½(toluene), **6-Y** • ½(toluene): C, 69.79; H, 6.98; N, 4.93. Found: C, 69.52; H, 6.80; N, 4.74.

X-ray Data Collection, Structure Solution and Refinement for $[(C_5Me_5)_2Gd(NCMe)_3][BPh_4]$, 2-Gd. A colorless crystal of approximate dimensions 0.321 x 0.270 x 0.182 mm was mounted on a glass fiber and transferred to a Bruker SMART APEX II diffractometer. The APEX2[42] program package was used to determine the unit-cell parameters and for data collection (25 sec/frame scan time for a sphere of diffraction data). The raw frame data was processed using SAINT[43] and SADABS[44] to yield the reflection data file. Subsequent calculations were carried out using the SHELXTL[45] program. The diffraction symmetry was 2/*m* and the systematic absences were consistent with the monoclinic space group $P2_1/n$ that was later determined to be correct. The structure was solved by direct methods and refined on F^2 by full-matrix least-squares techniques. The analytical scattering factors[46] for neutral atoms were used throughout the analysis. There were 1.5 toluene molecules of salvation present per formula unit and four unique molecules in the asymmetric unit. C(7), C(8), C(10), C(97), C(118), C(119), C(120), C(142), C(143), C(166), C(167), C(168), C(169) and C(170) were disordered and included using multiple components with partial site-occupancy-factors. Hydrogen atoms were included using a riding model. Least-squares analysis yielded wR2 = 0.1830 and Goof = 1.038 for 2203 variables refined against 48098 data (0.78 Å), R1 = 0.0681 for those 32882 data with $I > 2.0\sigma(I)$. The data may have been twinned but attempts to resolve any twinning issues were unsuccessful which may be a cause of less-than-satisfactory convergence. Attempts to obtain

better quality crystals were unsuccessful, however, molecular connectivity has been established. Details are included in Table 7.2.

X-ray Data Collection, Structure Solution and Refinement for $[(C_5Me_5)_2Y(NC^tBu)_3][BPh_4]$, 3-Y. A colorless crystal of approximate dimensions 0.560 x 0.067 x 0.034 mm was mounted on a glass fiber and transferred to a Bruker SMART APEX II diffractometer. The APEX2[42] program package was used to determine the unit-cell parameters and for data collection (90 sec/frame scan time for a sphere of diffraction data). The raw frame data was processed using SAINT[43] and SADABS[44] to yield the reflection data file. Subsequent calculations were carried out using the SHELXTL[45] program. The diffraction symmetry was 2/*m* and the systematic absences were consistent with the monoclinic space groups *Cc* and *C*2/*c*. It was later determined that space group *C*2/*c* was correct. The structure was solved by direct methods and refined on F^2 by full-matrix least-squares techniques. The analytical scattering factors[46] for neutral atoms were used throughout the analysis. There was half a toluene molecule of solvation in the asymmetric unit which was disordered and included using multiple components with partial site-occupancy-factors. C(14), C(16), C(17), C(18), C(19), C(20), C(23), C(24), C(33), C34), and C(35) were also disordered and included using multiple components with partial site-occupancy-factors. Hydrogen atoms were included using a riding model. Least squares analysis yielded wR2 = 0.2006 and Goof = 1.015 for 659 variables refined against 11755 data (0.8 Å), R1 = 0.0809 for those 5742 data with $I > 2.0\sigma(I)$. The low crystal quality may be a cause of less-than-satisfactory convergence. Attempts to obtain better quality crystals were unsuccessful; however, molecular connectivity has been established. Details are included in Table 7.2.

X-ray Data Collection, Structure Solution and Refinement for [$(C_5Me_5)_2$Gd(NCPh)3][BPh4], 4-Gd. A colorless crystal of approximate dimensions 0.266 x 0.086 x 0.060 mm was mounted on a glass fiber and transferred to a Bruker SMART APEX II diffractometer. The APEX2[42] program package was used to determine the unit-cell parameters and for data collection (120 sec/frame scan time for a sphere of diffraction data). The raw frame data was processed using SAINT[43] and SADABS[44] to yield the reflection data file. Subsequent calculations were carried out using the SHELXTL[45] program. There were no systematic absences nor any diffraction symmetry other than the Friedel condition. The centrosymmetric triclinic space group $P\bar{1}$ was assigned and later determined to be correct. The structure was solved by direct methods and refined on F^2 by full-matrix least-squares techniques. The analytical scattering factors[46] for neutral atoms were used throughout the analysis. There was one disordered toluene molecule and one disordered benzonitrile molecule of solvation present. Both were included using multiple components with partial site-occupancy-factors. Additionally, C(25), C(26), C(27), C(62), C(63) and C(64) were disordered and included using multiple components with partial site-occupancy-factors. Hydrogen atoms were included using a riding model. There were several high residuals present in the final difference-Fourier map. It was not possible to determine the nature of the residuals although it was probable that another toluene solvent molecule was present. The SQUEEZE routine in the PLATON[47] program package was used to account for the electrons in the solvent accessible voids. At convergence, wR2 = 0.0940 and Goof = 1.029 for 817 variables refined against 15004 data (0.78 Å), R1 = 0.0394 for those 12852 data with $I > 2.0\sigma(I)$. Details are included in Table 7.2.

X-ray Data Collection, Structure Solution and Refinement for [$(C_5Me_5)_2$La$(NCPh)_3$][BPh_4], 4-La. A yellow crystal of approximate dimensions 0.552 x 0.265

x 0.060 mm was mounted on a glass fiber and transferred to a Bruker SMART APEX II diffractometer. The APEX2[42] program package was used to determine the unit-cell parameters and for data collection (25 sec/frame scan time for a sphere of diffraction data). The raw frame data was processed using SAINT[43] and SADABS[44] to yield the reflection data file. Subsequent calculations were carried out using the SHELXTL[45] program. There were no systematic absences nor any diffraction symmetry other than the Friedel condition. The centrosymmetric triclinic space group $P\bar{1}$ was assigned and later determined to be correct. The structure was solved using the coordinates from jfc69 which is isomorphous. The analytical scattering factors[46] for neutral atoms were used throughout the analysis. There was one disordered toluene molecule and one disordered benzonitrile molecule of solvation present. Both were included using multiple components with partial site-occupancy-factors. Additionally, C(25), C(26), C(27), C(62), C(63) and C(64) were disordered and included using multiple components with partial site-occupancy-factors. Hydrogen atoms were included using a riding model. There were several high residuals present in the final difference-Fourier map. It was not possible to determine the nature of the residuals although it is probable that another toluene solvent molecule was present. The SQUEEZE routine in the PLATON[47] program package was used to account for the electrons in the solvent accessible voids. At convergence, wR2 = 0.0994 and Goof = 1.041 for 810 variables refined against 15240 data (0.78 Å), R1 = 0.0391 for those 13573 data with $I > 2.0\sigma(I)$. Details are included in Table 7.2.

X-ray Data Collection, Structure Solution and Refinement for $[(C_5Me_5)_2La(NCMe)_2(THF)][BPh_4]$, 5-La. A colorless crystal of approximate dimensions 0.272 x 0.161 x 0.101 mm was mounted on a glass fiber and transferred to a Bruker SMART APEX II diffractometer. The APEX2[42] program package was used to determine the unit-cell

parameters and for data collection (60 sec/frame scan time for a sphere of diffraction data). The raw frame data was processed using SAINT[43] and SADABS[44] to yield the reflection data file. Subsequent calculations were carried out using the SHELXTL[45] program. The diffraction symmetry was *mmm* and the systematic absences were consistent with the orthorhombic space group *Pmmn* that was later determined to be correct. The structure was solved by direct methods and refined on F^2 by full-matrix least-squares techniques. The analytical scattering factors[46] for neutral atoms were used throughout the analysis. Hydrogen atoms were included using a riding model. There were two half molecules in the asymmetric unit and a half a toluene molecule of solvation per formula unit. Least squares analysis yielded wR2 = 0.3790 and Goof = 1.086 for 417 variables refined against 13016 data (0.8 Å), R1 = 0.1534 for those 9173 data with $I > 2.0\sigma(I)$. There were several high residuals present in the final difference-Fourier map. It was not possible to determine the nature of the residuals although it is probable that acetonitrile solvent was present. The SQUEEZE routine in the PLATON[47] program package was used to account for the electrons in the solvent accessible voids. The low crystal quality may be a cause of less-than-satisfactory convergence. Attempts to obtain better quality crystals were unsuccessful; however, molecular connectivity has been established. Details are included in Table 7.2.

X-ray Data Collection, Structure Solution and Refinement for jfc72. A colorless crystal of approximate dimensions 0.378 x 0.337 x 0.173 mm was mounted on a glass fiber and transferred to a Bruker SMART APEX II diffractometer. The APEX2[42] program package was used to determine the unit-cell parameters and for data collection (20 sec/frame scan time for a sphere of diffraction data). The raw frame data was processed using SAINT[43] and SADABS[44] to yield the reflection data file. Subsequent calculations were carried out using the SHELXTL[45]

program. There were no systematic absences nor any diffraction symmetry other than the Friedel condition. The centrosymmetric triclinic space group $P\bar{1}$ was assigned and later determined to be correct. The structure was solved by direct methods and refined on F^2 by full-matrix least-squares techniques. The analytical scattering factors[46] for neutral atoms were used throughout the analysis. Hydrogen atoms were included using a riding model. There was one molecule of toluene per formula unit. Least squares analysis yielded wR2 = 0.1851 and Goof = 1.023 for 551 variables refined against 9997_ data (0.75 Å), R1 = 0.0710 for those 6424 data with $I > 2.0\sigma(I)$. Less-than-satisfactory convergence is due to the fact that data collection was stopped after 3 of 4 runs, and a full sphere of data was not collected. However, molecular connectivity has been established. Details are included in Table 7.2.

Table 7.2. X-ray data collection parameters for $[(C_5Me_5)_2Gd(NCMe)_3][BPh_4]$, **2-Gd**, $[(C_5Me_5)_2Y(NC^tBu)_3][BPh_4]$, **3-Y,** $[(C_5Me_5)_2Gd(NCPh)_3][BPh_4]$, **4-Gd,** $[(C_5Me_5)_2La(NCPh)_3][BPh_4]$, **4-La**, $[(C_5Me_5)_2La(NCMe)_2(THF)][BPh_4]$**,** **5-La**, and $[(C_5H_4SiMe_3)_2Y(NCMe)_3][BPh_4]$, **6-Y**.

	$C_{50}H_{59}BG$• $1½(C_7H_8)$	$C_{59}H_{77}BN_3Y$ • ½(C_7H_8)	$C_{65}H_{65}BGdN_3$ • $(C_7H_8)(C_7H_5N)$	$C_{65}H_{65}BLaN_3$ • $(C_7H_8)(C_7H_5N)$	$C_{52}H_{64}BLaN_2O$ • ½(C_7H_8)	$C_{46}H_{55}BN_3Si_2Y$ • (C_7H_8)
	2-Gd • $1½(C_7H_8)$	**3-Y • ½(C_7H_8)**	**4-Gd• $(C_7H_8)(C_7H_5N)$**	**4-La• $(C_7H_8)(C_7H_5N)$**	**5-La• ½(C_7H_8)**	**6-Y • (C_7H_8)**
formula weight	1008.26	974.02	1251.51	1234.18	928.83	897.96
T(K)	133(2)	133(2)	133(2)	133(2)	133(2)	133(2)
space group	$P2_1/n$	$C2/c$	$P\bar{1}$	$P\bar{1}$	$Pmmn$	$P\bar{1}$
a (Å)	19.0924(11)	41.369(8)	10.1948(10)	10.3564(8)	26.384(2)	12.806(4)
b (Å)	25.4127(15)	10.981(2)	16.9872(16)	16.9796(12)	31.097(3)	14.173(4)
c (Å)	45.876(3)	32.142(7)	20.798(2)	20.7326(15)	14.8912(12)	14.634(4)
α (deg)	90	90	100.1207(12)	99.9726(8)	90	91.100(3)
β (deg)	101.5453(7)	128.420(2)	103.1462(12)	102.8476(9)	90	106.408(4)
γ (deg)	90	90	93.2617(12)	93.0031(9)	90	98.109(3)
volume Å^3	21808(2)	11440(4)	3435.1(6)	3485.1(4)	12217.4(17)	2517.7(12)
Z	16	8	2	2	8	2
ρ_{calced} (Mg/m^3)	1.228	1.131	1.210	1.176	1.010	1.185
μ (mm^{-1})	1.255	1.058	1.010	0.657	0.731	1.242
R1[a] [I > 2.0σ(I)]	0.0681	0.0809	0.0394	0.0391	0.1534	0.0710
wR2[b]	0.1830	0.2006	0.0940	0.0994	0.3790	0.1851

[a] $R1 = \Sigma||F_o|-|F_c|| / \Sigma|F_o|$. [b] $wR2 = [\Sigma[w(F_o^2-F_c^2)^2] / \Sigma[w(F_o^2)^2]\ ]^{1/2}$

References

(1) Manriquez, J. M.; Fagan, P. J.; Marks, T. J. *Journal of the American Chemical Society* **1978**, *100*, 3939.

(2) Maynadié, J.; Berthet, J.-C.; Thuéry, P.; Ephritikhine, M. *Journal of the American Chemical Society* **2006**, *128*, 1082.

(3) Maynadié, J.; Berthet, J.-C.; Thuéry, P.; Ephritikhine, M. *Organometallics* **2006**, *25*, 5603.

(4) Maynadié, J.; Berthet, J.-C.; Thuéry, P.; Ephritikhine, M. *Organometallics* **2007**, *26*, 4585.

(5) Maynadié, J.; Barros, N.; Berthet, J.-C.; Thuéry, P.; Maron, L.; Ephritikhine, M. *Angewandte Chemie International Edition* **2007**, *46*, 2010.

(6) Meihaus, K. R.; Long, J. R. *Journal of the American Chemical Society* **2013**, *135*, 17952.

(7) Le Roy, J. J.; Korobkov, I.; Murugesu, M. *Chemical Communications* **2014**, *50*, 1602.

(8) Edelmann, A.; Blaurock, S.; Lorenz, V.; Hilfert, L.; Edelmann, F. T. *Angewandte Chemie International Edition* **2007**, *46*, 6732.

(9) Kinsley, S. A.; Streitwieser, A.; Zalkin, A. *Organometallics* **1985**, *4*, 52.

(10) Avdeef, A.; Raymond, K. N.; Hodgson, K. O.; Zalkin, A. *Inorganic Chemistry* **1972**, *11*, 1083.

(11) Rei; Poremba, P.; Lameyer, L.; Stalke, D.; T. Edelmann, F. *Chemical Communications* **1999**, 1865.

(12) Meermann, C.; Ohno, K.; Törnroos, K. W.; Mashima, K.; Anwander, R. *European Journal of Inorganic Chemistry* **2009**, *2009*, 76.

(13) Mashima, K.; Fukumoto, H.; Nakayama, Y.; Tani, K.; Nakamura, A. *Polyhedron* **1998**, *17*, 1065.

(14) Hodgson, K. O.; Raymond, K. N. *Inorganic Chemistry* **1972**, *11*, 3030.

(15) Hodgson, K. O.; Raymond, K. N. *Inorganic Chemistry* **1973**, *12*, 458.

(16) Le Roy, J. J.; Jeletic, M.; Gorelsky, S. I.; Korobkov, I.; Ungur, L.; Chibotaru, L. F.; Murugesu, M. *Journal of the American Chemical Society* **2013**, *135*, 3502.

(17) Evans, W. J.; Johnston, M. A.; Clark, R. D.; Ziller, J. W. *Journal of the Chemical Society, Dalton Transactions* **2000**, 1609.

(18) Evans, W. J.; Johnston, M. A.; Greci, M. A.; Ziller, J. W. *Organometallics* **1999**, *18*, 1460.

(19) Evans, W. J.; Schmiege, B. M.; Lorenz, S. E.; Miller, K. A.; Champagne, T. M.; Ziller, J. W.; DiPasquale, A. G.; Rheingold, A. L. *Journal of the American Chemical Society* **2008**, *130*, 8555.

(20) Edelmann, A.; Hrib, C. G.; Blaurock, S.; Edelmann, F. T. *Journal of Organometallic Chemistry*, *695*, 2732.

(21) Evans, W. J.; Clark, R. D.; Ansari, M. A.; Ziller, J. W. *Journal of the American Chemical Society* **1998**, *120*, 9555.

(22) Schumann, H.; Glanz, M.; Winterfeld, J.; Hemling, H. *Journal of Organometallic Chemistry* **1993**, *456*, 77.

(23) Tsoureas, N.; Summerscales, O. T.; Cloke, F. G. N.; Roe, S. M. *Organometallics* **2013**, *32*, 1353.

(24) Evans, W. J.; Davis, B. L.; Champagne, T. M.; Ziller, J. W. *Proceedings of the National Academy of Sciences* **2006**, *103*, 12678.

(25) Evans, W. J.; Seibel, C. A.; Ziller, J. W. *Journal of the American Chemical Society* **1998**, *120*, 6745.

(26) Evans, W. J.; Mueller, T. J.; Ziller, J. W. *Journal of the American Chemical Society* **2009**, *131*, 2678.

(27) Heeres, H. J.; Meetsma, A.; Teuben, J. H. *Journal of Organometallic Chemistry* **1991**, *414*, 351.

(28) Evans, W. J.; Ulibarri, T. A.; Chamberlain, L. R.; Ziller, J. W.; Alvarez, D. *Organometallics* **1990**, *9*, 2124.

(29) MacDonald, M. R.; Ziller, J. W.; Evans, W. J. *Inorganic Chemistry* **2011**, *50*, 4092.

(30) Corbey, J. F., University of California, Irvine, **2015**, *Dissertation*.

(31) Rinehart, J. D.; Long, J. R. *Chemical Science* **2011**, *2*, 2078.

(32) Peterson, J. K.; MacDonald, M. R.; Ziller, J. W.; Evans, W. J. *Organometallics* **2013**, *32*, 2625.

(33) MacDonald, M. R. University of California, Irvine, **2013**, *Dissertation*.

(34) Evans, W. J.; Montalvo, E.; Foster, S. E.; Harada, K. A.; Ziller, J. W. *Organometallics* **2007**, *26*, 2904.

(35) Shannon, R. *Acta Crystallographica Section A* **1976**, *32*, 751.

(36) Clarke, R. E.; Ford, P. C. *Inorganic Chemistry* **1970**, *9*, 227.

(37) N. Storhoff, B.; C. Lewis Jr, H. *Coordination Chemistry Reviews* **1977**, *23*, 1.

(38) Evans, W. J.; Montalvo, E.; Champagne, T. M.; Ziller, J. W.; DiPasquale, A. G.; Rheingold, A. L. *Journal of the American Chemical Society* **2008**, *130*, 16.

(39) Bellamy, L. J. *Advances in Infrared Group Frequencies*; Chapman and Hall: London, 1968.

(40) Achord, P.; Fujita, E.; Muckerman, J. T.; Scott, B.; Fortman, G. C.; Temprado, M.; Cai, X.; Captain, B.; Isrow, D.; Weir, J. J.; McDonough, J. E.; Hoff, C. D. *Inorganic Chemistry* **2009**, *48*, 7891.

(41) MacDonald, M. R.; Ziller, J. W.; Evans, W. J. *Journal of the American Chemical Society* **2011**, *133*, 15914.

(42) APEX2 Version 2014.1-1, Bruker AXS, Inc.; Madison, WI 2014.

(43) SAINT Version 8.34a, Bruker AXS, Inc.; Madison, WI 2013.

(44) Sheldrick, G. M. SADABS, Version 2014/5, Bruker AXS, Inc.; Madison, WI 2014.

(45) Sheldrick, G. M. SHELXTL, Version 2014/7, Bruker AXS, Inc.; Madison, WI 2014.

(46) International Tables for Crystallography 1992, Vol. C., Dordrecht: Kluwer Academic Publishers.

(47) Spek, A. L. PLATON, Acta. Cryst. 2009, D65, 148-155.

CHAPTER 8

Synthesis and Reduction of Tris(indenyl) Rare Earth Complexes Including C–H Bond Activation of an Indenyl Ligand

Introduction

After decades in which it was thought that Eu, Yb, Sm, Tm, Dy and Nd were the only rare earths that could form complexes with the metal in the +2 oxidation state, it was found that the reduction chemistry of yttrium and the f elements could provide +2 ions for yttrium,[1] all the lanthanides[2-4] (except Pm, which was not studied due to its radioactivity), uranium[5] and thorium.[6] These new oxidation states have been obtained by reduction of the tris(cyclopentadienyl) complexes, Cp'_3M and Cp''_3M ($Cp' = C_5H_4SiMe_3$, M = Y, lanthanide, U; $Cp'' = C_5H_3(SiMe_3)_2$, M = La, Ce, Th) to form $(Cp'_3M)^{1-}$ and $(Cp''_3M)^{1-}$ complexes, Figures 8.1 and 8.2.

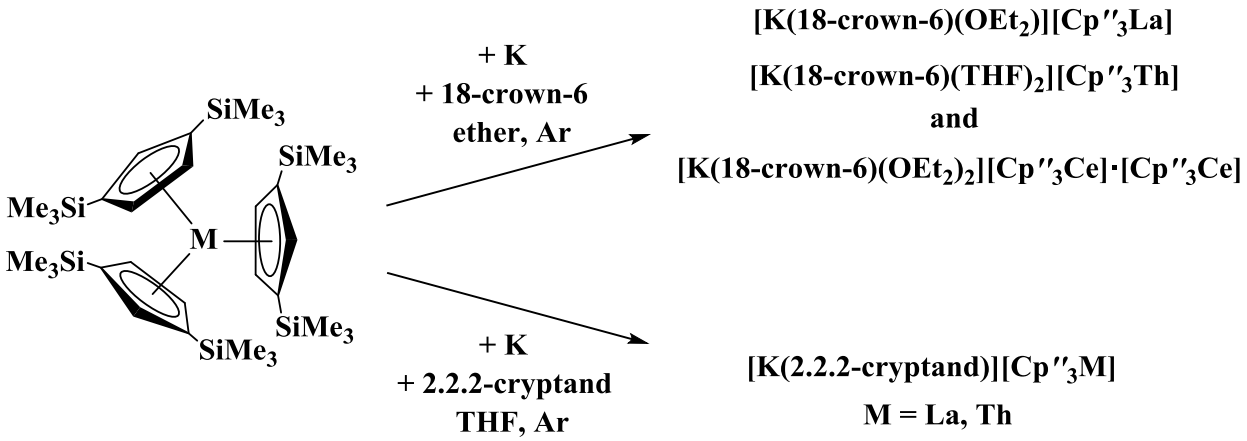

Figure 8.1. Crystallographically characterized products from reduction of Cp''_3M (M = La,[4] Ce,[4] and Th;[6] $Cp'' = C_5H_3(SiMe_3)_2$-1,3; ether = Et_2O or THF).

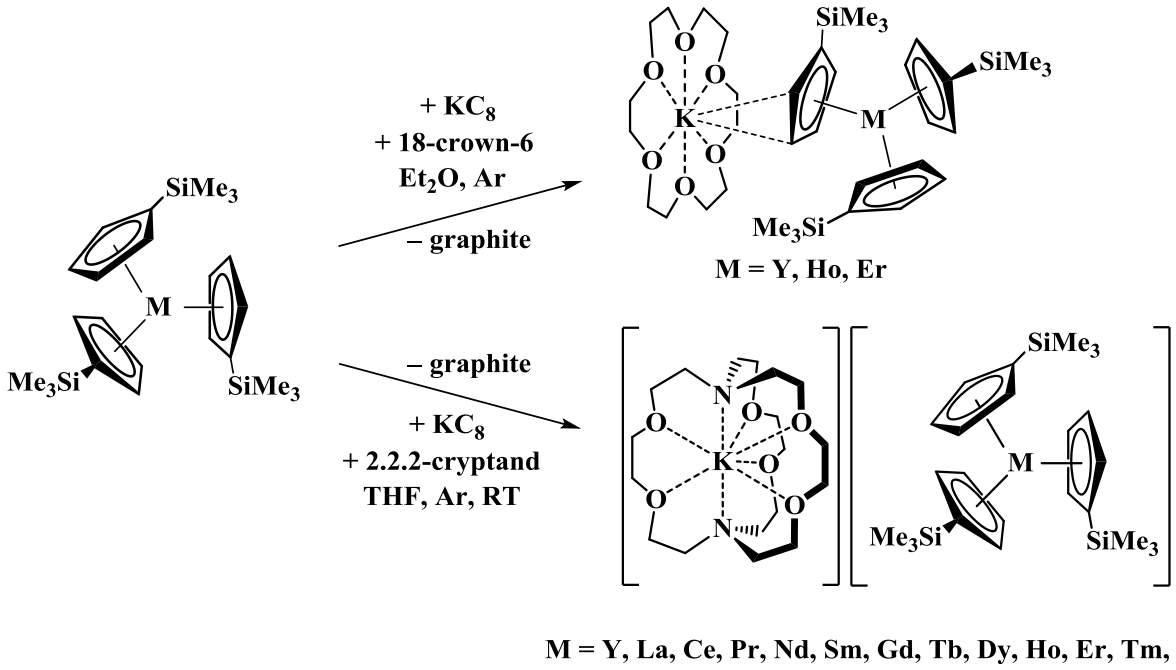

Figure 8.2. Crystallographically characterized products from reduction of Cp'_3M (M = Y,[1] La,[7] Ce,[7] Pr,[3] Nd,[7] Sm,[7] Gd,[3] Tb,[3] Dy,[7] Ho,[2] Er,[2] Tm,[7] Lu,[3] and U;[5] Cp′ = $C_5H_4SiMe_3$).

Structural, spectroscopic, and density functional theory analyses suggest that these new ions could be accessed for the first time because the $(Cp'_3)^{3-}$ and $(Cp''_3)^{3-}$ ligand sets allow the dz^2 orbital to be populated such that the new ions have $4f^n5d^1$ electron configurations for the lanthanides, $5f^36d^1$ for uranium, $6d^2$ for thorium, and $4d^1$ for yttrium. This is consistent with numerous theoretical analyses of the f elements in trigonal tris(cyclopentadienyl) coordination environments.[8-13] Whereas reduction of a $4f^n$ Ln^{3+} ion to a $4f^{n+1}$ Ln^{2+} product would be difficult due to the highly negative calculated generic reduction potentials for such a process (−2.7 to −3.9 V vs NHE[14,15]), reduction to $4f^n5d^1$ ions appears to be achievable. Recent magnetic measurements on the new Ln^{2+} complexes, performed by Katie Meihaus in the lab of Prof. Jeffrey R. Long at the University of California, Berkeley, have revealed that the holmium analog,

[K(2.2.2.-cryptand)][Cp'_3Ho], possesses the highest magnetic moment ever measured for a single metal ion with μ_{eff} = 11.4 μ_B, suggesting that these mixed configuration complexes could have important implications on how we understand fundamental magnetic properties of molecules.

Although these new ions are isolable in molecular form, the complexes are highly reactive. They are best formed at low temperature or with very short reaction times and should be stored at low temperature. Physical characterization of the complexes of the new ions is challenging, since decomposition can occur in the course of preparing the samples and making the measurements. To obtain more stable variants of these complexes for physical characterization studies, reductions of other tris(cyclopentadienyl) complexes were pursued since these coordination environments should also have dz^2 orbitals that could be populated. This chapter discusses results using the indenyl ligand C_9H_7 (Cp^{In}).

Yttrium was chosen as the initial metal for this investigation, since EPR spectroscopy can provide good evidence for the presence of Y^{2+} due to the 100% naturally abundant ^{89}Y nucleus that gives a doublet signal for this ion.[1,16] However, when reduction of the indenyl complex $Cp^{In}_3Y(THF)$ did not provide definitive products, other rare earth metals were examined. Only with Dy were definitive data obtained in the form of an unusual C–H activation product as identified by X-ray crystallography when an external magnet was present during crystallization.

C–H activation has previously been found in the reductive chemistry of Nd^{2+} by Deacon and coworkers using the $C_5H_2{}^tBu_3$ (Cp^{ttt}) ligand.[17] C–H bond activation has also been reported in the reduction of $Y[N(SiMe_3)_2]_3$ with potassium, but the metallacyclic species $\{[(Me_3Si)_2N]_2Y[CH_2Si(Me_2)NSiMe_3]\}[K(18\text{-crown-6})(THF)(toluene)]$[16,18] formed in that case is a common type of by-product in reactions with $M[N(SiMe_3)_2]_3$.[16,18-24] The reduction of

$Cp^{In}_3Dy(THF)$ reported here is another example that suggests C–H bond activation may be a viable reaction pathway in reactions that generate highly reactive f element Ln^{2+} ions.

Results

The synthesis of the indenyl complexes was more complicated than the synthesis of other tris(cyclopentadienyl) lanthanide complexes and this is one aspect of this ligand that distinguishes it from others cyclopentadienyl derivatives. The tris(indenyl) complexes, $Cp^{In}_3Ln(THF)$ (Ln = Y, Dy, Ho), were prepared by addition of $LnCl_3$ to either NaC_9H_7 or KC_9H_7, Figure 8.3. Unlike the larger known lanthanide analogs of $Cp^{In}_3Ln(THF)$ (Ln = La, Pr, Nd),[25] which are isomorphous and crystallize in the monoclinic space group $P2_1/c$, these new smaller metal analogs $Cp^{In}_3Ln(THF)$ (Ln = Y, Dy, Ho) are isomorphous with the Sm analog[25] which crystallizes in the hexagonal space group $P6_3$.

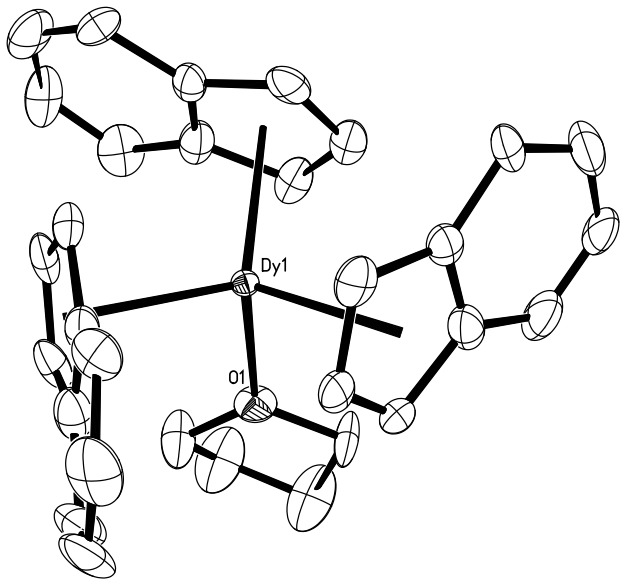

Figure 8.3. Thermal ellipsoid plot of $Cp^{In}_3Dy(THF)$ drawn at the 50% probability level. Hydrogen atoms are omitted for clarity. The yttrium and holmium analogs are isomorphous.

When 3 equiv of NaC_9H_7 are reacted with $DyCl_3$, YCl_3, or $HoCl_3$, two types of crystals with different morphologies crystallize from the same THF reaction mixture. One type was identified by X-ray crystallography to be the tris(indenyl) complex $Cp^{In}_3Ln(THF)$ described above, and the other is a NaCl adduct with the formula $[Cp^{In}_3Ln(\mu\text{-}Cl)LnCp^{In}_3][Na(THF)_6]$, which was identified by X-ray crystallography (Ln = Dy, Y), eq 8.1, Figure 8.4. The chloride-containing byproduct has been previously reported for Ln = Nd.[26]

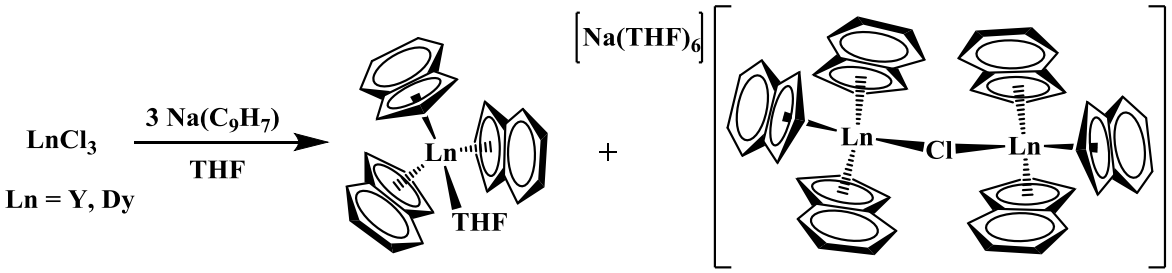

(8.1)

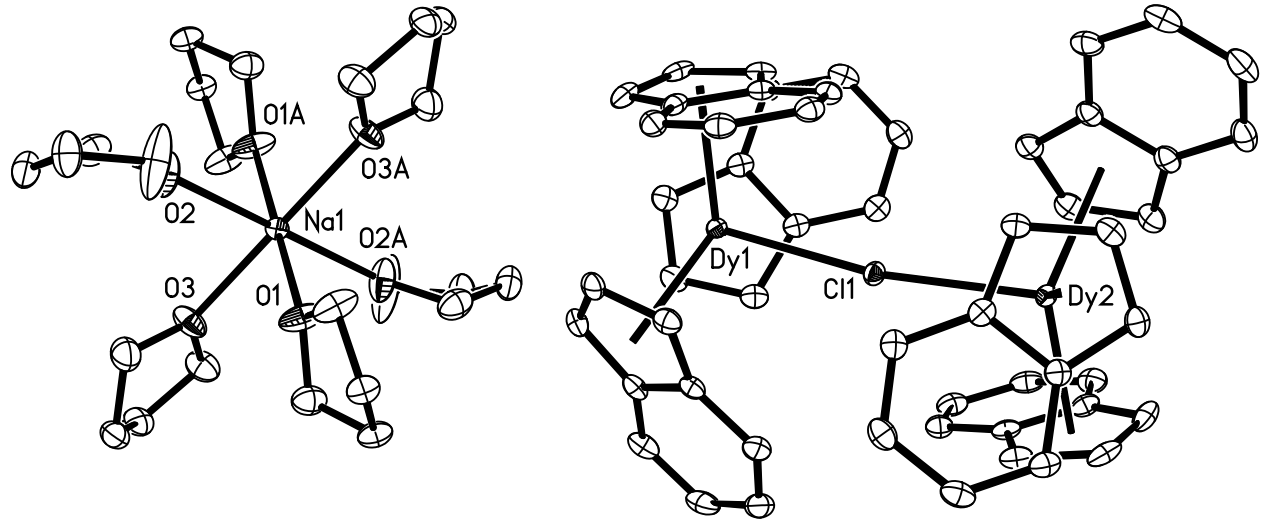

Figure 8.4. Thermal ellipsoid plot of $[Cp^{In}_3Dy(\mu\text{-}Cl)DyCp^{In}_3][Na(THF)_6]$ drawn at the 50% probability level. Hydrogen atoms and disorder in the THF ligands are omitted for clarity. The yttrium analog is isomorphous.

When KC_9H_7 is used instead of NaC_9H_7, the solvated tris(indenyl) species $Cp^{In}{}_3Ln(THF)$ can be washed with diethyl ether and isolated in pure form from THF. From the ether wash, in the cases of Ln = Dy and Ho, crystals of $[Cp^{In}{}_2Ln(\mu\text{-}Cl)_2K(Et_2O)]_\infty$ (Ln = Dy, Ho) could also be isolated and were identified by X-ray crystallography, Figure 8.5, eq 8.2. Although alkali metal halide adduct complexes of metallocenes, such as (cyclopentadienyl ring)$_2$Ln(halide)$_2$(alkali metal) are common in rare earth chemistry,[27-31] this example is unique in that the potassium ion bridges not only to four chloride ligands to generate a polymeric structure in the solid state, but it is also located near the phenyl portion of an indenyl ligand. A similar ether wash procedure using NaC_9H_7 as the indenyl source did not yield the same "ate-type" species as with KC_9H_7. In the case of Ho, crystals of a sodium-free trimetallic chloride complex, $[Cp^{In}Ho(THF)]_3(\mu\text{-}Cl)_3(\mu_3\text{-}Cl)(\mu_3\text{-}O)$, were isolated and identified by X-ray crystallography (Figure 8.6). These structures highlight differences between indenyl and the other cyclopentadienyl ligands, Cp′ and Cp″, mentioned above.

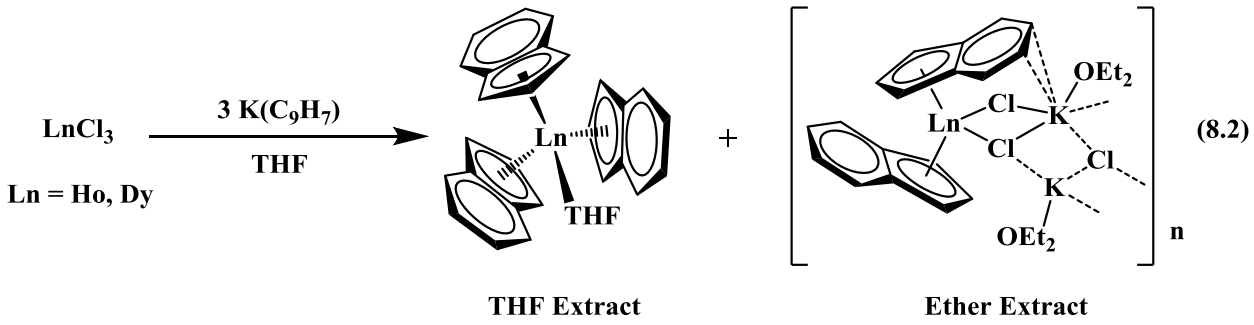

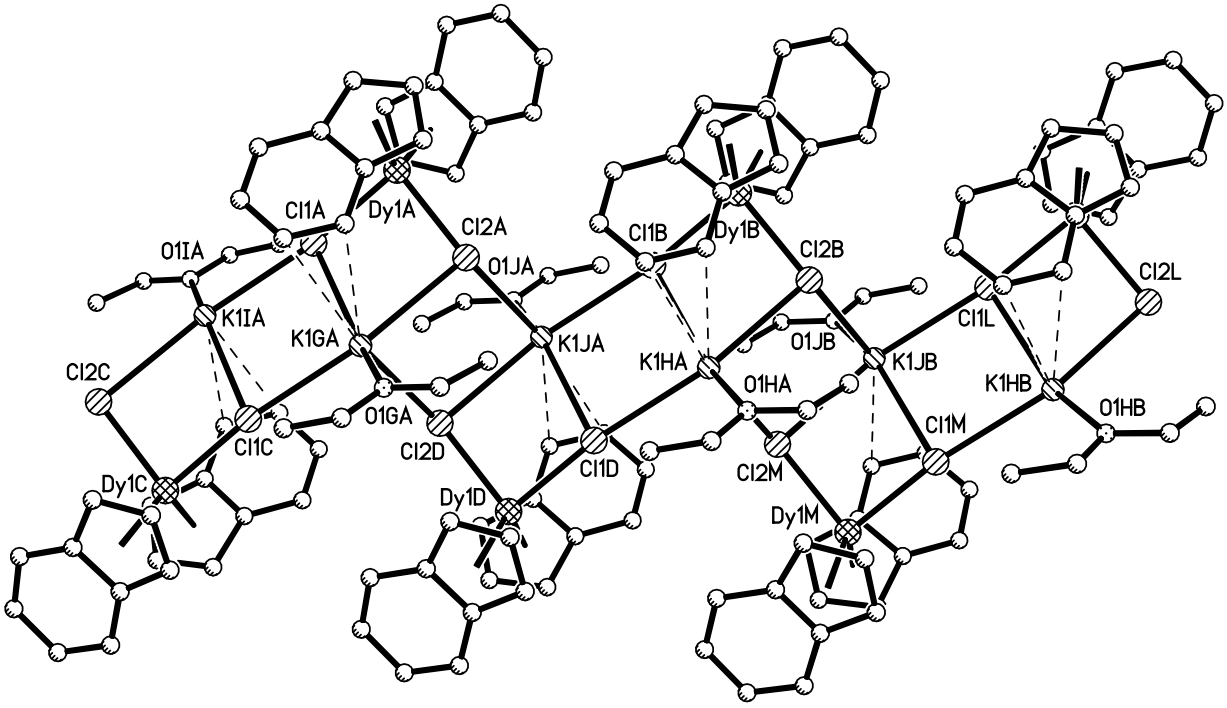

Figure 8.5. Crystal structure of $[Cp^{In}{}_2Dy(\mu\text{-}Cl)_2K(Et_2O)]_\infty$. Hydrogen atoms and outersphere solvent molecules are omitted for clarity. The holmium analog is isomorphous. The seven coordinate nature of each potassium ion can be seen with K1JA which is located near Cl1B, Cl1D, Cl2A, and Cl2D as well as ether oxygen O1JA and two carbon atoms of the indenyl ring at distances of 3.374(3) and 3.490(3) Å.

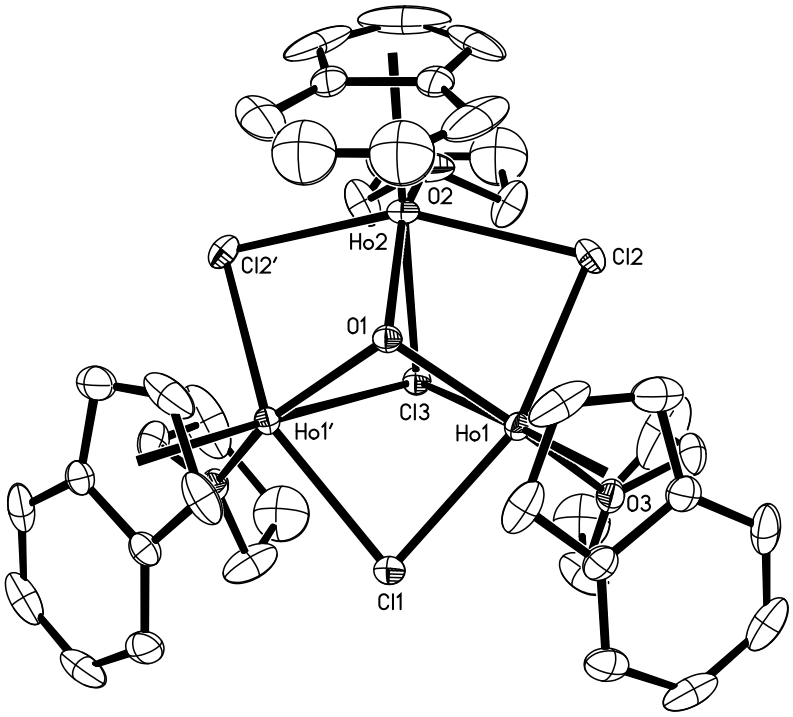

Figure 8.6. Thermal ellipsoid plot of $[Cp^{In}Ho(THF)]_3(\mu\text{-}Cl)_3(\mu_3\text{-}Cl)(\mu_3\text{-}O)$ drawn at the 50% probability level. Hydrogen atoms and disorder are omitted for clarity.

Reactions with Indenyl Complexes. C–H Bond Activation. Reduction of the tris(indenyl) complex $Cp^{In}{}_3Y$ ($Cp^{In} = C_9H_7$) with excess KC_8 gave a dark brown solution as in the reductions leading to the Ln^{2+} complexes mentioned in the introduction, but the characteristic doublet of Y^{2+} was not observed by EPR spectroscopy. Analogous reductions of complexes of the similarly sized metals, Dy and Ho, also gave dark colors, but only in the dysprosium reaction were crystals of a new complex involving the indenyl ligand fortuitously isolated. When an external NdFeB magnet was present during crystallization,[32] single crystals of $\{K(2.2.2\text{-cryptand})\}_2\{[(C_9H_7)_2Dy(\mu\text{-}\eta^5\text{:}\eta^1\text{-}C_9H_6)]_2\}$ could be obtained, Figure 8.7. This complex contains

the first example of the indenyl dianion, $(C_9H_6)^{2-}$, derived from C–H bond activation of the $(C_9H_7)^{1-}$ monoanion.

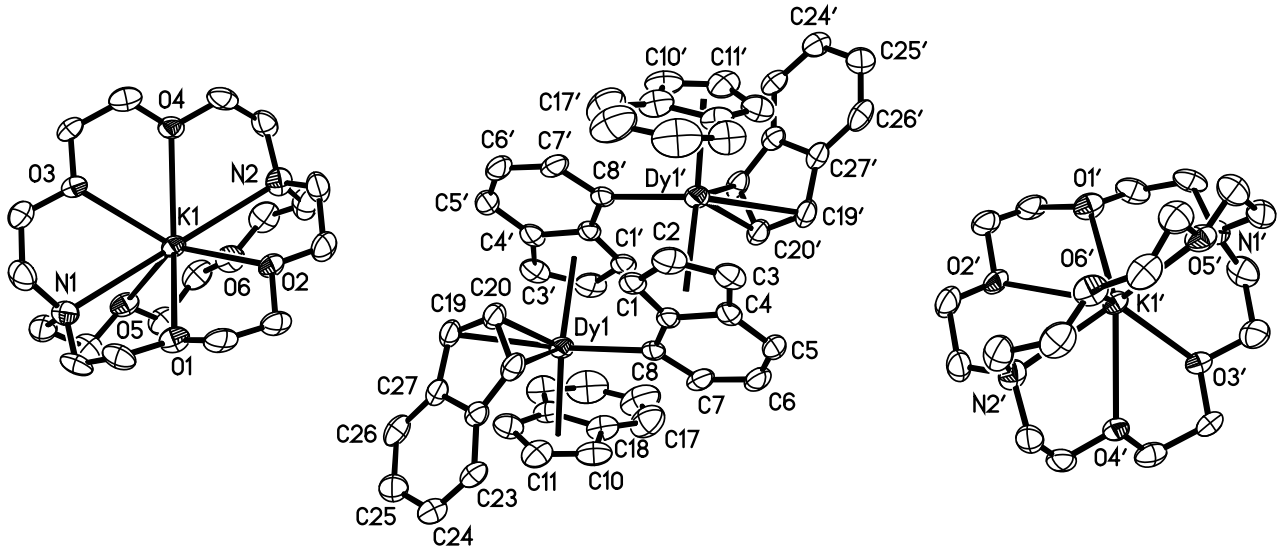

Figure 8.7. Thermal ellipsoid plot of $\{K(2.2.2\text{-cryptand})\}_2\{[(C_9H_7)_2Dy(\mu\text{-}\eta^5\text{:}\eta^1\text{-}C_9H_6)]_2\}$ drawn at the 50% probability level. Hydrogen atoms are omitted for clarity.

The structure of $\{K(2.2.2\text{-cryptand})\}_2\{[(C_9H_7)_2Dy(\mu\text{-}\eta^5\text{:}\eta^1\text{-}C_9H_6)]_2\}$ is a rare case in which three different indenyl binding modes are found in the same complex. Each Dy center is formally nine-coordinate, with two η^5-indenyl ligands, one η^3-indenyl group, and η^1-coordination to the metalated C8 carbon in the arene ring of an indenyl group bound to another Dy. It is not uncommon for the indenyl ligand to display η^3 binding modes, and, in some cases, this easily accessible mode is thought to facilitate unique reactivity when compared to other cyclopentadienyl derivatives.[33,34]

A comparison of the metrical data of $\{K(2.2.2\text{-cryptand})\}_2\{[(C_9H_7)_2Dy(\mu\text{-}\eta^5\text{:}\eta^1\text{-}C_9H_6)]_2\}$ with the ten-coordinate metal center in the $Cp^{In}{}_3Dy(THF)$ starting material as well as the $[Cp^{In}{}_3Dy(\mu\text{-Cl})DyCp^{In}{}_3][Na(THF)_6]$ byproduct is provided in Table 8.1. In $Cp^{In}{}_3Dy(THF)$, the

three symmetry-equivalent Dy-(η^5-ring centroid) distances are 2.496 Å. In {K(2.2.2-cryptand)}$_2${[$(C_9H_7)_2$Dy(μ-η^5:η^1-C_9H_6)]$_2$}, the analogous Dy-(η^5-ring centroid) distance involving the ring containing C10 is 2.542 Å, while the Dy-[(μ-η^1:η^5-C_9H_6)$^{2-}$ ring centroid] distance involving the ligand containing C1 is 2.423 Å. The distance from Dy to the (η^3-ring centroid) is much longer, 2.740 Å, as expected. The six unique Dy-(η^5-ring centroid) distances in [Cp^{In}_3Dy(μ-Cl)DyCp^{In}_3][Na(THF)$_6$] are similar to the distances to η^5-ring centroids in Cp^{In}_3Dy(THF) and {K(2.2.2-cryptand)}$_2${[$(C_9H_7)_2$Dy(μ-η^5:η^1-C_9H_6)]$_2$}.

For Cp^{In}_3Dy(THF), the dihedral angle formed between the planes of the 5- and 6-membered rings is 6.7°. Of the three unique indenyl ligands in {K(2.2.2-cryptand)}$_2${[$(C_9H_7)_2$Dy(μ-η^5:η^1-C_9H_6)]$_2$}, the one which binds in an η^3 fashion to the metal center displays the least amount of bending between the fused rings with a dihedral angle of 1.8°. The Dy1–C8(η^1) distance in {K(2.2.2-cryptand)}$_2${[$(C_9H_7)_2$Dy(μ-η^5:η^1-C_9H_6)]$_2$} (2.472(8) Å) is identical to the 2.475(4) Å Dy1–C1(η^1) distance in the "tuck-in" complex (η^5-$C_5Me_4SiMe_3$)Dy(η^5:η^1-$C_5Me_4SiMe_2CH_2$)(THF)[35] and is slightly longer than the 2.409(5) Å Dy1–C1(CH_2SiMe_3) distance in [(Cp′)Dy(CH_2SiMe_3)$_2$(THF)].[36]

Table 8.1. Selected interatomic distances (Å) and angles (º) for $Cp^{In}_3Dy(THF)$, $[Cp^{In}_3Dy(\mu\text{-}Cl)DyCp^{In}_3][Na(THF)_6]$ and $\{K(2.2.2\text{-cryptand})\}_2\{[(C_9H_7)_2Dy(\mu\text{-}\eta^5\text{:}\eta^1\text{-}C_9H_6)]_2\}$ where X = O, Cl, or C(η^1) for $Cp^{In}_3Dy(THF)$, $[Cp^{In}_3Dy(\mu\text{-}Cl)DyCp^{In}_3][Na(THF)_6]$ and $\{K(2.2.2\text{-cryptand})\}_2\{[(C_9H_7)_2Dy(\mu\text{-}\eta^5\text{:}\eta^1\text{-}C_9H_6)]_2\}$, respectively.

	Dy–(ring centroid)	Dy–X	Fused Ring Dihedral
$Cp^{In}_3Dy(THF)$	2.496	2.417(7)	6.7
$[Cp^{In}_3Dy(\mu\text{-}Cl)DyCp^{In}_3][Na(THF)_6]$	2.499		4.4
	2.490		4.5
	2.482	2.757(5)	4.9
	2.494	2.773(5)	4.8
	2.474		5.4
	2.535		3.5
$\{K(2.2.2\text{-cryptand})\}_2\{[(C_9H_7)_2Dy(\mu\text{-}\eta^5\text{:}\eta^1\text{-}C_9H_6)]_2\}$	2.432		3.9
	2.542	2.472(8)	6.7
	2.746 (η^3)		1.8

Density Functional Theory Analysis. Theoretical studies performed by Megan Fieser on the crystallographically characterized THF adducts, $Cp^{In}_3Ln(THF)$ (Ln = Y, La[37]), presumably present in the THF solutions during reduction, are different from those of the previously reported $Cp'_3M(THF)$ and $Cp''_3M(THF)$ complexes mentioned in the introduction above.[2,3,5-7] The LUMO of these THF-solvated indenyl complexes, $Cp^{In}_3Ln(THF)$, was not a d_{z2} orbital. Instead, it had mainly ligand character localized on the C_6 ring of the indenyl ligands, Figure 8.8, Table 8.2. This suggests reduction of these molecules would put more electron density on the ligands than in the other Cp^x_3Ln reductions. If the increased electron density on the ligand led to C–H bond activation, this would be consistent with the isolation of $\{K(2.2.2\text{-cryptand})\}_2\{[(C_9H_7)_2Dy(\mu\text{-}\eta^5\text{:}\eta^1\text{-}C_9H_6)]_2\}$, which contained a $(C_9H_6)^{2-}$ ligand formed by C–H bond activation in the arene ring.

Calculations were also performed on two unsolvated Cp^{In}_3Ln (Ln = Y, La) complexes with different indenyl geometries around the metal center, one in which the C_6 rings of the indenyl ligands orient above and below the plane of the three Cp^{In}(Cnt), **A**, and another in which the C_6 rings of indenyl ligands orient in the plane of the three Cp^{In}(Cnt), **B**.[38] For the **A** geometry, the LUMOs for both Y and La are primarily d_{z2} orbitals, but these orbitals have significantly more ligand character than any of the other Cp^x_3M complexes,[2,7] Figure 8.8, Table 8.2. For the **B** geometry, the LUMOs for both Y and La are also primarily d_{z2} orbitals, but the % metal character of these orbitals is much closer to that of the Cp^x_3Ln complexes previously characterized. This suggests that it may be possible to form an indenyl Ln^{2+} species in the absence of coordinating solvent if reduction can occur when the indenyl ligands are properly oriented.

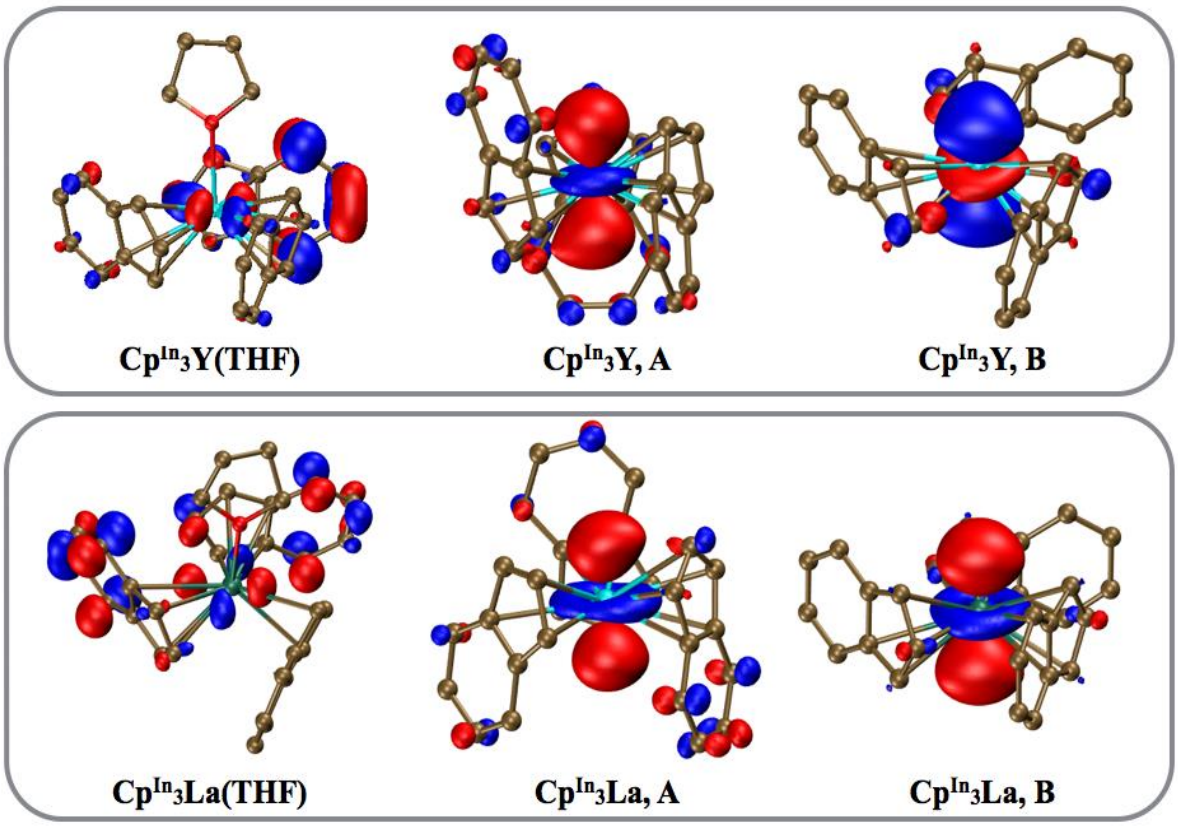

Figure 8.8. Molecular orbital plots of the LUMOs of Cp^{In}_3Y and $Cp^{In}_3Y(THF)$ (top) and the LUMOs of Cp^{In}_3La and $Cp^{In}_3La(THF)$ (bottom), using a contour value of 0.05.

Table 8.2. Mulliken population analysis (MPA) summary for the LUMOs of Cp^{In}_3Ln and $Cp^{In}_3Ln(THF)$ and HOMOs of the $(Cp^{In}_3Ln)^{1-}$ complexes, computed using TPSSh and TZVP basis sets. The % metal column indicates the total metal contribution to the molecular orbital and the % s and % d columns indicate how much of the total orbital comes directly from the metal s and d orbitals, respectively.

Compound	Neutral LUMO metal contribution			Anion HOMO metal contribution		
	% metal	% s	% d	% metal	% s	%d
$Cp^{In}_3Y(THF)$	35	0	33	—	—	—
Cp^{In}_3Y A	47	4	43	61	11	50
Cp^{In}_3Y B	62	13	49	75	18	57
$Cp^{In}_3La(THF)$	16	0	16	—	—	—
Cp^{In}_3La A	50	5	46	62	8	54
Cp^{In}_3La B	72	10	62	84	16	67

Discussion

Metalation of cyclopentadienyl rings on rare earth complexes has been known for decades[39] and was one of the reasons for the great success of the $(C_5Me_5)^{1-}$ ligand, which is more resistant to this problem. Nonetheless, C–H bond activation of $(C_5Me_5)^{1-}$ ligands also occurs to make $(C_5Me_4CH_2)^{2-}$ dianions that can attach to a single metal ("tuck-in")[40,41] or can bridge two metals ("tuck-over")[41,42] as is observed in $\{K(2.2.2\text{-cryptand})\}_2\{[(C_9H_7)_2Dy(\mu\text{-}\eta^5\text{:}\eta^1\text{-}$

$C_9H_6)]_2\}$. Given this history of C–H bond activation of cyclopentadienyl ligands, it is surprising that this type of reactivity has *not* previously been observed for the indenyl ligand system to our knowledge.

The isolation of the C–H bond activated product, $\{K(2.2.2\text{-cryptand})\}_2\{[(C_9H_7)_2Dy(\mu\text{-}\eta^5\text{:}\eta^1\text{-}C_9H_6)]_2\}$, was surprising in light of the uniform nature of the reductions of the other $Cp^x{}_3M$ complexes.[2,3,5-7] There was precedent for C–H bond activation in connection with Ln^{2+} chemistry as observed by Deacon and co-workers with the Nd^{2+} complex, $[Cp^{ttt}{}_2Nd(\mu\text{-}I)K(18\text{-crown-}6)]$ ($Cp^{ttt} = C_5H_2{}^tBu_3$), which decomposes to a Nd^{3+} complex in which one of the tert-butyl substituents is metalated, $[Cp^{ttt}\{\mu\text{-}C_5H_2{}^tBu_2(CH_2)\}Nd(\mu\text{-}I)K(\text{-}18\text{-crown-}6)]\bullet C_6H_{14}$.[17] However, there were no obvious similarities between the tris(tert-butyl)cyclopentadienyl and indenyl complexes.

Fortunately, DFT calculations provide a rationale for the observed C–H bond activation. Calculations on the indenyl complexes show that the LUMOs of $Cp^{Ind}{}_3Y$ and $Cp^{Ind}{}_3Y(THF)$ differ from those of $Cp'{}_3M$ and $Cp''{}_3M$.[2,6,7] In the indenyl case, there is more ligand character in the LUMO and correspondingly less d_{z^2} character. Hence, reduction might not simply populate the d_{z^2} orbital and lead to Ln^{2+}, but it could put more electron density on the ligand, making it more reactive. This in turn could lead to the observed metalation as one of the reaction pathways in this complicated reaction. Since $\{K(2.2.2\text{-cryptand})\}_2\{[(C_9H_7)_2Dy(\mu\text{-}\eta^5\text{:}\eta^1\text{-}C_9H_6)]_2\}$ was only isolated as a minor crystalline byproduct, the structure of $\{K(2.2.2\text{-cryptand})\}_2\{[(C_9H_7)_2Dy(\mu\text{-}\eta^5\text{:}\eta^1\text{-}C_9H_6)]_2\}$ should only be viewed as a demonstration that metalation of indenide is possible.

Conclusion

Attempts to make more stable derivatives of [K(2.2.2-cryptand)][Cp′$_3$Y], **1-Y**, via reduction of Cp$^{Ind}_3$Ln led to isolation of the metalated indenide complex, {K(2.2.2-cryptand)}$_2${[(C$_9$H$_7$)$_2$Dy(μ-η^5:η^1-C$_9$H$_6$)]$_2$}, demonstrating that C–H bond activation is possible in these highly reducing systems. DFT analysis of these reductions revealed that differences in the LUMOs of the Ln^{3+} precursors correlate with the observed reduction chemistry, since the LUMOs of the Cp$^x_3$M complexes are primarily d_{z^2} and those of the indenyl complexes have more ligand character.

Experimental Details

All manipulations and syntheses described below were conducted with rigorous exclusion of air and water using standard Schlenk line and glovebox techniques under an argon or dinitrogen atmosphere. Solvents were sparged with UHP argon and dried by passage through columns containing Q-5 and molecular sieves prior to use. Deuterated NMR solvents were dried over NaK alloy, degassed by three freeze-pump-thaw cycles, and vacuum transferred before use. Indene was dried over molecular sieves and degassed by three freeze-pump-thaw cycles. NaC$_9$H$_7$ and KC$_9$H$_7$ were prepared by treatment of indene with the alkali metal in THF. KC$_8$[43] and anhydrous LnCl$_3$[44] (Ln = Y, Ho, Dy) were prepared according to the literature. The Nd$_2$Fe$_{14}$B magnets used in the crystallizations were obtained from United Nuclear Scientific Equipment and Supplies. ^{1}H NMR spectra were recorded on Bruker GN500 or CRYO500 MHz spectrometers (^{13}C NMR at 125 MHz) at 298 K unless otherwise stated and referenced internally to residual protio-solvent resonances. Electron paramagnetic resonance spectra were collected using a Bruker EMX spectrometer equipped with an ER041XG microwave bridge in THF at 298

K and 77 K unless otherwise specified. IR samples were prepared as KBr pellets on a Varian 1000 FT-IR system. Elemental analyses were conducted on a Perkin-Elmer 2400 Series II CHNS elemental analyzer.

$Cp^{In}_3Dy(THF)$. This synthesis follows a previously reported procedure for the larger metals La, Pr, Nd and Sm.[25] In a glovebox, THF (8 mL) was added to $DyCl_3$ (324 mg, 1.21 mmol) to make a white slurry. A yellow THF solution (7 mL) of $NaCp^{In}$ (500 mg, 3.62 mmol) was added to the stirred slurry, and the cloudy yellow mixture was allowed to stir overnight. Centrifugation removed pale insoluble material, and the yellow supernatant was filtered and stored at –35 ℃ in a vial with a NdFeB magnet attached to the outside. After 1 d, yellow X-ray quality crystals of $Cp^{In}_3Dy(THF)$ (72 mg, 10%) had grown on the side of the vial where the magnet was attached. IR: 3067m, 3043m, 2978m, 2898w, 1795w, 1679w, 1475m, 1448m, 1407m, 1331s, 1253m, 1220m, 1109w, 1034m, 1008m, 866m, 792s, 752s cm^{-1}. Anal. Calcd for $C_{31}H_{29}ODy$: C, 64.19; H, 5.04. Found: C, 63.46; H, 5.03.

$Cp^{In}_3Dy(THF)$ can also be made by stirring KCp^{In} with $DyCl_3$ overnight, centrifuging to remove pale insoluble solids, and removing solvent from the supernatant via reduced pressure. The dried supernatant can then be washed with diethyl ether and collected via centrifugation. Pure $Cp^{In}_3Dy(THF)$ can be crystallized from THF solutions of the collected solids after washing with diethyl ether.

$Cp^{In}_3Y(THF)$. To a stirred yellow THF (10 mL) solution of KCp^{In} (250 mg, 1.62 mmol) was added YCl_3 (106 mg, 0.54 mmol) to yield a cloudy yellow mixture which was allowed to stir 2 d. Centrifugation removed white insoluble material, the yellow supernatant was filtered and solvent was removed under vacuum to yield pale yellow solids. Et_2O was added to the solids and the mixture was stirred overnight. Centrifugation separated white solids from pale yellow

supernatant, and the solids were redissolved in THF and stored at –35°. After several days, X-ray quality crystals of $Cp^{In}_3Y(THF)$ (18 mg, 7%), Figure S2, had grown. ^{1}H NMR (d_8-THF): δ 7.49 (m, C_9H_7, 6H), 6.97 (m, C_9H_7, 6H), 5.46 (m, C_9H_7, 6H), 4.52 (m, C_9H_7, 3H). ^{13}C NMR (d_8-THF): .δ 132.26 (C_9H_7), 122.98 (C_9H_7), 121.42 (C_9H_7), 120.94 (C_9H_7), 99.16 (C_9H_7). IR: 3098w, 3067w, 3031m, 2971m, 2922w, 2867w, 1793w, 1675w, 1599w, 1446m, 1331s, 1220s, 1033m, 1001m, 864m, 841m, 794s, 760s, 743s cm^{-1}. Anal. Calcd for $C_{31}H_{29}OY$: C, 73.52; H, 5.77. Found: C, 72.97; H, 5.86. When $NaCp^{In}$ was used in place of KCp^{In}, the NaCl adduct $[Cp^{In}_3Y(\mu\text{-Cl})YCp^{In}_3][Na(THF)_6]$ was isolated as crystals from the mother liquor of $Cp^{In}_3Y(THF)$ as determined by matching of the unit cell to that of the Dy analog.

$Cp^{In}_3Ho(THF)$. Similarly to $Cp^{In}_3Dy(THF)$, THF (6 mL) was added to $HoCl_3$ (131 mg, 0.48 mmol) to make a white slurry. A yellow THF solution of $NaCp^{In}$ (200 mg, 1.45 mmol) was added to the stirred slurry, and the cloudy yellow mixture was allowed to stir overnight. Centrifugation removed pale insoluble material, the yellow supernatant was filtered and solvent was removed under reduced pressure to yield tacky orange solid. The solids were stirred with Et_2O (12 mL) overnight, and the mixture was centrifuged to collect pale yellow solids which were dissolved in THF (6 mL) and stored at –35 °C in a vial with a NdFeB magnet attached to the outside. After 2 d, X-ray quality crystals of $Cp^{In}_3Ho(THF)$ (17 mg, 5%) had grown near the magnet. IR: 3085w, 3048w, 3028w, 2975w, 2863w, 1876w, 1774w, 1669w, 1595w, 1455w, 1446w, 1404w, 1331s, 1220m, 1032m, 1001m, 839m, 794s, 742s, 744s cm^{-1}. Anal. Calcd for $C_{31}H_{29}OHo$: C, 63.92; H, 5.02. Found: C, 63.57; H, 5.00. From the diethyl ether wash, crystals of $[Cp^{In}Ho(THF)]_3(\mu\text{-Cl})_3(\mu_3\text{-Cl})(\mu_3\text{-O})$ were isolated, Figure S4. When KCp^{In} was used in place of $NaCp^{In}$, crystals of $[Cp^{In}_2Ho(\mu\text{-Cl})_2K(Et_2O)]_\infty$ were isolated from the ether wash, as identified by matching the unit cell to that of the Dy analog.

{K(2.2.2-cryptand)}$_2${[(C$_9$H$_7$)$_2$Dy(μ-η^5:η^1-C$_9$H$_6$)]$_2$}. 2.2.2-Cryptand (47 mg, 0.125 mmol) was added to a yellow solution of $Cp^{In}_3Dy(THF)$ (72 mg, 0.124 mmol) in THF (10 mL). While stirring, KC_8 (50 mg, 0.370 mmol) was added and the reaction mixture was allowed to stir for 3 min. Black solids were filtered away to yield a dark brown filtrate. This filtrate was concentrated to 2 mL under reduced pressure and placed in a vial that had a NdFeB magnet attached to the outside. After several days at –35 °C, pale tan X-ray quality crystals of {K(2.2.2-cryptand)}$_2${[(C$_9$H$_7$)$_2$Dy(μ-η^5:η^1-C$_9$H$_6$)]$_2$} had grown near the magnet.

X-ray Data Collection, Structure Solution and Refinement for $Cp^{In}_3Dy(THF)$. A yellow crystal of approximate dimensions 0.312 x 0.097 x 0.028 mm was mounted on a glass fiber and transferred to a Bruker SMART APEX II diffractometer. The APEX2[45] program package was used to determine the unit-cell parameters and for data collection (10 sec/frame scan time for a sphere of diffraction data). The raw frame data was processed using SAINT[46] and SADABS[47] to yield the reflection data file. The systematic absences were consistent with the hexagonal space groups $P6_3$ and $P6_3/m$ and $P6_322$. The non-centrosymmetric space group $P6_3$ was assigned and later determined to be correct. The structure was solved by direct methods and refined on F^2 by full-matrix least-squares techniques.[48] The analytical scattering factors[49] for neutral atoms were used throughout the analysis. The molecule was located on a three-fold rotation axis. There was inherent disorder in the atoms comprising the THF ligand, O(1), C(10), C(11), C(12), and C(13), due to the three fold symmetry. Those atoms were included with 1/3 occupancy as well as restrained distances and thermal parameters. Hydrogen atoms were included using a riding model. At convergence, wR2 = 0.0544 and Goof = 1.095 for 124 variables refined against 1959 data (0.74 Å), R1 = 0.0224 for those 1796 data with I > 2.0σ(I).

The absolute structure was assigned by refinement of the Flack parameter.[50] Details are given in Table 8.3.

X-ray Data Collection, Structure Solution and Refinement for $Cp^{In}_3Y(THF)$. A colorless crystal of approximate dimensions 0.774 x 0.128 x 0.126 mm was mounted on a glass fiber and transferred to a Bruker SMART APEX II diffractometer. The APEX2[45] program package was used to determine the unit-cell parameters and for data collection (40 sec/frame scan time for a sphere of diffraction data). The raw frame data was processed using SAINT[46] and SADABS[47] to yield the reflection data file. The systematic absences were consistent with the hexagonal space groups $P6_3$ and $P6_3/m$ and $P6_322$. The non-centrosymmetric space group $P6_3$ was assigned and later determined to be correct. The structure was solved by direct methods and refined on F^2 by full-matrix least-squares techniques.[48] The analytical scattering factors[49] for neutral atoms were used throughout the analysis. The molecule was located on a three-fold rotation axis. There was inherent disorder in the atoms comprising the THF ligand, O(1), C(10), C(11), C(12), and C(13), due to the three fold symmetry. Those atoms were included with 1/3 occupancy as well as restrained distances and thermal parameters. Hydrogen atoms were included using a riding model. At convergence, wR2 = 0.0866 and Goof = 1.103 for 124 variables refined against 1965 data (0.74 Å), R1 = 0.0335 for those 1906 data with $I > 2.0\sigma(I)$. The absolute structure was assigned by refinement of the Flack parameter.[50] Details are given in Table 8.3.

X-ray Data Collection, Structure Solution and Refinement for $Cp^{In}_3Ho(THF)$. A yellow crystal of approximate dimensions 0.282 x 0.097 x 0.044 mm was mounted on a glass fiber and transferred to a Bruker SMART APEX II diffractometer. The APEX2[45] program package was used to determine the unit-cell parameters and for data collection (20 sec/frame

scan time for a sphere of diffraction data). The raw frame data was processed using SAINT[46] and SADABS[47] to yield the reflection data file. The systematic absences were consistent with the hexagonal space groups $P6_3$ and $P6_3/m$ and $P6_322$. The non-centrosymmetric space group $P6_3$ was assigned and later determined to be correct. The structure was solved by direct methods and refined on F^2 by full-matrix least-squares techniques.[48] The analytical scattering factors[49] for neutral atoms were used throughout the analysis. The molecule was located on a three-fold rotation axis. There was inherent disorder in the atoms comprising the THF ligand, O(1), C(10), C(11), C(12), and C(13), due to the three fold symmetry. Those atoms were included with 1/3 occupancy as well as restrained distances and thermal parameters. Hydrogen atoms were included using a riding model. At convergence, wR2 = 0.0464 and Goof = 1.163 for 125 variables refined against 2028 data (0.73 Å), R1 = 0.0190 for those 1895 data with $I > 2.0\sigma(I)$. The molecule was refined as a two-component inversion twin. Details are given in Table 8.3.

X-ray Data Collection, Structure Solution and Refinement for $[Cp^{In}_3Dy(\mu\text{-}Cl)DyCp^{In}_3][Na(THF)_6]$. A yellow crystal of approximate dimensions 0.342 x 0.315 x 0.284 mm was mounted on a glass fiber and transferred to a Bruker SMART APEX II diffractometer. The APEX2[45] program package was used to determine the unit-cell parameters and for data collection (15 sec/frame scan time for a sphere of diffraction data). The raw frame data was processed using SAINT[46] and SADABS[47] to yield the reflection data file. Subsequent calculations were carried out using the SHELXTL[48] program. There were no systematic absences nor any diffraction symmetry other than the Friedel condition. The centrosymmetric triclinic space group $P\bar{1}$ was assigned and later determined to be correct. The structure was solved using the Patterson method and refined on F^2 by full-matrix least-squares techniques. The analytical scattering factors[49] for neutral atoms were used throughout the analysis. Hydrogen

atoms were included using a riding model. C(67), C(74) and C(78) were disordered and included using multiple components with partial site-occupancy-factors The sodium atoms were located on inversion centers. At convergence, wR2 = 0.0594 and Goof = 1.059 for 823 variables refined against 15264 data (0.74 Å), R1 = 0.0237 for those 13847 data with I > 2.0σ(I). Details are given in Table 8.4.

X-ray Data Collection, Structure Solution and Refinement for [$Cp^{In}_2Dy(\mu$-Cl)$_2K(Et_2O)]_\infty$. A colorless crystal of approximate dimensions 0.516 x 0.096 x 0.051 mm was mounted on a glass fiber and transferred to a Bruker SMART APEX II diffractometer. The APEX2[45] program package was used to determine the unit-cell parameters and for data collection (45 sec/frame scan time for a sphere of diffraction data). The raw frame data was processed using SAINT[46] and SADABS[47] to yield the reflection data file. Subsequent calculations were carried out using the SHELXTL[48] program. The diffraction symmetry was 2/*m* and the systematic absences were consistent with the monoclinic space groups *Cc* and *C*2/*c*. It was later determined that space group *C*2/*c* was correct. The structure was solved by direct methods and refined on F^2 by full-matrix least-squares techniques. The analytical scattering factors[49] for neutral atoms were used throughout the analysis. The structure was polymeric and there was half of a diethyl ether molecule of solvation present per asymmetric unit. C(19), C(20), C(23) and C(24) were disordered and included using multiple components with partial site-occupancy-factors. Hydrogen atoms were included using a riding model. At convergence, wR2 = 0.0586 and Goof = 1.026 for 259 variables refined against 6442 data (0.73 Å), R1 = 0.0259 for those 5328 data with I > 2.0σ(I). Details are given in Table 8.4.

X-ray Data Collection, Structure Solution and Refinement for [$Cp^{In}Ho(THF)]_3(\mu$-Cl)$_3(\mu_3$-Cl)$(\mu_3$-O). A yellow crystal of approximate dimensions 0.283 x 0.214 x 0.198 mm was

mounted on a glass fiber and transferred to a Bruker SMART APEX II diffractometer. The APEX2[45] program package was used to determine the unit-cell parameters and for data collection (10 sec/frame scan time for a sphere of diffraction data). The raw frame data was processed using SAINT[46] and SADABS[47] to yield the reflection data file. Subsequent calculations were carried out using the SHELXTL[48] program. The diffraction symmetry was *mmm* and the systematic absences were consistent with the orthorhombic space groups *Pnma* and $Pna2_1$. It was later determined that space group *Pnma* was correct. The structure was solved using the Patterson method and refined on F^2 by full-matrix least-squares techniques. The analytical scattering factors[49] for neutral atoms were used throughout the analysis. The molecule was located on a mirror plane. C(15) was disordered and included using multiple components and partial site-occupant-factors. Hydrogen atoms were not included for this THF ligand. All other hydrogen atoms were included using a riding model. At convergence, wR2 = 0.0789 and Goof = 1.041 for 229 variables refined against 5420 data (0.73 Å), R1 = 0.0304 for those 5021 data with $I > 2.0\sigma(I)$. Details are given in Table 8.4.

X-ray Data Collection, Structure Solution and Refinement for {K(2.2.2-cryptand)}$_2${[(C$_9$H$_7$)$_2$Dy(μ-η^5:η^1-C$_9$H$_6$)]$_2$}. A bronze crystal of approximate dimensions 0.148 x 0.127 x 0.056 mm was mounted on a glass fiber and transferred to a Bruker SMART APEX II diffractometer. The APEX2[45] program package was used to determine the unit-cell parameters and for data collection (90 sec/frame scan time for a sphere of diffraction data). The raw frame data was processed using SAINT[46] and SADABS[47] to yield the reflection data file. Subsequent calculations were carried out using the SHELXTL[48] program. There were no systematic absences nor any diffraction symmetry other than the Friedel condition. The centrosymmetric triclinic space group $P\bar{1}$ was assigned and later determined to be correct. The structure was

solved by direct methods and refined on F^2 by full-matrix least-squares techniques. The analytical scattering factors[49] for neutral atoms were used throughout the analysis. The complex was situated about an inversion center. There were three THF solvent molecules per asymmetric unit. While the geometry of the solvents was reasonable, the thermal parameters were high, and it was necessary to fix those during refinement. As a test, the SQUEEZE[51] routine was employed in an effort to determine the best method for refining the solvent molecules and although the wR2 value did decrease significantly, refinement (esds, etc.) was not drastically improved. Therefore, it was determined that the use of SQUEEZE was not justified for the final refinement. Hydrogen atoms were included using a riding model. Least-squares analysis yielded wR2 = 0.2084 and Goof = 1.052 for 541 variables refined against 10946 data (0.8 Å), R1 = 0.0737 for those 7325 data with $I > 2.0\sigma(I)$. Details are given in Table 8.4.

Table 8.3. Crystal data and structure refinement parameters for $Cp^{In}_3Y(THF)$, $Cp^{In}_3Dy(THF)$, and $Cp^{In}_3Ho(THF)$.

	$Cp^{In}_3Y(THF)$	$Cp^{In}_3Dy(THF)$	$Cp^{In}_3Ho(THF)$
Empirical formula	$C_{31}H_{29}OY$	$C_{31}H_{29}ODy$	$C_{31}H_{29}OHo$
Formula weight	506.45	580.04	582.47
Temperature (K)	133(2)	133(2)	88(2)
Space group	$P6_3$	$P6_3$	$P6_3$
a (Å)	11.6507(11)	11.6494(11)	11.6521(16)
b (Å)	11.6507(11)	11.6494(11)	11.6521(16)
c (Å)	10.0984(10)	10.0857(9)	10.0884(14)
α (°)	90	90	90
β (°)	90	90	90
γ (°)	120	120	120
Volume (Å^3)	1187.1(3)	1185.3(2)	1186.2(4)
Z	2	2	2
ρ_{calcd} (Mg/m^3)	1.417	1.625	1.631
μ (mm^{-1})	2.478	3.173	3.356
$R1^a$	0.0335	0.0224	0.0190
$wR2^b$	0.0866	0.0544	0.0464

$^a R1 = \Sigma||F_o|-|F_c|| / \Sigma|F_o|$. $^b wR2 = [\Sigma[w(F_o^2-F_c^2)^2] / \Sigma[w(F_o^2)^2]]^{1/2}$

Table 8.4. Crystal data and structure refinement parameters for $[Cp^{In}_3Dy(\mu\text{-}Cl)DyCp^{In}_3][Na(THF)_6]$, $[Cp^{In}_2Dy(\mu\text{-}Cl)_2K(Et_2O)]_\infty$, $[Cp^{In}Ho(THF)]_3(\mu\text{-}Cl)_3(\mu_3\text{-}Cl)(\mu_3\text{-}O)$, and $\{K(2.2.2\text{-cryptand})\}_2\{[(C_9H_7)_2Dy(\mu\text{-}\eta^5\text{:}\eta^1\text{-}C_9H_6)]_2\}$.

	$[Cp^{In}_3Dy(\mu\text{-}Cl)DyCp^{In}_3][Na(THF)_6]$	$[Cp^{In}_2Dy(\mu\text{-}Cl)_2K(Et_2O)]_\infty$	$[Cp^{In}Ho(THF)]_3(\mu\text{-}Cl)_3(\mu_3\text{-}Cl)(\mu_3\text{-}O)$	$\{K(2.2.2\text{-cryptand})\}_2\{[(C_9H_7)_2Dy(\mu\text{-}\eta^5\text{:}\eta^1\text{-}C_9H_6)]_2\}$
Empirical formula	$C_{78}H_{90}ClDy_2NaO_6$	$[C_{22}H_{24}OCl_2DyK\bullet \frac{1}{2}(C_4H_{10}O)]_\infty$	$C_{39}H_{45}Cl_4Ho_3O_4$	$C_{114}H_{160}Dy_2K_2N_4O_{18}$
Formula weight	1506.93	1227.94	1214.34	2277.65
Temperature (K)	128(2)	143(2)	93(2)	128(2)
Space group	$P\bar{1}$	$C2/c$	$Pnma$	$P\bar{1}$
a (Å)	15.2268(8)	30.005(3)	20.6636(9)	13.807(3)
b (Å)	16.2771(9)	7.8383(8)	18.7523(8)	13.959(3)
c (Å)	16.3982(9)	24.439(3)	10.3659(5)	15.063(3)
α (°)	99.3597(6)	90	90	108.975(2)
β (°)	109.9880(6)	118.9116(12)	90	92.819(2)
γ (°)	113.9656(6)	90	90	101.386(2)
Volume (Å^3)	3268.0(3)	5031.3(9)	4016.7(3)	2671.2(10)
Z	2	4	4	1
ρ_{calcd} (Mg/m^3)	1.531	1.621	2.008	1.416
μ (mm^{-1})	2.371	3.363	6.156	1.534
$R1^a$	0.0237	0.0259	0.0304	0.0728
$wR2^b$	0.0594	0.0586	0.0789	0.2018

$^a R1 = \Sigma||F_o|-|F_c|| / \Sigma|F_o|$. $^b wR2 = [\Sigma[w(F_o^2-F_c^2)^2] / \Sigma[w(F_o^2)^2]]^{1/2}$

References

(1) MacDonald, M. R.; Ziller, J. W.; Evans, W. J. *Journal of the American Chemical Society* **2011**, *133*, 15914.

(2) MacDonald, M. R.; Bates, J. E.; Fieser, M. E.; Ziller, J. W.; Furche, F.; Evans, W. J. *Journal of the American Chemical Society* **2012**, *134*, 8420.

(3) MacDonald, M. R.; Bates, J. E.; Ziller, J. W.; Furche, F.; Evans, W. J. *Journal of the American Chemical Society* **2013**, *135*, 9857.

(4) Hitchcock, P. B.; Lappert, M. F.; Maron, L.; Protchenko, A. V. *Angewandte Chemie International Edition* **2008**, *47*, 1488.

(5) MacDonald, M. R.; Fieser, M. E.; Bates, J. E.; Ziller, J. W.; Furche, F.; Evans, W. J. *Journal of the American Chemical Society* **2013**, *135*, 13310.

(6) Langeslay, R. R.; Fieser, M. E.; Ziller, J. W.; Furche, F.; Evans, W. J. *Chemical Science* **2015**, *6*, 517.

(7) Fieser, M. E.; MacDonald, M. R.; Krull, B. T.; Bates, J. E.; Ziller, J. W.; Furche, F.; Evans, W. J. *Journal of the American Chemical Society* **2014**, *137*, 369.

(8) Bursten, B. E.; Rhodes, L. F.; Strittmatter, R. J. *Journal of the American Chemical Society* **1989**, *111*, 2756.

(9) Bursten, B. E.; Rhodes, L. F.; Strittmatter, R. J. *Journal of the American Chemical Society* **1989**, *111*, 2758.

(10) Strittmatter, R. J.; Bursten, B. E. *Journal of the American Chemical Society* **1991**, *113*, 552.

(11) Lauher, J. W.; Hoffmann, R. *Journal of the American Chemical Society* **1976**, *98*, 1729.

(12) Lukens, W. W.; Andersen, R. A. *Organometallics* **1995**, *14*, 3435.

(13) Denning, R. G.; Harmer, J.; Green, J. C.; Irwin, M. *Journal of the American Chemical Society* **2011**, *133*, 20644.

(14) Morss, L. R. *Chemical Reviews* **1976**, *76*, 827.

(15) Mikheev, N. B.; Auerman, L. N.; Rumer, I. A.; Kamenskaya, A. N.; Kazakevich, M. Z. *Russian Chemical Reviews* **1992**, *61*, 990.

(16) Fang, M.; Lee, D. S.; Ziller, J. W.; Doedens, R. J.; Bates, J. E.; Furche, F.; Evans, W. J. *Journal of the American Chemical Society* **2011**, *133*, 3784.

(17) Jaroschik, F.; Momin, A.; Nief, F.; Le Goff, X.-F.; Deacon, G. B.; Junk, P. C. *Angewandte Chemie International Edition* **2009**, *48*, 1117.

(18) Fang, M.; Bates, J. E.; Lorenz, S. E.; Lee, D. S.; Rego, D. B.; Ziller, J. W.; Furche, F.; Evans, W. J. *Inorganic Chemistry* **2011**, *50*, 1459.

(19) Fang, M.; Farnaby, J. H.; Ziller, J. W.; Bates, J. E.; Furche, F.; Evans, W. J. *Journal of the American Chemical Society* **2012**, *134*, 6064.

(20) Niemeyer, M. *Inorganic Chemistry* **2006**, *45*, 9085.

(21) Korobkov, I.; Gambarotta, S. *Inorganic Chemistry* **2010**, *49*, 3409.

(22) Deacon, G. B.; Forsyth, C. M. *Chemical Communications* **2002**, 2522.

(23) Wang, J.; Gardiner, M. G. *Chemical Communications* **2005**, 1589.

(24) Deacon, G. B.; Forsyth, C. M.; Junk, P. C.; Wang, J. *Inorganic Chemistry* **2007**, *46*, 10022.

(25) Guan, J.; Shen, Q.; Fischer, R. D. *Journal of Organometallic Chemistry* **1997**, *549*, 203.

(26) Chen, M.; Wu, G.; Wu, W.; Zhuang, S.; Huang, Z. *Organometallics* **1988**, *7*, 802.

(27) Albrecht, I.; Hahn, E.; Pickardt, J.; Schumann, H. *Inorganica Chimica Acta* **1985**, *110*, 145.

(28) Junk, P. C.; Smith, M. K. *Applied Organometallic Chemistry* **2004**, *18*, 252.

(29) Rausch, M. D.; Moriarty, K. J.; Atwood, J. L.; Weeks, J. A.; Hunter, W. E.; Brittain, H. G. *Organometallics* **1986**, *5*, 1281.

(30) Jaroschik, F.; Nief, F.; Le Goff, X.-F.; Ricard, L. *Organometallics* **2007**, *26*, 1123.

(31) Evans, W. J.; Davis, B. L.; Champagne, T. M.; Ziller, J. W. *Proceedings of the National Academy of Sciences* **2006**, *103*, 12678.

(32) Meihaus, K. R.; Corbey, J. F.; Fang, M.; Ziller, J. W.; Long, J. R.; Evans, W. J. *Inorganic Chemistry* **2014**, *53*, 3099.

(33) Habib, A.; Tanke, R. S.; Holt, E. M.; Crabtree, R. H. *Organometallics* **1989**, *8*, 1225.

(34) O'Connor, J. M.; Casey, C. P. *Chemical Reviews* **1987**, *87*, 307.

(35) Takenaka, Y.; Hou, Z. *Organometallics* **2009**, *28*, 5196.

(36) Nishiura, M.; Baldamus, J.; Shima, T.; Mori, K.; Hou, Z. *Chemistry – A European Journal* **2011**, *17*, 5033.

(37) Xia, J.; Jin, Z.; Lin, G.; Chen, W. *Journal of Organometallic Chemistry* **1991**, *408*, 173.

(38) *For geometry **A**, the structure of the known unsolvated Cp^{In}_3Sm (Atwood, J. L.; Burns, J. H.; Laubereau, P. G. J. Am. Chem. Soc. 1973, 95, 1830) was used in which Sm was replace with Y or La. For geometry B, the structure of Cp^{In}_3LnTHF [Ln = Y, La[37]] was used with the THF removed from the structure.*

(39) Ballard, D. G. H.; Courtis, A.; Holton, J.; McMeeking, J.; Pearce, R. *Journal of the Chemical Society, Chemical Communications* **1978**, 994.

(40) Bercaw, J. E.; Marvich, R. H.; Bell, L. G.; Brintzinger, H. H. *Journal of the American Chemical Society* **1972**, *94*, 1219.

(41) Evans, W. J.; Miller, K. A.; DiPasquale, A. G.; Rheingold, A. L.; Stewart, T. J.; Bau, R. *Angewandte Chemie* **2008**, *120*, 5153.

(42) Siladke, N. A.; Webster, C. L.; Walensky, J. R.; Takase, M. K.; Ziller, J. W.; Grant, D. J.; Gagliardi, L.; Evans, W. J. *Organometallics* **2013**, *32*, 6522.

(43) Bergbreiter, D. E.; Killough, J. M. *Journal of the American Chemical Society* **1978**, *100*, 2126.

(44) Meyer, G.; Ax, P. *Materials Research Bulletin* **1982**, *17*, 1447.

(45) APEX2 Version 2013.10-1, Bruker AXS, Inc.; Madison, WI 2013.

(46) SAINT Version 8.34a, Bruker AXS, Inc.; Madison, WI 2013.

(47) Sheldrick, G. M. SADABS, Version 2014/4, Bruker AXS, Inc.; Madison, WI 2014.

(48) Sheldrick, G. M. SHELXTL, Version 2014/6, Bruker AXS, Inc.; Madison, WI 2014.

(49) International Tables for Crystallography 1992, Vol. C., Dordrecht: Kluwer Academic Publishers.

(50) Parsons, S., Flack, H. D., Wagner, T. Acta Cryst. B69, 249-259, 2013.

(51) Spek, A. L. PLATON, Acta. Cryst. 2009, D65, 148-155.

APPENDIX A

Results on Projects Beyond Those in the Chapters: Summaries and Structures

Synthesis of the $(N=N)^{2-}$ Complex $\{[(Me_3Si)_2N]_2(THF)Y\}_2(\mu\text{-}\eta^2\text{:}\eta^2\text{-}N_2)$ Using Lithium

As mentioned in the introduction and throughout this dissertation, it has been shown that potassium and sodium can be used in the LnA_3/M (Ln = Y, lanthanide; A = anionic ligand; M = KC_8, K, Na) reduction system to form rare earth reduced dinitrogen complexes such as $[A_2(THF)Ln]_2(\mu\text{-}\eta^2\text{:}\eta^2\text{-}N_2)$.[1-3] When A = $[N(SiMe_3)_2]^-$, not only does the $(N_2)^{2-}$ complex $[(Me_3Si)_2N]_2(THF)Ln\}_2(\mu\text{-}\eta^2\text{:}\eta^2\text{-}N_2)$ form, but other products including the cyclometallated species $\{[K(18\text{-crown-6})(THF)(toluene)]\}\{[(Me_3Si)_2N]_2Ln[CH_2Si(Me_2)NSiMe_3]\}\{[K(18\text{-crown-6})(THF)(toluene)]\}$,[4,5] the radical $(N_2)^{3-}$ complex $[K(THF)_6][\{[(Me_3Si)_2N]_2(THF)Ln\}_2(\mu_3\text{-}\eta^2\text{:}\eta^2\text{:}\eta^2\text{-}N_2)]$[6,7] and the $(N_2H_2)^{2-}$-containing complex $[(Me_3Si)_2N]_2(THF)Ln\}_2(\mu\text{-}N_2H_2)$[5] have also been known to form in the initial reaction mixture, Figure A.1. It was of interest to determine whether rare earth reduced dinitrogen species could also be synthesized using M = Li and if the enhanced reducing power of lithium might lead to fewer byproducts when A = $[N(SiMe_3)_2]^-$. This section discusses preliminary results exploring the reduction of $Y[N(SiMe_3)_2]_3$ with lithium in a nitrogen atmosphere. Yttrium was the rare earth of choice for this investigation, because, as mentioned in earlier chapters, its diamagnetic nature in the 3+ oxidation state and its nuclear spin of I = ½ are useful for spectroscopic characterization.

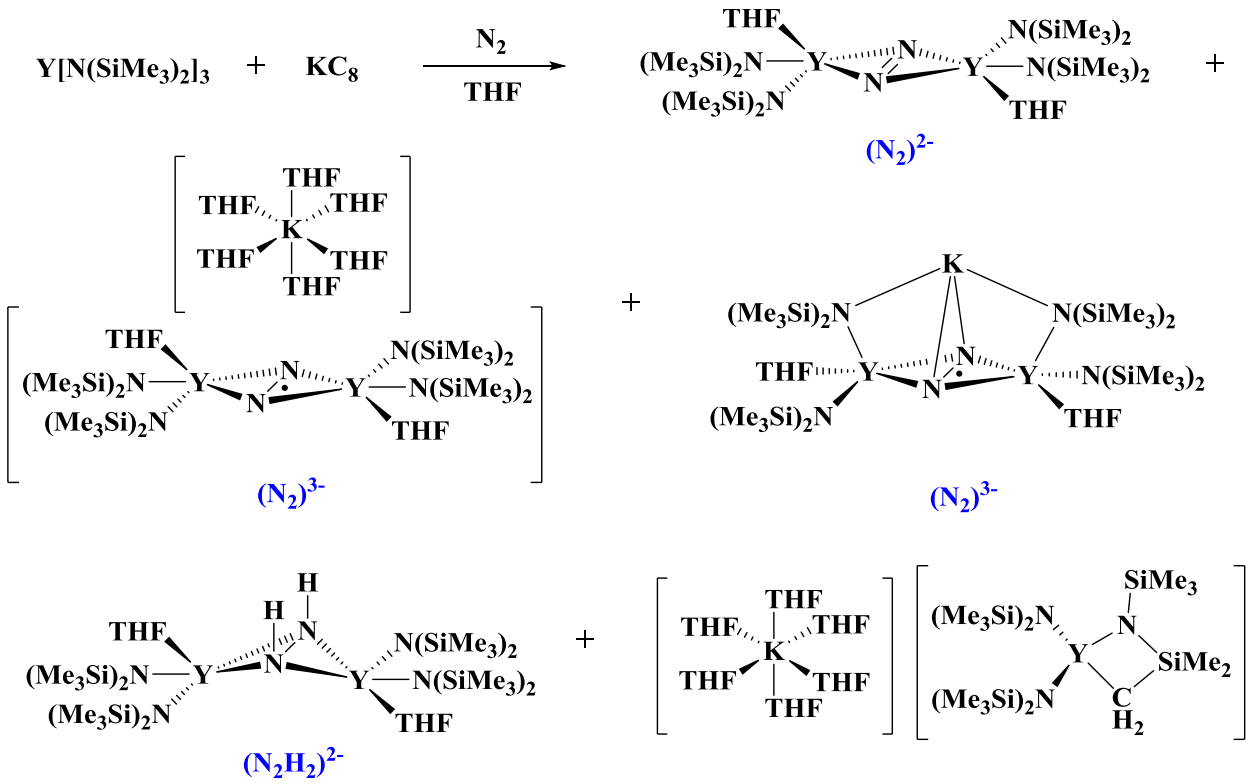

Figure A.1. Five of the crystallographically characterized products from the reaction of $Y[N(SiMe_3)_2]_3$ with KC_8, as mentioned in the text.

Addition of a colorless THF solution of $Y[N(SiMe_3)_2]_3$ to a vial containing lithium granules smeared along the vial walls results in a color change to dark amber consistent with the formation of the radical $(N_2)^{3-}$ complex $[K(THF)_6][\{[(Me_3Si)_2N]_2(THF)Y\}_2(\mu_3\text{-}\eta^2\text{:}\eta^2\text{:}\eta^2\text{-}N_2)]$,[6] one of the several products formed in the analogous reaction when M = KC_8. After stirring for 1 h, the crude reaction mixture was analyzed by NMR spectroscopy. Figure A.2 shows the ^1H NMR spectrum of the region where the $[N(SiMe_3)_2]^-$ ligand is expected to resonate. In addition to unreacted starting material, $Y[N(SiMe_3)_2]_3$, which is assigned to the peak at 0.306 ppm, the NMR spectrum shows that multiple products are generated in this initial reaction. Indeed, a small peak at 0.344 ppm, which can be assigned to the $(N_2)^{2-}$ complex

{[$(Me_3Si)_2N]_2$(THF)Y}$_2$(μ_3-η^2:η^2:η^2-N_2), is present in this spectrum suggesting dinitrogen reduction has occurred. However, peaks appear in this region at 0.376 and 0.484 ppm which do not match any of the above mentioned by products and are currently unassigned. The NMR spectrum for the crude reaction with Li (Figure A.2) can be compared to the analogous reaction with KC_8 (Figure A.3), in which a mixture of products is also observed. Peaks in Figure A.3 are assigned to the cyclometallated species {[$(Me_3Si)_2N]_2$Ln[$CH_2Si(Me_2)NSiMe_3$]}{[K(18-crown-6)(THF)(toluene)]}[4,5] (0.581 and 0.601 ppm), the $(N_2H_2)^{2-}$-containing complex [$(Me_3Si)_2N]_2$(THF)Ln}$_2$(μ-N_2H_2)[5] (0.394 ppm), {[$(Me_3Si)_2N]_2$(THF)Y}$_2$(μ_3-η^2:η^2:η^2-N_2) (0.341 ppm) and Y[$N(SiMe_3)_2]_3$ (0.304 ppm).

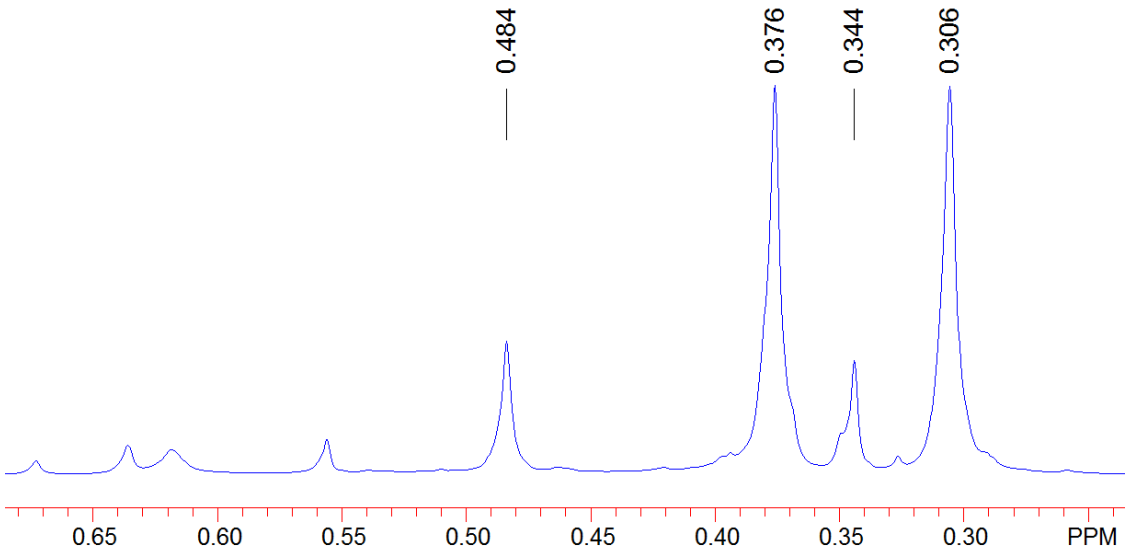

Figure A.2. ^{1}H NMR spectrum of the reaction of Y[$N(SiMe_3)_2]_3$ with Li for the region in which signals for the $[N(SiMe_3)_2]^-$ ligands would be expected.

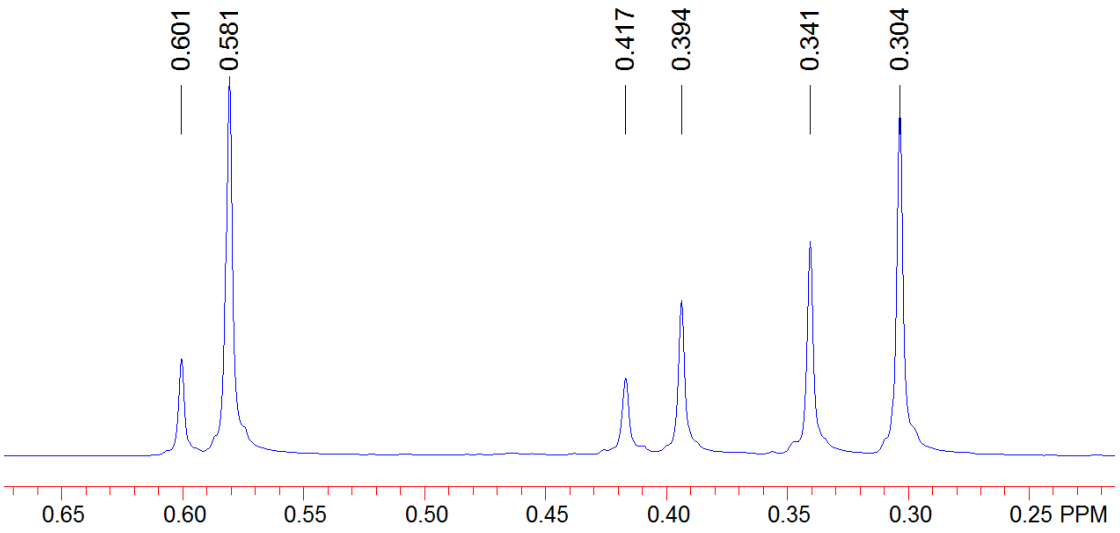

Figure A.3. ^{1}H NMR spectrum of the reaction of $Y[N(SiMe_3)_2]_3$ with KC_8 for the region in which signals for the $[N(SiMe_3)_2]^-$ ligands would be expected.

In one case, colorless crystals were obtained from the toluene extract of the amber reaction mixture resulting from addition of $Y[N(SiMe_3)_2]_3$ to Li metal and were identified by X-ray crystallography as the lithium "ate complex" $\{[(Me_3Si)_2N]_3Y\}(\mu\text{-Cl})[Li(THF)_3]$ shown in Figure A.4. The source of the chloride ion in $\{[(Me_3Si)_2N]_3Y\}(\mu\text{-Cl})[Li(THF)_3]$ is unclear, however, it is possible that residual KCl may not have been completely removed upon hexane extraction of $Y[N(SiMe_3)_2]_3$, which is made from YCl_3 and $K[N(SiMe_3)_2]$ in THF. This crystallographic result subsequently has led to alteration of the procedure for synthesizing $Y[N(SiMe_3)_2]_3$ which now includes hexane extraction and workup in a glovebox free from coordinating solvents, which are more likely to dissolve small amounts of water from the environment than noncoordinating solvents, potentially causing KCl to be sparingly soluble.[8,9] In conclusion, these NMR experiments indicate that like the K and Na reactions, the reaction of

$Y[N(SiMe_3)_2]_3$ with Li metal also forms the $(N_2)^{2-}$ species $\{[(Me_3Si)_2N]_2(THF)Y\}_2(\mu_3\text{-}\eta^2\text{:}\eta^2\text{:}\eta^2\text{-}N_2)$ along with other products.

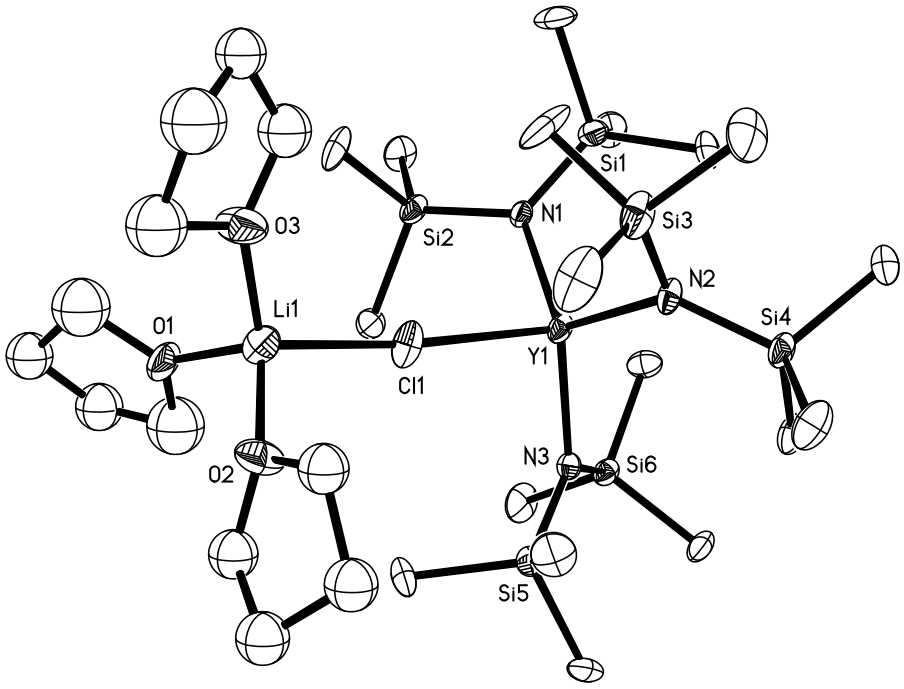

Figure A.4. Thermal ellipsoid plot of $\{[(Me_3Si)_2N]_3Y\}(\mu\text{-Cl})[Li(THF)_3]$ drawn at the 30% probability level. Hydrogen atoms and disorder in the THF ligands has been omitted for clarity.

Experimental. All syntheses and manipulations described below were conducted under nitrogen with rigorous exclusion of air and water using glovebox, Schlenk, and vacuum line techniques. Solvents used were dried over columns containing Q-5 and molecular sieves. Benzene-d_6 was dried over sodium-potassium alloy, degassed using three freeze-pump-thaw cycles, and vacuum transferred before use. Potassium and sodium were washed with hexanes and scraped to provide fresh surfaces before use. Lithium granules were purchased from Strem Chemicals. $Y[N(SiMe_3)_2]_3$ was synthesized according to literature methods.[10] ^1H and ^{13}C NMR

spectra were obtained on a Bruker CRYO500 MHz spectrometer at 25 ºC and referenced internally to residual protio solvent.

Synthesis of $\{[(Me_3Si)_2N]_2(THF)Y\}_2(\mu\text{-}\eta^2\text{:}\eta^2\text{-}N_2)$ Using Lithium. In a nitrogen filled glovebox, a colorless THF solution (1 mL) of $Y[N(SiMe_3)_2]_3$ (100 mg, 0.18 mmol) was added to a vial containing lithium granules (6 mg, 1 mmol) smeared on the vial walls. After stirring for about 5 min, the solution was dark amber. After stirring for 1 h, the solution was filtered and solvent was removed. The NMR spectrum in benzene-d_6 of the residual solid shows multiple peaks in the $[N(SiMe_3)_2]^-$ region including those assigned to unreacted $Y[N(SiMe_3)_2]_3$ starting material (0.306 ppm) and the known $(N_2)^{2-}$ complex $[(Me_3Si)_2N]_2(THF)Ln\}_2(\mu\text{-}\eta^2\text{:}\eta^2\text{-}N_2)$ (0.344 ppm). ^{1}H NMR (500 MHz, benzene-d_6): δ 0.306 (s, $Y[N(SiMe_3)_2]_3$), 0.344 (s, $[(Me_3Si)_2N]_2(THF)Ln\}_2(\mu\text{-}\eta^2\text{:}\eta^2\text{-}N_2)$), 0.376 (s), 0.484 (s), 1.353 (THF), 3.588 (THF). ^{13}C NMR (126 MHz, benzene-d_6): δ 4.85 (s, $Y[N(SiMe_3)_2]_3$), 5.83 (s, $[(Me_3Si)_2N]_2(THF)Ln\}_2(\mu\text{-}\eta^2\text{:}\eta^2\text{-}N_2)$), 5.97 (s), 6.49 (s). In one case, toluene extraction of the crude material afforded colorless crystals identified by X-ray crystallography as $\{[(Me_3Si)_2N]_3Y\}(\mu\text{-}Cl)[Li(THF)_3]$ (Figure A.4).

Inelastic Neutron Scattering (INS) on the Terbium $(N_2)^{3-}$ Single-Molecule Magnet, [K(18-crown-6)(THF)$_2$]{[(Me$_3$Si)$_2$N]$_2$(THF)Tb}$_2$(μ-η^2:η^2-N$_2$)

Inelastic neutron scattering (INS) is an experimental technique that has been used to interrogate magnetic properties, such as the magnetic ground state and spin excitations, in molecular magnets.[11] In collaboration with the group of Professor Oliver Waldmann of the University of Freiburg, preliminary INS measurements were obtained on the previously reported single-molecule magnet (SMM) [K(18-crown-6)(THF)$_2$]{[(Me$_3$Si)$_2$N]$_2$(THF)Tb}$_2$(μ-η^2:η^2-N$_2$),[7] containing an $(N_2)^{3-}$ radical bridge, as well as its $(N_2)^{2-}$ precursor {[(Me$_3$Si)$_2$N]$_2$(THF)Tb}$_2$(μ-η^2:η^2-N$_2$)[1] which is not an SMM. These data were collected at the ISIS Facility at the STFC Rutherford Appleton Laboratory in the United Kingdom. Figures A.5 and A.6 include measurements for the SMM [K(18-crown-6)(THF)$_2$]{[(Me$_3$Si)$_2$N]$_2$(THF)Tb}$_2$(μ-η^2:η^2-N$_2$) at various temperatures, and Figure A.7 shows comparative data for [K(18-crown-6)(THF)$_2$]{[(Me$_3$Si)$_2$N]$_2$(THF)Tb}$_2$(μ-η^2:η^2-N$_2$) and its $(N_2)^{2-}$ precursor {[(Me$_3$Si)$_2$N]$_2$(THF)Tb}$_2$(μ-η^2:η^2-N$_2$) collected at 2 K. Theoretical analysis remains to be done on these data.

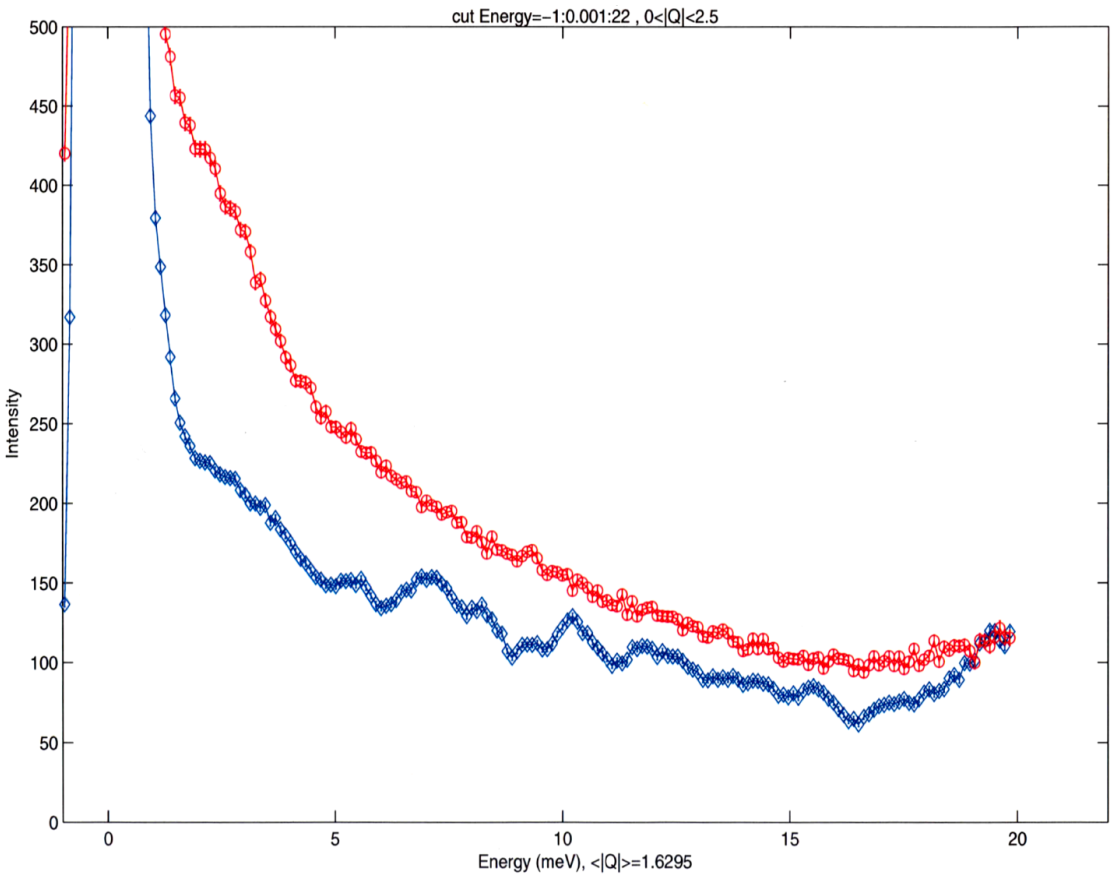

Figure A.5. INS intensity as a function of energy for [K(18-crown-6)(THF)$_2$]{[(Me$_3$Si)$_2$N]$_2$(THF)Tb}$_2$(μ-η^2:η^2-N$_2$) at 3 K (blue diamonds) and 125 K (red circles).

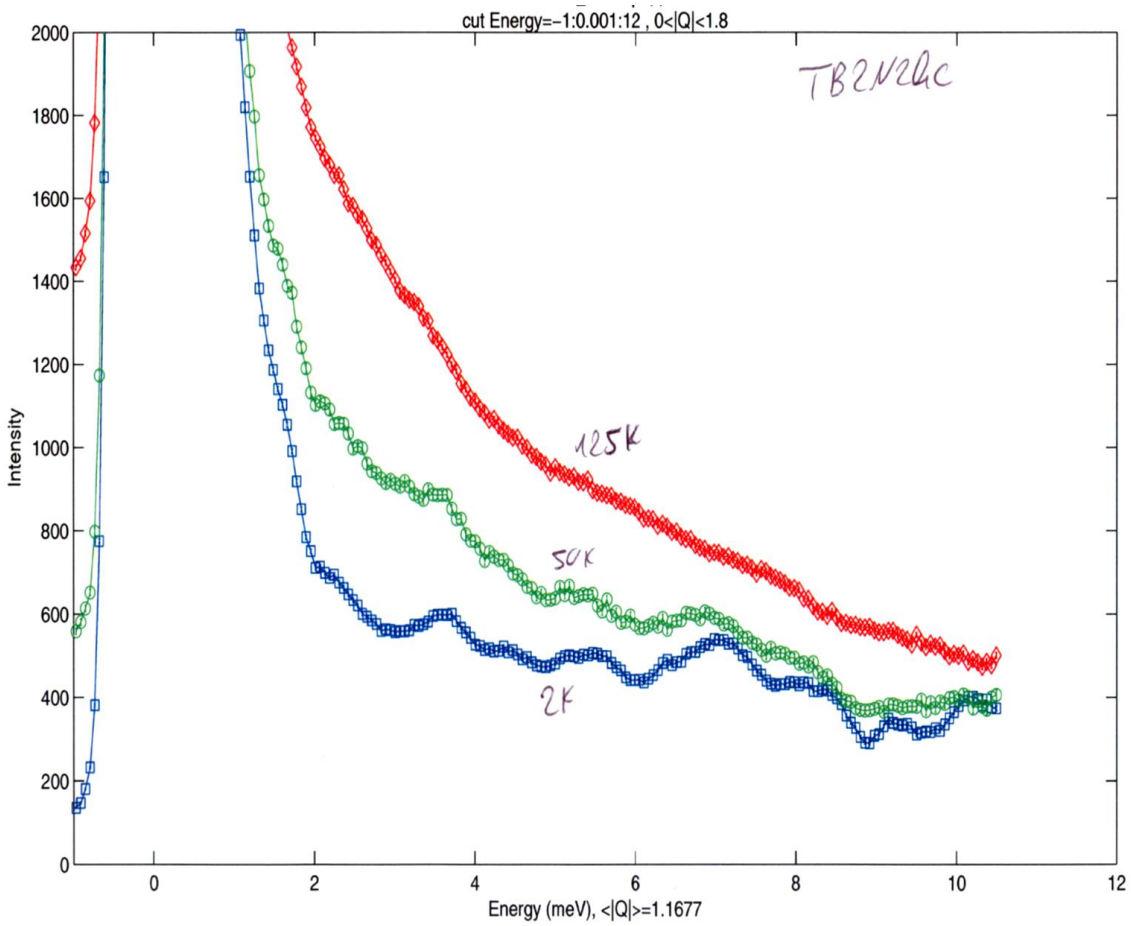

Figure A.6. A second plot of INS intensity as a function of energy measured for [K(18-crown-6)(THF)$_2$]{[(Me$_3$Si)$_2$N]$_2$(THF)Tb}$_2$(μ-η^2:η^2-N$_2$) this time at 2 K (blue squares), 50 K (green circles) and 125 K (red diamonds).

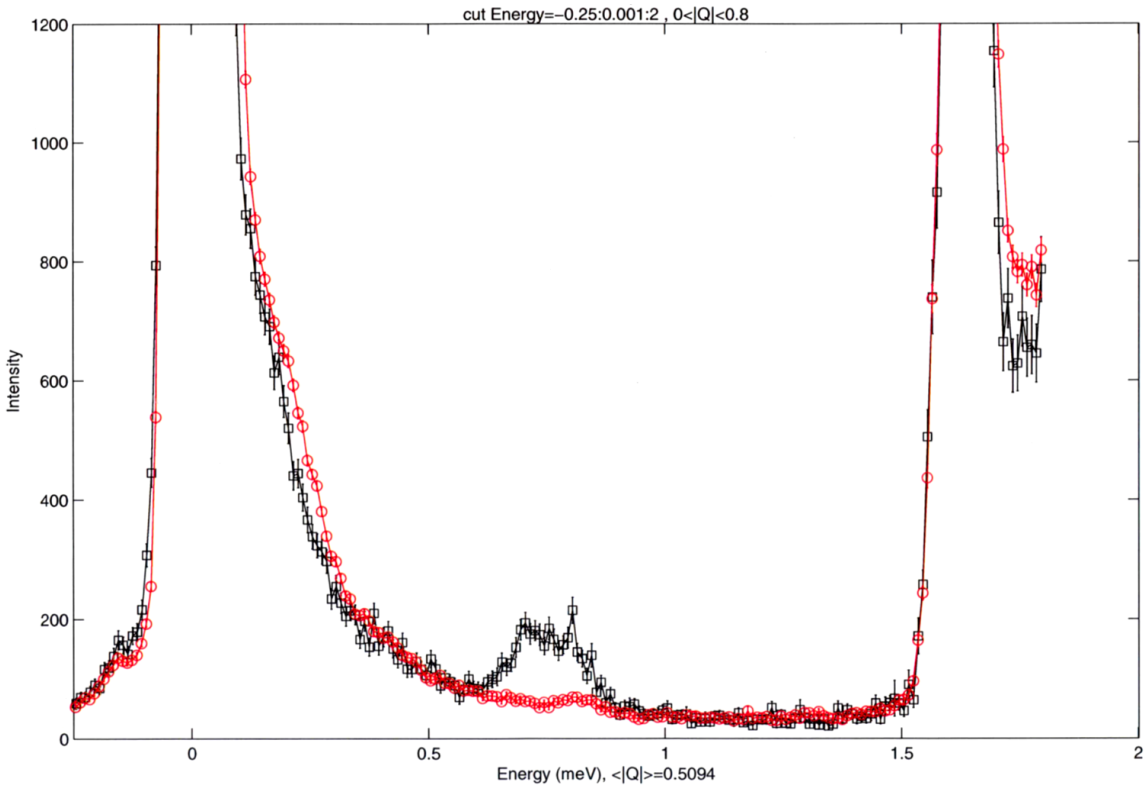

Figure A.7. INS intensity as a function of energy measured at 2 K comparing [K(18-crown-6)(THF)$_2$]{[(Me$_3$Si)$_2$N]$_2$(THF)Tb}$_2$(μ-η^2:η^2-N$_2$) (red circles) and {[(Me$_3$Si)$_2$N]$_2$(THF)Tb}$_2$(μ-η^2:η^2-N$_2$) (black squares). The rise of intensity above 1.5 meV is to be neglected.

Experimental. All syntheses and manipulations described below were conducted under nitrogen with rigorous exclusion of air and water using glovebox, Schlenk, and vacuum line techniques. Solvents used were dried over columns containing Q-5 and molecular sieves. [K(18-crown-6)(THF)$_2$]{[(Me$_3$Si)$_2$N]$_2$(THF)Tb}$_2$(μ-η^2:η^2-N$_2$)[7] and {[(Me$_3$Si)$_2$N]$_2$(THF)Tb}$_2$(μ-η^2:η^2-N$_2$)[1] were prepared according to the literature and submitted as crystalline samples.

Dinitrogen Reduction Reactions Using Aryloxide Ancillary Ligands Including Synthesis of a Dysprosium Hydroxide Trimer

Due to the exceptional SMM properties of the $(N_2)^{3-}$ amide-containing series of rare earth complexes [K(18-crown-6)(THF)$_2$]{[(Me$_3$Si)$_2$N]$_2$(THF)Ln}$_2$(μ-η^2:η^2-N$_2$) (Ln = Tb,[7] Dy[12]), it was of interest to analyze the magnetic properties of the previously reported aryloxide-containing $(N_2)^{3-}$ complex [K(THF)$_6$][Dy(OC$_6$H$_3$^{t}Bu$_2$-2,6)$_2$(THF)]$_2$(μ-η^2:η^2-N$_2$),[4,6]. Although many attempts were made to reproduce the synthesis of its $(N_2)^{2-}$ precursor [Dy(OC$_6$H$_3$^{t}Bu$_2$-2,6)$_2$(THF)]$_2$(μ-η^2:η^2-N$_2$)[4,6] by reduction of the monomeric species Dy(OC$_6$H$_3$^{t}Bu$_2$-2,6)$_3$ with KC$_8$,[4] in my hands, this complex could never be isolated in pure form. The only crystallographically characterizable product obtained was the trimeric hydroxide cluster, {K(THF)$_6$}$_2${[Dy(OC$_6$H$_3$^{t}Bu$_2$-2,6)$_2$(THF)]$_3$(μ_2-OH)$_3$(μ_3-OH)$_2$}, shown in Figure A.8.

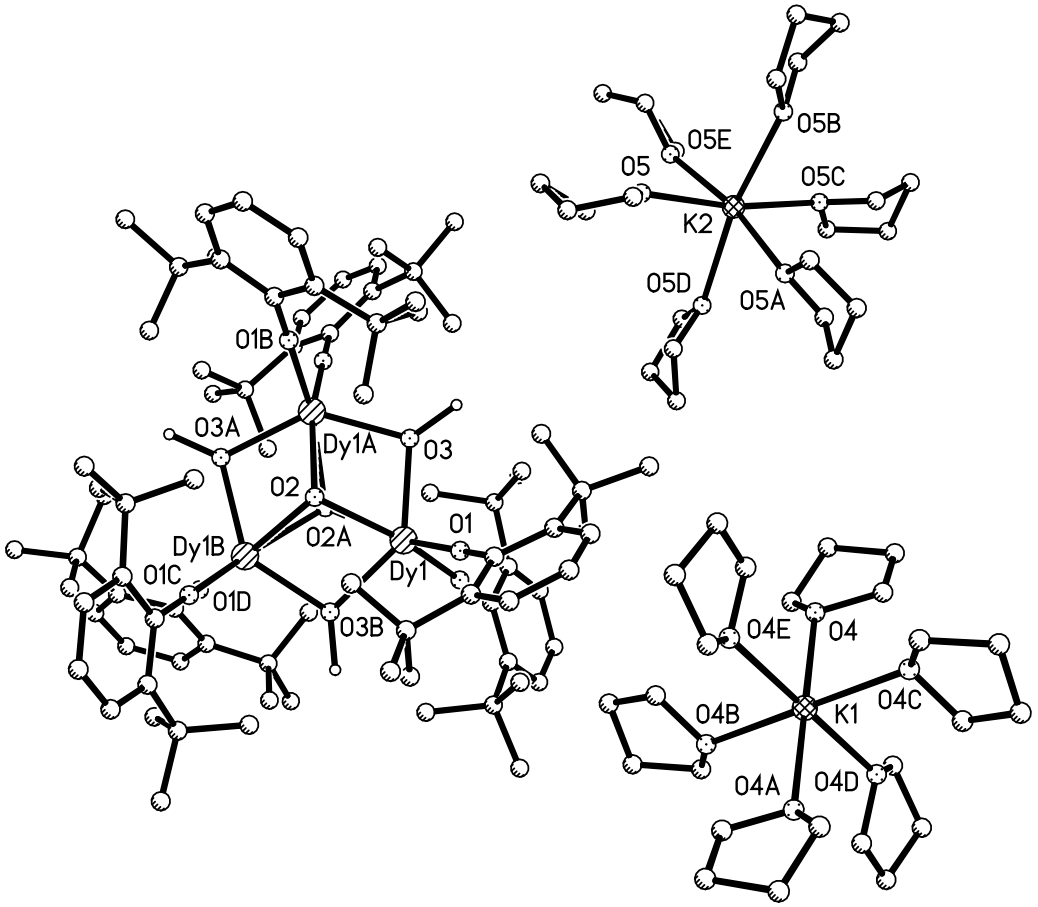

Figure A.8. Crystal structure of $\{K(THF)_6\}_2\{[Dy(OC_6H_3{}^tBu_2\text{-}2,6)_2(THF)]_3(\mu_2\text{-}OH)_3(\mu_3\text{-}OH)_2\}$ isolated from a single reaction of $Dy(OC_6H_3{}^tBu_2\text{-}2,6)_3$ with KC_8. All hydrogen atoms, except those of the hydroxyl groups, have been omitted for clarity. Disorder in the THF ligands has also been omitted. The hydrogen atoms on the (μ_3-OH) groups could not be located.

This inability to isolate the desired $(N_2)^{2-}$ complex $[Dy(OC_6H_3{}^tBu_2\text{-}2,6)_2(THF)Dy]_2(\mu\text{-}\eta^2\text{:}\eta^2\text{-}N_2)$ may have been due to impurities in the tris(aryloxide) starting material $Dy(OC_6H_3{}^tBu_2\text{-}2,6)_3$ which was synthesized via two routes, eq A.1 and A.2.[10] In most cases, the tris($OC_6H_3{}^tBu_2$-2,6) compound was isolated as a tacky solid and could not be crystallized. In some cases, NMR spectra of the Y reaction analogous to that of eq A.2 revealed incomplete

substitution of the $[N(Me_3Si)_2]^{1-}$ ligands, to generate heteroleptic complexes. Attempts were also made to substitute the $[N(Me_3Si)_2]^{1-}$ ligands in the $(N_2)^{2-}$ species $\{[(Me_3Si)_2N]_2(THF)Ln\}_2(\mu\text{-}\eta^2\text{:}\eta^2\text{-}N_2)$ (Ln = Y,[2] Dy,[1]) with $(OC_6H_3{}^tBu_2\text{-}2,6)^{1-}$ by addition of $HOC_6H_3{}^tBu_2$-2,6. In some case, NMR peaks consistent with the expected product could be observed for reactions with Y; however, crystals were never obtained.

$$\mathbf{DyCl_3 + 3\ Na(O\text{-}2,6\text{-}{}^tBuC_6H_3) \longrightarrow Dy(O\text{-}2,6\text{-}{}^tBuC_6H_3)_3} \qquad \mathbf{A.1}$$

$$\mathbf{Dy[N(SiMe_3)_2]_3 + 3\ 2,6\text{-}{}^tBuC_6H_3OH \longrightarrow Dy(O\text{-}2,6\text{-}{}^tBuC_6H_3)_3} \qquad \mathbf{A.2}$$

An Anionic Terbium Tetrakis(Amide) Complex, $\{Na(THF)_6\}\{Tb[N(SiMe_3)_2]_4\}$

It is known that addition of strong reducing agents such as KC_8 to the tris(amide) complexes $Ln[N(SiMe_3)_2]_3$ yields a mixture of products, among which are the $K\{[(Me_3Si)_2N]_2(THF)Ln\}_2(\mu_3\text{-}\eta^2\text{:}\eta^2\text{:}\eta^2\text{-}N_2)$,[4,6] $\{[(Me_3Si)_2N]_2(THF)Ln\}_2(\mu\text{-}\eta^2\text{:}\eta^2\text{-}N_2)$,[1,2] $\{[K(18\text{-crown-6})(THF)(toluene)]\}\{[(Me_3Si)_2N]_2Ln[CH_2Si(Me_2)NSiMe_3]\}$,[4,5] and $[(Me_3Si)_2N]_2(THF)Ln\}_2(\mu\text{-}N_2H_2)$[5] species (Figure A.1). The tetrakis(amide) complexes $\{K(THF)_6\}\{Ln[N(SiMe_3)_2]_4\}$ have also been identified for Ln = La and Pr from these reaction mixtures.[1] In an attempt to reproduce the LnA_3/M chemistry using M = Na in place of M = KC_8,[1] colorless crystals of $\{Na(THF)_6\}\{Tb[N(SiMe_3)_2]_4\}$, Figure A.9, were isolated. Although this complex has a much smaller rare earth metal than the La and Pr complexes,$\{K(THF)_6\}\{Ln[N(SiMe_3)_2]_4\}$, and a different alkali metal, it is isomorphous with the previously reported analogs, as shown in Table A.1.

Table A.1. Preliminary unit cell parameters for $\{Na(THF)_6\}\{Tb[N(SiMe_3)_2]_4\}$ as compared with the previously reported complexes $\{K(THF)_6\}\{Ln[N(SiMe_3)_2]_4\}$ (Ln = La, Pr).[1]

	$\{K(THF)_6\}$ $\{La[N(SiMe_3)_2]_4\}$	$\{K(THF)_6\}$ $\{Pr[N(SiMe_3)_2]_4\}$	$\{Na(THF)_6\}$ $\{Tb[N(SiMe_3)_2]_4\}$
Space Group	*C*2/*c*	*C*2/*c*	*C*2/*c*
a (Å)	26.623(3)	26.627(3)	26.724
b (Å)	30.624(3)	30.590(3)	30.807
c (Å)	17.357(2)	17.345(2)	17.335
α (deg)	90	90	90
β (deg)	91.339(2)	91.169(2)	90.996
γ (deg)	90	90	90

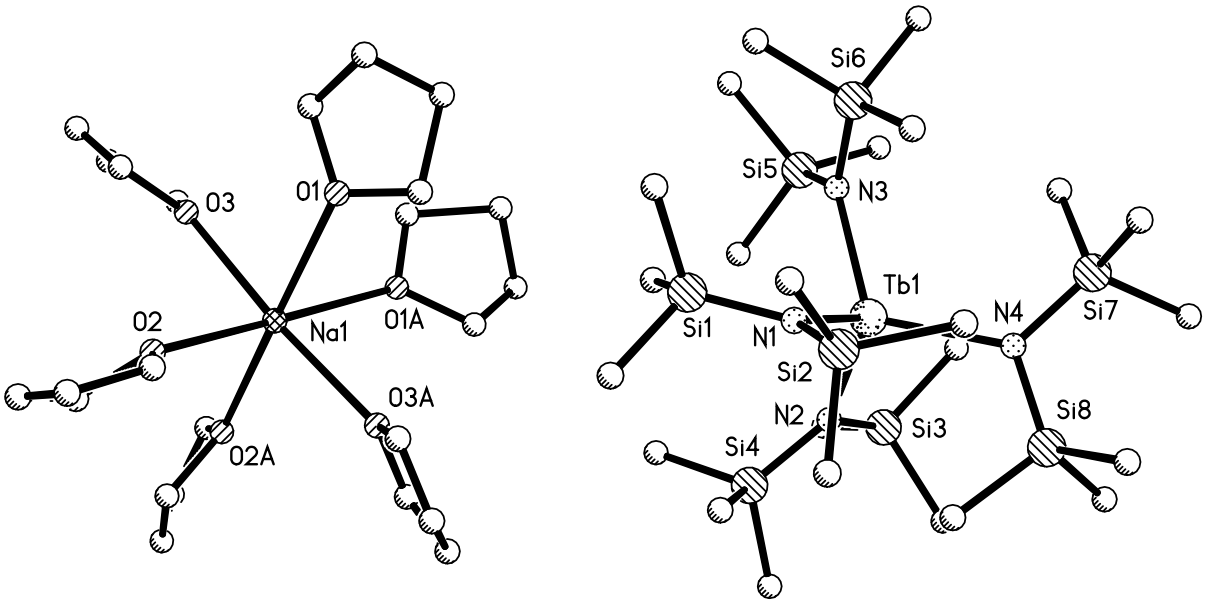

Figure A.9. Crystal structure of $\{Na(THF)_6\}\{Tb[N(SiMe_3)_2]_4\}$. Hydrogen atoms have been omitted for clarity.

Experimental. All syntheses and manipulations described below were conducted under nitrogen with rigorous exclusion of air and water using glovebox, Schlenk, and vacuum line techniques. Solvents used were dried over columns containing Q-5 and molecular sieves. Sodium was washed with hexanes and scraped to provide fresh surfaces before use. $Tb[N(SiMe_3)_2]_3$ was synthesized according to literature methods.[10] $\{Na(THF)_6\}\{Tb[N(Me_3Si)_2]_4\}$ was synthesized analogously to $\{K(THF)_6\}\{Ln[N(Me_3Si)_2]_4\}$ (Ln = La, Pr).[1]

Cryptand Analogs of Single-Molecule Magnets: [K(2.2.2.-cryptand)]-{[$(Me_3Si)_2N]_2(THF)Ln\}_2(\mu$-$\eta^2$:$\eta^2$-$N_2$)

In the course of studying the $(N_2)^{3-}$ complexes $K\{[(Me_3Si)_2N]_2(THF)Ln\}_2(\mu_3$-$\eta^2$:$\eta^2$:$\eta^2$-$N_2$), **A**, [1,6,13] $[K(THF)_6]\{[(Me_3Si)_2N]_2(THF)Ln\}_2(\mu$-$\eta^2$:$\eta^2$-$N_2$), **B**,[6] and [K(18-crown-6)$(THF)_2$]$\{[(Me_3Si)_2N]_2(THF)Ln\}_2(\mu$-$\eta^2$:$\eta^2$-$N_2$), **C**,[4,7,12] (Ln = Y, Gd, Tb, Dy), Figure A.10, for their utility to better understand the properties of radical-bridged SMMs, it was observed that the inner-sphere K^+ analog **A** displays faster magnetic relaxation than the outer-sphere K^+ 18-crown-6 ligated analog **C**[13] when Ln = Tb or Dy, as described in Chapter 2 of this dissertation. This suggested that the proximity of the counter cation plays a significant role in the type of magnetic coupling present in the $(N_2)^{3-}$ systems. It was of interest to determine if a more thorough encapsulation of the K^+ ion might enhance the SMM properties of the Ln_2N_2 core. For this purpose, a new series of $(N_2)^{3-}$ complexes has been synthesized, namely [K(2.2.2-cryptand)]$\{[(Me_3Si)_2N]_2(THF)Ln\}_2(\mu$-$\eta^2$:$\eta^2$-$N_2$)}, **D**, (Ln = Y, Gd, Tb, Dy), Figures A.10 and A.11.

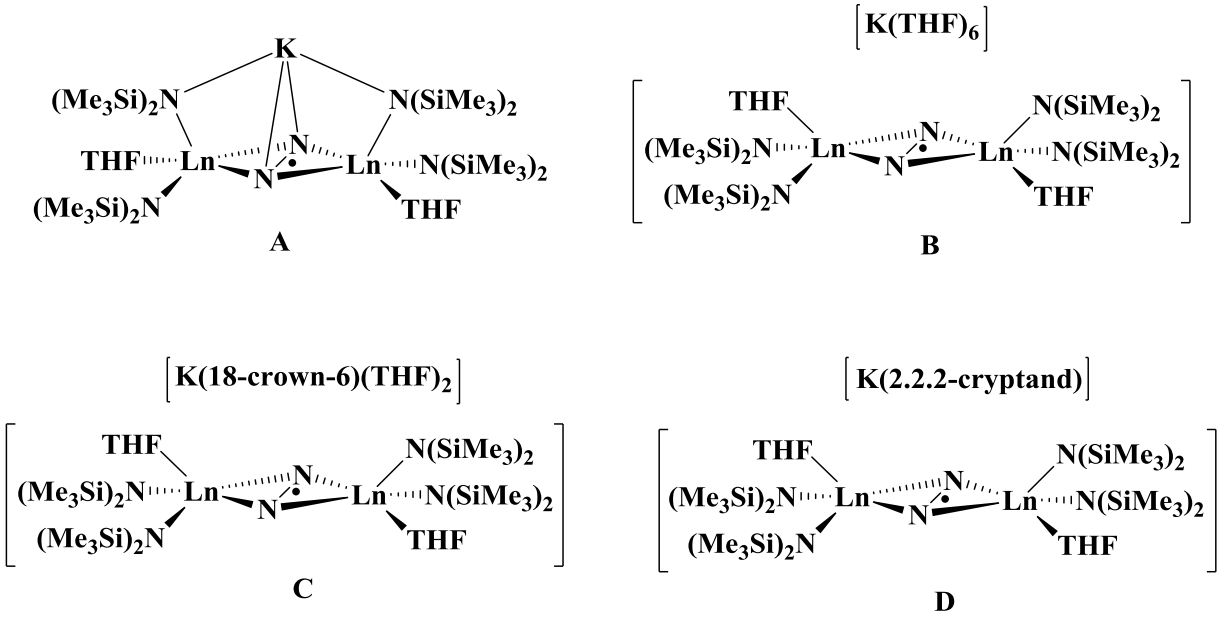

Figure A.10. The four crystallographically characterized variations of the $(N_2)^{3-}$ rare earth series using the $[N(SiMe_3)_2]^{1-}$ ligand set with increasing degree of cation/anion separation from **A** to **D**.

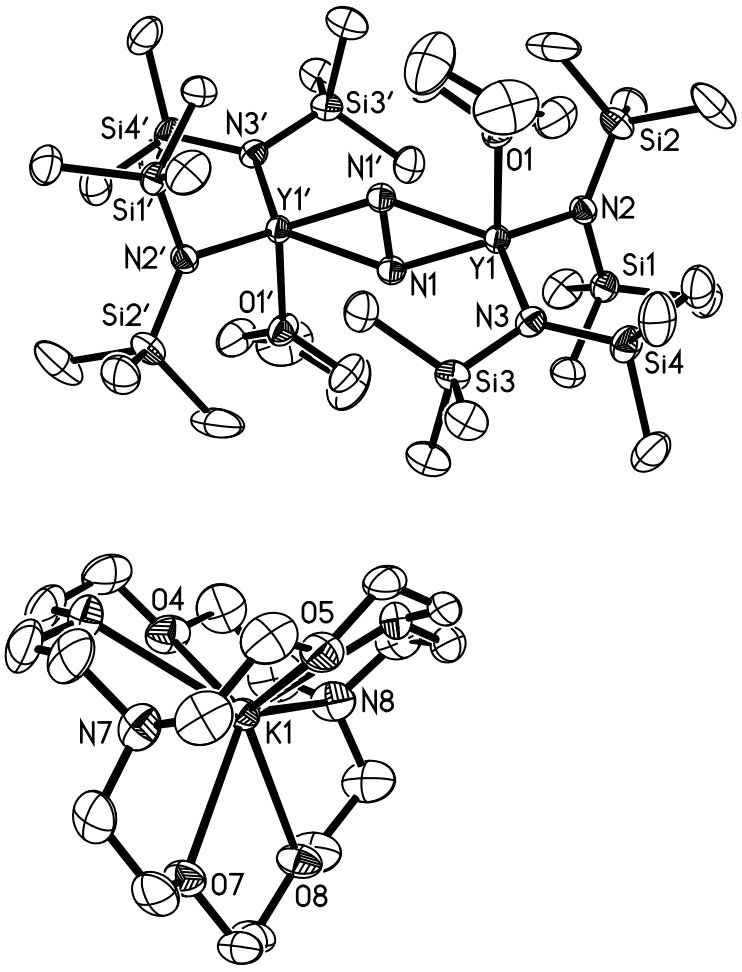

Figure A.11. Thermal ellipsoid plot of [K(2.2.2-cryptand)]{[$(Me_3Si)_2N]_2$(THF)Y}$_2$(μ-η^2:η^2-N_2), **D**-**Y**, drawn at the 50% probability level. Hydrogen atoms have been omitted for clarity. The Gd and Dy analogs are isomorphous.

The Y, Gd, Dy, and Tb analogs of **D** all crystallize in the triclinic space group $P\bar{1}$. However, two different unit cells have been obtained for the Y analog, **D**-**Y**, depending on the crystalline batch. One is isomorphous with the Dy and Gd analogs and contains two half dimer units along with one full occupancy [K(2.2.2-cryptand)] moiety per asymmetric unit (see Appendix B). The second cell is isomorphous with the Tb analog in which the asymmetric unit

appears to consists only of one half dimer and one half occupancy [K(2.2.2-cryptand)] moiety. Generally, the cell consistent with the Tb analog seems to indicate disorder in the 2.2.2-cryptand ligand which is not prevalent in the refined solutions for the Gd, Dy and Y analogs which possess a different unit cell. Magnetic measurements have not yet been performed on these complexes.

Experimental. All syntheses and manipulations described below were conducted under nitrogen with rigorous exclusion of air and water using glovebox, Schlenk, and high-vacuum line techniques. Solvents were sparged with UHP argon and dried over columns containing Q-5 and molecular sieves. Potassium was washed with hexane and scraped to provide fresh surfaces before use. The compounds $\{[(Me_3Si)_2N]_2(THF)Ln\}_2(\mu\text{-}\eta^2\text{:}\eta^2\text{-}N_2)$ (Ln = Y, Tb, Dy, Gd) were synthesized according to the literature method for the yttrium analog.[4] KC_8 was prepared according to the literature procedure.[14] $Nd_2Fe_{13}B$ magnets used in the crystallizations were obtained from United Nuclear Scientific Equipment and Supplies. EPR spectra were collected using a Bruker EMX spectrometer equipped with an ER041XG microwave bridge.

[K(2.2.2-cryptand)]{[(Me$_3$Si)$_2$N]$_2$(THF)Y}$_2$(μ-η^2:η^2-N$_2$), D-Y. Following a previously reported procedure for the 18-crown-6 analog,[4] in a nitrogen filled glovebox, $\{[(Me_3Si)_2N]_2(THF)Y\}_2(\mu\text{-}\eta^2\text{:}\eta^2\text{-}N_2)$ (100 mg, 0.1 mmol) and 2.2.2-cryptand (40 mg, 0.1 mmol) were dissolved in THF (10 mL) to make a pale blue solution. While stirring, KC_8 (14 mg, 0.1 mmol) was added and the solution immediately became orange with black solids. After 5 min, the reaction mixture was filtered and solvent was removed from the dark orange filtrate via reduced pressure to yield [K(2.2.2-cryptand)]$\{[(Me_3Si)_2N]_2(THF)Y\}_2(\mu\text{-}\eta^2\text{:}\eta^2\text{-}N_2)$, **D-Y**, as a red-orange solid. Orange X-ray quality crystals were grown from concentrated Et_2O solutions. EPR

spectra of the orange crystals show the same 11 peak pattern that was reported for the other outer-sphere K^+ analogs, complexes **B-Y** and **C-Y**.[6]

[K(2.2.2-cryptand)]{[(Me$_3$Si)$_2$N]$_2$(THF)Tb}$_2$(μ-η^2:η^2-N$_2$), D-Tb. Following the procedure for the Y analog above, orange X-ray quality crystals of [K(2.2.2-cryptand)]{[(Me$_3$Si)$_2$N]$_2$(THF)Tb}$_2$(μ-η^2:η^2-N$_2$), **D-Tb**, were grown from concentrated Et$_2$O solutions in the presence of an external magnetic field.

[K(2.2.2-cryptand)]{[(Me$_3$Si)$_2$N]$_2$(THF)Dy}$_2$(μ-η^2:η^2-N$_2$), D-Dy. Following the procedure for the Y analog above, dark orange X-ray quality crystals of [K(2.2.2-cryptand)]{[(Me$_3$Si)$_2$N]$_2$(THF)Dy}$_2$(μ-η^2:η^2-N$_2$), **D-Dy**, were grown from concentrated Et$_2$O solutions in the presence of an external magnetic field.

[K(2.2.2-cryptand)]{[(Me$_3$Si)$_2$N]$_2$(THF)Gd}$_2$(μ-η^2:η^2-N$_2$), D-Gd. Following the procedure for the Y analog above, dark orange X-ray quality crystals of [K(2.2.2-cryptand)]{[(Me$_3$Si)$_2$N]$_2$(THF)Gd}$_2$(μ-η^2:η^2-N$_2$), **D-Gd**, could be grown from concentrated Et$_2$O solutions.

An Anthracenide Dianion-Containing Complex, {K(2.2.2.-cryptand)}{[$C_5H_3(Me_3Si)_2]_2Gd(C_{14}H_{10})$}

Aromatic substrates such as anthracene ($C_{14}H_{10}$), naphthalene ($C_{10}H_8$), and benzene (C_6H_6) are interesting prospects as radical bridges between rare earth metal centers for SMM studies. In Chapter 6 of this dissertation, radical phenazine-bridged complexes where shown to display SMM properties, and other aromatic substrates have also been employed as radical bridging units in SMMs.[15,16] Lappert and coworkers have reported a crystallographically characterized radical bridging benzene complex with lanthanum, namely [K(18-crown-6)(η^2-$C_6H_6)_2$][$(LaCp^{tt}_2)_2$-(μ-η^6:η^6-C_6H_6)],[17] synthesized by addition of 1.5 equiv of potassium and 18-crown-6 to 1 equiv of the tris(cyclopentadienyl) precursor $La(Cp^{tt})_3$ where $Cp^{tt} = C_5H_3(^tBu)_2$. This result prompted the exploration of analogous reactions with aromatic substrates including benzene, using derivatized tris(cyclopentadienyl) precursors containing paramagnetic lanthanides such as Gd, Dy, and Tb, which have demonstrated optimal properties as choice metals in rare earth SMMs.[7,12,18] One of these reactions, shown in eq A.3, involved addition of KC_8 and 2.2.2-cryptand to the bis(trimethylsilyl)-substituted cyclopentadienyl complex $Gd[C_5H_3(SiMe_3)_2]_3$ in the presence of anthracene. This led to isolation of black crystals that were identified by X-ray crystallography as {K(2.2.2.-cryptand)}{$[C_5H_3(Me_3Si)_2]_2Gd(C_{14}H_{10})$}, Figure A.12, which contains a dianionic anthracenide ligand. This complex is similar to other cyclopentadienyl rare earth species in the literature containing doubly reduced aromatic substrates such as {K(18-crown-6)}{$[C_5H_3(SiMe_3)_2]_2La(C_6H_6)$},[17] {K(2.2.2-cryptand)}{$[C_5H_4(SiMe_3)]_2Y(C_{10}H_8)$},[19] and {K(2.2.2-cryptand)}{$[C_5H_4(SiMe_3)]_2Y(C_6H_5Ph)$}.[19]

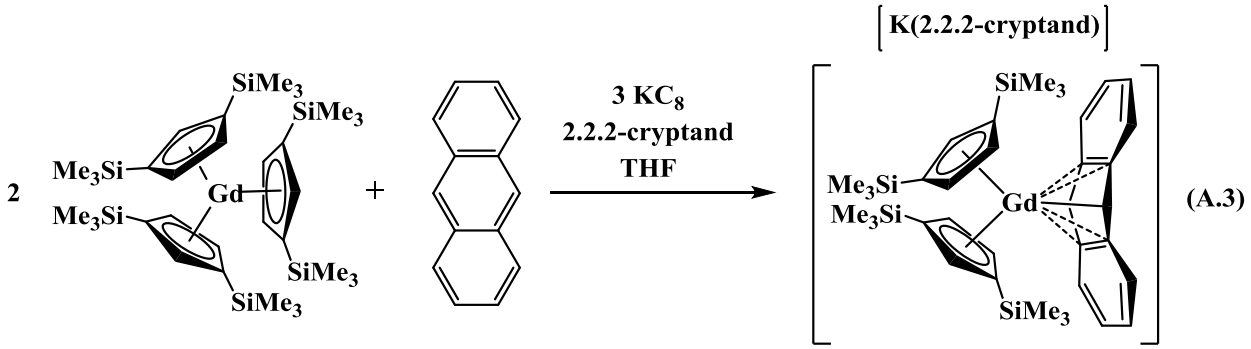

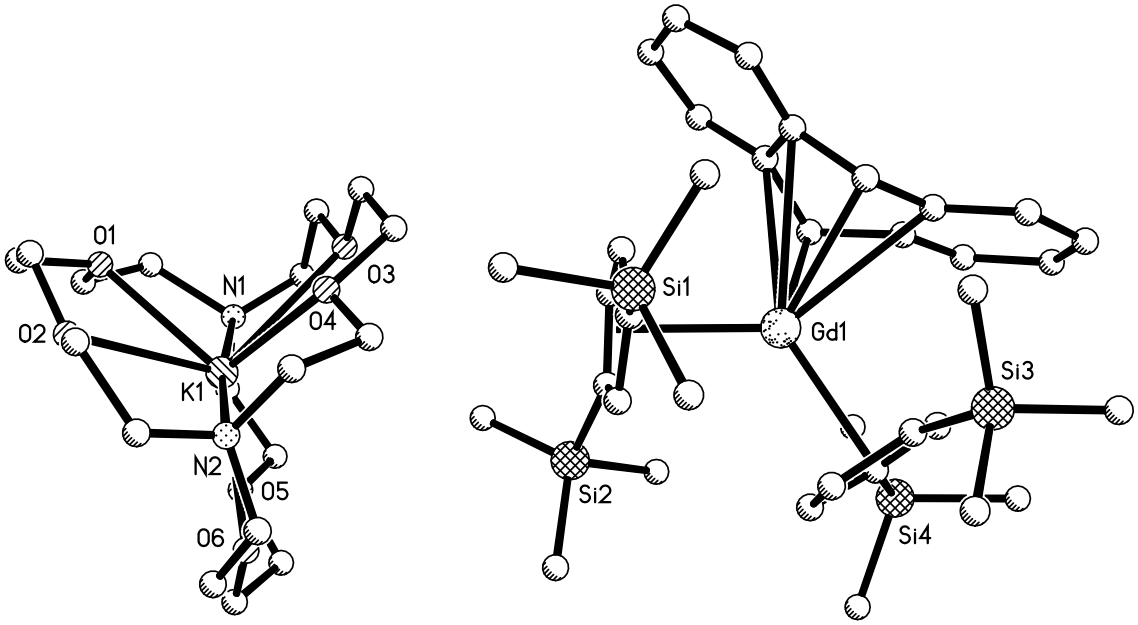

Figure A.12. Crystal structure of {K(2.2.2.-cryptand)}{[$C_5H_3(SiMe_3)_2$]$_2$Gd($C_{14}H_{10}$)}. Hydrogen atoms have been omitted for clarity.

Experimental. All syntheses and manipulations described below were conducted under nitrogen or argon with rigorous exclusion of air and water using glovebox, Schlenk, and high-vacuum line techniques. Solvents were sparged with UHP argon and dried over columns

containing Q-5 and molecular sieves. Potassium was washed with hexane and scraped to provide fresh surfaces before use. $Gd[C_5H_3(SiMe_3)_2]_3$[20] and KC_8[14] were prepared according to the literature procedures. Anthracene and 2.2.2-cryptand (4,7,13,16,21,24-hexaoxa-1,10-diazabicyclo[8.8.8]hexacosane) were purchased from Aldrich.

{K(2.2.2.-cryptand)}{[$C_5H_3(Me_3Si)_2]_2Gd(C_{14}H_{10})$}. In a nitrogen filled glovebox, a yellow THF solution (5 mL) of $[C_5H_3(SiMe_3)_2]_3Gd$ (48 mg, 0.06 mmol) was added to a colorless THF solution (3 mL) containing anthracene (5 mg, 0.03 mmol) and 2.2.2-cryptand (12 mg, 0.03 mmol). While stirring, KC_8 (12 mg, 0.09 mmol) was added, and the dark suspension was left to stir for 40 min. Black solids were removed via filtration and solvent was removed from the black filtrate to yield a tacky black solid which was dissolved in 5 mL of Et_2O and stored at –35°. After 2 d, black X-ray quality crystals of {K(2.2.2.-cryptand)}{$[C_5H_3(Me_3Si)_2]_2Gd(C_{14}H_{10})$} were obtained.

Isolation of the Cryptand Analog of the Dy^{3+} "Ate" Complex $(C_5Me_5)_2DyCl_2K(THF)_2$

With the discovery that yttrium,[21] all the lanthanides,[22-24] uranium,[25] and thorium[26] can access the +2 oxidation state as $[Cp_3^xM]^-$ complexes, as discussed in Chapter 8 of this dissertation, it was of interest to determine if other trivalent lanthanides species could be reduced to form divalent ions. In the course of these exploratory studies, the reduction of the "ate-type" complex $(C_5Me_5)_2DyCl_2K(THF)_2$ was attempted in the presence of 2.2.2-cryptand and KC_8, eq A.4, which afforded crystals of the outer sphere $[K(cryptand)]^+$ analog, $[K(cryptand)][(C_5Me_5)_2DyCl_2]$, Figure A.13. Similar $Cp^R{}_2LnX_2K$ complexes, such as $(Cp^{ttt})_2Dy(\mu\text{-}Cl_2)K(18\text{-crown-6})$, have been reported by Nief and coworkers as products of reactions involving Ln^{2+}-containing species.[27] Additionally, the Dy^{2+} "ate" complexes $(Cp^{ttt})_2Dy(\mu\text{-}X)K(18\text{-crown-6})$ (X = BH_4, Br, I) could be synthesized via KC_8 reduction of the trivalent precursors $(Cp^{ttt})_2DyX$.[28] However, further reduction attempts on isolated crystals of $[K(cryptand)][(C_5Me_5)_2DyCl_2]$ did not result in formation of observable Ln^{2+} species. $[K(cryptand)][(C_5Me_5)_2DyCl_2]$ is an unusual type of $Cp^R{}_2LnX_2K$ complex in that the chloride ligands are terminal. In most complexes of this type, at least one X ligand bridges to the potassium.

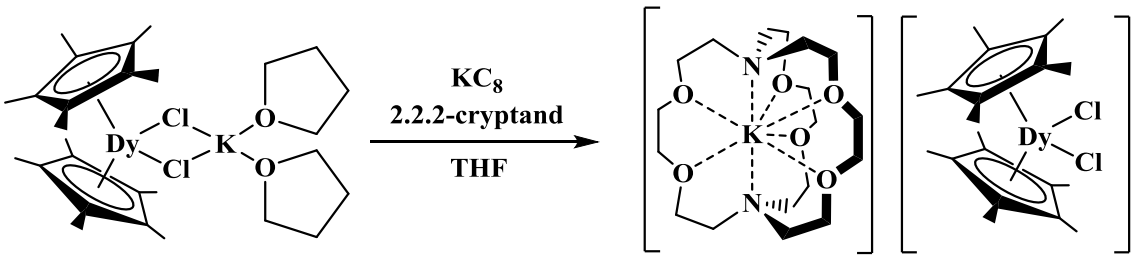

(A.4)

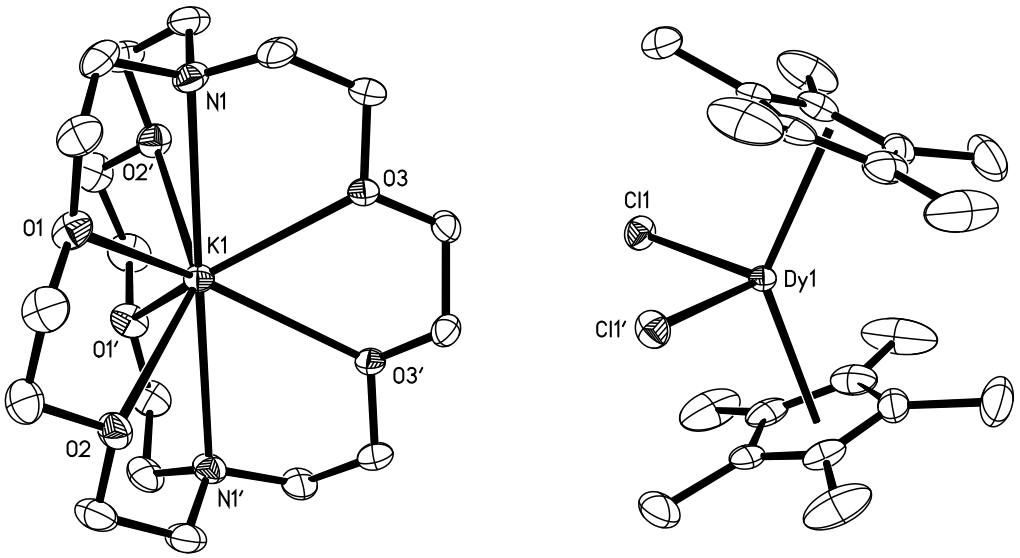

Figure A.13. Thermal ellipsoid plot of [K(cryptand)][$(C_5Me_5)_2DyCl_2$] drawn at the 50% probability level. Hydrogen atoms have been omitted for clarity.

Experimental. All syntheses and manipulations described below were conducted under nitrogen with rigorous exclusion of air and water using glovebox, Schlenk, and high-vacuum line techniques. Solvents were sparged with UHP argon and dried over columns containing Q-5 and molecular sieves. Potassium was washed with hexane and scraped to provide fresh surfaces before use. $(C_5Me_5)_2DyCl_2K(THF)_2$[29,30] and KC_8[14] were prepared according to the literature procedures. $Nd_2Fe_{13}B$ magnets used in the crystallizations were obtained from United Nuclear Scientific Equipment and Supplies.

[K(cryptand)][$(C_5Me_5)_2DyCl_2$]. In a nitrogen filled glovebox, 2.2.2-cryptand (30 mg, 0.08 mmol) was added to a tan THF solution (5 mL) of $(C_5Me_5)_2DyCl_2K(THF)_2$ (50 mg, 0.08 mmol) and no color change was observed. While stirring, KC_8 (10 mg, 0.08 mmol) was added, and the dark suspension was left to stir overnight. Black solids were removed via centrifugation,

and the yellow supernatant was concentrated then stored at –35 ° in a vial with an $Nd_2Fe_{13}B$ magnet attached to the outside. After 3 d, colorless X-ray quality crystals of $[K(cryptand)][(C_5Me_5)_2DyCl_2]$ (35 mg, 51%) were observed growing near the magnet.

Dysprosium Metallocene Complexes of Redox Active Metal Coordination Complexes, $(C_5Me_5)_2Dy[M(SNS)_2]$ (M = Mo, W; $[SNS]^{3-}$ = bis(thiophenolato)amide)

It has been shown that some sulfur-containing bridging ligands can provide sufficient exchange pathways for magnetic coupling in paramagnetic lanthanide complexes.[31,32] It has also been demonstrated that radical-containing bridging units can drastically enhance the strength of this coupling. The marrying of these two concepts led to a collaboration with the laboratory of Professor Alan F. Heyduk at UC Irvine, whose group has been able to synthesize Mo and W complexes containing the $[SNS]^{3-}$ = bis(thiophenolato)amide ligand, $Mo[SNS]_2$ and $W[SNS]_2$, respectively, Figure A.14.[33] The Heyduk lab has also shown that additional metal moieties can bind $Mo[SNS]_2$ and $W[SNS]_2$ through the sulfur ligands to generate bimetallic and trimetallic species. It was of interest to incorporate these transition metal complexes as ligands on paramagnetic lanthanide centers. In their fully oxidized form, each transition metal complex contains a metal in the +6 oxidation state with a diamagnetic d^0 configuration. However, both Mo and W are known to access the +5 oxidation state which would leave one unpaired electron on the metal center that, if bound to a paramagnetic lanthanide, might couple to the unpaired f electrons.

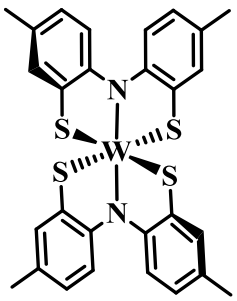

$W[SNS]_2$

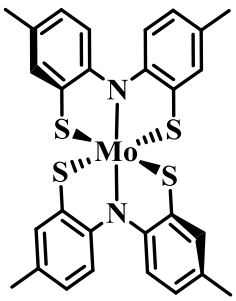

$Mo[SNS]_2$

Figure A.14. Graphical representations of the previously reported $Mo[SNS]_2$ and $W[SNS]_2$ complexes.[33]

In literature pertaining to organometallic rare earth chemistry and throughout this dissertation, the desolvated cationic complexes $[(C_5Me_5)_2Ln][(\mu\text{-}Ph)_2BPh_2]$ have proven to be useful precursors in the activation of a variety of substrates.[30,34,35] The Dy analog, $[(C_5Me_5)_2Dy][(\mu\text{-}Ph)_2BPh_2]$, was initially chosen to explore the reaction chemistry of the $Mo[SNS]_2$ and $W[SNS]_2$ complexes since Dy has proven to be highly useful in the design of molecular magnets due to its high anisotropy and paramagnetism.[16,18] It was found that reaction of 2 equiv of the cationic precursor $[(C_5Me_5)_2Dy][(\mu\text{-}Ph)_2BPh_2]$ with 1 equiv of $Mo[SNS]_2$ leads to substitution of the BPh_4 anion to generate the mixed metal complex $[(C_5Me_5)_2Dy][Mo(SNS)_2]$, **1**, eq A.5, Figure A.15. Crystallization of **1** was aided by the presence of an external magnetic field.[13] Crystallographic characterization of **1** suggests that molybdenum is in the +5 oxidation state, since the metrical parameters of the "SNS" chelate indicate this ligand is in its fully reduced form and charge balance for the Dy^{3+} ion requires three anionic ligands. One of these must be the singly reduced $[Mo(SNS)_2]^{1-}$ moiety. The byproducts of this reaction have not yet been identified, however, it is possible that BPh_4 is acting as a one electron reducing agent, as has been previously reported.[34]

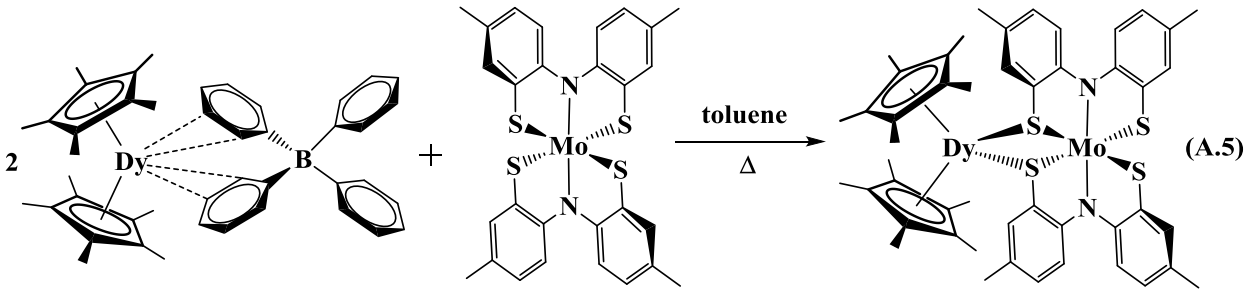

1

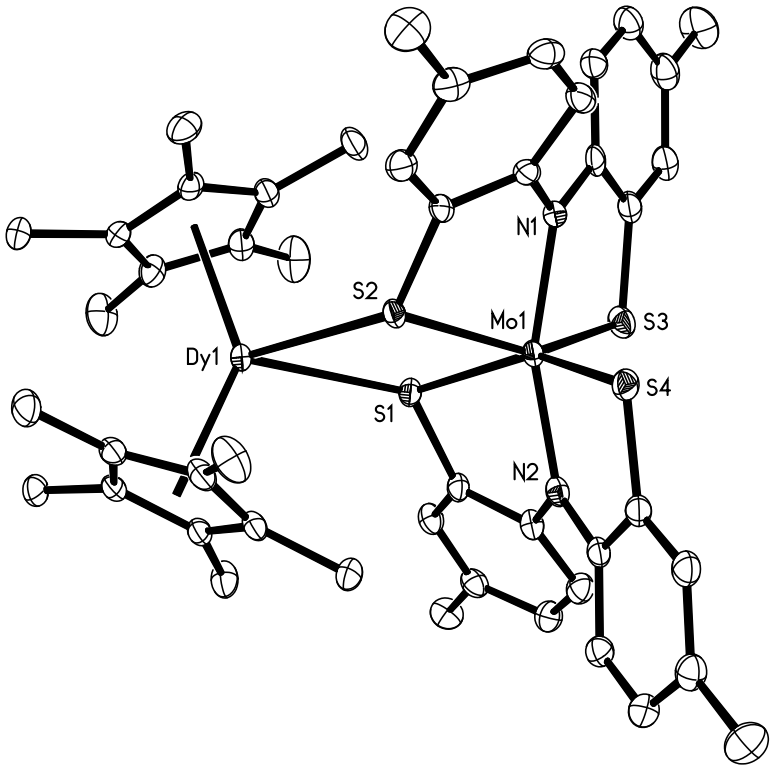

Figure A.15. Thermal ellipsoid plot of $[(C_5Me_5)_2Dy][Mo(SNS)_2]$, **1**, drawn at the 30% probability level. Hydrogen atoms have been omitted for clarity.

Preliminary reactions were also carried out with the W complex, $W[SNS]_2$, in which 2 equiv of KC_8 were first added to $W[SNS]_2$ to generate a reduced form of the complex before it was combined with 2 equiv of $[(C_5Me_5)_2Dy][(\mu\text{-}Ph)_2BPh_2]$ to generate the W analog of complex **1**, namely $[(C_5Me_5)_2Dy][W(SNS)_2]$, **2**, eq A.6, Figure A.16. Dark red crystals of **2** were isolated in the presence of an external magnetic field and crystallographically characterized. The structure of **2** contains two unique molecules in the asymmetric unit, therefore, **2** is not isomorphous with the Mo analog **1**, which contains only one molecule in the asymmetric unit. Again, the $[W(SNS)_2]^{1-}$ moiety suggests the transition metal W is in the +5 oxidation state.

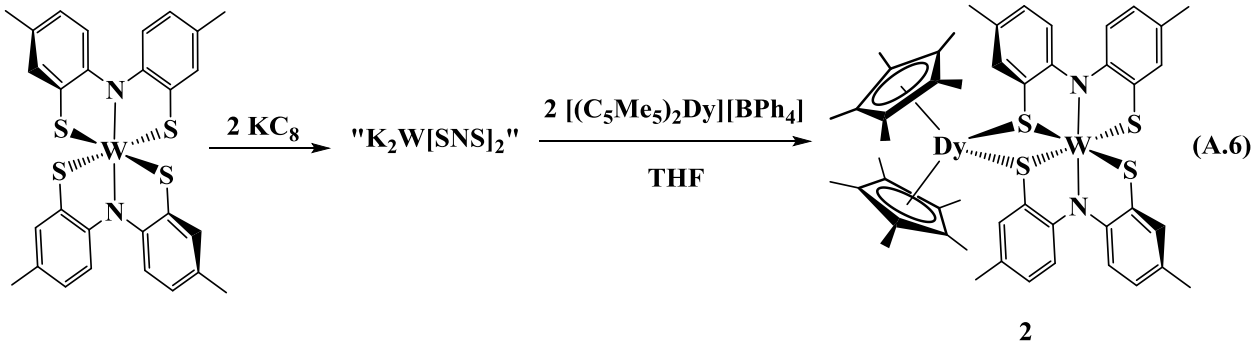

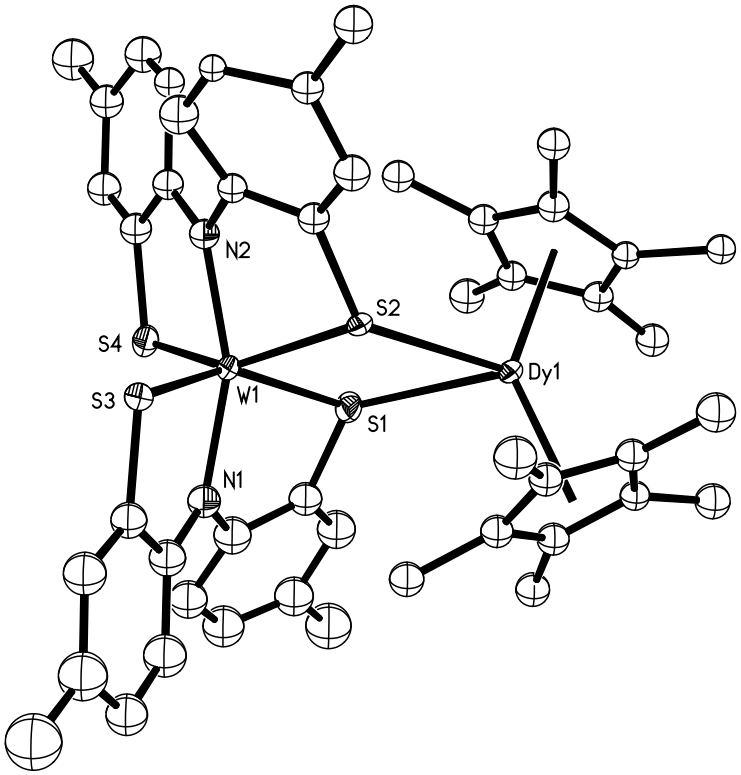

Figure A.16. Crystal structure of $[(C_5Me_5)_2Dy][W(SNS)_2]$, **2**. Heteratoms are drawn as thermal ellipsoids at the 30% probability level. Hydrogen atoms have been omitted for clarity.

In both the reactions shown above, eq A.5 and A.6, it was expected that a trimetallic complex, $[(C_5Me_5)_2Dy][M(SNS)_2][Dy(C_5Me_5)_2]$ (M = Mo, W), would form rather than the resulting bimetallic species. It is interesting that the same general formula and structure,

$[(C_5Me_5)_2Dy][M(SNS)_2]$, can be obtained with or without addition of an external reductant such as KC_8. Magnetic measurements have not yet been performed on complexes **1** or **2** to learn whether the radical $[M(SNS)_2]^{1-}$ moiety can couple the unpaired spins on the Dy^{3+} center. Analogous reactions with the Y precursor $[(C_5Me_5)_2Y][(\mu\text{-}Ph)_2BPh_2]$ are underway so that EPR spectroscopy can be used to verify the presence of a M^{5+} transition metal in **1** and **2**.

Experimental. All syntheses and manipulations described below were conducted under nitrogen with rigorous exclusion of air and water using glovebox, Schlenk, and high-vacuum line techniques. Solvents were sparged with UHP argon and dried over columns containing Q-5 and molecular sieves. Potassium was washed with hexane and scraped to provide fresh surfaces before use. $[(C_5Me_5)_2Dy][(\mu\text{-}Ph)_2BPh_2]$[30] and KC_8[14] were prepared according to the literature procedures. The $W[SNS]_2$ and $Mo[SNS]_2$ precursors were provided by Kyle Rosenkoetter and Mikey Wojnar. $Nd_2Fe_{13}B$ magnets used in the crystallizations were obtained from United Nuclear Scientific Equipment and Supplies.

$[(C_5Me_5)_2Dy][Mo(SNS)_2]$, 1. In a nitrogen filled glovebox, a dark purple toluene solution (5 mL) of $Mo[SNS]_2$ (15 mg, 0.02 mmol) was added to a cloudy white toluene suspension (10 mL) of $[(C_5Me_5)_2Dy][(\mu\text{-}Ph)_2BPh_2]$ and the dark solution was left to stir overnight. It was then transferred to 100 mL sealable Schlenk flask and heated to reflux for 12 h while stirring. The dark purple solution was brought back into the glovebox, centrifuged to remove a small amount of dark gray solids, and solvent was removed from the supernatant to yield a dark purple solid. The solids were dissolved in Et_2O (18 mL) and stored at –35 ° in a vial with a $Nd_2Fe_{13}B$ magnet attached to the side. After 4 days, dark purple X-ray quality crystals of $[(C_5Me_5)_2Dy][Mo(SNS)_2]$, **1**, were observed growing on the wall in contact with the magnet.

$[(C_5Me_5)_2Dy][W(SNS)_2]$, 2. In a nitrogen filled glovebox, KC_8 (8 mg, 0.06 mmol) was added to a dark brown THF solution (5 mL) of $W[SNS]_2$ (20 mg, 0.03 mmol) and the dark mixture was stirred for 10 min. This mixture was then filtered to remove black solids and the filtrate was directly added to a colorless THF solution (5 mL) of $[(C_5Me_5)_2Dy][(\mu\text{-}Ph)_2BPh_2]$ to make a dark brown mixture which was left to stir overnight. Centrifugation removed black and gray solids and solvent was removed from the dark red supernatant to yield dark brown solids. The product was extracted using Et_2O and X-ray quality crystals of $[(C_5Me_5)_2Dy][W(SNS)_2]$, **2**, were grown from Et_2O solutions in the presence of an external magnetic field.

References

(1) Evans, W. J.; Lee, D. S.; Rego, D. B.; Perotti, J. M.; Kozimor, S. A.; Moore, E. K.; Ziller, J. W. *Journal of the American Chemical Society* **2004**, *126*, 14574.

(2) Evans, W. J.; Lee, D. S.; Ziller, J. W. *Journal of the American Chemical Society* **2003**, *126*, 454.

(3) Evans, W. J.; Lee, D. S.; Lie, C.; Ziller, J. W. *Angewandte Chemie International Edition* **2004**, *43*, 5517.

(4) Fang, M.; Bates, J. E.; Lorenz, S. E.; Lee, D. S.; Rego, D. B.; Ziller, J. W.; Furche, F.; Evans, W. J. *Inorganic Chemistry* **2011**, *50*, 1459.

(5) Fang, M.; Lee, D. S.; Ziller, J. W.; Doedens, R. J.; Bates, J. E.; Furche, F.; Evans, W. J. *Journal of the American Chemical Society* **2011**, *133*, 3784.

(6) Evans, W. J.; Fang, M.; Zucchi, G. l.; Furche, F.; Ziller, J. W.; Hoekstra, R. M.; Zink, J. I. *Journal of the American Chemical Society* **2009**, *131*, 11195.

(7) Rinehart, J. D.; Fang, M.; Evans, W. J.; Long, J. R. *Journal of the American Chemical Society* **2011**, *133*, 14236.

(8) McNaney, J.; Zimmerman, F.; Zimmerman, H. *Monatshefte fuer Chemie* **1986**, *117*, 1.

(9) Strong, J.; Tuttle, T. R. *The Journal of Physical Chemistry* **1973**, *77*, 533.

(10) W. A. Herrmann, G. B.; Edelmann, F. T., Ed. 1997; Vol. 6.

(11) Baker, M. L.; Waldmann, O.; Piligkos, S.; Bircher, R.; Cador, O.; Carretta, S.; Collison, D.; Fernandez-Alonso, F.; McInnes, E. J. L.; Mutka, H.; Podlesnyak, A.; Tuna, F.; Ochsenbein, S.; Sessoli, R.; Sieber, A.; Timco, G. A.; Weihe, H.; Güdel, H. U.; Winpenny, R. E. P. *Physical Review B* **2012**, *86*, 064405.

(12) Rinehart, J. D.; Fang, M.; Evans, W. J.; Long, J. R. *Nature Chemistry* **2011**, *3*, 538.

(13) Meihaus, K. R.; Corbey, J. F.; Fang, M.; Ziller, J. W.; Long, J. R.; Evans, W. J. *Inorganic Chemistry* **2014**, *53*, 3099.

(14) Bergbreiter, D. E.; Killough, J. M. *Journal of the American Chemical Society* **1978**, *100*, 2126.

(15) Demir, S.; Nippe, M.; Gonzalez, M. I.; Long, J. R. *Chemical Science* **2014**, *5*, 4701.

(16) Demir, S.; Jeon, I.-R.; Long, J. R.; Harris, T. D. *Coordination Chemistry Reviews* **2015**, *289–290*, 149.

(17) Cassani, M. C.; Duncalf, D. J.; Lappert, M. F. *Journal of the American Chemical Society* **1998**, *120*, 12958.

(18) Woodruff, D. N.; Winpenny, R. E. P.; Layfield, R. A. *Chemical Reviews* **2013**, *113*, 5110.

(19) Kotyk, C. M.; MacDonald, M. R.; Ziller, J. W.; Evans, W. J. *Organometallics* **2015**.

(20) Xie, Z.; Chui, K.; Liu, Z.; Xue, F.; Zhang, Z.; Mak, T. C. W.; Sun, J. *Journal of Organometallic Chemistry* **1997**, *549*, 239.

(21) MacDonald, M. R.; Ziller, J. W.; Evans, W. J. *Journal of the American Chemical Society* **2011**, *133*, 15914.

(22) MacDonald, M. R.; Bates, J. E.; Fieser, M. E.; Ziller, J. W.; Furche, F.; Evans, W. J. *Journal of the American Chemical Society* **2012**, *134*, 8420.

(23) MacDonald, M. R.; Bates, J. E.; Ziller, J. W.; Furche, F.; Evans, W. J. *Journal of the American Chemical Society* **2013**, *135*, 9857.

(24) Hitchcock, P. B.; Lappert, M. F.; Maron, L.; Protchenko, A. V. *Angewandte Chemie International Edition* **2008**, *47*, 1488.

(25) MacDonald, M. R.; Fieser, M. E.; Bates, J. E.; Ziller, J. W.; Furche, F.; Evans, W. J. *Journal of the American Chemical Society* **2013**, *135*, 13310.

(26) Langeslay, R. R.; Fieser, M. E.; Ziller, J. W.; Furche, F.; Evans, W. J. *Chemical Science* **2015**, *6*, 517.

(27) Nief, F. *Dalton Transactions* **2010**, *39*, 6589.

(28) Jaroschik, F.; Nief, F.; Le Goff, X.-F.; Ricard, L. *Organometallics* **2007**, *26*, 3552.

(29) Demir, S.; Zadrozny, J. M.; Nippe, M.; Long, J. R. *Journal of the American Chemical Society* **2012**, *134*, 18546.

(30) Evans, W. J.; Seibel, C. A.; Ziller, J. W. *Journal of the American Chemical Society* **1998**, *120*, 6745.

(31) Tuna, F.; Smith, C. A.; Bodensteiner, M.; Ungur, L.; Chibotaru, L. F.; McInnes, E. J. L.; Winpenny, R. E. P.; Collison, D.; Layfield, R. A. *Angewandte Chemie International Edition* **2012**, *51*, 6976.

(32) Pointillart, F.; Klementieva, S.; Kuropatov, V.; Le Gal, Y.; Golhen, S.; Cador, O.; Cherkasov, V.; Ouahab, L. *Chemical Communications* **2012**, *48*, 714.

(33) Shaffer, D. W.; Szigethy, G.; Ziller, J. W.; Heyduk, A. F. *Inorganic Chemistry* **2013**, *52*, 2110.

(34) MacDonald, M. R.; Ziller, J. W.; Evans, W. J. *Inorganic Chemistry* **2011**, *50*, 4092.

(35) Schultz, M.; Boncella, J. M.; Berg, D. J.; Tilley, T. D.; Andersen, R. A. *Organometallics* **2002**, *21*, 460.

APPENDIX B

List of Crystal Structures, Cell Parameters, and UCI X-ray Codes

Code	Compound	a (Å)	b (Å)	c (Å)	α (°)	β (°)	γ (°)	Volume (Å^3)
jfc1	$\{[(Me_3Si)_2N]_3Y\}(\mu\text{-}Cl)[Li(THF)_3]$	35.9	16.1	24.8	90	132.1	90	10623
jfc4	$\{[(Me_3Si)_2N]_2(py)Y\}_2(\mu\text{-}\eta^2\text{:}\eta^2\text{-}N_2)$	11.4	11.5	11.8	97.5	96.1	117.0	1353
jfc5	$\{[(Me_3Si)_2N]_2(Ph_3PO)Y\}_2(\mu\text{-}\eta^2\text{:}\eta^2\text{-}N_2)\bullet(C_7H_8)_2$	13.3	17.3	20.7	106.5	91.0	108.3	4295
jfc6	$\{[(Me_3Si)_2N]_2(PhCN)Y\}_2(\mu\text{-}\eta^2\text{:}\eta^2\text{-}N_2)$	11.7	12.1	12.1	106.0	114.5	104.5	1442
jfc7	$\{[(Me_3Si)_2N]_2(DMAP)Y\}_2(\mu\text{-}\eta^2\text{:}\eta^2\text{-}N_2)$	11.7	21.4	11.9	90	95.1	90	2960
jfc8	$\{[(Me_3Si)_2N]_2(THF)Y\}_2(\mu\text{-}\eta^2\text{:}\eta^2\text{-}N_2)$	11.7	12.4	13.7	114.0	102.9	110.4	1546
jfc9	$\{[(C_5Me_5)_2Tb]_2(\mu\text{-phz})\}\{BPh_4\}\bullet 5(C_6H_6)$	10.6	15.0	16.2	64.5	71.5	82.3	2208
jfc10	$K\{[(Me_3Si)_2N]_2(THF)Gd\}_2(\mu_3\text{-}\eta^2\text{:}\eta^2\text{:}\eta^2\text{-}N_2)]\bullet\frac{1}{2}(C_7H_8)$	12.5	21.4	22.4	90	105.0	90	5763
jfc11	$\{[(Me_3Si)_2N]_2(THF)Gd\}_2(\mu\text{-}\eta^2\text{:}\eta^2\text{-}N_2)\bullet(C_8H_8)$	11.7	12.3	12.8	101.7	109.1	110.7	1522
jfc12	$\{[Dy(OC_6H_3{}^tBu_2\text{-}2,6)_2(THF)]_3(\mu_2\text{-}OH)_3(\mu_3\text{-}OH)_2\}\{K(THF)_6\}_2$	19.7	19.7	20.5	90	90	120	6897
jfc13	$\{[Dy(OC_6H_3{}^tBu_2\text{-}2,6)_2(THF)]_3(\mu_2\text{-}OH)_3(\mu_3\text{-}OH)\}\{K(THF)_6\}$	19.3	19.3	20.9	90	90	120	6755
jfc14	$\{[(Me_3Si)_2N]_2(THF)Dy\}_2(\mu\text{-}\eta^2\text{:}\eta^2\text{-}N_2)$	11.7	12.3	12.8	101.3	109.9	110.3	1514
jfc15	$[(C_5Me_5)_2Y](bpym)][BPh_4]\bullet(THF)$	10.6	17.8	26.2	101.8	94.8	90.6	4815

jfc16	$\{[(Me_3Si)_2N]_2(Ph_3PO)Y\}_2(\mu\text{-}\eta^2\text{:}\eta^2\text{-}N_2)$	12.0	12.5	16.6	75.4	73.0	65.0	2142
jfc17	$\{Na(THF)_6\}\{Tb[N(SiMe_3)_2]_4\}$	26.7	30.8	17.3	90	91.0	90	14269
jfc18	$\{[(C_5Me_5)_2Dy]_2(\mu\text{-phz})\}\{BPh_4\}\bullet 4(C_6H_6)$	10.6	15.0	16.1	64.7	71.4	82.2	2196
jfc21	$\{[(Me_3Si)_2N]_2(THF)Tb\}_2(\mu\text{-}\eta^2\text{:}\eta^2\text{-NO})\bullet(C_7H_8)$	11.6	12.3	12.9	101.9	110.0	110.2	1518
jfc24	$\{[(Me_3Si)_2N]_2Y(THF)\}_2(\mu\text{-}\eta^2\text{:}\eta^2\text{-}S_2)/\{[(Me_3Si)_2N]_2Y(THF)\}_2(\mu\text{-S}) \bullet (C_7H_8)$	11.7	12.1	13.0	99.4	110.4	111.5	1525
jfc25	$\{[(Me_3Si)_2N]_2(THF)Y\}_2(\mu\text{-}\eta^2\text{:}\eta^2\text{-}N_2)$	11.2	11.4	13.3	107.6	104.6	94.0	1558
jfc26	$\{[(C_5Me_5)_2Dy]_2(\mu\text{-phz})\}\{BPh_4\}\bullet (C_6H_6)$	13.6	18.5	27.2	90	90	90	6838
jfc27	$\{K(cryptand)\}\{[(Me_3Si)_2N]_2(THF)Y\}_2(\mu\text{-}\eta^2\text{:}\eta^2\text{-}N_2)$	10.0	12.9	19.3	90.6	93.9	102.4	2423
jfc28	$K\{[(Me_3Si)_2N]_2(THF)Dy\}_2(\mu_3\text{-}\eta^2\text{:}\eta^2\text{:}\eta^2\text{-}N_2)]\bullet\frac{1}{2}(C_6H_{14})$	12.5	21.5	22.2	90	105.1	90	5777
jfc29	$\{K(cryptand)\}\{[(Me_3Si)_2N]_2(THF)Y\}_2(\mu\text{-}\eta^2\text{:}\eta^2\text{-}N_2)$	10.1	13.0	19.2	90.3	94.4	102.4	2451
jfc30	$\{K(cryptand)\}\{[(Me_3Si)_2N]_2(THF)Y\}_2(\mu\text{-}\eta^2\text{:}\eta^2\text{-}N_2)$	10.0	13.0	19.2	90.5	94.5	102.2	2429
jfc31	$\{K(cryptand)\}\{[(Me_3Si)_2N]_2(THF)Y\}_2(\mu\text{-}\eta^2\text{:}\eta^2\text{-}N_2)$	11.6	14.8	23.5	86.0	78.1	76.9	3867
jfc32	$K\{[(Me_3Si)_2N]_2(THF)Gd\}_2(\mu_3\text{-}\eta^2\text{:}\eta^2\text{:}\eta^2\text{-}N_2)]\bullet\frac{1}{2}(C_5H_{12})$	12.6	21.5	22.2	90	104.8	90	5806
jfc33	$[(C_5Me_5)_2Gd]_2(\mu\text{-phz})\bullet(C_7H_8)$	10.4	11.0	11.4	80.7	77.0	85.5	1260
jfc34	$\{K(cryptand)\}\{[(Me_3Si)_2N]_2(THF)Dy\}_2(\mu\text{-}\eta^2\text{:}\eta^2\text{-}N_2)$	11.6	14.8	23.7	86.0	78.3	77.1	3896

jfc35	{K(cryptand)}{[$(Me_3Si)_2N]_2$(THF)Tb}$_2$(μ-η^2:η^2-N_2)	10.2	13.1	19.3	90.4	94.9	102.3	2513
jfc36	{K(cryptand)}{[$(Me_3Si)_2N]_2$(THF)Gd}$_2$(μ-η^2:η^2-N_2)	11.7	14.8	23.7	85.9	78.1	77.1	3912
jfc37	$(C_5Me_5)Dy(C_3H_5)_2$(THF)	8.6	8.9	13.1	85.0	76.6	80.1	953
jfc39	$(C_5Me_5)_2Dy(C_3H_5)$	8.9	13.6	17.6	90	90	90	2136
jfc40	[K(cryptand)][1,4- $C_6H_4(SiMe_3)_2$]	11.8	12.5	13.9	86.8	85.1	63.1	1816
jfc41	{$[(C_5Me_5)_2Tb]_2$(μ-phz)}{BPh_4}, no solvent	10.4	12.4	25.3	97.8	95.9	96.0	3171
jfc42	$[(C_5Me_5)_2Dy(NH_3)_2][BPh_4]$•½($C_7H_8$)	16.1	18.8	29.9	93.8	104.0	109.4	8148
jfc43	{$[(Me_3Si)_2N]_2$Y(THF)}$_2$(μ-S)	10.4	12.2	12.2	61.5	80.2	89.1	1333
jfc44	{$[(Me_3Si)_2N]_2$Y(THF)}$_2$(μ-Se)	10.4	12.2	12.2	62.0	88.8	80.6	1341
jfc45	{$[(Me_3Si)_2N]_2$Y(THF)}$_2$(μ-η^2:η^2-S_2)/{$[(Me_3Si)_2N]_2$Y(THF)}$_2$(μ-S)	10.7	12.1	12.1	61.0	79.5	88.5	1340
jfc46	$[(Me_3Si)_2N]_2Y[\eta^2$-$S_3N(SiMe_3)_2]$(THF)	8.8	10.1	23.8	101.1	91.0	101.8	2022
jfc47	$[Cp^{In}{}_3Y(\mu$-Cl)$YCp^{In}{}_3][Na(THF)_6]$	15.2	16.2	16.6	99.7	109.8	113.8	3294
jfc48	$Cp^{In}{}_3$Ho(THF)	11.7	11.7	10.1	90	90	120	1186
jfc49	$[Cp^{In}{}_3Pr(\mu$-Cl)$PrCp^{In}{}_3][Na(THF)_6]$	10.7	12.5	12.6	87.0	82.7	88.4	1661
jfc50	$Cp^{In}{}_3$Y(THF)	11.7	11.7	10.1	90	90	120	1187
jfc51	$[Cp^{In}{}_3La(\mu$-Cl)$LaCp^{In}{}_3][Na(THF)_6]$	10.7	12.4	12.6	87.5	88.5	83.9	1666
jfc52	KCp^{In}	12.8	12.9	40.3	83.0	81.5	61.4	5747
jfc53	$Cp^{In}{}_3$La(THF)	23.4	10.5	21.6	90.0	114.5	90.0	4831
jfc54	$[Cp^{In}{}_3La(\mu$-Cl)$LaCp^{In}{}_3][Na(THF)_6]$	10.6	12.3	12.6	87.5	88.4	83.9	1634
jfc55	$Cp^{In}{}_3$Dy(THF)	11.7	11.7	10.1	90	90	120	1185
jfc56	{$[(Me_3Si)_2N]_2$(THF)Y}$_2$(μ-η^2:η^2-Se_2) (ICED)	10.8	12.1	12.2	61.7	80.0	87.6	1375

jfc57	{K(2.2.2-cryptand)}$_2${[(C$_9$H$_7$)$_2$Dy(μ-η^5:η^1-C$_9$H$_6$)]$_2$}	13.8	13.9	15.0	108.9	92.8	101.3	2663
jfc58	[(C$_5$Me$_5$)$_2$Y(NC^{t}Bu)$_3$][BPh$_4$]	41.4	11.0	32.1	90	128.4	90	11440
jfc59	{[(Me$_3$Si)$_2$N]$_2$Y(THF)}$_2$(μ-O)	10.9	12.0	12.2	60.7	76.3	89.2	1341
jfc60	{K(18-crown-6)}$_2${[(Me$_3$Si)$_2$N]$_2$(THF)Y}$_2$(μ-SO?)$_2$	14.2	15.7	16.7	116.7	94.3	110.2	3002
jfc61	{[(Me$_3$Si)$_2$N]$_2$Y(THF)}$_2$(μ-η^2:η^2-S$_2$)/{[(Me$_3$Si)$_2$N]$_2$Y(THF)}$_2$(μ-S)•(C$_7$H$_8$)	11.7	12.2	13.0	99.6	110.2	111.1	1520
jfc62	[(C$_5$Me$_5$)$_2$Y(NCMe)$_3$][BPh$_4$]	46.0	25.5	18.6	90	101.6	90	21310
jfc63	[K(cryptand)][BPh4]	13.9	14.3	17.6	107.3	126.6	98.7	2427
jfc64	[Cp$^{In}_3$Dy(μ-Cl)DyCp$^{In}_3$][Na(THF)$_6$]	15.2	16.3	16.4	99.4	110.0	114.0	3268
jfc65	[(C$_5$Me$_5$)$_2$La(NCMe)$_2$(THF)][BPh$_4$]	14.9	26.4	31.1	90	90	90	12217
jfc66	[K(18-crown-6)][(C$_8$H$_8$)$_2$La]	9.2	9.2	17.4	96.6	96.6	98.1	1429
jfc67	[(C$_5$Me$_5$)$_2$Gd(NCMe)$_3$][BPh$_4$]	19.1	25.4	45.9	90	101.5	90	21808
jfc68	[K(cryptand)]{[(Me$_3$Si)$_2$N]$_2$Y[CH$_2$Si(Me$_2$)NSiMe$_3$]}	15.6	34.6	44.0	90	90	90	23739
jfc69	[(C$_5$Me$_5$)$_2$Gd(NCPh)$_3$][BPh$_4$]	10.2	17.0	20.8	100.1	103.2	93.3	3435
jfc70	[(C$_5$Me$_5$)$_2$La(NCPh)$_3$][BPh$_4$]	10.4	17.0	20.7	100.0	102.8	93.0	3485
jfc71	[K(cryptand)][C$_5$H$_3$(SiMe$_3$)$_2$]$_2$Gd(C$_{14}$H$_{10}$)	14.9	19.2	21.2	90.1	90.0	100.8	5955
jfc72	[(C$_5$H$_4$SiMe$_3$)$_2$Y(NCMe)$_3$][BPh$_4$]	12.8	14.2	14.6	91.1	106.4	98.1	2518
jfc73	[(C$_5$H$_4$SiMe$_3$)$_2$Y(OH)]$_2$	12.3	13.5	14.2	62.1	68.3	81.2	1942
jfc74	[K(cryptand)]BPh$_4$•(THF)$_2$	13.3	13.7	14.3	93.5	116.3	95.7	2301
jfc75	[K(cryptand)][C$_{14}$H$_{10}$]	10.9	11.8	13.9	88.1	74.1	67.0	1584
jfc76	Cp^{In}DyCl$_2$(THF)$_3$	22.3	11.7	26.8	90	107.2	90	6676

jfc77	$[Cp^{In}_2Dy(\mu\text{-}Cl)_2K(Et_2O)]_\infty$	7.8	15.5	22.0	95.5	100.3	104.6	2514
jfc78	$[K(cryptand)][(C_5Me_5)_2DyCl_2]\bullet(THF)$	18.4	21.6	14.1	90	112.9	90	5151
jfc79	$[Cp^{In}_2Ho(\mu\text{-}Cl)_2K(Et_2O)]_\infty$	7.8	15.4	21.8	79.3	79.8	75.4	2466
jfc80	$[Cp^{In}Ho(THF)]_3(\mu\text{-}Cl)_3(\mu_3\text{-}Cl)(\mu_3\text{-}O)$	10.4	18.8	20.7	90	90	90	4017
jfc81	$[(C_5Me_5)_2Dy][Mo(SNS)_2]$	11.9	12.8	19.3	72.0	80.1	73.6	2666
jfc82	$[(C_5Me_5)_2Dy][W(SNS)_2]$	11.9	19.3	22.5	70.4	87.0	88.5	4842